

UNCLASSIFIED

AD NUMBER
AD860365
NEW LIMITATION CHANGE
TO Approved for public release, distribution unlimited
FROM Distribution authorized to U.S. Gov't. agencies and their contractors; Operational and Administrative Use; 30 Jun 1969. Other requests shall be referred to Air Force Aero Propulsion Laboratory, Attn: APLP-3, Wright-Patterson AFB, OH, 45433.
AUTHORITY
AFAPL ltr, 12 Apr 1972

THIS PAGE IS UNCLASSIFIED

AFAPL-TR-69-57

SILVER-ZINC ELECTRODES
AND
SEPARATOR RESEARCH

J. A. Keralla

Delco-Remy Division, General Motors Corporation

TECHNICAL REPORT AFAPL-TR-69-57

30 June 1969

STATEMENT #2 UNCLASSIFIED

This document is subject to special export controls and each transmittal to foreign governments or foreign nationals may be made only with prior approval of -----

Air Force Aero Propulsion Laboratory

Air Force Systems Command

Wright-Patterson Air Force Base, Ohio 45433

Attch 1 APHP-3

Reproduced by the
CLEARINGHOUSE
for Federal Scientific & Technical
Information Springfield Va. 22151



H20

AD 860365

AFAPL-TR-69-57

SILVER-ZINC ELECTRODES
AND
SEPARATOR RESEARCH

J. A. Keralla

Delco-Remy Division, General Motors Corporation

TECHNICAL REPORT AFAPL-TR-69-57

30 June 1969

Air Force Aero Propulsion Laboratory
Air Force Systems Command
Wright-Patterson Air Force Base, Ohio 45433

FOREWORD

This report was prepared by Delco-Remy Division of General Motors Corporation, Anderson, Indiana, on Air Force Contract Nr. AF33(615)-3487, under Task Nr. 314522 of Project Nr. 3145, "Silver-Zinc Electrodes and Separator Research." The work was administered under the direction of the Static Energy Conversion Section, Flight Vehicle Power Branch, Aero Space Power Division, Aero Propulsion Laboratory; Mr. J. E. Cooper was task engineer for the laboratory.

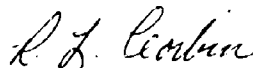
The assistance of Dr. T. P. Dirkse, Professor of Chemistry, Calvin College, Grand Rapids, Michigan, as consultant on this project is greatly appreciated.

This report was submitted by the authors on 31 August 1968.

Publication of this report does not constitute Air Force approval of the report's findings or conclusions. It is published only for the exchange and stimulation of ideas.



J. A. Keralla
Engineer - Power Systems
Delco-Remy Division, GMC



R. L. Corbin
Supervisor - Power Systems
Delco-Remy Division, GMC

NOTICE

When Government drawings, specifications, or other data are used for any purpose other than in connection with a definitely related Government procurement operation, the United States Government thereby incurs no responsibility nor any obligation whatsoever; and the fact that the Government may have formulated, furnished, or in any way supplied the said drawings, specifications, or other data, is not to be regarded by implication or otherwise as in any manner licensing the holder or any other person or corporation, or conveying any rights or permission to manufacture, use, or sell any patented invention that may in any way be related thereto.

Copies of this report should not be returned unless return is required by security considerations, contractual obligations, or notice on a specific document.

ABSTRACT

Emulphogene BC-610 used in quantities of .5% to 1% by weight in the negative active material tends to increase cycle life.

The use of 1% Pb in the negative active material tends to increase cycle life at 60% depth-of-discharge. The presence of Fe in zinc oxide in concentrations over .010% is detrimental to cycle life at any depth-of-discharge.

The use of inert polyethylene crosslinked at 90 Mrads, radiation grafted with methacrylic acid can be used as a satisfactory separator material for long cycling silver zinc cells.

TABLE OF CONTENTS

<u>Item</u>	<u>Title</u>	<u>Page</u>
I	<u>Introduction</u>	1
II	<u>Factual Data</u>	2
	A. Mechanical Barriers to Zinc Agglomeration	2
	B. Surfactant Additions	9
	C. Fundamental Studies on Surfactants	16
	D. Particle Size and Morphology of Zinc Oxides	16
	E. Zinc Electrode Fabrication Techniques	26
	F. Influence of Membrane Separator Characteristics	30
	G. Sites for ZnO Overgrowths	30
	H. Development of Failure Analysis Techniques	34
	I. Sizes of Zincate Ion & Soluble Silver Species in KOH	39
	J. Membrane Pore Size Measurements in KOH	39
	K. Stoichiometric Ratio of Formed Zinc	42
	L. Alternate Method of Surface Area Measurement	43
	M. Separator Development	43
	N. Electrolytes	53
III	<u>General Discussion</u>	54
IV	<u>Recommendations</u>	60
	Appendix I - Preparation & Characterization of Special Zinc Oxides for Evaluation in Silver Oxide-Zinc Secondary Batteries	136
	Appendix II - Adsorption of Organic Materials on Zinc Electrodes	190
	Appendix III - Surface Area Studies of Zinc Electrodes	230
	Appendix IV - A Literature Survey on the Solubility of ZnO in Other Divalent Metal Oxides and of Zn(OH) ₂ in Other Divalent Metal Hydroxides	262
	Appendix V - Sizes of Zincate Ion and Soluble Silver Species in KOH	270
	Appendix VI - Development of Improved Separator Materials for the Alkaline Silver Oxide Zinc Battery	288
	Distribution List	

LIST OF FIGURES

<u>Figure</u>		<u>Page</u>
1	Negative Plate in Control Cell at 140 Cycles 100X .	62
2	Negative Plate Containing 5% Asbestos Fibers at 134 Cycles 140X	63
3	Negative Plate Containing 10% Asbestos Fibers at 134 Cycles 140X	64
4	Negative Plate Containing 15% Asbestos Fibers at 134 Cycles 140X	65
5	Negative Plate Containing 5% FSC Fibers at 146 Cycles 140X	66
6	Negative Plate Containing 10% FSC Fibers at 146 Cycles 140X	67
7	Negative Plate Containing 15% FSC Fibers at 146 Cycles 140X	68
8	Negative Plate Containing 5% Zinc Fibers at 171 Cycles 140X	69
9	Negative Plate Containing 10% Zinc Fibers at 108 Cycles 140X	70
10	Negative Plate Containing 15% Zinc Fibers at 168 Cycles 140X	71
11	Negative Plate Containing .2% LSA at 84 Cycles 200X	72
12	Negative Plate Containing 1.2% LSA at 168 Cycles 200X	73
13	Negative Plate Containing 2% LSA at 144 Cycles 200X	74
14	Negative Plate as Control at 157 Cycles 200X . . .	75
15	Negative Plate Containing 1% Cotton Fibers at 144 Cycles 100X	76
16	Negative Plate Containing 3% Cotton Fibers at 144 Cycles 100X	77

LIST OF FIGURES (Continued)

<u>Figure</u>	<u>Title</u>	<u>Page</u>
17	Negative Plate Containing 5% Cotton Fibers at 144 Cycles 100X	78
18	Photomicrograph of a Negative Plate Containing 15% Avicel 200X	79
19	Negative Plate Containing 30% Cellulosic Fibers at 300 Cycles 100X	80
20	Negative Plate Containing .15% BC-420 at 168 Cycles 200X	81
21	Negative Plate Containing 1% BC-420 at 168 Cycles 200X	82
22	Negative Plate Containing .15% BC-720 at 120 Cycles 200X	83
23	Negative Plate Containing 1% BC-720 at 108 Cycles 200X	84
24	Negative Plate Containing .15% BC-840 at 168 Cycles 200X	85
25	Negative Plate Containing 1% BC-840 at 144 Cycles 200X	86
26	Negative Plate Containing .5% BC-610 at 168 Cycles Control Cell 200X	87
27	Negative Plate Containing .15% BC-610 at 76 Cycles at 40°F 200X	88
28	Negative Plate Containing .6% BC-610 at 52 Cycles at 40°F 200X	89
29	Negative Plate Containing 1% BC-610 at 58 Cycles at 40°F 200X	90
30	Negative Plate Containing .15% BC-610 at 110 Cycles at 100°F 200X	91

LIST OF FIGURES (Continued)

<u>Figure</u>	<u>Title</u>	<u>Page</u>
31	Negative Plate Containing .6% BC-610 at 121 Cycles at 100°F 200X	92
32	Negative Plate Containing 1% BC-610 at 124 Cycles at 100°F 200X	93
33	Negative Plate Containing .1% FC-95 at 150 Cycles 200X	94
34	Negative Plate Containing .6% FC-95 at 152 Cycles 200X	95
35	Negative Plate Containing 1% FC-95 at 168 Cycles 200X	96
36	Negative Plate Containing 1% Carbowax with a Molecular Weight Range of 6000 after 132 Cycles 100X	97
37	Negative Plate Containing 1% Carbowax with a Molecular Weight Range of 1000 after 200 Cycles 100X	98
38	Negative Plate Containing 1% Carbowax with a Molecular Weight Range of 200 after 100 Cycles 100X	99
39	Negative Plate Containing 1.1% LSA After 108 Cycles 200X	100
40	Negative Plate Containing 1.1% LSA and 5% ZnSO ₄ after 96 Cycles 200X	101
41	Negative Plate Containing .0008% Pb after 202 Cycles 200X	102
42	Negative Plate Containing .028% Pb after 214 Cycles 200X	103
43	Negative Plate Containing 1.02% Pb after 221 Cycles 200X	104
44	Negative Plate Containing 2.4% Pb after 214 Cycles 200X	105

LIST OF FIGURES (Continued)

<u>Figure</u>	<u>Title</u>	<u>Page</u>
45	Negative Plate Containing .0006% Fe after 178 Cycles 200X	106
46	Negative Plate Containing .0086% Fe after 168 Cycles 200X	107
47	Negative Plate Containing .0092% Fe after 120 Cycles 200X	108
48	Negative Plate Containing .26% Pb and .010% Fe after 192 Cycles 200X	109
49	Negative Plate Containing .07% Al and .0010% Fe after 156 Cycles 200X	110
50	Negative Plate Containing .9% Al and .0008% Fe after 167 Cycles 200X	111
51	Negative Plate Containing .25% Pb after 221 Cycles 200X	112
52	Negative Plate Containing .3% Al after 170 Cycles 200X	113
53	Negative Plate Containing Kadox 15 after 170 Cycles 200X	114
54	Negative Plate Containing Zinc Dust after 168 Cycles 200X	115
55	Negative Plate Containing Zinc Flake after 204 Cycles 100X	116
56	Negative Plate of Electrodeposited Zinc after 96 Cycles 200X	117
57	Negative Plate Containing 1% CaO after 156 Cycles 200X	118
58	Negative Plate Containing 3% CaO after 96 Cycles 200X	119
59	Negative Plate Containing 5% CaO after 156 Cycles 200X	120

LIST OF FIGURES (Continued)

<u>Figure</u>	<u>Title</u>	<u>Page</u>
60	Electronmicrograph of the Surface of VF WP Millipore Material at 150,000 X 100X	121
61	Electronmicrograph of the Surface of VM WF Millipore Material at 150,000 X 100X	122
62	Electronmicrograph of the Surface of Dow Corning Porous Glass at 300,000 X 100X	123
63	Electronmicrograph of the Surface of 2.2XH Membrane Material by RAI at 61,000 X 100X	124
64	Electronmicrograph of the Surface of Dow Corning Porous Glass at 300,000 X	125
65	Electronmicrograph of the Surface of 2.2XH Membrane Material by RAI at 61,000 X 100X	126
66	Electronmicrograph of Surface of 2.2XH Membrane Material by RAI at 300,000 X 100X	127
67	Electronmicrograph of Surface of 2.2XH Membrane Material by RAI at 300,000 X 100X	128
68	Negative Plate with a 2:1 Construction after 184 Cycles 100X	129
69	Negative Plate with a 3:1 Construction After 204 Cycles 100X	130
70	Negative Plate with a 4:1 Construction after 220 Cycles 100X	131
71	Appearance of the Negative Material After Cycle Failure in the Separator Test 100X	132
72	Comparison of Cycle Life of Separators in Various KOH Concentrations	133
73	Comparison of Cycle Life of Percent Aluminum in Zinc Oxide in Separators	134
74	Comparison of Cycle Life of Percent Lead in Zinc Oxide in Separators	135

LIST OF TABLES

<u>Table</u>	<u>Title</u>	<u>Page</u>
I	Mechanical Barriers to Zinc Agglomeration	6
II	Surfactants	11
III	Concentration & Cycle Life at 60% Depth-of-Discharge	13
IV	Surfactants	14
V	Percentages of Additives & Number of Cycles at 60% Depth-of-Discharge	16
VI	Particle Size & Morphology of Zinc Oxides	18
VII	Particle Size & Morphology of Zinc Oxides	20
VIII	Particle Size & Morphology of Zinc Oxides	22
IX	Particle Size & Morphology of Zinc Oxide	24
X	Particle Size & Morphology of Zinc Oxide	25
XI	Particle Size & Morphology of ZnO	27
XII	Zinc Electrode Fabrication Techniques	28
XIII	Cells Constructed Using Electrodeposited Negative Plates with Results at 3 Different Depths-of- Discharge	29
XIV	Initial Capacity & Cycle Life of Cells with Negative Plates Containing Insoluble CaO	31
XV	Reduction Potentials	33
XVI	Stoichiometric Ratio of Formed Zinc	42
XVII	Separator Development	44
XVIII	Separators.	46
XIX	Initial Capacity & Cycle Life at Various Depths- of-Discharge	45
XX	Number of Cells that Failed by Short Circuiting . .	48

LIST OF TABLES (Continued)

<u>Table</u>	<u>Title</u>	<u>Page</u>
XXI	Separators	50
XXII	Cells Containing Four Layers of RAI 90 Mrad Crosslinked Acrylic & Methacrylic Acid Graft	51
XXIII	Electrolyte Concentration	53
XXIV	Electrolyte and Separator Test	55
XXV	Capacity Available at Cycle-Life Test Rates	56
XXVI	Allowable Capacity Loss Before Failure Related to % DOD	57

I. INTRODUCTION

The objectives of this program are to provide design criteria for long life (5000 cycles), light weight (25 ah/#) silver-zinc batteries for military aerospace applications. Effort will be concentrated on the zinc electrode and separator since these are recognized as the major causes of premature failure of the silver-zinc battery.

The specific items under study in this contract are:

- A. Mechanical Barriers to Zinc Agglomeration
- B. Surfactant Additions
- C. Fundamental Studies on Surfactants
- D. Particle Size and Morphology of Zinc Oxides
- E. Zinc Electrode Fabrication Techniques
- F. Influence of Membrane Separator Characteristics
- G. Sites for Zinc Oxide Overgrowths
- H. Development of Failure Analysis Techniques
- I. Sizes of Zincate Ion and Soluble Silver Species in KOH
- J. Membrane Pore Size Measurements in KOH
- K. Stoichiometric Ratio of Formed Zinc
- L. Alternate Method of Surface Area Measurement
- M. Separator Development
- N. Electrolytes

This report covers the entire three years work on the above items.

All test cells were cycled at 60% depth-of-discharge at the two hour cycle program of 35 minutes discharge and 85 minute charge.

II. FACTUAL DATA

A. Mechanical Barriers to Zinc Agglomeration

In an effort to minimize the agglomeration of particles in the negative active material, addition of the following materials to the negative plate mix were tested:

1. Shredded fibrous sausage casing
2. Shredded asbestos
3. Zinc metal
4. Lignosulfonic acid
5. Cotton fibers
6. Avicel (a finely powdered cellulosic material)

One hundred and ninety-one 25 a.h. cells were constructed utilizing various percentages of the above materials. Table I shows the construction details, initial capacity, cycle data and appearance of cell components of inspected cells after failure. Control cells on this test ran from 84 to 180 cycles, averaging 140 cycles. The major cause of failure was loss of zinc at the tops and edges of the zinc plate and agglomeration of the zinc. Figure 1 shows a typical zinc plate from a control cell after failure at 140 cycles. Control cells on this program are made with negative plates containing 20g Kadox-15 zinc oxide, 2% HgO, and 0.5% Emulphogene BC-610.

1. Effects of Asbestos

Cells #1 through #27 containing asbestos fibers in the negative plate in quantities 5, 10 and 15% did not increase the cycle life of the zinc plate, yielding 134 cycles. These failed by loss of zinc plate capacity due to washout around the edges and in spite of the fact that the photomicrographs of failed zinc plates (Figures 2, 3 and 4) show reduced agglomeration by comparison with Figure 1. Except for cells #1, 2, 10, 11 and 27, which were opened for examination after the first discharge, all cells had received an accumulated overcharge of 22-24 a.h. (~1.14% per cycle) at the end of life and failure examination disclosed the active material to be in the form of zinc.

Considerable trouble was experienced in getting these cells ready for test. They were given what appeared to be a normal formation charge, based on charge voltage behavior; however, on the first capacity discharge, all cells gave less than one minute capacity. At this point the above-mentioned cells (1, 2, 10, 11 and 27) were opened for examination and it was found that the zinc plates were substantially unformed. The remaining cells were soaked for an additional two weeks (standard procedure is to soak cells one week before giving the formation charge), then they were given an additional charge of 50 hours at one ampere. The initial capacity data shown in Table I was then obtained on a 15 ampere discharge rate.

Subsequently, 3-cell groups containing 0.5, 1.0 and 1.5% asbestos were tested. These failed very suddenly at 74 cycles, even though plates were well-formed and showed relatively little loss of electrolyte around the plate edges. These were, however, 19-plate cells, and it is thought that the additional 8 layers of fibrous sausage casing separation may have dried out the negative plates.

2. Effects of Shredded Fibrous Sausage Casing

Cells 31 through 59 contained 5, 10 and 15% shredded fibrous sausage casing in the negative plates and yielded an average of 146 cycles. The individual groups received a minimum of 16-24 a.h. of accumulated overcharge and on teardown the negative plates were substantially 100% metallic zinc. Figures 5, 6 and 7 show representative photomicrographs of failed negative plates. It appears that the fibers have done a good job of keeping the metal dispersed; however, there are many gaping voids and along with the loss of material around the edges, there may have been a good deal of loss in electrical contact from place to place in the active material contributing to loss in negative plate capacity.

This test was repeated with 9-cell groups containing 1, 3 and 5% shredded fibrous sausage casing in 19-plate cells. These all gave 134 cycles or less with some very early failures (v.g. 14 cycles). In spite of the fact that these cells had received an accumulated overcharge of 40 a.h., teardown examination

revealed the negative plates to be mostly zinc oxide. It is evident that these plates were not accepting charge for some reason, or the large quantities of overcharge oxygen was oxidizing the negative plates.

The 19-plate construction was used for some of the cell group: during this phase to determine whether going to more, but thinner, plate construction could improve cycle life. Obviously, it didn't.

3. Effects of Zinc Metal

Cells 60 through 86 contained elongated metallic zinc particles (#1208 zinc powder) to the extent of 5, 10 and 15% by weight. The groups containing 5% and 15% zinc powder averaged very well at 171 and 168 cycles, while the group containing 10% zinc failed at 108 cycles. These groups accumulated 13 to 25 a.h. of overcharge during life and showed substantially 100% zinc metal on teardown. Figures 8, 9 and 10 show photomicrographs of failed zinc plates. That for 5% zinc (Figure 8) is comparable in density to the control (Figure 1). The others exhibit a considerable loss in active material.

4. Effects of Lignosulfonic Acid

Cells 126 to 143 contained lignosulfonic acid in the negative mix in concentrations of 0.2, 1.2 and 2%. These concentrations yielded average cycle lives of 84, 168 and 132 cycles, respectively. It appears that too little of this additive is not enough to be effective, and that an optimum quantity around 1.2% for best life exists. Figures 11, 12 and 13 show photomicrographs of zinc plates from failed cells. Figure 14 shows a photomicrograph of a zinc plate from a failed control cell for comparison. Apparently, the lignosulfonic acid can have some dispersing effect although comparing the particle sizes in Figures 12 and 14 would lead to the conclusion that this is not the major effect.

5. Effects of Cotton Fibers

Cells 150 through 167 contained concentrations of 5, 3 and 1% of cotton fibers in the negative plate.

Control cells (168 through 173) which were run with this group averaged 122 cycles, while those with the fibers averaged 128, 144 and 138 for 5, 3 and 1% respectively. These cells accumulated 37 a.h. of overcharge throughout cell life for 1.7% per cycle and showed substantially 100% metallic zinc in the negative plates on teardown. Figures 15, 16 and 17 show photomicrographs of failed negative plates. This additive appears to aid materially in keeping the metallic zinc dispersed; moreover, it was the only one examined (of the mechanical barrier type) which appeared to have any effect at all in retaining the zinc active material at the tops and edges of the plates.

6. Effects of Avicel*

Avicel is a very finely powdered microcrystalline cellulose (particles in the $10\ \mu$ range). Cells 174 through 191 contained concentrations of 5, 10 and 15% of this material and averaged 130, 96 and 72 cycles respectively. These showed substantially 100% metallic zinc on teardown and they had accumulated 24 a.h. overcharge through cycle-life testing. However, their voltage behavior throughout life was very erratic and it is concluded that this material has no merit as an addition agent. Figure 18 shows a photomicrograph of a plate from a cell averaging 96 cycles.

As a matter of curiosity, three cells (147, 148 and 149) were built with 30% by weight shredded fibrous sausage casing and cycled at 40% depth-of-discharge. These gave 300 cycles, which may be compared with the 400-600 cycles obtained with 0.5% Emulphogene BC-610 obtained on the last contract. Figure 19 shows a photomicrograph of a failed zinc plate. It appears that 30% by weight of this low-density material is just too much bulk and it keeps the zinc dispersed so well that the particles fail to maintain contact.

*FMC Corporation, American Viscose Division, Newark, N.J.

TABLE I

Study: Mechanical Barriers to Zinc Agglomeration

Note: The separation system was one layer of acrylonitrile monomer and four layers of reinforced cellulosic material. The electrolyte amount was 90 c.c. of 50% KOH. Upon cell examination, the separator appearance was good.

Cell Nr.	Cycles	Initial Capacity	Pos. Plate Construction	Neg. Plate Construction	Additive Material	Negative Plate		
						Extent Form.	Treeling	Creeping Washout
1	0	0 a.h.	Eight plates .020"-.023"	Seven plates 20 g	5% Asbestos fibers	90% Oxide	Unformed	
2	0	0	4" x 2.5"	Kadox-15		"	"	
3-9	134	36 a.h.	15 g Ag + 1% Pd	+ 2% H ₂ O + .5% BC-610	10% "	100% Zn	None	Light 1- 2 layers 30%
10	0	29	"	"	"	90% Oxide	Unformed	
11	0	29	"	"	"	"	"	
12-18	134	29 a.h.	"	"	"	100% Zn	None	" 30-35%
19-26	134	29	"	"	15% "	"	"	"
27	0	29	"	"	"	90% Oxide	Unformed	
28*	156	33 a.h.	"	"	None	100% Zn	None	Light 3 layers 30-45%
29*	144	33	"	"	"	"	"	"
30*	180	33	"	"	"	"	"	"
31-38	146	32 a.h.	"	"	5% Shredded Cellulosic fibers	"	"	"
39	132	32	"	"	10% "	"	"	"
40-49	146	33 a.h.	"	"	15% "	"	"	"
50-59	146	31 a.h.	"	"	5% Zinc Metal fibers (1208)	"	"	"
60-68	171	31	"	"	10% "	"	Yes, at top	"
69-77	108	31	"	"	"	"	"	"
78-86	168	34 a.h.	"	"	15% "	"	Very light on edges	"

*Control Cells.

TABLE I (Continued)

Study:		Mechanical Barriers to Zinc Agglomeration (Continued)			Note: Same as previous Table			
Cell No.	Cycles	Initial Capacity	Pos. Plate Construction	Neg. Plate Construction	% Addition Material	Extent Form.	Negative Plate Freeing Creeping	Washout
87-93	122	25 a.h.	Ten plates .015"-.017"	Nine plates 15 g Kadox-15	1% Shredded Cellulosic fibers	mostly oxide	None	Light 2 layers
94	14	"	"	"	"	"	"	"
95	98	"	"	"	"	"	"	None
96	122	"	4" x 2.5"	2% HgO	"	"	"	Light 2 layers
97-99	134	"	10 g Ag	+ .5% BC-610	3%	"	"	20-25%
100	98	"	+ 1% Pd	"	"	"	"	"
101-104	134	"	"	"	"	"	"	"
105-113	134	"	"	"	5%	"	"	"
114-116	73	"	"	"	.5% Asbestos fibers 1%	90% Zn	"	10-15% around 2 layers
117-119	73	"	"	"	"	"	"	"
120-122	73	"	"	"	1.5%	"	"	"
123*	157	24 a.h.	"	"	None	"	"	25-35%
124*	157	"	"	"	"	"	"	"
125*	157	"	"	"	"	"	"	"
126-131	84	22a.h.	Eight plates .015"-.017"	Seven plates 20 g Kadox-15 + 2% HgO	.2% ISA	90% ZnO	"	10-20%
132	168	21a.h.	"	"	1.2%	95% Zn	Light	40-50%
133	156	"	4" x 2.5"	"	"	"	"	"
134-135	168	20a.h.	10 g Ag	"	"	"	"	"
136-137	168	21a.h.	+ 1% Pd	"	"	"	"	"
138-139	144	20a.h.	"	"	2%	90% ZnO	None	Light 2 layers
140	60	"	"	"	"	"	"	"
141	144	"	"	"	"	"	"	"
142	132	"	"	"	"	"	"	"
143	168	21a.h.	"	"	"	"	"	"

* Control Cells.

TABLE I (Continued)

Study:

Mechanical Barriers to Zinc Agglomeration

Note: Same as previous Table

Cell No.	Cycles	Initial Capacity	Pos. Plate Construction	Neg. Plate Construction	% Addition Material	Extent Form. Freeing	Negative Plate Creeping	Washout
144*	156	33 a.h.	Eight plates .015"-.017" 4" x 2.5"	Seven plates 20 g Kadox-15 + 2% HgO + .5% BC-610	None	90% Zn	Light 2 layers	20-25%
145*	144	33	"	"	"	"	"	"
146*	130	33	"	"	"	"	"	"
147	300**	21	10 g Ag + 1% Pd	"	30% Cellulosic fibers	"	"	None
148	300**	21	"	"	"	"	"	"
149	300**	21	"	"	"	"	"	"
150	144	23	"	"	5% cotton fibers	95% Zn	Light 3 layers	20-25%
151	108	"	"	"	"	"	"	"
152	144	"	"	"	"	"	"	"
153	108	"	"	"	"	"	"	"
154	144	"	"	"	"	"	"	"
155	124	"	"	"	"	"	"	"
156-161	144	24 a.h.	"	"	3% cotton fibers	"	"	"
162	108	23 a.h.	"	"	1% "	"	"	"
163-167	144	"	"	"	None	"	"	"
168*	132	24 a.h.	"	"	"	"	"	"
169*	144	"	"	"	"	"	"	"
170*	132	"	"	"	"	"	"	"
171*	108	"	"	"	"	"	"	"
172*	132	"	"	"	"	"	"	"
173*	84	"	"	"	"	"	"	"
174-177	132	22 a.h.	"	"	5% Avicel powdered cellulose	"	"	"
178	120	"	"	"	"	"	"	"
179	132	"	"	"	10% "	"	"	Very slight
180-182	72	"	"	"	"	"	"	"
183	132	"	"	"	"	"	"	"
184	96	"	"	"	"	"	"	"
185	120	"	"	"	"	"	"	"
186-191	72	21 a.h.	"	"	15% "	"	"	"

* Control Cells.

** Cells cycled at 40% depth-of-discharge.

B. Surfactant Additions

The following Emulphogene-type surfactants were tested in order to complete the Emulphogene series, which is characterized by longer and longer polyethylene-oxide chains as the series goes up in number from BC-420 to BC-840; BC-420, BC-720 and BC-840. The increasing chain length of the polyethylene-oxide structure renders the material more and more soluble in water and water solutions. BC-610 in 0.5% concentration was used in the control cells. FC-95, an anionic fluorochemical surfactant*, was also tested.

In addition, a group of alcohols were tested to determine whether the alcoholic functional group, in combination with various chain lengths, might function in the same way as the Emulphogene. These were: tridecanol, propanol, ethanol, tertiary amyl alcohol and butanol.

Table II shows the construction features, initial capacities, cycle life data, and appearance of the cell components after failure.

Cells 1 through 91 were constructed with 21 plates and three layers of fibrous sausage casing separation. This was an attempt to ascertain whether thin plate construction with reduced numbers of layers of cellulosic separation might provide longer cycle life for the same internal cell volume. The results speak pretty clearly: the major cause of failure was short-circuiting in combination with a very high degree of washout of the zinc plate active material. Initial capacities and discharge voltage characteristics of these cells were very good, at the expense of cycle life, however. The most noteworthy feature of this group of cells is (although those made with 0.5% BC-610 washed and shorted) like most of the others that it achieved 166 cycles, where other groups were shorting or otherwise failing around 100-120 cycles, or less.

*Minnesota Mining and Manufacturing Co., St. Paul, Minnesota

Because of the short-circuiting failure mode, the thin-plate construction did not allow a good evaluation of the surfactant series in terms of their capability to extend zinc plate life and the test was repeated with the standard 15-plate construction and four layers of fibrous sausage casing using 3-cell groups.

Cells 91 through 120 show the pertinent data. The BC-420 is probably as good as but no better than the standard 0.5% BC-610. The BC-720 and BC-840 show somewhat reduced average cycle life in comparison. Figures 20 through 26 show photomicrographs of the negative material from failing cells for the surfactants. A good deal of loss of active material, or separation of active material from the grid, seems to be involved in this whole series.

Cells 121 through 156 and 157 through 192 contain various concentrations of BC-610 and were life-tested at 40°F. and 100°F. respectively at Dayrad Laboratories, Dayton, Ohio. Cycle life at either temperature was less than that obtained at room temperature. The spread of data at any one temperature is low. If any conclusion can be drawn, it is that for best cycle life at low temperatures a low concentration of surfactant is favored; at the high temperature, a high concentration is favored.

Figures 27, 28 and 29 show photomicrographs of failed negative plates at 40°F for 0.15, 0.6 and 1.0% BC-610, respectively. They look much like the material when it fails at room temperature around 160 cycles. Figures 30, 31 and 32 show photomicrographs of failed negative plates at 100°F. for the same surfactant concentrations. The low temperature cells failed in spite of the fact that they were given 1-10% overcharge and the negatives appeared to consist mostly of metallic zinc on failure examination. The high temperature cells lost negative plate capacity in spite of 1-2% overcharge per cycle.

Cells 289 through 306 contained FC-95 in concentrations of 0.1, 0.6 and 1%. There was a slight improvement as concentration increased. In fact, the 1% solution gave as good cycle life as 0.5% Emulphogene. The photomicrographs are shown in

TABLE II

Surfactants

Note: The separator system for the first 90 cells was one layer acrylonitrile monomer and three layers of reinforced cellulosic material; remaining cells were same but with four layers of reinforced cellulosic material. The electrolyte amount was 90 c.c. of 50% KOH. Accumulated overcharge is 20 ampere-hours.

Cell Nr.	Cycles	Initial Capacity	Pos. Plate Construction	Neg. Plate Construction	Surfactant	Negative Plate			
						Extent Formed	Treering	Creeping	Washout
1-9	108	31 a.h.	Eleven plates	Ten plates	.15% BC-420	50% Zn	Light	Light	4.5-50%
10-18	108	30 a.h.	.015"-0.017"	15g Kadox-15	.6%	"	"	2 layers	"
19-27	108	28 a.h.	10g Ag + 1% Pd	+ 2% HgO	1.0%	"	"	"	"
28-30	114	39 a.h.	"	"	.15% BC-720	90% Zn	Heavy	Heavy	40-50%
31-32	114	"	"	"	"	Shorted	"	2 layers	"
33-35	114	"	"	"	"	90% Zn	"	"	"
36	84	"	"	"	"	"	"	"	"
37-39	114	37 a.h.	"	"	.6%	Shorted	"	"	"
40-45	114	"	"	"	"	90% Zn	"	"	"
46-50	114	30 a.h.	"	"	1%	Shorted	"	"	"
51-54	114	"	"	"	"	90% Zn	"	"	"
55-57	36	32 a.h.	"	"	.15% BC-840	Shorts	"	"	"
58	116	"	"	"	"	"	"	"	"
59-62	36	"	"	"	"	"	"	"	"
63	116	"	"	"	"	90% Zn	"	"	"
64-66	36	34 a.h.	"	"	.6%	Shorts	"	"	"
67	119	"	"	"	"	"	"	"	"
68	34	"	"	"	"	"	"	"	"
69	100	"	"	"	"	"	"	"	"
70-71	36	"	"	"	"	"	"	"	"
73-80	36	39 a.h.	"	"	1%	Shorted	"	"	"
81	155	"	"	"	"	90% Zn	"	"	"
82*-89*	166	27 a.h.	"	"	.5% BC-610	Shorted	"	"	"
90*	166	"	"	"	"	90% Zn	"	"	"
91	168	25 a.h.	Eight plates	Seven plates	.15% BC-420	Mostly Zn	Medium	Heavy	"
92-93	132	"	.015"-0.017"	20g Kadox-15	"	"	sides	4 layers	"
94-96	168	24 a.h.	10g Ag + 1% Pd	+ 2% HgO	.6%	"	ard	"	"
97-99	168	"	"	"	1%	"	bottom	"	"
100-101	120	25 a.h.	"	"	.15% BC-720	"	None	Light	35-40%
*Control Cells.									3 layers

TABLE II (Continued)

Study: Surfactants		Initial		Pos. Plate		Neg. Plate		Surfactant		Extent Formed		Negative Plate		Creeping		Washout	
Cell	Cycles	Capacity	Construction	Eight plates	Seven plates	Construction	plates			Mostly Zn	Zn	Creeping	Plate				
Nr.				plates	plates												
102	108	25 a.h.		.015"-.017"	20g Kadox-			.15% BC-720		"	None	Light 3				35-40%	
103	108	"		10 g Ag +	15 + 2%			.6%		"	"	layers				"	
104	120	"		1% Pd	HgO			"		"	"	"				"	
105	108	"		"	"			1% BC-720		"	"	"				"	
106-108	108	22 a.h.		"	"			.15% BC-840		"	"	"				"	
109	144	25 a.h.		"	"			"		"	"	"				"	
110-111	168	"		"	"			.6%		"	"	"				"	
112	132	24 a.h.		"	"			"		"	"	"				"	
113	144	"		"	"			"		"	"	"				"	
114	132	"		"	"			"		"	"	"				"	
5-116	144	22 a.h.		"	"			1% BC-840		"	"	"				"	
117	132	"		"	"			"		"	"	"				"	
118*-120*168	76**	"		"	"			.5% BC-610		"	"	"				"	
121-132	76**	25 a.h.		"	"			.15%		90% ZnO	None	"				30-40%	
133-144	52**	"		"	"			.6%		"	"	"				15-25%	
145-156	58**	"		"	"			1%		"	"	"				"	
157-168	110***	24 a.h.		"	"			.15%		"	"	"				20-30%	
169-180	121***	25 a.h.		"	"			.5%		"	"	Light 2				"	
181-192	124***	26 a.h.		"	"			1%		"	"	layers				"	
193-198	120	27 a.h.		"	"			.1% Tridecanol		"	"	"				35-40%	
199-204	108	"		"	"			.6%		"	"	"				"	
205-210	108	"		"	"			1%		"	"	"				"	
211-216	72	26 a.h.		"	"			.1% Propanol		"	"	"				20-30%	
217-222	72	"		"	"			.6%		"	"	"				"	
223-228	40	"		"	"			1%		"	"	"				"	
229-234	157	27 a.h.		"	"			.1% Ethanol		90% Zn	Light	"				"	
235-240	135	25 a.h.		"	"			.6%		"	"	"				"	
241-246	111	23 a.h.		"	"			1%		"	"	"				"	
247-252	124	26 a.h.		"	"			.1% Tert. Amyl		90% ZnO	None	"				35-45%	
253-258	130	25 a.h.		"	"			.6%		"	"	"				"	
259-264	108	24 a.h.		"	"			1%		"	"	"				"	
265-270	92	23 a.h.		"	"			.1% Butyl Alco.		"	"	"				25-30%	
271-276	100	"		"	"			.6%		"	"	"				"	
277-282	58	"		"	"			1%		"	"	"				"	
283*-288*104	104	25 a.h.		"	"			.1% BC-610		"	"	"				"	
289-294	150	23 a.h.		"	"			.1% BC-95		"	"	"				20-30%	
295-300	152	"		"	"			.6%		"	"	"				"	
301-306	168	"		"	"			1%		"	"	"				"	

***At 100°F.

**At 40°F.

*Control Cells.

Figures 33, 34 and 35. They look much like the photomicrographs for Emulphogene. The FC-95 test had a total of 40 a.h. overcharge, which is ample.

Cells 193 through 282 contained various percentages of the alcohols. The control cells for this group (cells 283-288) gave only 104 cycles. Cycle life for these groups ran from 60 to 159 (except for the ethanol) and the zinc plates showed mostly oxide on teardown examination.

An additional one-hundred and eight 25 a.h. cells have been constructed in two groups of 54 cells. One group having 2% cotton fibers in the negative material along with various concentrations of carbowaxes of three different molecular weight ranges. The second group of 54 cells is the same, but does not contain 2% cotton fibers in the negative material. The following table shows the concentration and cycle life obtained at 60% depth-of-discharge.

TABLE III
Concentration & Cycle Life at 60% Depth-of-Discharge

<u>Cells</u>	<u>Molec- ular Weight</u>	<u>Carbo- wax Concen- tration</u>	<u>Initial Capacity</u>	<u>Cycles Without 2% Cotton</u>	<u>Cycles With 2% Cotton</u>
6	6000	.3%	24 a.h.	156	148
6	6000	.6%	23	132	148
6	6000	1.0%	23	132	148
6	1000	.3%	22 a.h.	204	132
6	1000	.6%	22	204	156
6	1000	1.0%	22	204	156
6	200	.3%	22 a.h.	120	108
6	200	.6%	23	108	108
6	200	1.0%	22	98	108
6	Controls		21.0	84	

The cause of failure in all cells was loss of negative plate capacity. The use of cotton fibers in the negative electrode does not appear to improve cell cycle ability. The carbowax mecular weight range of 1000 appears to have a strong effect on increasing cycle life. Table IV shows

TABLE IV
SURFACTANTS

NOTE: All cells contained 8 positive plates 4" x 2-1/2" x .015" with 12g silver; 7 negative plates 4" x 2-1/2" x .050" with 20g ZnO and 2% HgO. The separator system was one layer of acrylonitrile monomer & four layers of reinforced cellulosic material. Electrolyte was 90cc, 50% KOH.

Cell No.	Surfactant	Condition of Positive Plate	Condition of Separation	Extent Formed	Treeing	Material Creeping	Material Washout	Cause of Failure
307-312	.7% LSA	Good-well formed	Good-no pin holes or tears	90% ZnO	None	None	10-20%	Shedding of material and subsequent loss of plate capacity
313-318	1.1% LSA	"	"	"	"	Light-2 layers	20-30%	"
319-324	1.1% LSA + 5% ZnSO ₄	"	1st layer deteriorated-rest O.K.	75% ZnO	Light	Medium-around 4 layers	40-50%	"
325-330	1.1% LSA + 1% FC95	"	"	75% ZnO	Medium	"	20-30%	"
331-336*	None	"	"	"	"	"	50-60%	"
337-342	.3% carbowax 6000	"	Good	75%-90% ZnO	None	Light-2 layers	40-50%	"
343-348	.6% carbowax 6000	"	"	"	"	"	"	"
349-354	1% carbowax 6000	"	"	"	"	"	"	"
355-360	.3% carbowax 6000	"	"	"	"	"	"	"
361-366	+ 2% cotton fibers	"	"	"	"	"	"	"
367-372	.6% carbowax 6000 + 2% cotton fibers	"	"	"	"	"	"	"
373-378	1% carbowax 6000 + 2% cotton fibers	"	1st layer deteriorated-rest O.K.	70% ZnO	Medium	Medium-4 layers	50-60%	"
379-384	.3% carbowax 1000	"	"	"	"	"	"	"
385-390	.6% carbowax 1000	"	"	"	"	"	"	"
391-396	1% carbowax 1000	"	Good	"	None to light	"	50%	"
397-402	.3% carbowax 1000 + 2% cotton fibers	"	"	"	"	"	"	"
403-408	.6% carbowax 1000 + 2% cotton fibers	"	"	"	"	"	"	"
409-414	1% carbowax 1000 + 2% cotton fibers	"	"	"	"	"	"	"
415-420	.3% carbowax 200 + 2% cotton fibers	"	"	90% ZnO	None	2 layers	40-50%	"
	.6% carbowax 200 + 2% cotton fibers	"	"	"	"	"	"	"

TABLE IV (Continued)

STUDY: SURFACTANTS

NOTE: All cells contained 8 positive plates 4" x 2-1/2" x .015" with 12g silver; 7 negative plates 4" x 2-1/2" x .050" with 20g ZnO and 2% HgO. The separator system was one layer of acrylonitrile monomer & four layers of reinforced cellulosic material. Electrolyte was 90cc, 50% KOH.

Cell No.	Surfactant	Condition of		Condition of Negative Plate			Cause of Failure
		Positive Plate	Separation	Extent Formed	Treeing	Material Creeping	Material Washout
421-426	1% carbowax 200 + 2% cotton fibers	Good-well formed	Good	90% ZnO	None	2 layers	40-50%
427-432	.# carbowax 200	"	"	"	Heavy	Medium-4 layers	30-40%
433-438	.6% carbowax 200	"	"	"	"	"	"
439-444	1% carbowax 200	"	"	"	"	"	"

(*) Control Cells

the appearance of cell components after cycle testing. Figures 36, 37 and 38 show the photomicrographs of negative plates containing 1% carbowax in the three molecular weight ranges.

Thirty 25 a.h. cells were constructed containing various percentages of LSA (lignosulfonic acid) $ZnSO_4$ and FC95 incorporated in the negative plate. Table V shows the cells with the percentages of additives and the number of cycles obtained at 60% depth-of-discharge.

TABLE V

Percentages of Additives & Number of Cycles at 60% Depth-of-Discharge

<u>No. of Cells</u>	<u>Percent Additive</u>	<u>Initial Capacity</u>	<u>Cycles</u>
6	.7% LSA	23 a.h.	108
6	1.1% LSA	24 a.h.	108
6	5% $ZnSO_4$ + 1.1% LSA	24 a.h.	96
6	5% $ZnSO_4$ + 1% FC95	23 a.h.	96
6	Controls	24 a.h.	148

The cause of failure was loss of negative plate capacity. Table IV shows the appearance of cell components after cycle testing. Figure 39 shows a photomicrograph of a negative plate containing 1.1% LSA after 108 cycles. Figure 40 shows a negative plate containing 5% $ZnSO_4$ and 1.1% LSA after 96 cycles.

C. Fundamental Studies on Surfactants

The final report on "Adsorption of Organic Materials on Zinc Electrodes" from the University of Texas is in Appendix I.

D. Particle Size and Morphology of Zinc Oxides

In an effort to determine whether the starting zinc oxide has any effect on cycle life, a variety of oxides, embodying variations in preparation

process particle size, crystal morphology, surface area, doping agents to improve oxide conductivity, and impurities have been prepared and tested. Thirty-five variations plus three repeat samples have been tested with results shown in Table VI. These cells were cycled at 60% DOD.

The oxides containing various percentages of Pb due show an increase in cycle life, as well as those oxides containing AL. The samples containing iron were tested to determine allowable limits as an impurity that is not detrimental to cycle life. These limits ranged from a high of .07% to a low of .0003%. The cause of failure for these cells not containing high concentrations of iron was loss of negative plate capacity. The cells containing lead and flaked zinc dust gave the largest cycle life. Cells containing an excessive (over .010%) iron did not cycle; in fact, the zinc oxide did not reduce to zinc on initial formation due to the lowered Zn/ZnO potential.

Figures 41 through 55 show the photomicrographs of negative plates representative of the ZnO samples after completion of the indicated cycles.

Based on the performance of these samples, the following three batches of 25# each were obtained from the New Jersey Zinc Company.

1. .25% Pb doped ZnO
2. High conductivity ZnO with .3% AL
3. Flaked zinc dust

The iron content as impurity was held to .004% where feasible.

Table VII shows the life obtained at 60% DOD and the appearance of the cell components after testing. The main cause of failure was loss of negative plate capacity. An additional 12 cells were constructed with Zn Flake as the negative active material. The initial capacity of these cells was 18 a.h. and they only delivered 60 cycles at 60% DOD. However, a continuation of cycling at 25% DOD yielded 440 cycles. The cause of failure was excessive short circuiting.

TABLE VI

STUDY: PARTICLE SIZE AND MORPHOLOGY OF ZINC OXIDES

NOTE: Separator system same as listed in Table I. Cells contain eight positive plates .015" and seven negative plates of 20g test ZnO + 2% HgO + .5% BC610.

Cell No.	Cycles	Initial Capacity	Zinc Oxide	Additive	Condition of Separator	Condition of Negative Plate			Cause of Failure
						Am't. Formed	Creeping	Washout	
1-6	108	23 ah	243-7-1	French Process	Good	90% ZnO	2 Layers	30%	Loss of negative capacity
7-12	96	25 ah	243-11-1	As	"	"	"	"	"
13-18	106	24 ah	243-15-1	French Process	"	"	"	"	"
19-24	140	24 ah	243-19-1	"	"	"	"	"	"
25-30	96	26 ah	243-23-1	"	"	"	"	"	"
31-36	80	25 ah	243-27-1	"	"	"	"	"	"
37-42	130	25 ah	243-31-1	"	"	"	"	"	"
43-48	12	23 ah	243-35-1	"	"	"	"	"	"
49-54	150	24 ah	243-41-1	.3% Al	"	"	"	"	"
55-60	135	25 ah	243-45-1	.48% In	"	"	"	"	"
61-66	148	25 ah	243-63-1	Basic ZnCO ₃	"	"	"	"	"
67-72	132	22 ah	243-71-1	Wet Process	"	"	"	"	"
73-78	126	21 ah	243-75-1	Wet Process	"	"	"	"	"
79-84	122	24 ah	243-79-1	Wet Process	"	"	"	"	"
85-90*	130	23 ah	KADOX-15	None	90% Zn	"	"	"	"
91-96	135	24 ah	243-67-2	Basic ZnCO ₃	"	"	"	50%	"
97-102	150	27 ah	243-83-1	None	"	"	"	"	"
103-108	132	26 ah	243-87-1	Sn	"	"	"	"	"
109-114	120	25 ah	243-91-1	Cd	"	"	"	"	"
115-120	132	25	243-95-1	Cu	"	"	"	"	"
121-126	156	26	243-49-4	Zn	"	"	"	"	"

(*) Control Cells

TABLE VI (Continued)

STUDY: PARTICLE SIZE AND MORPHOLOGY OF ZINC OXIDES

NOTE: Same as Table II

Cell No.	ZnO Sample	Additive	Initial Capacity	Cycles	Condition of Negative Plate			Cause of Failure
					Extent Formed	Treeing	Material Creeping	
1-6	243-127-2	.0008% Pb	23.5 ah	202	50%	None	Medium-around 3 layers	35-45% Loss of negative capacity
7-12	243-107-4	.0003% Fe	24 ah	214	"	"	"	"
13-18	243-107-2	.028% Pb	21 ah	221	"	"	30-40%	"
19-24	243-107-3	.0003% Fe	22.5 ah	214	"	"	"	"
25-30	243-131-1	2.42% Pb	23.5	178	"	"	"	"
21-36	243-131-2A	.0004% Fe	20	168	"	"	"	"
37-42	243-131-2B	.0086% Fe	24	120	"	"	Light-around 2 layers	25-30% 30-40%
43-48	243-135-1	.0092% Fe	23	192	"	"	"	"
49-54	243-139-1	.26% Pb	23	156	"	"	"	"
55-60	243-139-2	.010% Fe	24	167	"	Light	Medium-around 3 layers	35-45%
61-66	243-107-1	.07% Al	23	221	"	None	None	"
67-72	243-99-1	.92% Al	0	0	0%	None	None	Fe lowered An/AnO Potential Loss of negative capacity.
73-78	243-41-1	.0008% Fe	24	170	50%	"	Light-2 layers	40-50% Fe lowered An/AnO Potential Loss of negative capacity.
79-84*	KADOX-15	.25% Pb	24	170	"	"	Medium-3 layers	40-50% Fe lowered Zn/ZnO Potential Loss of negative capacity.
85-90	243-115-1	.07% Fe	0	0	"	"	None	50-60%
91-96	243-119-1	Zinc Dust Flaked	23	168	25%	"	3-layers	None 40-50%
97-102	243-123-1	Zinc Dust	23	204	50%	"	Heavy-3 layers	"
103-108*	KADOX-15	None	24	130	"	"	Light-3 layers	"
109-114	243-111-1	.027% As	20	80	"	"	None	20-30%
115-120	243-103-1	.089% Mn	23	130	"	"	"	"

(*) Control Cells

TABLE VII

STUDY: PARTICLE SIZE AND MORPHOLOGY OF ZINC OXIDES

Cell No.	Initial Capacity	Cycles	ZnO Doped	Condition of Separator	Condition of Neg. Plate	Condition of Neg. Plate	Condition of Neg. Plate	Cause of Failure
					Am't. Formed	Creeping	Washout	
1	23 ah	212	.25% Pb	1st layer deteriorated	40% ZnO	Heavy 4 layers	60%	Loss of negative plate capacity
2	"	"	"	"	"	"	"	"
3	"	"	"	"	"	"	"	"
4	"	"	"	"	"	"	"	"
5	"	"	"	"	"	"	"	"
6	"	"	"	"	"	"	"	"
7	"	"	"	"	"	"	"	"
8	"	"	"	"	"	"	"	"
9	"	"	"	"	"	"	"	"
10	"	"	"	"	"	"	"	"
11	24 ah	180	.3% Al	Good	"	"	"	"
12	"	"	"	"	"	"	"	"
13	"	"	"	"	"	"	"	"
14	"	"	"	"	"	"	"	"
15	"	"	"	"	"	"	"	"
16	"	"	"	"	"	"	"	"
17	"	"	"	"	"	"	"	"
18	"	"	"	"	"	"	"	"
19	"	"	"	"	"	"	"	"
20	"	"	"	"	"	"	"	"
21-32*	20 ah	110	Kadox-15	"	50% ZnO	"	40%	"

(*) Control cells

A shipment from the New Jersey Zinc Company of 75 lbs. each of .25% Pb and .3% Al doped zinc oxide was made into cells containing both cellulosic and polyethylene cross linked, and grafted membranes.

Table VIII shows the life obtained, and the appearance of the cell components after testing. These cells were cycled at 60% DOD.

It can be seen that the cells containing the polyethylene membranes did not have any zinc creeping about or through the membranes. They remained in good condition throughout cycle life. The use of .24% Pb in the zinc oxide did show an increase in cycle life. The chief cause of failure was loss of negative plate capacity.

Additional cells were constructed containing .3% Al and .2% Pb doped zinc oxide were tested at 60% DOD in 30%, 35%, 40%, 45% and 50% KOH electrolyte. These cells contained four layers of polyethylene membrane and 17 plates. Table IX shows the initial capacities and cycles obtained. Again, the main cause of cell failure is the loss of negative plate capacities. There does not seem to be much difference in the Al or Pb doped ZnO; the lower KOH concentrations appear to shorten cycle life.

At the suggestion of Dr. J. J. Lander, additional Al and Pb doped ZnO were obtained in concentrations of 1%, 3% and 5%. In actuality, these concentrations turned out to be .89%, 2.7% and 4.5% of Al, and .99%, 2.5% and 4.5% Pb.

Cells were constructed with these oxides using 4 layers of polyethylene separators, with control cells using four layers of cellulosic separators. These cells were cycled at 60% DOD. Table X shows the cycles obtained by the different doped oxides and separators. The addition of large quantities of Pb in ZnO has a detrimental effect on the cellulosic separation to the extent that the cause of failure is short circuiting because of separator disintegration. The use of Al in ZnO does not have this effect on the separators. The cause of failure in these cells was loss of negative plate capacity.

TABLE VIII

STUDY: PARTICLE SIZE AND MORPHOLOGY OF ZINC OXIDES

NOTE: test cells contain polyethylene separators cross-linked 90 Mrad and radiation grafted with methacrylic acid. Each cell contains 7 positives .015" and 8 negatives of 20g test oxide. The control cell's contain cellulosic membranes with 7 positives .015" and 8 negatives of 20g test oxide.

Cell No.	Initial Capacity	Cycles	ZnO Doped	Number of Layers and Condition of Separators	Condition of Neg. Plates			Cause of Failure
					Am't. Formed	Creeping	Washout	
1	33 ah	160	.3% Al	3 layers good	40%	None	60%	Shorts
2	"	"	"	"	"	"	"	"
3	"	"	"	"	"	"	"	"
4	"	"	"	"	"	"	"	"
5	31 ah	180	.3% Al	4 layers good	40%	None	60%	Loss of negative capacity
6	"	"	"	"	"	"	"	"
7	"	"	"	"	"	"	"	"
8	"	"	"	"	"	"	"	"
9	30 ah	175	.3% Al	5 layers good	40%	None	60%	Loss of negative capacity
10	"	"	"	"	"	"	"	"
11	"	"	"	"	"	"	"	"
12	"	"	"	"	"	"	"	"
13*	20 ah	178	.3% Al	4 layers cellulosic 1st layer deteriorated	40%	Around 3 layers	60%	Loss of negative capacity
14*	"	"	"	"	"	"	"	"
15*	"	"	"	"	"	"	"	"
16*	"	"	"	"	"	"	"	"
1	33 ah	212	.25% Pb	4 layers good	30%	None	65%	Loss of negative capacity
2	"	"	"	"	"	"	"	"
3	"	"	"	"	"	"	"	"
4	"	"	"	"	"	"	"	"
5	"	"	"	"	"	"	"	"
6	"	"	"	"	"	"	"	"
7	"	"	"	"	"	"	"	"
8	"	"	"	"	"	"	"	"
9	"	"	"	"	"	"	"	"
10	"	"	"	"	"	"	"	"

TABLE VIII (Continued)

Cell No.	Initial Capacity	Cycles	ZnO Doped	Number of Layers and Condition of Separators	Condition of Neg. Plates			Cause of Failure
					Am't. Formed	Creeping	Washout	
11*	27 ah	180	.25% Pb	4 layers cellulosic.	40%	Around 3 layers	60%	Loss of negative capacity
12*	"	"	"	1st layer deteriorated	"	"	"	"
13*	"	"	"	"	"	"	"	"
14*	"	"	"	"	"	"	"	"
15*	"	"	"	"	"	"	"	"
16*	"	"	"	"	"	"	"	"
17*	"	"	"	"	"	"	"	"
18*	"	"	"	"	"	"	"	"
19*	"	"	"	"	"	"	"	"
20*	"	"	"	"	"	"	"	"

(*) control cells

TABLE IX

STUDY: PARTICLE SIZE AND MORPHOLOGY OF ZINC OXIDE

NOTE: Same as Table VIII

Cell No.	Initial Capacity	Cycles	Electrolyte Concentration	ZnO Doped	Cause of Failure
1-6	26 ah	60	30% KOH	.3% Al	Loss of neg. plate capacity
7-8*	20	48	"	"	"
9-14	27	72	35% KOH	"	"
15-16*	31	108	"	"	"
17-22	29	108	40% KOH	"	"
23-24*	30	192	"	"	"
25-30	28	120	45% KOH	"	"
31-32*	27	192	"	"	"
33-38	28	216	50% KOH	"	"
39-40*	27	156	"	"	"
41-46	24	60	30% KOH	.25% Pb	"
47-48*	21	36	"	"	"
49-54	24	60	35% KOH	"	"
55-56*	21	60	"	"	"
57-62	23	96	40% KOH	"	"
63-64*	20	96	"	"	"
65-70	19	96	45% KOH	"	"
71-72*	21	132	"	"	"
73-78	19	108	50% KOH	"	"
79-80*	25	192	"	"	"

(*) Control Cells

TABLE X

STUDY: PARTICLE SIZE AND MORPHOLOGY OF ZINC OXIDE

NOTE: Same as Table VIII

A.	.25% Pb Doped ZnO		.99% Pb Doped ZnO		2.5% Pb Doped ZnO		4.5% Pb Doped ZnO	
	Test	Control	Test	Control	Test	Control	Test	Control
	Cells	Cells	Cells	Cells	Cells	Cells	Cells	Cells
	Cycles		Cycles		Cycles		Cycles	
	150	192	264	132	192	96	156	72
B.	.3% Al Doped ZnO		.89% Al Doped ZnO		2.7% Al Doped ZnO		4.5% Al Doped ZnO	
	Test	Control	Test	Control	Test	Control	Test	Control
	Cells	Cells	Cells	Cells	Cells	Cells	Cells	Cells
	Cycles		Cycles		Cycles		Cycles	
	150	178	240	240	186	187	240	192
	170	178	108	240	186	187	216	264
	180	178	204	204	186	186	216	276
	180	178	204	108	185	186	216	276
	150	178	204	108	182	185	216	276

Table XI shows the appearance of the cell components after inspection. The final report submitted by the New Jersey Zinc Company is included in Appendix II.

E. Zinc Electrode Fabrication Techniques

In an effort to determine whether negative plate cycle life could be increased by achieving an interlacing network of basic zinc oxides and, subsequently, of zinc crystals by means of wet pasting with ZnCO_3 and ZnSO_4 additions, the following wet pastes were tested: zinc oxide plus various concentrations of ZnCO_3 and zinc oxide plus various concentrations of ZnSO_4 . In addition, admixtures of the acicular zinc oxides XX601 and XX4 to the Kadox-15 were tested.

After drying plates made with wet pastes of the ZnSO_4 additions showed the presence of basic zinc sulfates in the X-ray pattern. Wet-pasted plates made with ZnCO_3 additions showed simple mixtures of ZnO and ZnCO_3 in their X-ray patterns.

Table XII shows the initial capacity, cycle data, construction and appearance of cell components on failure analysis.

Cells 1 through 18 were fabricated with thin plates and 21-plate construction with the usual four layers of fibrous sausage casing separation. Trouble on cycling was immediately experienced, some cells failing before 20 cycles. These could be brought back by extended overcharges but they wouldn't last long anyway even after the over-charge. This is believed to be an electrolyte starvation situation at the zinc electrode due to the high ratio of separator weight. Control cells (19-27) behaved the same way.

It is interesting and must be significant of something that the 21-plate construction which utilized ZnCO_3 and ZnSO_4 additions to the negative plates did not experience this difficulty (cells 38-55). These gave respectable cycle lives ranging from 132 to 180 cycles with the cells having ZnSO_4 -containing negatives showing up a little better. These cells

TABLE XI

STUDY: PARTICLE SIZE AND MORPHOLOGY OF ZnO

NOTE: Same as Table VIII

Cell Nr.	Initial Capacity	ZnO Addition	Separator Condition	Negative Plate Condition			Cause of Failure
				Am't. Formed	Creeping	Wash-Out	
1-5	28 ah	.25% Pb	Good	40% Zn	None	50%	Loss of neg. plate capacity
6-10*	26 ah	.25% Pb	1st layer deteriorated	40% Zn	3 Layers	50%	"
11-15	27 ah	.99% Pb	Good	20% Zn	None	70%	"
16-20*	26 ah	.99% Pb	1st & 2nd layer deteriorated	40% Zn	3 Layers	50%	Shorts
21-25	28 ah	2.5% Pb	Good	40% Zn	None	50%	Loss of neg. capacity
26-30*	23 ah	2.5% Pb	1st, 2nd layer deteriorated	50% Zn	3 Layers	40%	Shorts
31-35	28 ah	4.5% Pb	Good	50% Zn	None	50%	Loss of neg. capacity
36-40*	23 ah	4.5% Pb	1st, 2nd, 3rd layers deteriorated	40% Zn	3 Layers	40%	Shorts
41-45	29 ah	.3% Al	Good	40% Zn	None	50%	Loss of neg. capacity
46-50*	27 ah	.3% Al	Good	40% Zn	None	50%	"
51-55	28 ah	.89% Al	Good	40% Zn	None	50%	"
56-60*	25 ah	.89% Al	Good	40% Zn	None	50%	"
61-65	29 ah	2.7% Al	Good	40% Zn	None	50%	"
66-70*	24 ah	2.7% Al	Good	40% Zn	None	50%	"
71-75	31 ah	4.5% Al	Good	40% Zn	None	50%	"
76-80*	26 ah	4.5% Al	Good	40% Zn	None	50%	"

(*) Control Cells

TABLE XII

Study: Zinc Electrode Fabrication Techniques

Note: Same as Table I

Cell Nr.	Cycles	Initial Capacity	Pos. Plate Construction	Neg. Plate Construction	Variable Tested	Accumulated Overcharge	Extent Formed	Negative Plate Treering Creeping	Washout
1	41	24 a.h.	Eleven .015"-.017"	Ten 15g Kadox + 2% HgO	5% XX601 Zinc Oxide	-20 a.h.	90% Zinc	Very Around light 4 layers	30-40%
2	77	"	"	"	"	"	"	"	"
3	26	"	10g Ag + 1% Pd	"	"	"	"	"	"
4	65	"	"	"	"	"	"	"	"
5	26	"	"	BC-610	"	"	"	"	"
6-8	77	"	"	"	"	"	"	"	"
9	67	"	"	"	"	"	"	"	"
10-12	77	25 a.h.	"	"	10% XX601 Zinc Oxide	"	"	"	"
13	65	"	"	"	"	"	"	"	"
14-16	77	"	"	"	"	"	"	"	"
17	65	"	"	"	"	"	"	"	"
18	77	"	"	"	"	"	"	"	"
19*-27*	77	24 a.h.	"	"	None	"	"	"	"
28-30	157	19 a.h.	Nine .015"-.017"	Eight 15g Kadox + 2% HgO	2% XY-4	-2 a.h.	"	"	40-50%
31-33	157	22 a.h.	"	"	5% "	+50 a.h.	"	"	"
34-37	157	23 a.h.	10g Ag + 1% Pd	"	10% "	"	Heavy	"	"
38-40	157	37 a.h.	Eleven plates .015"-.017"	Ten plates 15g Kadox + 2% HgO	2% ZnCO ₃	+16 a.h.	"	"	"
41-43	156	34 a.h.	"	"	5% "	"	"	"	"
44-46	132	28 a.h.	10g Ag + 1% Pd	"	10% "	"	"	"	"
47-49	180	38 a.h.	"	"	2% ZnSO ₄	"	"	"	"
50-52	166	33 a.h.	"	"	5% "	"	"	"	"
53-55	180	36 a.h.	"	"	10% "	"	"	"	"
56*	204	38 a.h.	Eight plates .020"-.023"	Seven plates 20g ZnO + 2% HgO + .5% BC-610	None	"	None	Light 2 layers	15-25%
57*	96	"	15g Ag + 1% Pd	"	"	"	"	"	"
58*	120	"	"	"	"	"	"	"	"
59	156	21 a.h.	"	"	2% ZnSO ₄	"	"	"	"
60	168	17 a.h.	"	"	"	"	"	"	"
61	168	22 a.h.	"	"	"	"	"	"	"
62	204	25 a.h.	"	"	5% "	"	"	"	"
63	168	"	"	"	"	"	"	"	"
64	204	"	"	"	"	"	"	"	"
65-67	132	"	"	"	10% "	"	"	"	"
68-70	132	24 a.h.	"	"	2% ZnCO ₃	"	"	"	"
71-73	132	25 a.h.	"	"	5% "	"	"	"	"
74	24	24 a.h.	"	"	10% "	"	"	"	"
75	48	"	"	"	"	"	"	"	"
76	120	"	"	"	"	"	"	"	"

*Control Cells.

exhibited very heavy zinc mossing around the bottom and edges of the plates, although they did not fail by short-circuiting but by loss of active material.

Cells 28 through 37 contained admixtures of XX4 zinc oxide in 2, 5 and 10% by weight concentrations. These utilized thin-plate, 17-plate construction, so the ratio of plate weight to separator weight was higher than in the case of the 21-plate construction. These cycled without any problem, but their life of 157 cycles doesn't represent any increase over that obtained with the 15-plate construction and the addition of Emulphogene BC-610.

A repeat test was made with the standard 15-plate construction with negative plates containing $ZnCO_3$ and $ZnSO_4$ (cells 59-76). Some improvement in cycle life was achieved by cells containing negatives with 5% $ZnSO_4$ and 5% appears to be a near-optimum concentration. The addition of $ZnCO_3$ was definitely harmful on this test. These cells accumulated 14.4 a.h. of overcharge for about 0.6% per cycle and they exhibited a relatively low amount of washout. The negatives showed mixed oxide and metallic zinc on tear-down. It seems possible that these cells may have done slightly better if given a little more overcharge.

In an effort to determine if an electrodeposited zinc electrode would increase cycle life of the cell system six 25 a.h. cells were constructed using electrodeposited negative plates with results at three different depths-of-discharge as shown in Table XIII.

TABLE XIII

Cells Constructed Using Electrodeposited Negative Plates
With Results at 3 Different Depths-of-Discharge

<u>No. of Cells</u>	<u>Initial Capacity</u>	<u>Cycles at 60% DOD</u>	<u>Cycles at 40% DOD</u>	<u>Cycles at 25% DOD</u>
2	20 a.h. 18	96 96		
2	22 28		228 228	
2	29 29			700* 700*
<u>Controls</u> <u>1 - 6</u>	28.5	204 204	400** 400**	850 850

* failure due to shorts

** test stopped

The main cause of failure was due to loss in negative plate capacity. The plated negative, upon inspection, showed the same pattern of shedding and agglomeration as did the regular production plates. Figure 56 shows a photomicrograph of a plated negative after 96 cycles at 60% DOD.

An experimental 25 a.h. cell containing three layers of cellulosic membranes was constructed as follows: All the negative plates had a center section removed in the shape of a rectangle, and a plastic shim was inserted in the cavity. This area was 2" x 3/4". Additional plates were utilized in the element such that the surface area of active material was the same as in regular 25 a.h. cell construction. This cell delivered 290 cycles at 60% DOD. However, additional cells constructed with standard 25 a.h. size plates having a smaller opening at the plate centers (1" x 1/2") only yielded 130 cycles at 60% DOD.

Additional cells were constructed to try to optimize the hole size which seems to prohibit the zinc material from agglomerating at the plate centers; but no success was obtained by this method.

F. Influence of Membrane Separator Characteristics

The final report on this subject will be published separately by the Whittaker Corporation.

G. Sites for ZnO Overgrowths

The basis for this approach toward extending the capacity and, perhaps, cycle life is to provide crystal sites for precipitation of ZnO within the zinc plate itself, thus discouraging its transport through the separator and to the bottom of the plate. Fast precipitation should tend to increase the zinc plate capacity by slowing down the accumulation of zincate ion in solution, which might be expected in turn to slow down the onset of passivation. Also, if precipitation could be induced at the location where the zinc is going into solution during discharge, on the subsequent charge the formation of metallic zinc might be expected to take place at the same location, thus tending to stabilize the geometrical distribution of zinc on the electrode and so promote longer life.

Russian work (N. Julidov, Author's Certificate No. 116812 of 3/7/58) had shown the possibility of using $\text{Ca}(\text{OH})_2$, which is quite insoluble in alkali, to accomplish this purpose in the study of zinc-nickel oxide cells. Based on that work, 18 cells were constructed, 6 cells each containing 1, 3 and 5% by weight of finely divided CaO in the negative plate, initial capacities were checked, and the cells cycle-life tested. The data are shown in Table XIV.

TABLE XIV

Initial Capacity and Cycle Life of Cells with
Negative Plates Containing Insoluble CaO

<u>No. of Cells</u>	<u>CaO in Negative (% by Weight)</u>	<u>Initial Capacity (A.H.)</u>	<u>Cycle Life</u>
6	1	24.1	156
6	3	24.1	96
6	5	23.8	156

The data show no obvious effects on either initial capacity or cycle life, and it is concluded that the use of CaO does not achieve the desired result, at least in these small concentrations. This is in sharp contrast to the behavior of BaSO_4 in lead-acid cells which has appreciable effects on capacity of lead plates when used in quantities of less than 0.5%. Figures 57 through 59 show photographs of negative plates containing 1%, 3% and 5% CaO .

The reason for the ineffectiveness of CaO additions (which was also found to be true by V.V. Romanov, "On approaches to Extend Service Life of the Nickel-Zinc Battery") was shown by him to be due to the slowness with which $\text{Ca}(\text{OH})_2$ induces precipitation of zincate ion from solution. Although substantially complete precipitation could be achieved in a 90-day period, it takes 30 days to reduce the zincate ion concentration by one-half. Romanov used a $\text{Ca}(\text{OH})_2$ concentration in the ratio of 1:2.2 to ZnO in his plates, and he abandoned this approach toward extending zinc plate cycle life.

A literature search has been made by Dr. W. VanDoorne (Calvin College, Grand Rapids, Michigan) in order to disclose, if possible, other oxides or hydroxides which might possibly be tried out to achieve the desired effects. This survey is included in this report as Appendix III in order to preserve the referencing system in his report.

The search disclosed the following oxides as possibilities - all of which form solid solutions with ZnO: BeO, MnO, FeO, CoO, NiO, CuO, PdO, MgO, CdO, SnO. In addition it was found that both Ni(OH)₂ and Co(OH)₂ form solid solutions with Zn(OH)₂. Thus, from the point of view of crystal structure, any one or all of these might be tried for their possible effects along the desired lines.

If the slowness of precipitation of zincate ion from solution were to hold, regardless of the nature of the host crystal, then this approach is doomed to failure in any case (for the 2-hour cycle); however, inasmuch as this is not known at this time, such of these materials as meet the criteria described below might be tried out in the next year's work.

The criteria are:

- (1) the oxide or hydroxide must be insoluble;
- (2) the oxide or hydroxide must have a reduction potential more negative than that for the $\text{ZnO} \rightarrow \text{Zn}$ charging reaction.

The reasons for these criteria are fairly obvious. If the material is soluble, it can't remain in the plate in its crystalline form. If it is reduced to metal at potentials less negative than that for the $\text{ZnO} \rightarrow \text{Zn}$, then on the formation charge it would go to the metallic state and remain that way on the plate. In the latter instance, it would, furthermore, be disastrous to incorporate a substance with a low hydrogen overvoltage, because then hydrogen gas generation rates would be expected to become unbearable for sealed cell operation. FeO is a good example of the latter situation. It is well known that the iron electrode of the Edison cell has a very short charged stand life because of the rate at which it generates hydrogen in the KOH electrolyte environment.

Reference to Latimer, "Oxidation Potentials," 2nd ed., Table 85 (Prentice-Hall, Inc. 1952, Englewood Cliffs, N.J.) gives the line-up in Table VI for the oxidation-reduction potentials of the candidate oxides or hydroxides in alkaline solutions.

TABLE XV

Reduction Potentials

Couple	E°
$\text{Ca} + 2 \text{OH}^- = \text{Ca(OH)}_2 + 2\text{e}$	-3.03
$\text{Mg} + 2 \text{OH}^- = \text{Mg(OH)}_2 + 2\text{e}$	-2.69
$2\text{Be} + 6 \text{OH}^- = \text{Be}_2\text{O}_3 + 3 \text{H}_2\text{O} + 4\text{e}$	-2.62
$\text{Mn} + 2 \text{OH}^- = \text{Mn(OH)}_2 + 2\text{e}$	-1.55
$\text{Zn} + 2 \text{OH}^- = \text{Zn(OH)}_2 + 2\text{e}$	-1.245
$\text{Zn} + 4 \text{OH}^- = \text{ZnO}_2 + 2 \text{H}_2\text{O} + 2\text{e}$	-1.216
$\text{Cr} + 4 \text{OH}^- = \text{CrO}_2^- + \text{H}_2\text{O} + 3\text{e}$	-1.2
$\text{Sn} + 3 \text{OH}^- = \text{HSnO}_3^- + \text{H}_2\text{O} + 2\text{e}$	-0.91
$\text{Fe} + 2 \text{OH}^- = \text{Fe(OH)}_2 + 2\text{e}$	-0.877
$\text{H}_2 + 2 \text{OH}^- = 2 \text{H}_2\text{O} + 2\text{e}$	-0.828
$\text{Cd} + 2 \text{OH}^- = \text{Cd(OH)}_2 + 2\text{e}$	-0.809
$\text{Co} + 2 \text{OH}^- = \text{Co(OH)}_2 + 2\text{e}$	-0.73
$\text{Ni} + 2 \text{OH}^- = \text{Ni(OH)}_2 + 2\text{e}$	-0.72
$2 \text{Cu} + 2 \text{OH}^- = \text{Cu}_2\text{O} + \text{H}_2\text{O} + 2\text{e}$	-0.358
$\text{Cu}_2\text{O} + 2 \text{OH}^- + \text{H}_2\text{O} = 2 \text{Cu(OH)}_2 + 2\text{e}$	-0.080
$\text{Pd} + 2 \text{OH}^- = \text{Pd(OH)}_2 + 2\text{e}$	+0.07

On the basis of these data, only Ca, Mg, Be and Mn oxides or hydroxides would not be expected to be

reduced to metal at the zinc electrode. Romanov has given up on Ca(OH)_2 and Mg(OH)_2 and the data of this report show that addition of CaO has no beneficial effect.

BeO is quite soluble in strong NaOH , to the extent of 3 + gm/100 gm saturated solution. While it would be a simple matter to saturate the solution (assuming that it would have a similar solubility in KOH) and then add excess BeO to the plate, the solid phase in existence with BeO in concentrated solutions is not BeO , but $\text{BeO} \cdot \text{NaOH} \cdot \text{H}_2\text{O}$ (Seidell, "Solubilities of Inorganic and Metal Organic Compounds," 4th Ed., Vol. I, p. 412. D. VanNostrand Company, Inc., New York, 1958). If a similar compound were to form in KOH solutions, the crystal structure would be changed, of course.

Solubility data for Mn(OH)_2 in NaOH solutions show 0.03 grams per 4.14 molal solution with solubility increasing with concentration (Seidell, Vol. II, p. 558). The presence of manganese in the system is to be eschewed, however, because soluble permanganates are certain to be formed on charge at the silver oxide plate which would oxidize the separator.

It is concluded from the available information that this approach appears to be hopeless, and abandonment is recommended.

H. Development of Failure Analysis Techniques

Throughout this program, all cells that have failed cycle life tests have been inspected and analysis has been undertaken to determine the cause of failure.

In general, the major causes of cell failure have been loss of negative plate capacity, and shorting. A third cause is lack of cell charge acceptance, particularly at 60% DOD, which ties in with the loss of negative plate capacity.

The loss of negative plate capacity is due to actual loss of active material from the grid. The material moves down toward the bottom center of the grid

losing surface area and developing high current density sites which tend to produce hydrogen. There is also some solubility of the zinc oxide in KOH electrolyte.

When cells have failed, the components such as separators, plates, and any free electrolyte are inspected. Samples of plates are sectioned and photomicrographs are obtained. Chemical analysis for silver, zinc and zinc oxide are made to determine their presence in separators, and adjoining electrodes.

The following chemical procedures are in use in this program.

1. Determination of Zinc in Separator Materials

- a. Depending on the choice of the person desiring the analysis, either measure and calculate the actual area of the separator material or assume a standard 6 square inch area.
- b. Dissolve the zinc on the separator sample by placing HNO_3 on the separator into a 250 ml. beaker and adding 25 ml. of 1:3 HCl .
- c. After the zinc has been dissolved from the separator material, neutralize the solution with concentrated NH_4OH to a pH of approxi- 8.5 - 9.0. Use the Beckman pH meter for this step and the following step also.
- d. Add a few drops of a saturated aqueous solution of sodium acetate; then add enough 50% by weight acetic acid to bring the solution to a pH of 5.0 - 4.5. The pH of the cold solution should not be lower than 4.5.
- e. Add 2-3 drops of the COPPER-EDTA solution and enough PAN indicator solution to turn the sample solution a deep violet color.
- f. Heat the solution to boiling and titrate with 0.1 molar EDTA solution until the sample solution changes to a clear yellow color. (A very definite end-point.)

- g. Run a blank determination and subtract the value of the blank from the value for zinc.
- h. A 10 ml. burette graduated in 0.02 ml. may be used to dispense the EDTA solution.

CALCULATIONS

* TOTAL GRAMS ZN = ml EDTA x An FACTOR FOR EDTA

GRAMS Zn PER SQ. IN. = TOTAL GRAMS Zn/AREA

* In Zn factor for the EDTA solution will be found in the standard solutions book. 1 ml. of EDTA solution should equal approximately 7 mg of zinc.

NOTES

- i. Better results are achieved if steps 3 through 5 are carried out on a cool solution.
 - j. Answers are reported in total grams of zinc found and in grams of zinc per square inch.
2. Determination of Silver in Separator Materials
- a. Depending on the choice of the person desiring the analysis, either measure the exact area of the separator material or assume a 6 square inch area.
 - b. Put the separator material into a 250 ml. beaker and add 25 ml. of 1:2 HNO₃. Swirl beaker to wet entire separator. Place beaker on medium heat hot plate to aid the solution of the silver. Normally it will not be necessary to boil the acid and separator to cause solution of the silver.
 - c. Upon dissolving the silver, add 75 ml. of water and stir solution.
 - d. The silver is titrated with 0.1N NH₄SCN using a ferric ion as an internal indicator. Add 5 ml. of FeNH₄(SO₄)₂, ferric ammonium sulfate, to the solution of silver and titrate with 0.1N NH₄SCN to a reddish-brown or rust-colored end-point.

- c. Calculate the total grams of silver by the following method:

$$\text{*TOTAL GRAMS Ag} = \text{Ml 0.1N NH}_4\text{SCN} \times \text{Ag FACTOR OF 0.1N NH}_4\text{SCN}$$

* The Ag factor of NH_4SCN will vary with the normality of the solution, and should be calculated every time a new solution is prepared by standardizing against AgNO_3 . The Ag factor should fall in the area of 0.010777 gms. Ag per ml. NH_4SCN .

- f. Divide total grams of silver calculated by the area to get grams of silver per square inch.
- g. Answers are reported in grams of silver per square inch, and in total grams of silver.

NOTES

- h. The end-point of the titration is quite distinct but requires some care and practice in determining it. A definite rust color is desired but not to the extent of over-titration.
- i. Normally the Ag factor for the NH_4SCN will be recorded in the standard solutions book and on the bottle containing the NH_4SCN .
3. Determination of Silver & Palladium in Silver-Zinc Negative (Zinc) Plates
- a. Reagents:
1. Nitric Acid (1:1)
 2. Nitric Acid, Conc.
 3. Hydrochloric Acid (1:3)
 4. Methyl Orange Indicator
 5. Ammonium Hydroxide, Conc.
 6. Nioxime, 0.8% solution in H_2O
- b. Procedure for Silver:
- 1) Cut the sample into small pieces to facilitate dissolution. Dissolve in a

300 ml. beaker; dampen sample with distilled water; slowly add 20 ml. of (1:1) HNO_3 ; place on oscillating hot plate, medium heat; add conc. HNO_3 and distilled water to complete dissolution of sample.

- 2) When sample is clear, cool to room temperature, then filter through a Black Ribbon paper. If filtrate is not clear, re-filter through a Whatman #42 filter paper.
- 3) Add 10 ml. of HCl (1:3) and simmer for 30 minutes.
- 4) Filter, hot, through a previously weighed Gooch crucible. Use hot water and rubber policeman to remove precipitate from beaker sides. Retain filtrate for palladium determination.
- 5) Dry precipitate one hour at 110°C ., cool in dessicator, reweigh, for AgCl .

$$\text{Mg. Ag per in}^2 = \frac{\text{mg. AgCl} \times 0.7526}{\text{Plate area, in}^2}$$

c. Procedure for Palladium:

- 1) Add 5 drops of Methyl Orange indicator to the filtrate from the silver analysis, agitate on a magnetic stirrer.
- 2) Add conc. NH_4OH until sample turns yellow (pH5-6). Add more methyl orange as color tends to fade rapidly. Zinc hydroxide will probably be precipitated, slight to heavy precipitate. The zinc hydroxide is filtered, Black Ribbon paper.
- 3) If solution is not yellow clear, refilter.
- 4) Complete palladium per procedure for palladium in separators starting with ... agitate on magnetic stirrer.

300 ml. beaker; dampen sample with distilled water; slowly add 20 ml. of (1:1) HNO_3 ; place on oscillating hot plate, medium heat; add conc. HNO_3 and distilled water to complete dissolution of sample.

- 2) When sample is clear, cool to room temperature, then filter through a Black Ribbon paper. If filtrate is not clear, re-filter through a Whatman #42 filter paper.
- 3) Add 10 ml. of HCl (1:3) and simmer for 30 minutes.
- 4) Filter, hot, through a previously weighed Gooch crucible. Use hot water and rubber policeman to remove precipitate from beaker sides. Retain filtrate for palladium determination.
- 5) Dry precipitate one hour at $110^\circ\text{C}.$, cool in dessicator, reweigh, for AgCl .

$$\text{Mg. Ag per in}^2 = \frac{\text{mg. AgCl} \times 0.7526}{\text{Plate area, in.}^2}$$

c. Procedure for Palladium:

- 1) Add 5 drops of Methyl Orange indicator to the filtrate from the silver analysis, agitate on a magnetic stirrer.
- 2) Add conc. NH_4OH until sample turns yellow (pH 5-6). Add more methyl orange as color tends to fade rapidly. Zinc hydroxide will probably be precipitated, slight to heavy precipitate. The zinc hydroxide is filtered, Black Ribbon paper.
- 3) If solution is not yellow clear, refilter.
- 4) Complete palladium per procedure for palladium in separators starting with ... agitate on magnetic stirrer.

600-2000 angstroms. Again, Figure 61, the pores of the VM millipore material would be 170-250 angstroms for the black dots and 1300-4000 angstroms for the white areas. The Dow Corning glass disk had pores in the 50-75 angstrom range, Figure 62. The 2.2XH polyethylene separator pore size was 40-100 angstroms, Figure 63. The plain unirradiated polyethylene surface was basically smooth and without detail.

The VF WP millipore material was manufactured by the Millipore Corp., Bedford, Mass. According to their literature, this material is made of mixed esters of cellulose in a white plain surface with a mean pore size of 100 angstroms plus or minus 20 angstroms. Its porosity is 70%. The second material (VM WP millipore) was also made of mixed esters of cellulose but had a mean pore size of 500 angstroms plus or minus 30 angstroms according to the manufacturer's specifications. The third type of separator was 2.2XH polyethylene, a radiated grafted polyethylene sheet made by Radiation Applications Inc. The mean pore size of this separator, as claimed by the manufacturer, was 40 angstroms or less. Also, a plain sheet of RAI's polyethylene was submitted so that its surface could be ascertained. The disk of Dow Corning glass was reputed to have pore sizes of 36-54 angstroms.

Direct one-step carbon replicas were made of the millipore type materials in a vacuum evaporator shadow caster. Gold or chromium was pre-shadowed on small strips of the separators and then 100-200 angstrom thick carbon was put down on the surfaces in a continuous film. Small pieces of this replicated material were placed on 1/8 inch specimen grids of 200 mesh and into an acetone reflux column equipped with a cold finger. After three hours in the reflux column, the original cellulose material was dissolved away leaving a clean direct replication of the material's surface.

A two stage replica technique was used for the polyethylene and the porous glass. Two drops of Ladd's replication solution were placed on an inch strip of Ladd's plastic replicating tape and this tape was placed on the surface of the polyethylene and left to dry. When dry, the replicating tape was peeled carefully from the polyethylene and fastened to a glass slide with scotch tape. A carbon replica

was then made of the surface of the plastic tape by the vacuum evaporator and reflux column techniques.

The replicas were viewed with an RCA EMU-3F electron microscope and the images were recorded on Kodak electron image photographic plates. The total magnification of the prints was based upon a replica of a 28,800 lines per inch grating.

Several attempts were made to pot some of the materials in epoxies and to slice ultra thin sections of the cross-sectional areas with a Porter Blum ultramicrotome. This technique did not work - primarily because the polyethylene would not be cut by our diamond knife. The epoxy would not saturate or permeate the sample so there was little bonding of the epoxy to the polyethylene.

Figure 60 shows the surface of the VF WP millipore material at 150,000 X magnification. This separator should have pores of about 100 angstroms in diameter. The size of the small black dots in this photo is about 100 angstroms. According to the manufacturer's specifications, this material is 70% porous; however, these dots do not cover 70% of the surface area. If the large white areas are the pores, then their pore size would range from 600-2000 angstroms and still they would not occupy 70% of the area.

Figure 61 shows the small black dots of the VM WP millipore separator to be in the 170-250 angstrom range. Its magnification was also 150,000 X. Now if the white areas were the pores, the dimensions of these would be 1300-4000 angstroms. Again its porosity according to the manufacturer was supposed to be 72%.

The porous glass made by Dow Corning is pictured in Figure 62 at 300,000 X. The small black and gray projections represent the pores which range from 50-75 angstroms. Figure 64 is another view of the porous glass.

The surface of the 2.2XH polyethylene separator at 61,000 X looked like that pictured by Figures 30 and 65. Replica number 30 was not pre-shadowed with a metal; replica number 32 was shadowed with

chromium. At this magnification the pores cannot be seen. Figures 66 and 67 show parts of "5" and "6" respectively at 300,000 X. The pores in the separator are represented by the small round projections which are similar to those of the porous glass. The diameters of these pores range from 40-1000 angstroms.

The actual pore size openings of the separator surfaces are represented in the photos. The shape and size of the pores as they proceed through the interior of the separators could not be determined using our known techniques.

K. Stoichiometric Ratio of Formed Zinc

Groups of three 25 a.h. cells were constructed with weight ratios of formed zinc material to silver in 2:1, 3:1 and 4:1. Cycling was done at temperatures of 30°F, 40°F, 75°F and 110°F, and at 40% DOD and 60% DOD. The results of these cells are shown in Table XVI.

TABLE XVI
Stoichiometric Ratio of Formed Zinc

<u>Ratio</u>	<u>Initial Capacity</u>	<u>Temperature</u>	<u>Cycles @ 40% DOD</u>	<u>Cycles @ 60% DOD</u>
2:1	24 ah	30°F	12	2
2:1	23	40	84	0
2:1	26	75	380	184
2:1	23	110	410	175
3:1	24	30	50	3
3:1	22	40	60	0
3:1	22	75	460	204
3:1	24	110	349	204
4:1	25	30	2	2
4:1	25	40	60	0
4:1	25	75	435	220
4:1	25	110	336	210

The cause of failure was due to loss of capacity of the zinc electrodes. In general, the failures at low temperatures were due to the inability of the zinc electrodes to accept the recharge in the 85-minute charge time.

Figure 68 shows a photomicrograph of a negative plate with a 2:1 construction.

Figure 69 shows a photomicrograph of a negative plate with a 3:1 construction.

Figure 70 shows a photomicrograph of a negative plate with a 4:1 construction.

Ratios above 2:1 show a little increase in cycle life at room temperatures, but the resulting increase in volume area does not warrant a cell design change.

L. Alternate Method of Surface Area Measurement

This section is written by Prof. T. P. Dirkse, Calvin College, and is included in Appendix V.

M. Separator Development

The initial study by RAI Research Inc., was to prepare experimental batches of membranes from three different polyethylene base materials; namely, Bakelite 0602, Phillips 1712 and USI 280. The three base materials were crosslinked to 90 Mrads, and radiation grafted with acrylic and methacrylic acid. The samples were of 100' lengths, about 1-1/2 mils thick and had a resistance of about 30-90 milliohm inches.²

Five 25 a.h. cells were constructed with 2, 3 and 4 layers each from the three base material samples, and cycled at 60% depth-of-discharge. The results are listed in Table XVII.

TABLE XVII
Separator Development

<u>Cells</u>	<u>RAI Membrane</u>	<u>Initial Capacity</u>	<u>Acrylic Acid Graft</u>	<u>Methacrylic Acid Graft</u>
10	4 Layers Bakelite 0602	24 a.h.	60(5)*	116(5)*
10	3 Layers Bakelite 0602	26	60(5)*	116(5)*
10	2 Layers Bakelite 0602	24	60(2) ¹ 76(3) ¹	50(1) ¹ 80(4) ¹
10	4 Layers Phillips 1712	30	40(5)*	140(3) ¹ 112(2) ¹
10	3 Layers Phillips 1712	30	48(1) ¹ 60(4) ¹	103(5) ¹
10	2 Layers Phillips 1712	30	60(5) ¹	36(5) ¹
10	4 Layers USI 280	30	48(1) ¹ 60(4)*	140(5)*
10	3 Layers USI 280	30	48(3) ¹ (2)*	56(3) ¹ (2)*
10	2 Layers USI 280	30	36(5) ¹	24(5) ¹
3	Controls 4 Layers FSC	22	120(3)*	
3	Controls 3 Layers FSC	25	123(3)*	
4	Controls 2 Layers FSC	31	76(4) ¹	

* = Capacity Failure
() = No. of Cells
()¹ = Failure by shorts

Table XVIII shows the appearance of the cell components. The results of the teardown inspection revealed that in all cases, the zinc electrode had material bunching along the center and bottom portions of the grid showing the effect of heavy agglomeration. There was no indication of zinc creepage on any layer of membrane with the acrylic acid graft. With the methacrylic acid graft, however, there was zinc creepage around the layers. This occurred only in the Bakelite 0602 and Phillips 1712 base materials.

Cells containing two layers of Bakelite material, both acrylic and methacrylic acid graft, delivered as many cycles as the control cells containing two layers of FSC. Cells containing three and four layers of the Bakelite methacrylic acid graft cycled nearly as well as the control cells. Although cells containing four layers of Phillips 1712 and USI 280 methacrylic acid graft did obtain more cycles than the controls, the two layer samples did not perform as well as either the two layer Bakelite or control cells.

On the basis of this test, 500 foot lots of Bakelite acrylic and methacrylic acid radiation graft, crosslinked at the 90 Mrad level were prepared by RAI, Inc. A third sample, containing chemically grafted methacrylic acid was also furnished.

Groups of eighteen 25 a.h. cells were constructed with each of the three membrane samples. The eighteen cell group contained 5, 4 and 3 layers of each membrane. These cells were cycled at 60%, 40% and 25% depth-of-discharge. In addition, cells containing 4 layers of each membrane are presently under cycle test at the indicated depth-of-discharge at the Quality Assurance Laboratory, Crane, Indiana. This is done so that a comparison of cycle life can be made with cells containing 4 layers of separation.

Table XIX shows the initial capacity and cycle life obtained at the various depths of discharge for these cells containing the three membrane samples. The control cells contained 4 layers of cellulosic membrane.

TABLE XVIII

SEPARATORS

Note: All cells were constructed as in Table I except for separator combinations. All cells contained one layer of acrylonitrile monomer next to the positive plate. Electrolyte concentration was 40% KOH. MA = methacrylic acid graft. AA = acrylic acid graft. The general condition of the RA1 separator after cycle life was good.

Cell No.	O.C. Voltage	Number and Kind of Separators*	Condition of Positive Plate	Extent Formed	Treeing	Creeping	Penetration	Washout	Cause of Failure
1-5	1.80	Bakelite MA 4L	Buckled + ZnO	Zinc 90%	None	Light 3L	None	55%-75%	Loss of negative capacity
6-10	1.82	3L	Deposit	Oxide 90%	"	"	"	"	Shorts
11-15	0.30	2L				None		20%	
16-20	1.12	Phillips MA 4L	"	"	"	Light 3L	"	65%-75%	"
21-25	0.70	3L	"	"	"	Light 2L	"	"	"
26-30	0.00	2L	"	"	"	None	"	30%	"
31-35	1.82	US1 MA 4L	"	50%-50%	"	"	"	50%-60%	Loss of capacity
36-40	1.8-0.5	3L	"	Oxide 90%	"	"	"	"	Loss of cap. & shorts
41-45	0.00	2L	"	"	"	"	"	10%-20%	Shorts
46-50	1.82	Bakelite AA 4L	"	Zinc 90%	"	"	"	65%-75%	Loss of capacity
51-55	1.82	3L	"	"	"	"	"	"	"
56-60	0.00	2L	"	Oxide 90%	"	"	"	"	Shorts
61-65	1.82	Phillips AA 4L	"	Zinc 90%	"	"	"	50%-60%	Loss of capacity
66-70	0.00	3L	"	Oxide 90%	"	"	"	"	Shorts
71-75	0.00	2L	"	"	"	"	"	"	"
76-80	1.82	US1 AA 4L	"	Zinc 90%	"	"	"	"	Loss of capacity
81-85	0.50	3L	"	Oxide 90%	"	"	"	"	Shorts
86-90	0.50	2L	"	"	"	"	"	"	"
91-93*	1.84	Cellulosic 4L	Good	Zinc 60%	"	Light 3L	"	"	Loss of capacity
94-96*	1.84	3L	"	"	"	Light 2L	"	"	"
97-100*	0.00	2L	Discharged	Oxide 90%	"	Heavy 2L	Yes	"	Shorts

* Control Cells. The first layer of cellulosic material was deteriorated in these cells.

The failure mode is by loss of negative material and/or short circuiting. All cells in this test are considered to have failed by short circuiting if the open circuit voltage is below 1.52 V. after a week's charged stand time after completion of cycle testing.

TABLE XIX

Initial Capacity and Cycle Life at Various Depths-of-Discharge

A. 90 Mrad Methacrylic Acid Radiation Graft Membrane

	<u>Controls</u>	<u>3 Layers</u>	<u>4 Layers</u>	<u>5 Layers</u>
Initial Capacity	22 a.h.	27 a.h.	28 a.h.	27 a.h.
Cycles at 60% DOD	156(4)*	120(6)*	72(3)*	132(2)* 96(2)* 108(2)*
40% DOD	288(2)* 312(2)*	180(1) ¹ 288(2) ¹ 276(2) 288(1)*	253(3)*	120(2)* 216(3)* 240(1)*
25% DOD	396(2)* 480(1) 528(1)	432(1) ¹ 444(1) ¹ 456(2) ¹ 492(1) ¹ 601(1) ¹	400(1) 428(2)	553(1)* 600(5) ^c

B. 90 Mrad Acrylic Acid Radiation Graft Membrane

	Same as A	25 a.h.	28 a.h.	25.5 a.h.
Initial Capacity				
Cycles at 60%DOD	"	48(1) ¹ 72(3) ¹ 72(1)*	84(3)*	48(2) ¹ 72(4) ¹
40% DOD	"	144(1) ¹ 156(1)* 180(1) ¹ 204(1) ¹ 240(2)*	144(2)* 144(1) ¹	120(3)* 156(3)*
25% DOD	"	408(1)* 468(1) ¹ 492(2) ¹ 517(2)*	324(2)* 300(1)*	336(2)* 408(1)* 468(2)*

TABLE XIX (Cont'd)

C. 90 Mrad Methacrylic Acid Chemical Graft

	<u>Controls</u>	<u>3 Layers</u>	<u>4 Layers</u>	<u>5 Layers</u>
Initial Capacity	24 a.h.	22 a.h.	20 a.h.	23 a.h.
Cycles at 60% DOD	144(1)*	48(2) ¹ 84(2) ¹ 96(2) ¹ 96(3)*	2(3)	30(3) ¹
40% DOD	Awaiting Tests	- - - - -	- - - - -	- - - - -
25% DOD	Awaiting Tests		348(1)* 400(2)	Awaiting Test

* = Failure
 () = Number of Cells
 ()¹ = Failure by Shorts
 ()^c = Cycling

Table XX shows the number of cells that failed by short circuiting with the number of layers of membranes tested at the indicated depths-of-discharge.

TABLE XX

Number of Cells that Failed by Short Circuiting

	<u>3L MA</u>	<u>3L AA</u>	<u>3L CMA</u>
60% DOD	0	5	6
40% DOD	5	3	2
25% DOD	6	2	6
	<u>4L MA</u>	<u>4L AA</u>	<u>4L CMA</u>
60% DOD	0	0	4
40% DOD	0	1	3
25% DOD	0	0	6
	<u>5L MA</u>	<u>5L AA</u>	<u>5L CMA</u>
60% DOD	0	6	3
40% DOD	0	0	3
25% DOD	3	3	6

TABLE XX (Cont'd.)

	<u>Control Cells</u>
60% DOD	0
40% DOD	0
25% DOD	3

MA = Methacrylic Acid

AA = Acrylic Acid

CMA = Chemically Grafted Methacrylic Acid

Table XXI shows the appearance of the cell components after cycle testing. The main differences here in the polyethylene treated membranes and the cellulosic controls are:

1. The cellulosics will deteriorate (rot) while the polyethylenes will not.
2. The zinc material will creep around layers in big splotches in and on the cellulosics, while in the polyethylenes the same material will penetrate in one or two areas in each layer about the size of a dime if it does occur. In many instances, the penetration can not be seen, yet cell shorts have occurred.
3. The cellulosics will swell to over twice the original thickness, while the polyethylenes will not. In fact, there appears to be a "deswelling" causing a stretching of the membrane across the plate. This is probably what is making the positive plates buckle and, since pressure is reduced in the perpendicular direction to the face of the plate, this is causing increased shedding of the negative material.

Figure 70 shows the appearance of the negative plate material after the indicated cycle failure due to loss of negative plate capacity. These plates are from cells containing 3 and 5 layers of the radiated methacrylic acid graft. The control plate is in the center from a cell containing 4 layers of cellulosic

TABLE XXI
SEPARATORS

Note: Same as Table X

Number and Kind of Separator**	Depth of Discharge	Cell No.	O.C. Voltage	Condition of Positive Plate	Condition of Negative Plate			Cause of Failure
					Extent Formed	Treering Creeping	Penetration	
3 Layers MA	60%	1-6	1.83V	Buckled +ZnO Deposit	60% Zinc	None	None	Loss of neg. cap.
" " "	40%	7-12	1.54	"	90% Oxide	"	All layers	Shorts
" " "	25%	13-18	0.70	"	"	"	"	"
4 Layers MA	60%	19-21	1.82	"	60% Zinc	"	2 layers	Loss of neg. capacity
" " "	40%	22-24	1.82	"	"	"	3 layers	"
" " "	25%	25-27	1.77	"	"	"	3 layers	"
5 Layers MA	60%	28-33	1.83	"	"	"	3 layers	"
" " "	40%	34-39	1.82	"	"	"	None	"
3 Layers AA	60%	46-51	0.50	Buckled +ZnO Deposit	90% Oxide	None	None	Shorts
" " "	40%	52-57	1.77	"	"	"	"	Loss of capacity
" " "	25%	58-63	1.59	"	"	"	3 layers	and shorts
4 Layers AA	60%	64-66	1.82	"	60% Zinc	"	"	Loss of capacity
" " "	40%	67-69	1.60	"	50%-50%	"	None	"
" " "	25%	70-72	1.80	"	"	"	All layers	"
5 Layers AA	60%	73-78	0.90	"	90% Oxide	"	None	Shorts
" " "	40%	79-81	1.76	"	60% Zinc	"	"	Loss of capacity
" " "	25%	82-87	1.80	"	"	"	3 layers	"
Control Cells*	60%	88-91	1.83	Good	"	Medium 4 layers	None	"
" " "	40%	92-95	1.82	"	"	Heavy	"	"
" " "	25%	96-99	0.80	Discharged	90% Oxide	"	"	Shorts

* The cellulosic membranes were in general badly deteriorated in cells at 40% & 25% DOD; at 60% DOD, the first layer only was deteriorated.

** The MA and AA radiated grafted membranes were in very good condition at all depths-or-discharge.

membrane material. In all cases after cycle failure, the negative material resulted in this configuration.

In general from the cycle data obtained to date, the 90 Mrad crosslinked polyethylene methacrylic acid radiation grafted membrane gave longer cycle life, layer for layer, than did the acrylic acid grafted membrane at each depth-of-discharge. In addition, three layers of the methacrylic acid graft are as good as or better than the separator for the control cells. The best cycles obtained so far are with the 5-layer methacrylic acid graft at 25% depth-of-discharge. It is believed that loose element pack construction could be a factor in some early cycle failures at all depths-of-discharge. All cells now under construction have proper shimming.

The results of the tests on cells containing four layers of RAI 90 Mrad crosslinked acrylic and methacrylic acid graft performed at the Quality Assurance Laboratory at Crane, Indiana are compared with those obtained at Delco-Remy.

TABLE XXII

Cells Containing Four Layers of RAI 90 Mrad Crosslinked Acrylic and Methacrylic Acid Graft

1. Cells containing four layers of acrylic acid graft.

<u>DOD</u>	<u>Cell No.</u>	<u>Crane</u>	<u>Delco-Remy</u>
25%	1	203*	324*
	2	369*	324*
	3	357*	300 ¹
40%	4	84*	144*
	5	84*	144*
	6	84*	144*
60%	7	34*	84*
	8	34*	84*
	9	34*	84*

TABLE XXII (Cont'd.)

2. Cells containing 4 layers methacrylic acid graft.

<u>DOD</u>	<u>Cell #</u>	<u>Crane</u>	<u>Delco-Remy</u>
25%	1	215 ¹	400*
	2	237 ¹	428*
	3	237 ¹	428*
40%	4	84*	253*
	5	84*	253*
	6	84*	253*
60%	7	34*	72*
	8	34*	72*
	9	34	72*

3. Control cells containing 4 layers FSC

<u>DOD</u>	<u>Cell #</u>	<u>Crane</u>	<u>Delco-Remy</u>
25%	1	1100	396*
	2	900	396 ¹
	3	---	480 ¹
	4	---	528 ¹
40%	1	100*	228*(2)
	2	100*	312*(2)
60%	1	38*	156*(4)
	2	38*	

* = failure by loss of capacity
 1 = failure by short circuiting
 () = number of cells
 c = cycling

An additional 5000 feet of 90 Mrad crosslinked polyethylene methacrylic acid radiation graft has been utilized in 25 a.h. cells throughout the remainder of the program. This material was consistently uniform. The resistance was 60 milliohms in.² throughout, and had a constant thickness of 1.7".

Much of the separator has been used in the cells testing the various zinc oxide samples as reported under Section D.

An additional test of electrolyte concentration was accomplished with cells containing seventeen plates, and four layers of polyethylene grafted membranes along with control cells of seventeen plates and four layers of cellulosic materials. The following table shows the number of cells, electrolyte concentration and initial capacity of the cells tested at 60% DOD.

TABLE XXIII
Electrolyte Concentration

<u>No. of Cells</u>	<u>Electrolyte Concentration</u>	<u>Initial Capacity</u>	<u>No. of Cycles</u>
4 polyethylene 2 controls	30% KOH 30% KOH	28 a.h. 13 a.h.	84 60
4 polyethylene 2 controls	35% KOH 35% KOH	30 a.h. 15 a.h.	112 112
4 polyethylene 2 controls	40% KOH 40% KOH	24 a.h. 19 a.h.	124 124
4 polyethylene 2 controls	45% KOH 45% KOH	25 a.h. 19 a.h.	84 112
4 polyethylene 2 controls	50% KOH 50% KOH	25 a.h. 23 a.h.	150 150

The cause of failure was loss of negative plate capacity. It is interesting to note here that the best capacities are obtained by cells containing polyethylene separators at the lowest electrolyte concentrations, and the opposite is true of the cells containing the cellulosic separators.

N. Electrolytes

A study of electrolyte mixtures, using percentages of 45% and 50% KOH and 45% NaOH in addition to varying layers of separator material was accomplished.

Table XXIV shows the cell construction, cycle data and appearance of cell components of some 60 cells tested. The best combination tested prior to the development of the polyethylene radiated graft membranes was four layers of cellulosic membranes in 50% KOH electrolyte yielding a cycle life of 220 cycles at 60% DOD.

The mixtures of KOH and NaOH were tried out because previous experience at lower depths-of-discharge (25% and 40%) had shown that NaOH increased cycle life over equivalent weight concentrations of KOH. The NaOH-containing electrolytes just could not support the rates of charge necessary on the 2-hour cycle regimen at 60% DOD. Charge voltages went way up; the cells heated up, and gassing resulted, indicating inefficiency of charge.

III. GENERAL DISCUSSION

As a prelude to examination of the effects on cycle life of the several variations incorporated in the negative plate during this program, consideration should be given to the pure effect of the depth-of-discharge factor. That is to say, the question should be asked: what actual capacities are available from these nominal 25 a.h. cells at various rates of discharge for the cell design concerned? Reduction in capacity as a function of discharge rate is expected for any electrochemical cell and it may vary as a function of cell design. In order to determine this for the 15-plate, 4-layer cellulosic 0.5% BC-610, cells were discharged at 25 and 50 amperes and found to have capacities of 19.0 and 15.0 a.h., respectively. The average of all the control cells run on this program to date is 26.7 a.h. at the 15-ampere rate. On the basis of these data, the following table was constructed.

ELECTROLYTE AND SEPARATOR TEST

Cell No.	Initial Capacity	Pos. Plate Construction	Neg. Plate Construction	Electrolyte	Extent of Zinc Formed & Accumulative Overcharge	Light	Negative Plate Treeing Creeping Washout		
1-3	192	28 a.h.	Eight plates	Seven plates	45% KOH	90% Zinc	+ 11 a.h.	Light	around 25-35%
4-6	220	29 "	.020"-.023"	20 g ZnO	50% KOH	"	"	"	"
7-9	192	30 "	15 g Ag + 1% Pd	+ 2% HgO	45% KOH	"	"	"	"
10-12	192	28 "		+ .5% BiClO	50% KOH	"	"	"	"
13	192	30 "	"	"	45% KOH	"	"	"	"
14	60	30 "	"	"	"	90% ZnO	"	None	"
15	192	30 "	"	"	"	90% Zn	"	Light	"
16-17	192	29 "	"	"	50% KOH	"	"	"	"
18	180	29 "	"	"	"	"	"	"	"
19	60	30 "	"	"	45% KOH	90% ZnO	"	None	"
20	192	30 "	"	"	"	90% Zn	"	Light	"
21	192	30 "	"	"	"	"	"	"	"
22	180	28 "	"	"	50% KOH	"	"	"	"
23-24	192	28 "	"	"	"	"	"	"	"
25-30	210	34 "	"	"	100% (45% KOH)				
31-36	162	30 "	"	"	80% (45% KOH), 20% (45% NaOH)				
37-42	70	28 "	"	"	60% (45% KOH), 40% (45% NaOH)				
43-48	33	21 "	"	"	40% (45% KOH), 60% (45% NaOH)				
49-54	33	22 "	"	"	20% (45% KOH), 80% (45% NaOH)				
55-60	33	18 "	"	"	100% (45% NaOH)				

TABLE XXV

Capacity Available at Cycle-Life Test Rates

<u>Depth-of-Discharge (% of Nominal Capacity*)</u>	<u>Required Depth-of-Discharge a.h.</u>	<u>Required Rate on 2-Hour Cycle (35-min. discharge) amperes</u>	<u>Capacity Available at Cycle-Life Test Rates a.h.</u>
100	25	43	15.5
80	20	34.3	17
70	17.5	29.8	18
60	15	25.8	19
40	10	17.2	23
25	6.25	10.7	31

* Nominal Capacity = 25 ampere-hours at 15-ampere rate

It is apparent that this cell design would not be able to cycle at all on the 2-hour regimen at depth-of-discharges of 100% or 80%, because it does not have sufficient capacity at the required test rate of discharge.

From Table XXV we may construct another table relating the allowable capacity loss before failure from the data in columns 2 and 4 of the table for depth-of-discharges of 70% or less. This is shown in the following table:

TABLE XXVI

Allowable Capacity Loss Before Failure Related to % DOD

<u>% DOD</u>	<u>Allowable Capacity Loss Until Failure a.h.</u>	<u>Expected Cycle Life</u>
70	0.5	28
60	4	226
40	13	735
25	24.7	1400*

*Actual cycle life from data of Table 12,
AFAPL-TR-66-79.

Now, assuming that there is a direct ratio between the allowable capacity loss until failure and the actual cycle life, data for expected cycle life as a function of DOD may be calculated, as in the third column of the table. The actual cycle life at 25% DOD was used to estimate expected cycle life at the higher depths-of-discharge. An actual cycle life of 600 cycles at 40% DOD for negative plates with 0.5% BC-610 Emulphogene additions may be compared with the value of 735 from the table. (See Table 11, AFAPL-TR-66-79.) The average cycle life of 33 control cells on this program, so far, is 164 ± 36 cycles with some groups going over 200 cycles. This may be compared with the value of 226 cycles in Table XXVI.

In estimating the expected cycle life as a function of depth-of-discharge and the allowable capacity loss, it is obvious that the condition of the negative plate will be much better at the end of life at 60% depth-of-discharge than it is at 40% depth-of-discharge and so on. This is evident from the fact that if the depth-of-discharge is reduced after failure at 60%, the cell will continue to cycle.

The point of this discussion is this: during the first year of this program we have been looking very intensively at the effects of the several variations on agglomeration and dispersity of the active material. This was a natural sequitur to the discovery that cycle life could nearly double with the use of Emulphogene BC-610 and that this resulted from reduction of the rate of agglomeration (AFAPL-TR-66-79, Table 11 and Figures 47 through 51), and the maintenance of dispersity of the metallic zinc. It seems possible, judging from the photomicrographs, that even at 60% depth-of-discharge there is sufficient true surface area (i.e. lack of agglomeration or particle size growth) to support the discharge and that loss of active material around the top and sides of the plate may have been a predominant factor in determining life. (Actually, true surface area of the available zinc needs to be measured to support this possible conclusion.)

Several other possible effects can be thought of that could come into play in shortening life: one, the loss of small amounts of active material would be more serious in reducing life at the higher depths-of-discharge; two, the loss in geometric area of the active

material would be more serious, due to increased IR losses; and three, if availability of electrolyte is a controlling factor in determining capacity then the reduced geometric area might mean that the electrolyte at the top and the sides is not available for reaction and, moreover, the change in the electrolyte concentration due to inhibition of diffusion by the separator would be more serious, due to the increase in geometric current density and the reduced geometric area.

If these effects are dominating factors in determining cycle life, there are two obvious ways to go in order to alleviate the situation. One way is to find the cause for the rearrangement of the active material from the tops and sides to the center and bottom of the plate and see what can be done about it. In a very interesting study made recently (J. McBreen and G. A. Dalin, "The Mechanism of Zinc Shape Change in Secondary Batteries," Extended Abstracts of the Battery Division of the Electrochemical Society - Fall Meeting, Philadelphia, 1966, p. 123), gravitational effects, "washing" caused by rise and fall of the electrolyte in the negative plate compartment, and cell case taper were ruled out as possible causes. The second way to go is to provide a separator which will reduce the extent of electrolyte concentration change, and perhaps provide a higher energy yield in the equivalent cell volume.

Based on the predominance of short-circuiting failures when only three layers of fibrous sausage casing were used, and the low cycle life resulting (around 110 - 120 cycles, see Table II), four layers of fibrous sausage casing were used for standard construction in order to insure zinc plate failure.

Results of the electrolyte study seems to indicate the use of 50% KOH electrolyte for maximum cycle life. A repeat test using radiated polyethylene grafted membranes also verifies this fact, although this test only produced some 150 cycles at 60% DOD. Figure 72 shows the results obtained using various electrolyte concentrations and two different separator systems.

In the study of zinc oxide powders furnished by the New Jersey Zinc Company, the additions of 1% Al and 1% Pb in the zinc oxide showed an increased cycle life at 60% DOD. The use of cellulosic membranes combined with

increased concentrations of Pb show a decrease in cycle life due to severe deterioration of the cellulosic membranes. There is no detrimental effect on the radiated polyethylene grafted membrane. Figure 73 and Figure 74 show the cycles obtained with the various concentrations of Al and Pb doped zinc oxides and the two different separator systems used.

Limits on the concentration of Fe in the zinc oxide were established, and a maximum limit of .010% Fe appears to be tolerable in the zinc oxide for battery usage, although a limit of .004% Fe is called for where possible.

In the study of surfactants it has been resolved that Emulphogene BC-610 in concentration of .4% to 1% has a beneficial effect on cycle life of the zinc electrode.

A stoichiometric ratio of 2:1 zinc to silver should be maintained for maximum cycle life on this 2-hour regimen.

In the separator development work, a successful inert membrane has been produced by RAI Research Corporation. This is a polyethylene base, crosslinked at 90 Mrad, and radiated grafted with methacrylic acid monomer. Cycle life obtained by cells using these membranes has been equal to or better than cellulosic control membranes. Inspections after cycle life show the material to be unaffected by electrode or electrolyte environment.

Studies on base polymer material, precrosslink, dosage, grafting techniques and the graft monomer have resulted in producing a membrane of uniform characteristics. Three polyethylene base materials were used; i.e., Bakelite 0602, Phillips 1712, and USI 280 and precrosslinked at 90 Mrad.

Two monomers, acrylic and methacrylic acid were radiation grafted and 100 ft. samples were furnished for cycle test at 60% depth-of-discharge. The results indicated that the Bakelite 0602 base polyethylene grafted with methacrylic acid produced the best cycle life, and was fairly equal to the controls.

Additional 500 ft. samples containing the 90 Mrad precrosslinked film with radiation grafted methacrylic and acrylic acid were furnished. A third sample of 90 Mrad precrosslinked film was chemically grafted with methacrylic acid.

The results show that the radiation grafted methacrylic acid membranes yield longer cycle life than the acrylic acid grafted membrane, and are equal to, and in some cases better than the control membranes. The importance of the data here is that 3 layers of the methacrylic acid grafted membrane were as good as 4 layers of the cellulosic membrane in nearly all depths-of-discharge. This indicates that a higher energy yield can be expected since less space and weight are required with this membrane system and, as cell manufacturing techniques improve with the use of this membrane, it is expected that no more than three layers will be required for many applications of this cell system.

The test results on the chemically grafted membranes are not favorable, and this method of grafting will not be studied further on this program.

At the present time, it appears that controls used in the manufacture of the 90 Mrad precrosslinked Bakelite 0602 polyethylene base, radiation grafted methacrylic acid membrane, are adequate to produce a membrane having uniform chemical and physical characteristics.

An additional 5000 ft. pilot run was produced and this material was found to be uniform in thickness and resistivity. This material was used in cells involved in zinc oxide and electrolyte concentration studies. In all cases, it was noted in cell inspections after cycle failure that no zinc creeping was detected around or through this separator system. The silver penetration is on the order of .2 to .4 milligrams per square inch.

This membrane, as presently manufactured by the techniques outlined in the Final Report by RAI Research Corporation, is found to be satisfactory and in many instances superior to cellulosic materials in silver-zinc sealed or vented secondary cells.

IV. RECOMMENDATIONS

Study NaOH electrolyte concentrations in cells containing polyethylene membranes. Earlier work with cells utilizing NaOH electrolyte and cellulosic membranes showed an increase in cycle life by quite a margin,

but failure modes were due to separator deterioration. It is possible that the inert polyethylene membranes will sustain a larger cycle life because of immunity to electrolyte environment.

Additional study of Pb and Al doped ZnO in higher concentrations; 5% to 10% and also with or without the HgO additive, to determine cycle life and corrosion of the zinc electrode.

Methods of charging the zinc electrode such as pulse charging techniques which use A.C. imposed on D.C. current which may retard shape change.

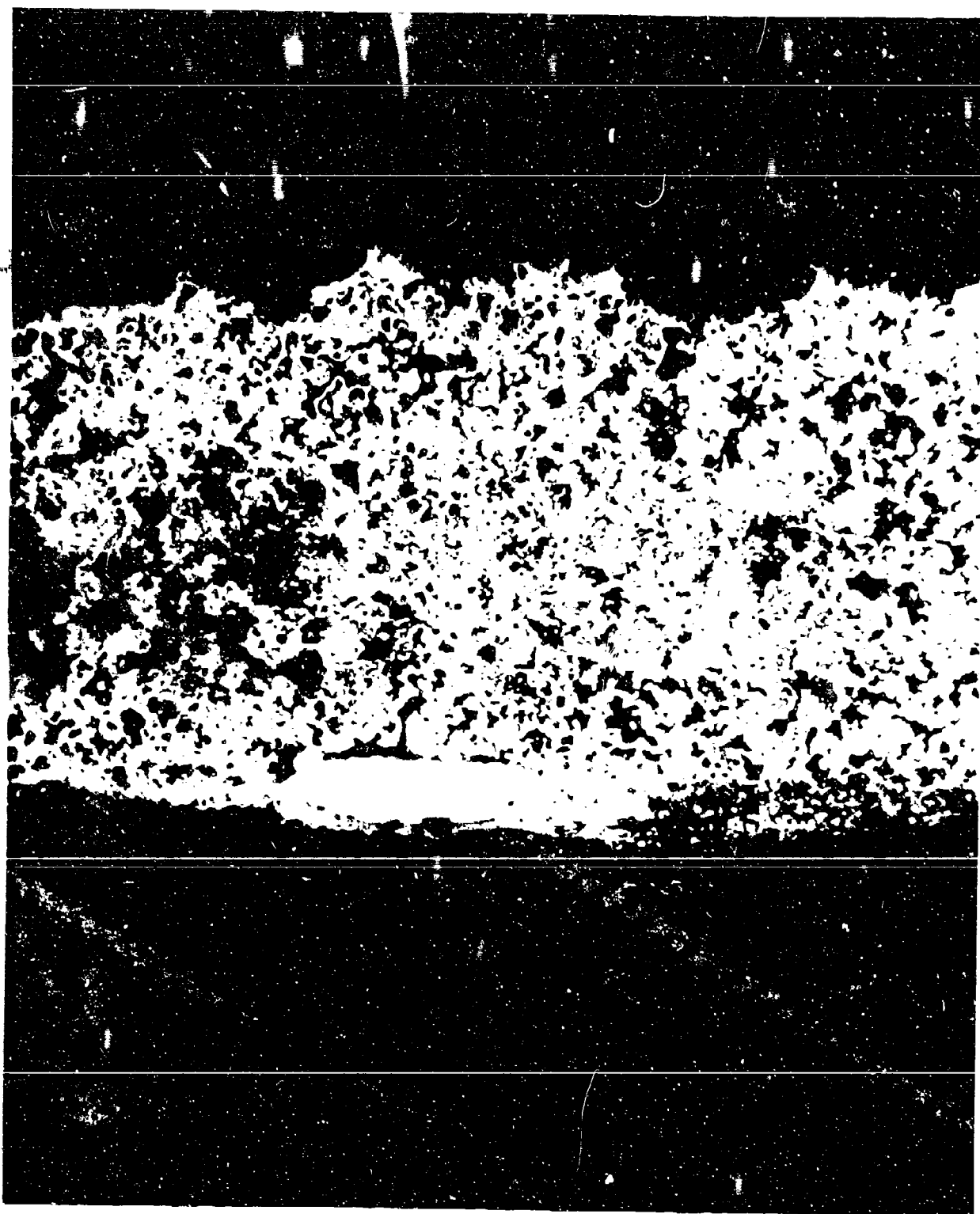


Figure 1. Negative Plate in Control Cell at 140 Cycles
100X

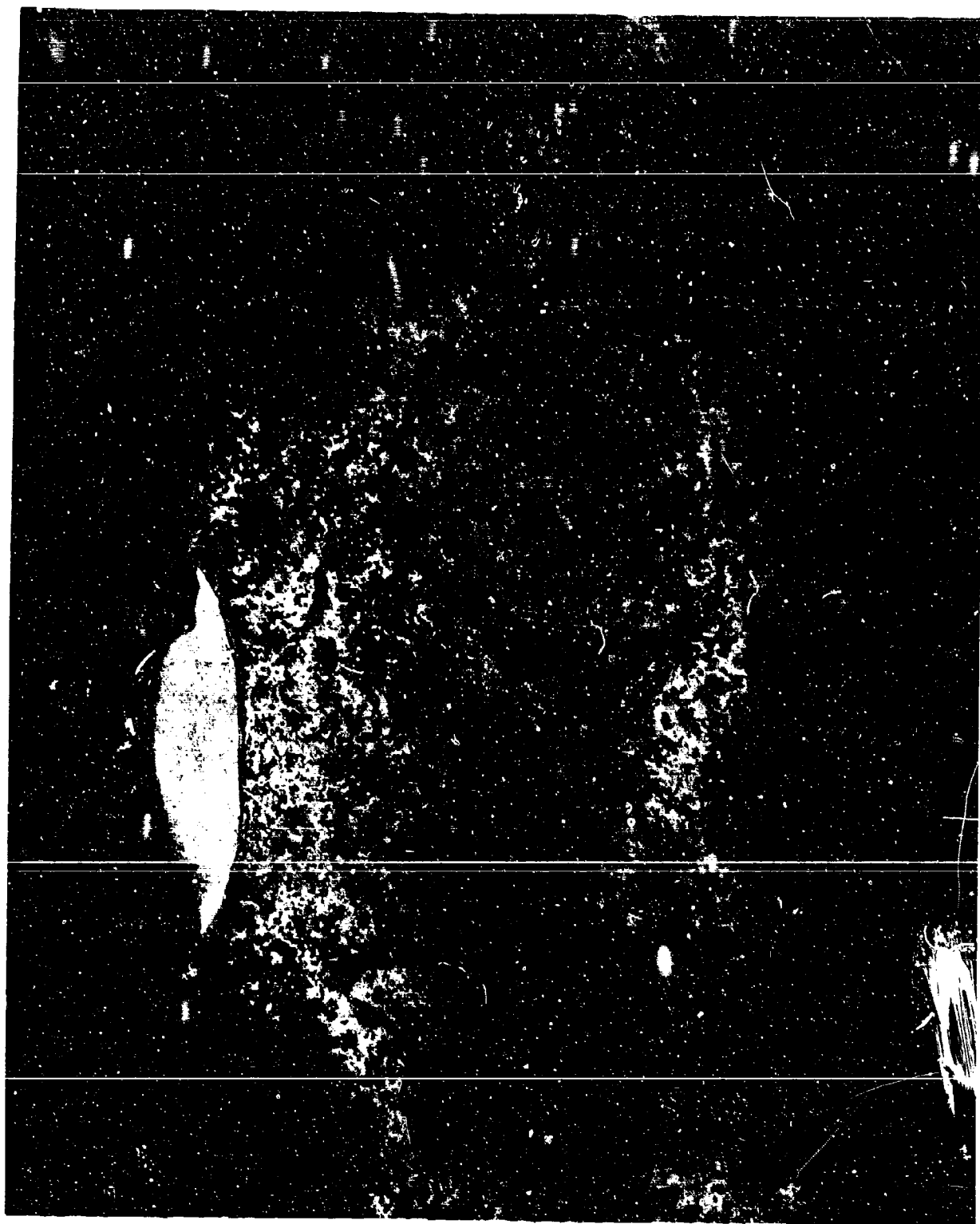


Figure 2. Negative Plate Containing 5% Asbestos Fibers
at 134 Cycles. 140X 140X

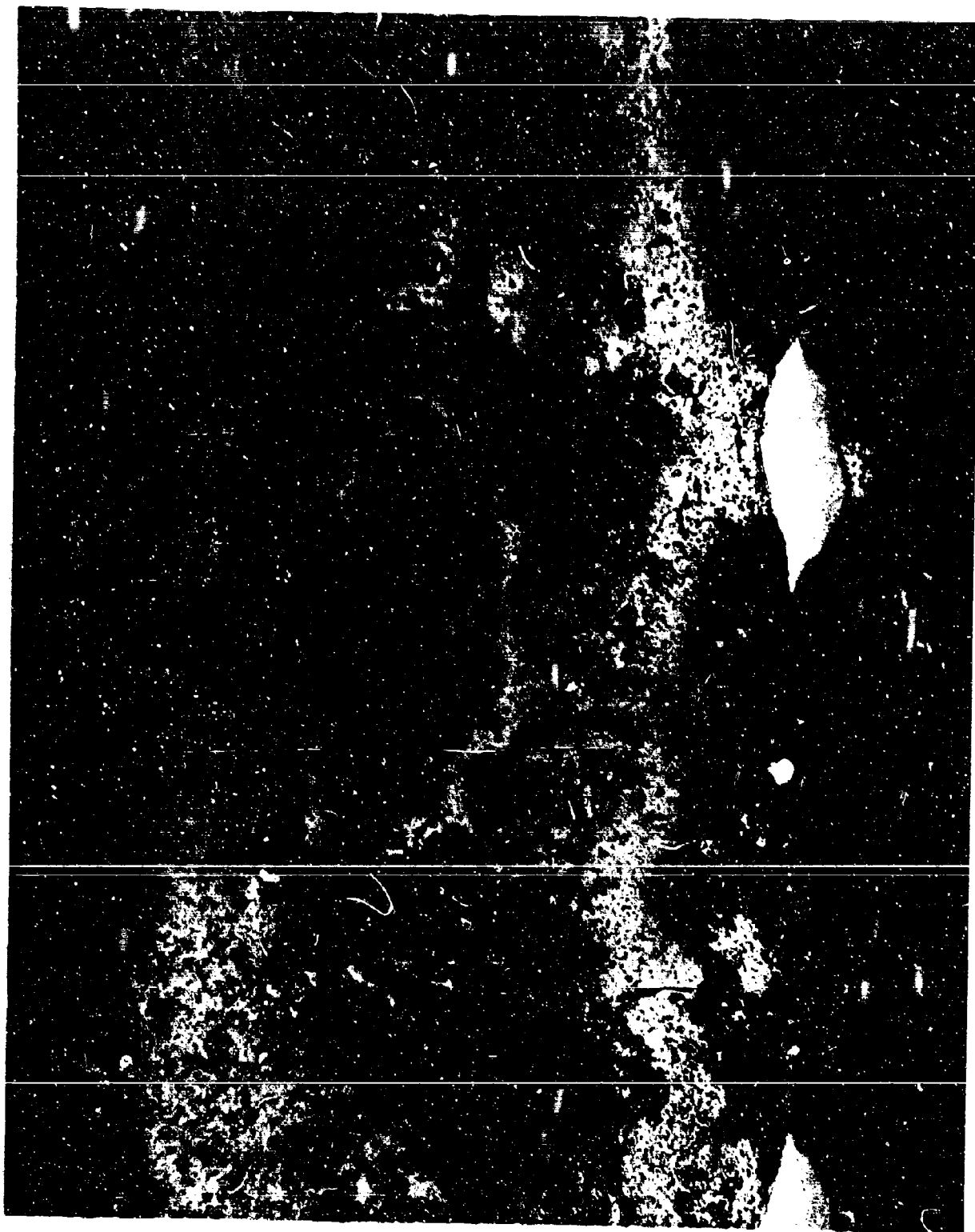


Figure 3. Negative Plate Containing 10% Asbestos Fibers at 134
Cycles 140X



Figure 4. Negative Plate Containing 15% Asbestos Fibers at 134 Cycles.

140X

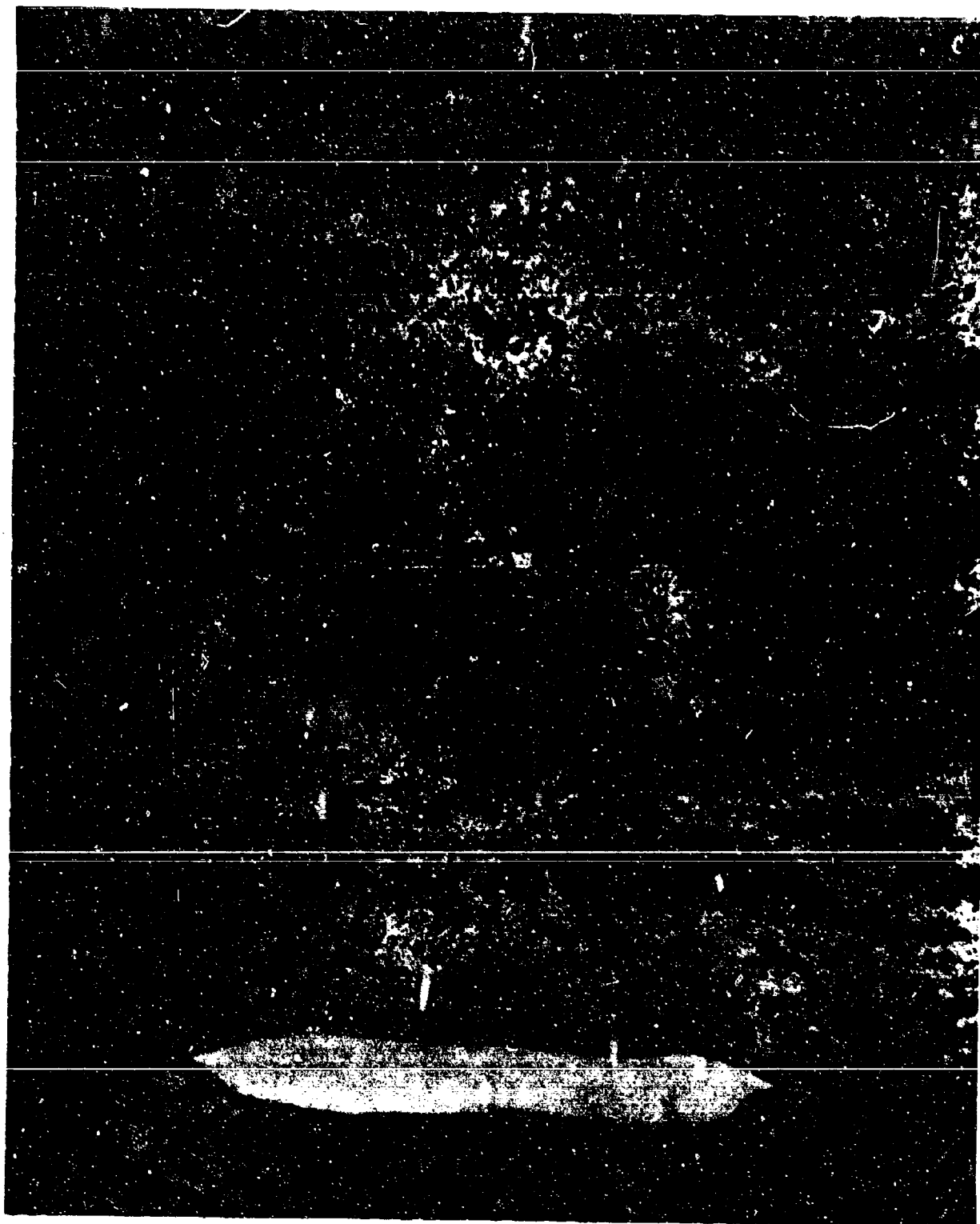


Figure 5. Negative Plate Containing 5% FSC Fibers at 146 Cycles
140X



Figure 6. Negative Plate Containing 10% FSC Fibers at 146 Cycles
140X

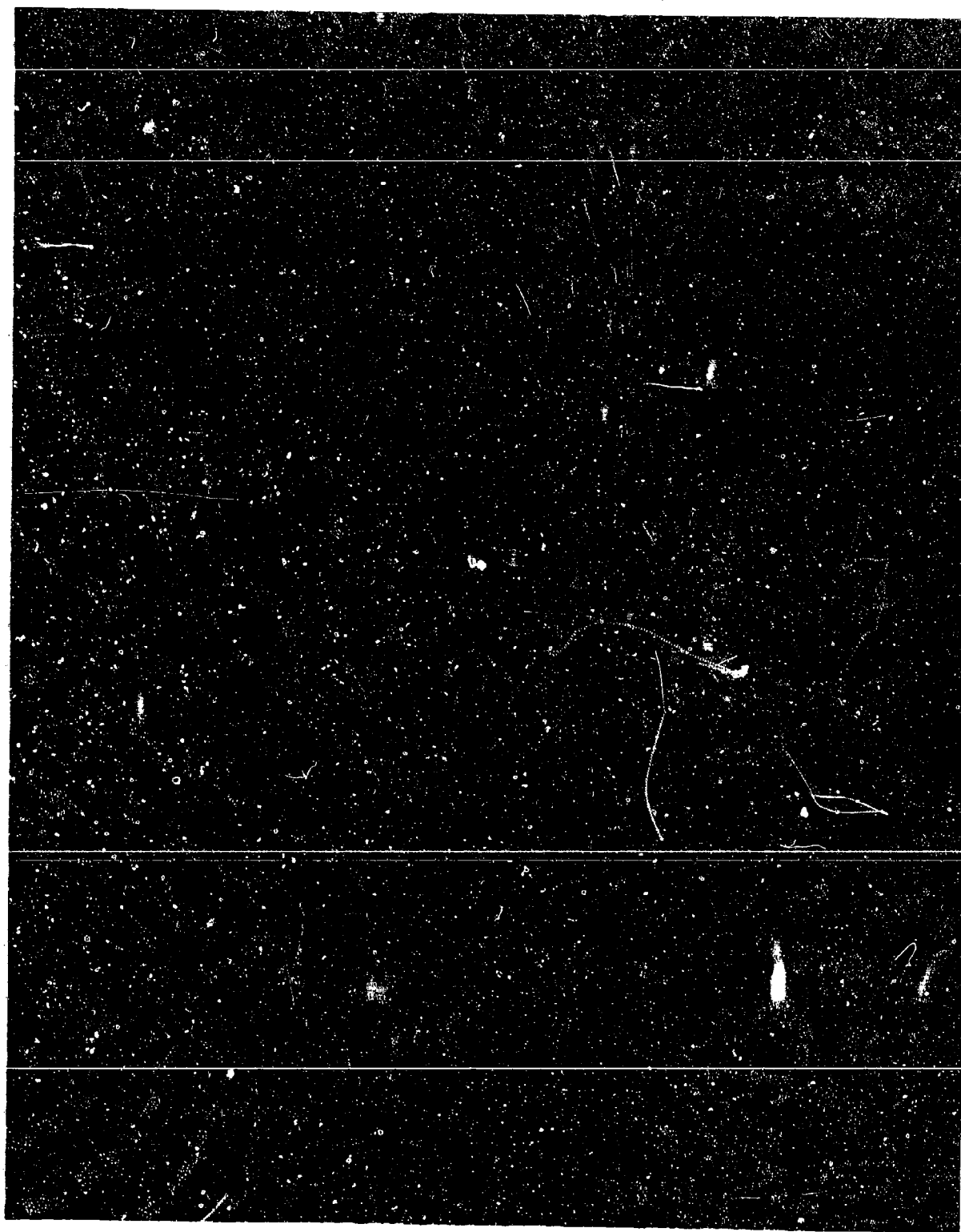


Figure 7. Negative Plate Containing 15% FSC Fibers at 146 Cycles
-68- 140X

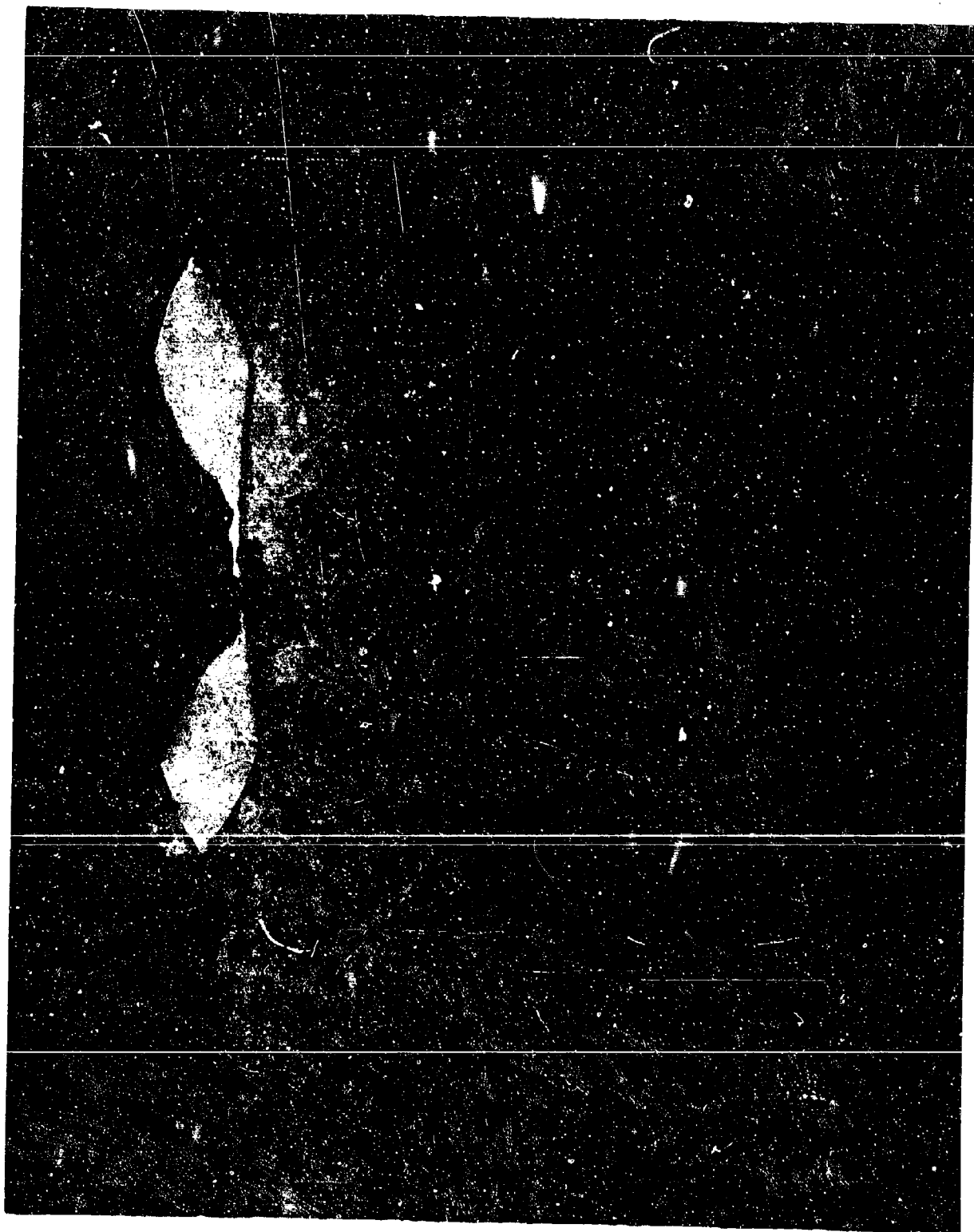


Figure 8. Negative Plate Containing 5% Zinc Fibers at 171 Cycles
140X

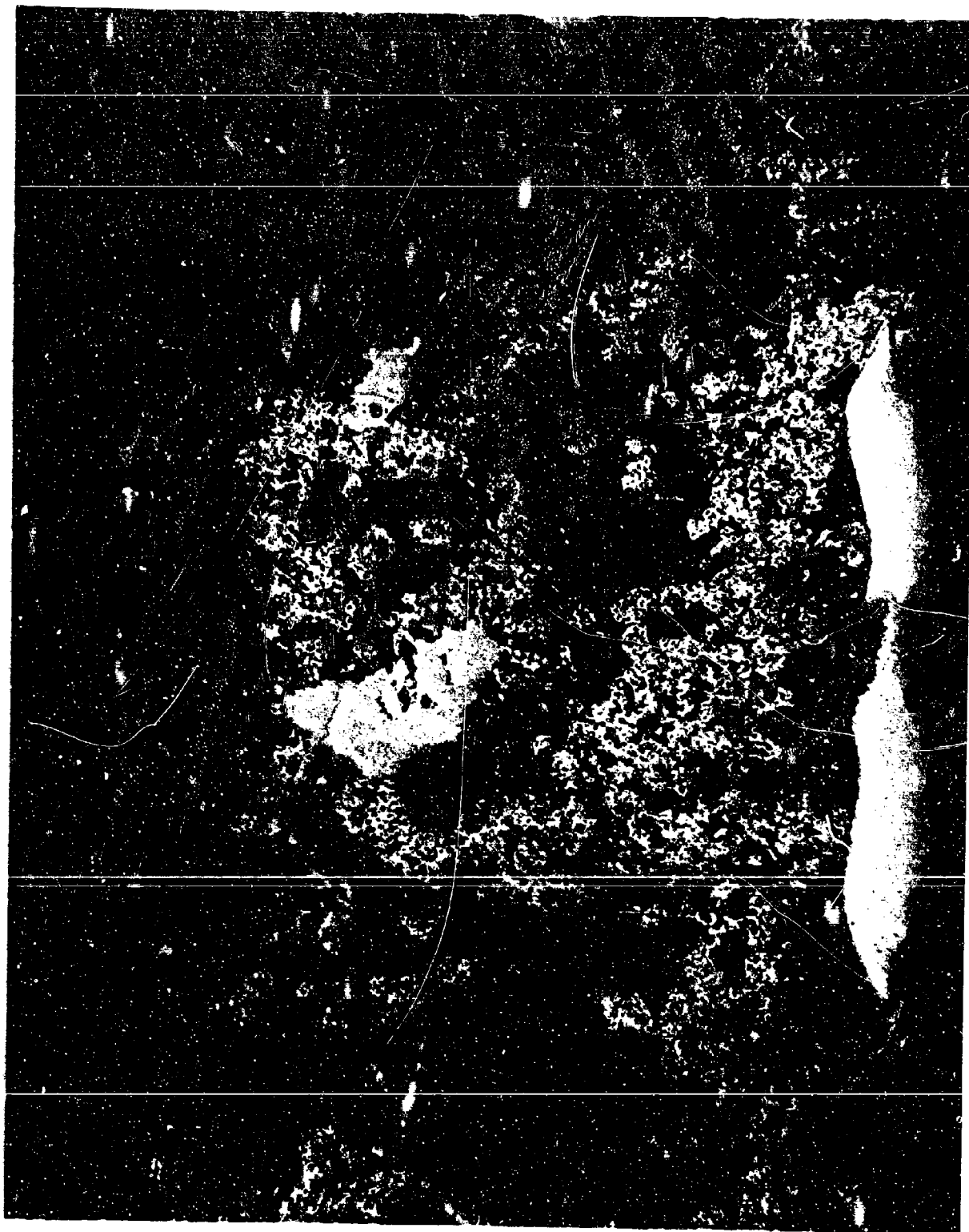


Figure 9. Negative Plate Containing 10% Zinc Fibers at 108 Cycles
140X

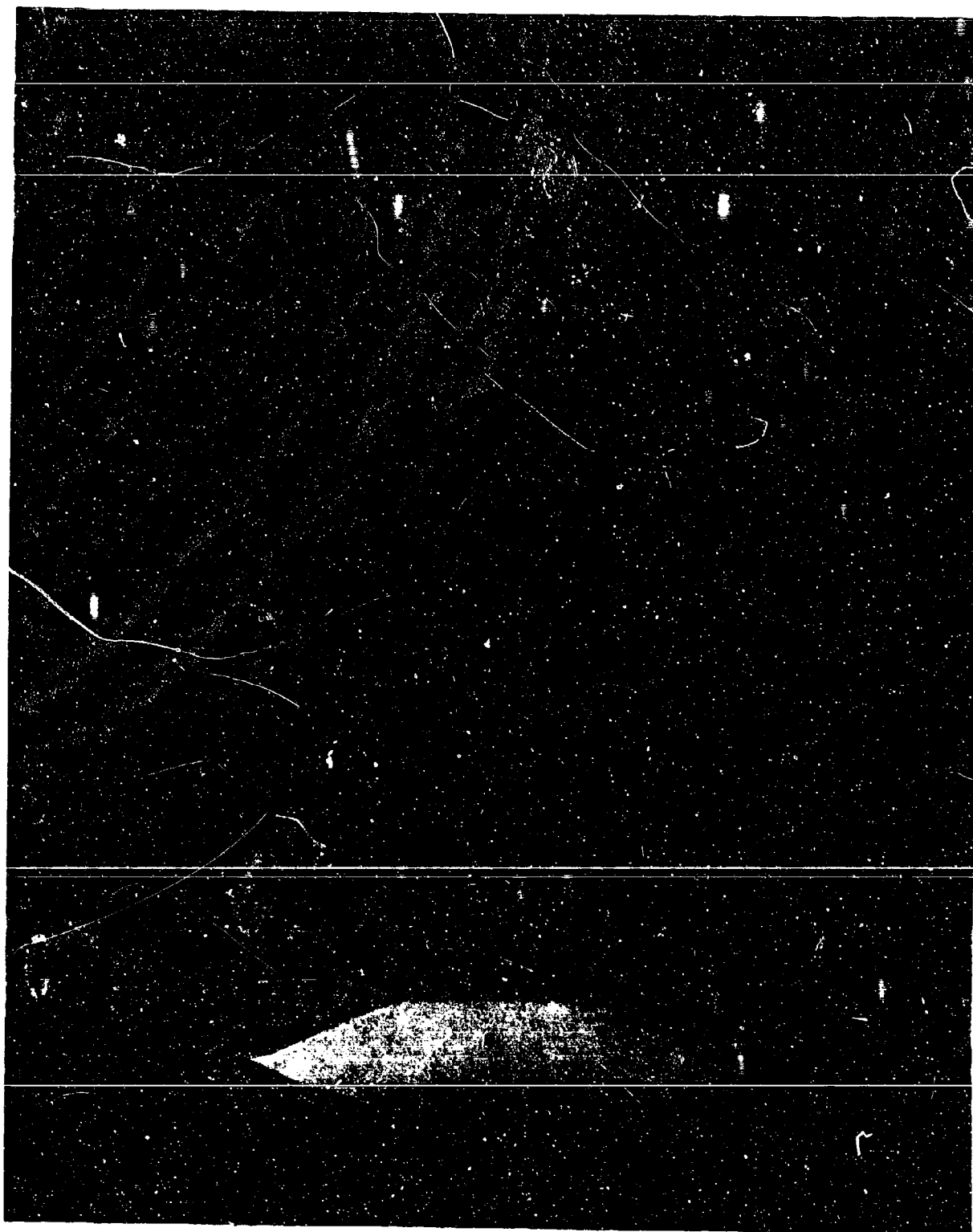


Figure 10. Negative Plate Containing 15% Zinc Fibers at 168 Cycles
140X

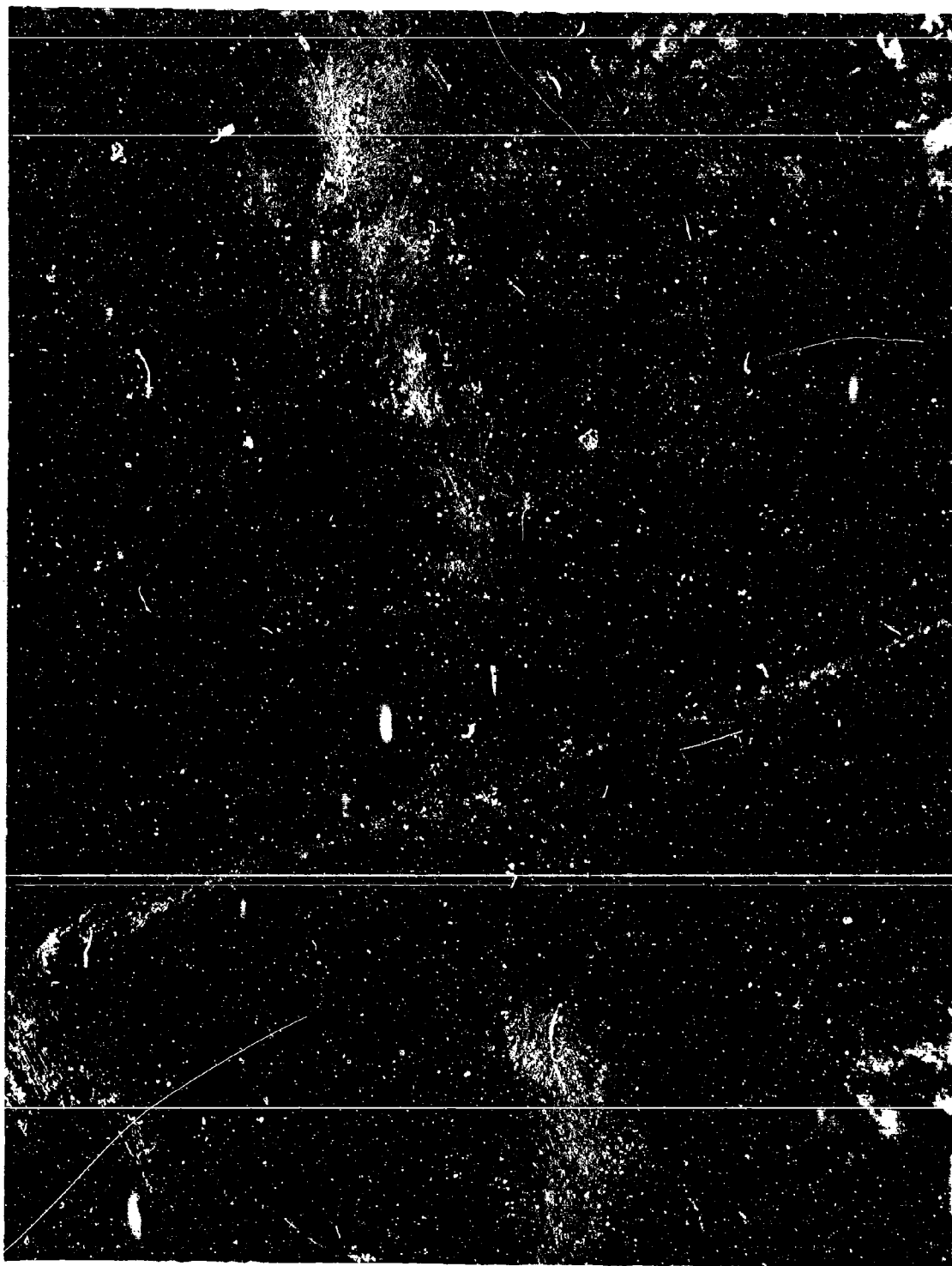


Figure 11. Negative Plate Containing .2% LSA at 84 Cycles

-72

200X

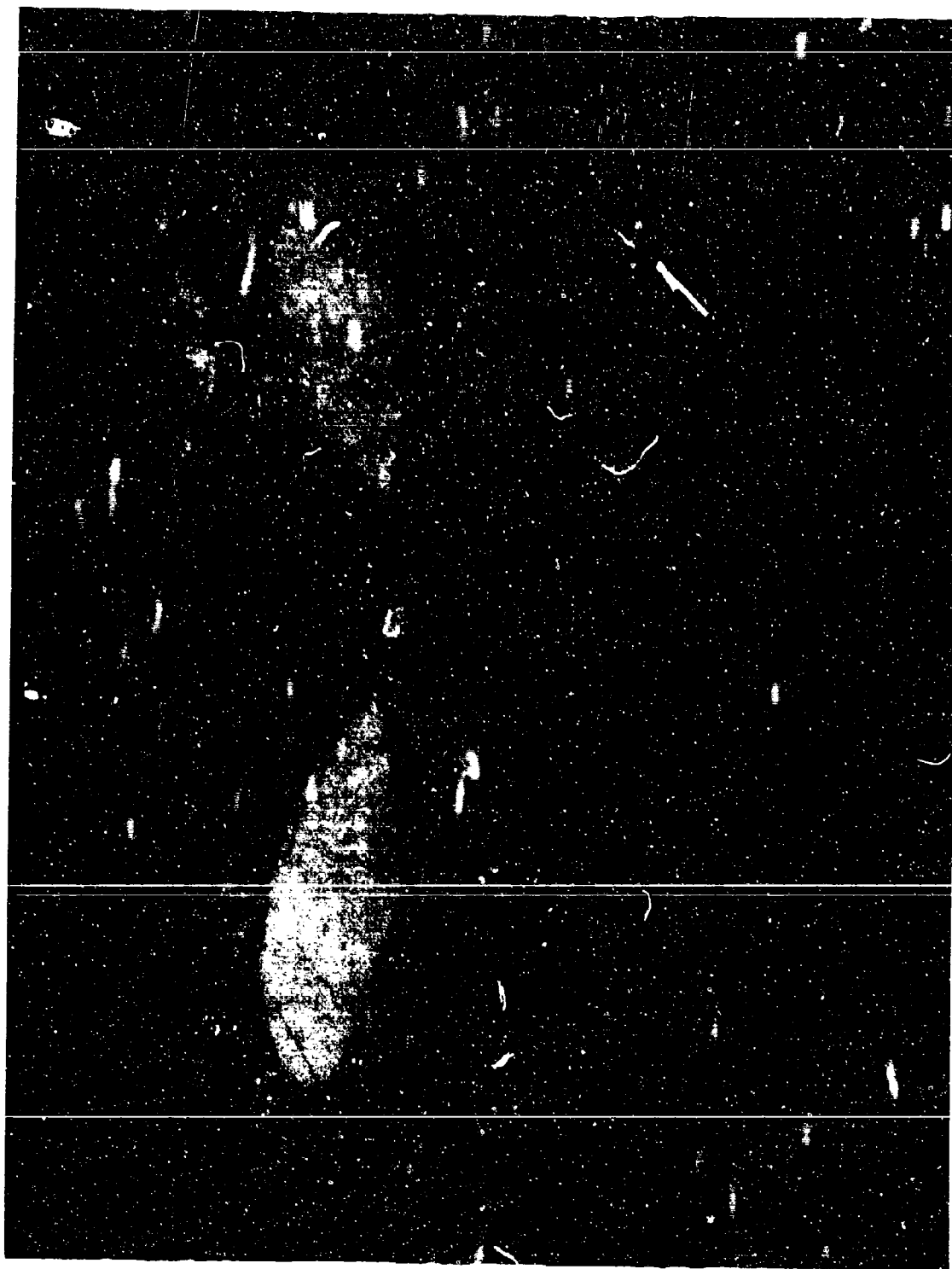


Figure 12. Negative Plate Containing 1.2% LSA at 168 Cycles. 200X



Figure 13. Negative Plate Containing 2% LSA at 144 Cycles. 200X

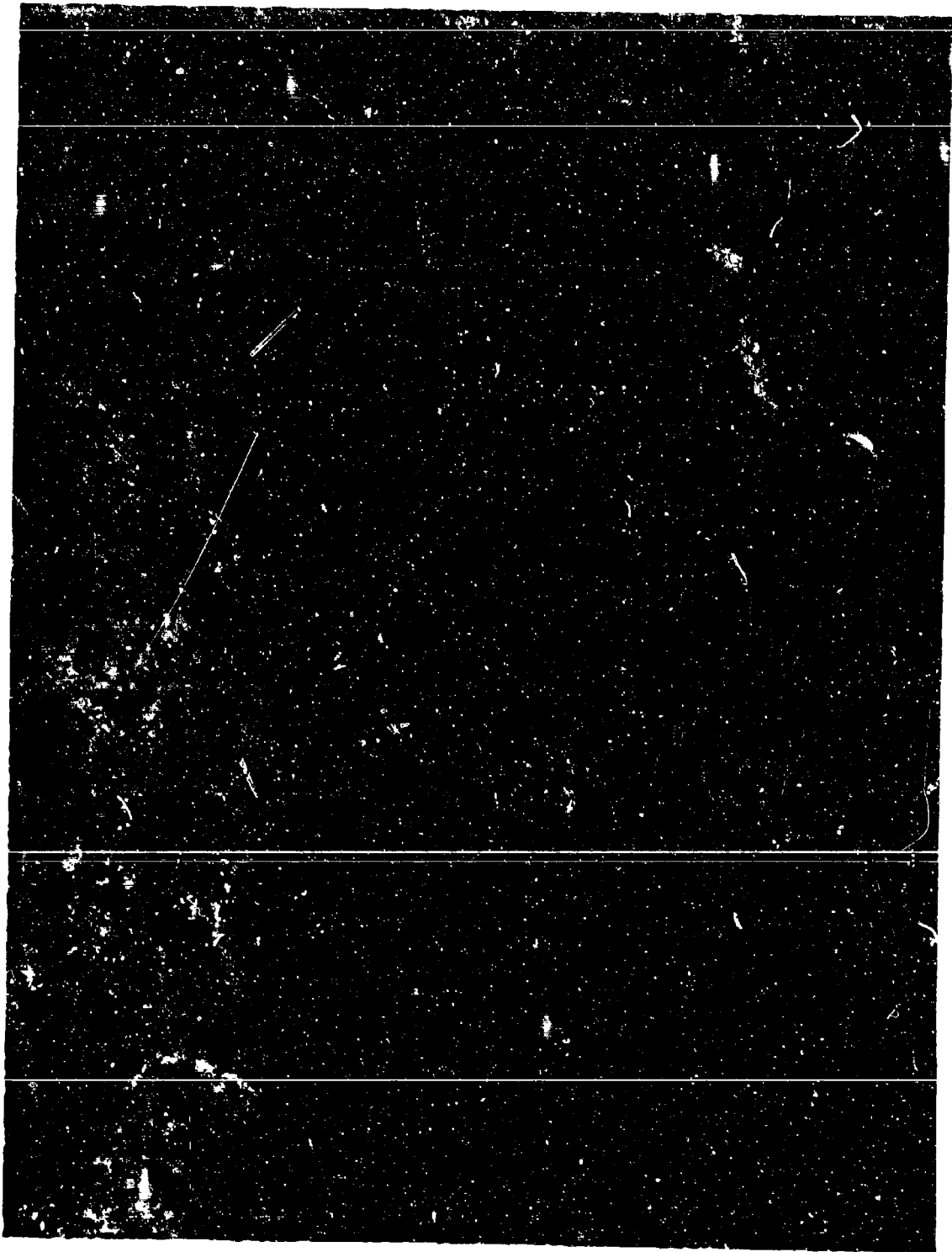


Figure 14. Negative Plate as Control at 157 Cycles

200X

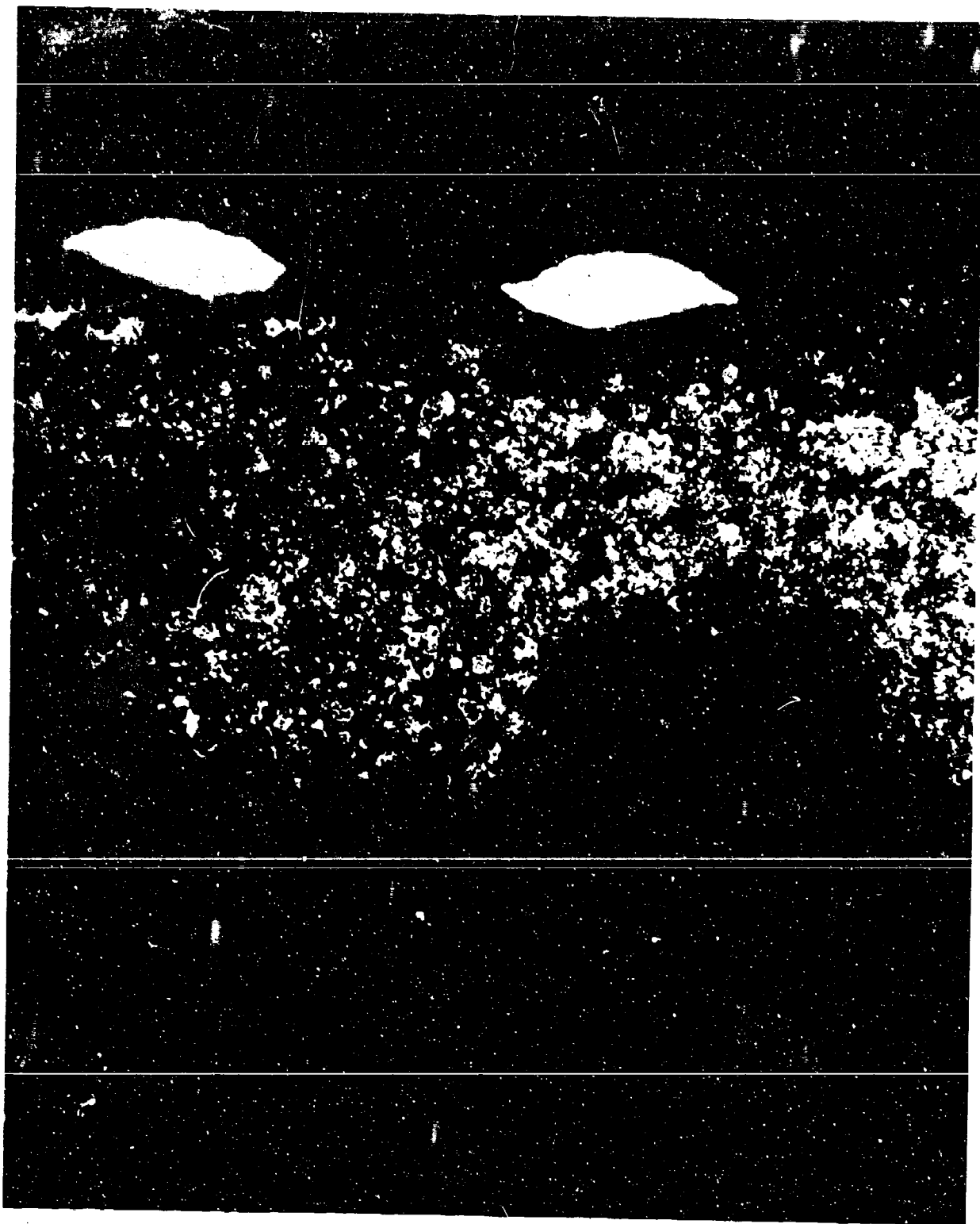


Figure 15. Negative Plate Containing 1% Cotton Fibers at 144 Cycles
100X

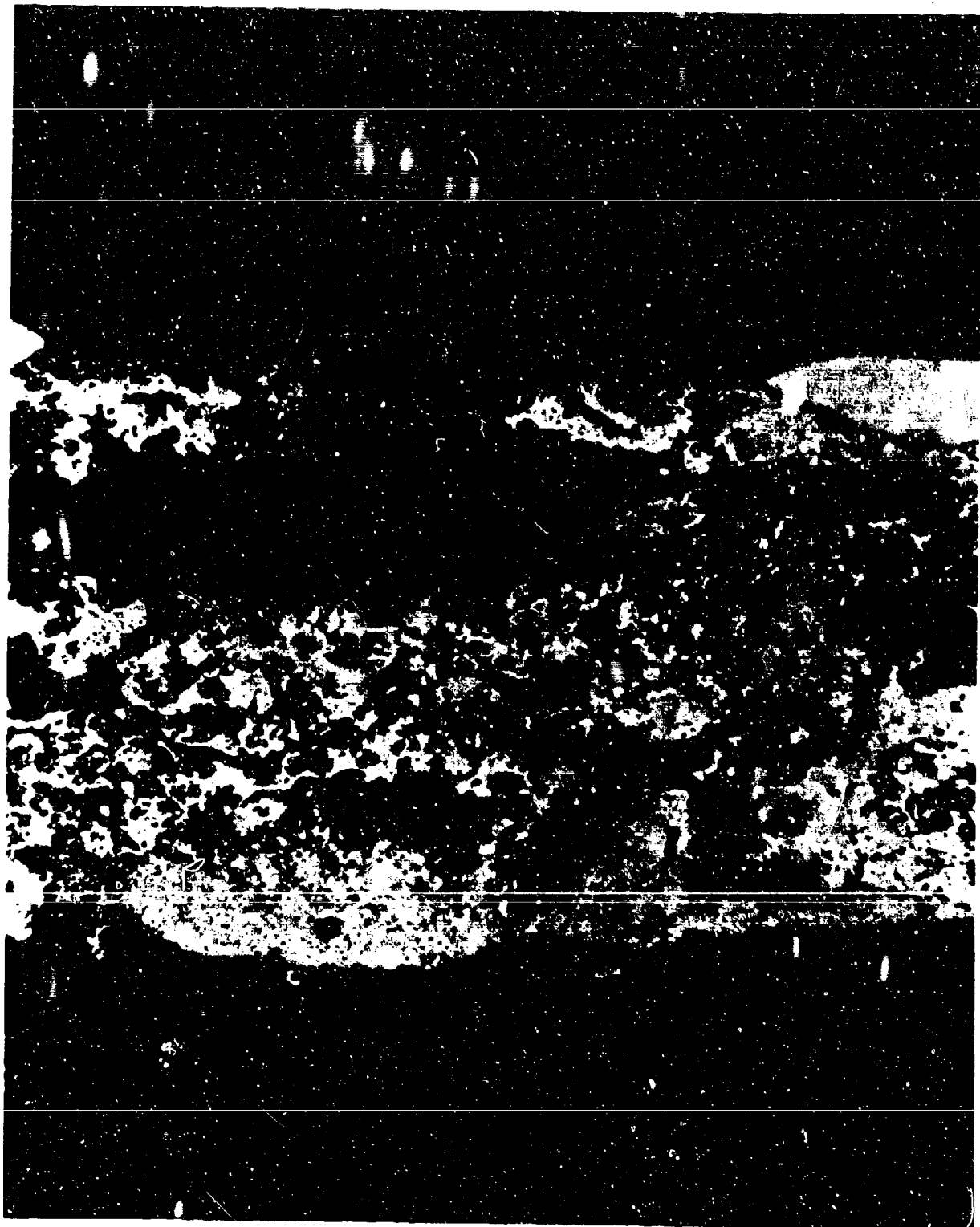


Figure 16. Negative Plate Containing 3% Cotton Fibers at 144 Cycles
100X

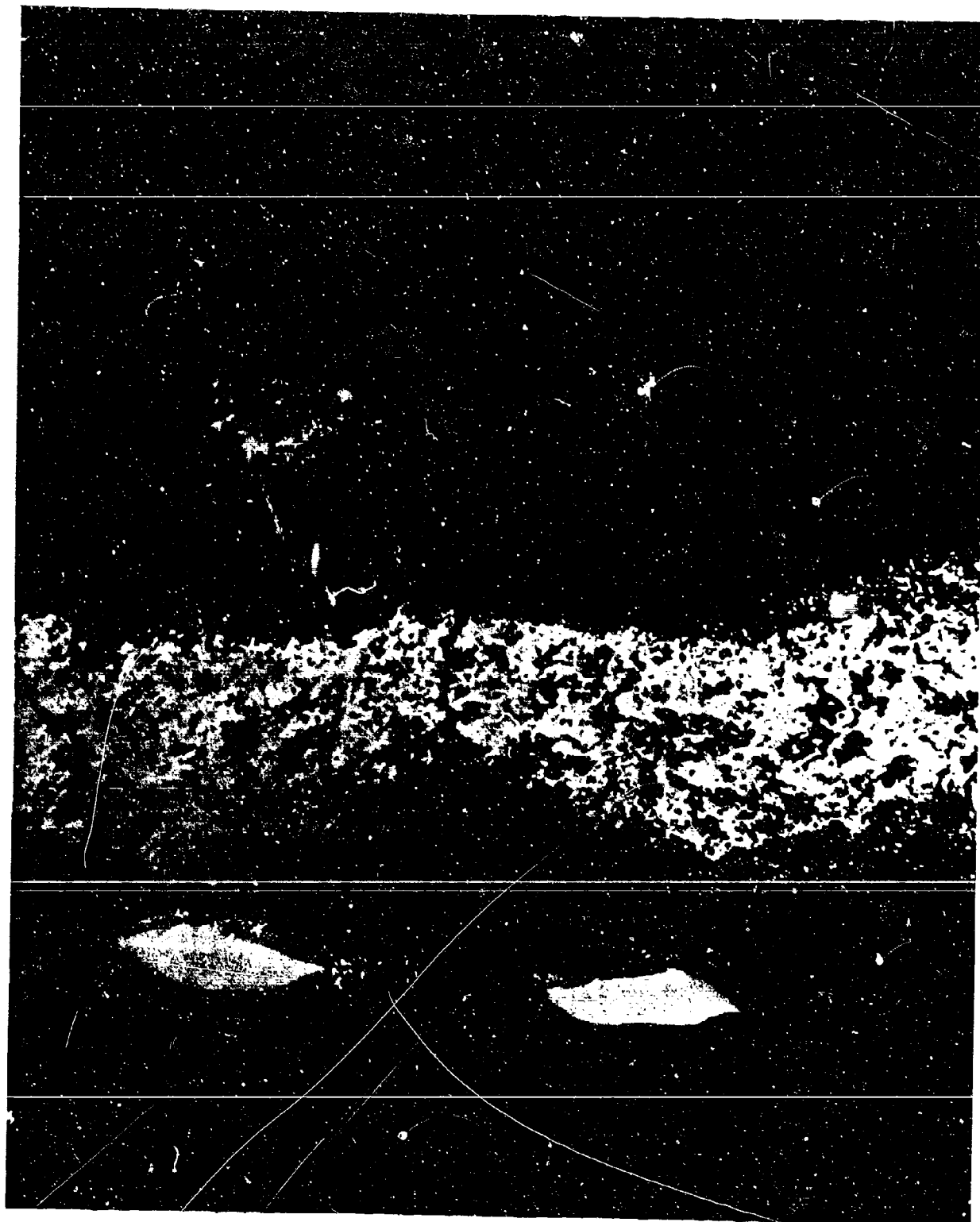


Figure 17. Negative Plate Containing 5% Cotton Fibers at 144 Cycles
-78- 100X

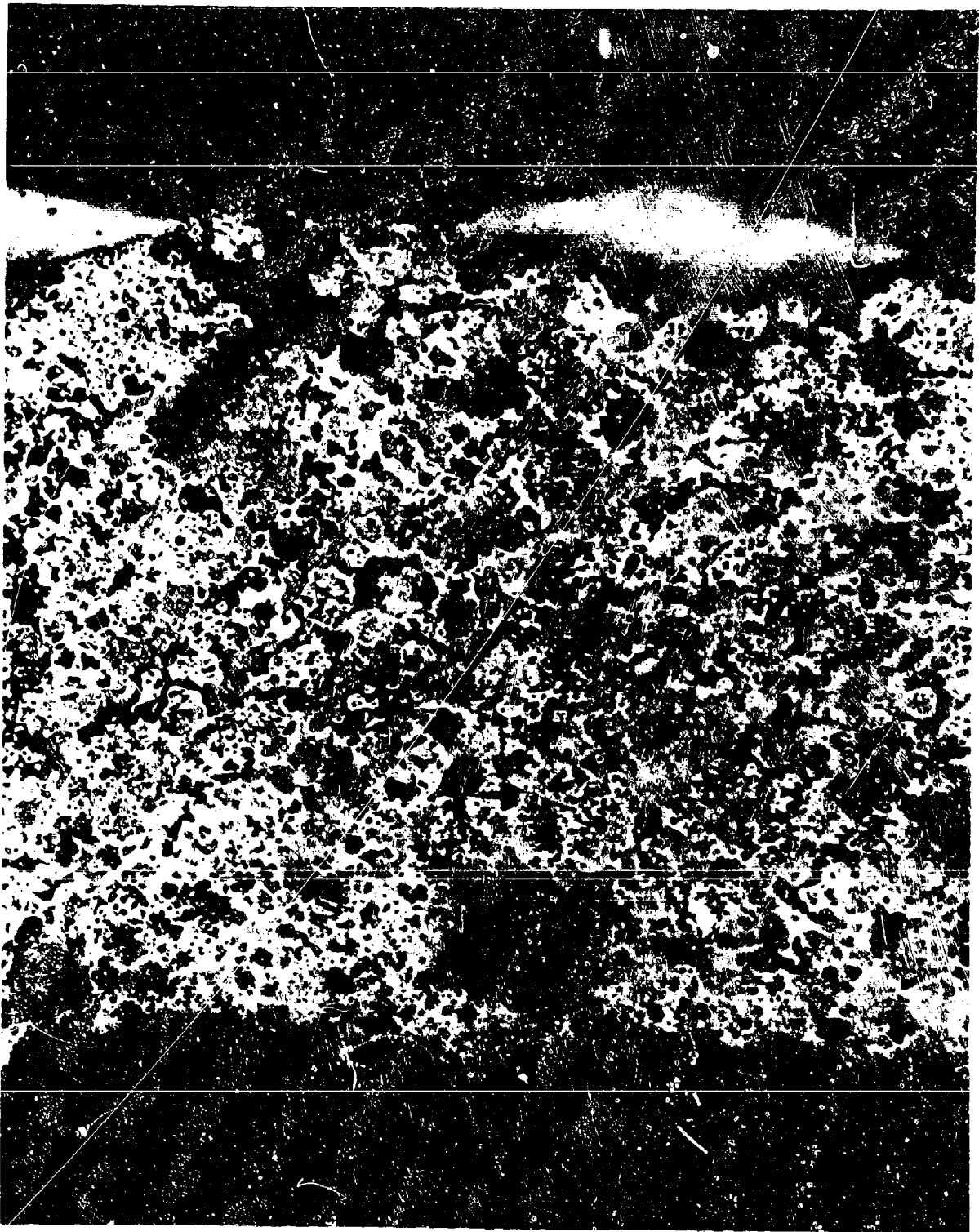


Figure 18. Photomicrograph of a Negative Plate Containing 15% AVICEL
-79- 200X

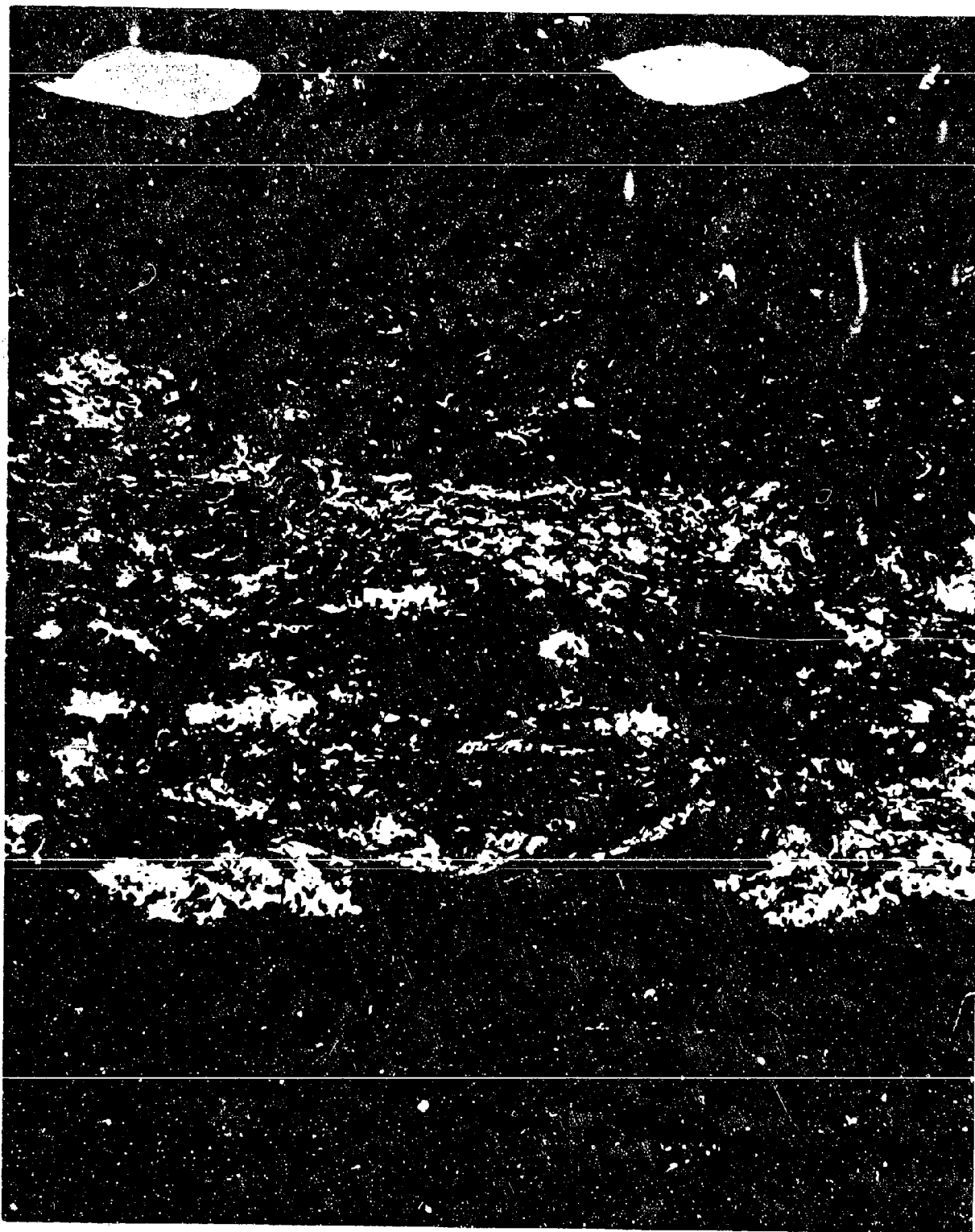


Figure 19. Negative Plate Containing 30% Cellulosic Fibers at 300 Cycles
100X

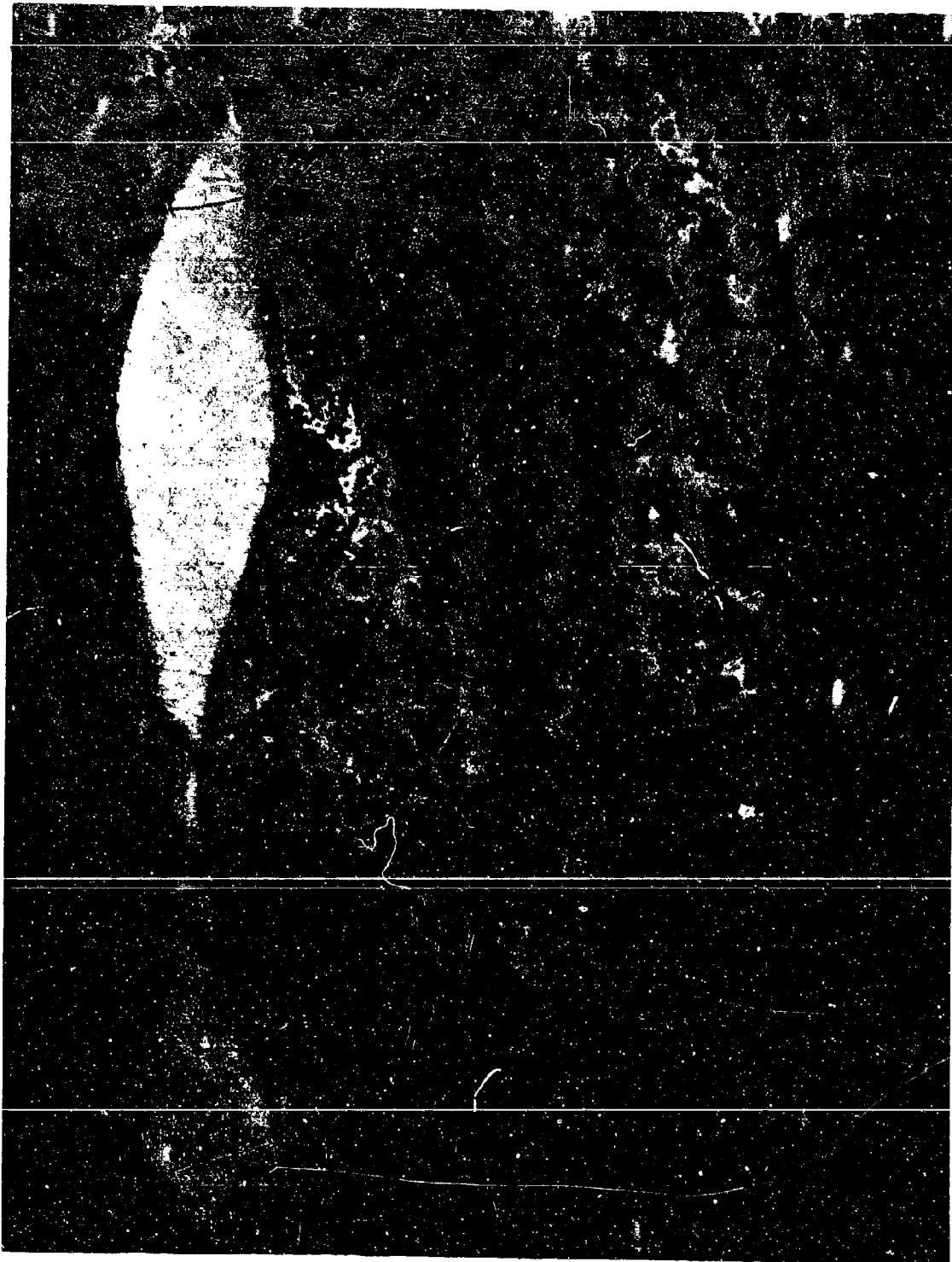


Figure 20. Negative Plate Containing .15% BC-420 at 168 Cycles 200X
-81-



Figure 21. Negative Plate Containing 1% BC-420 at 168 Cycles.

200X

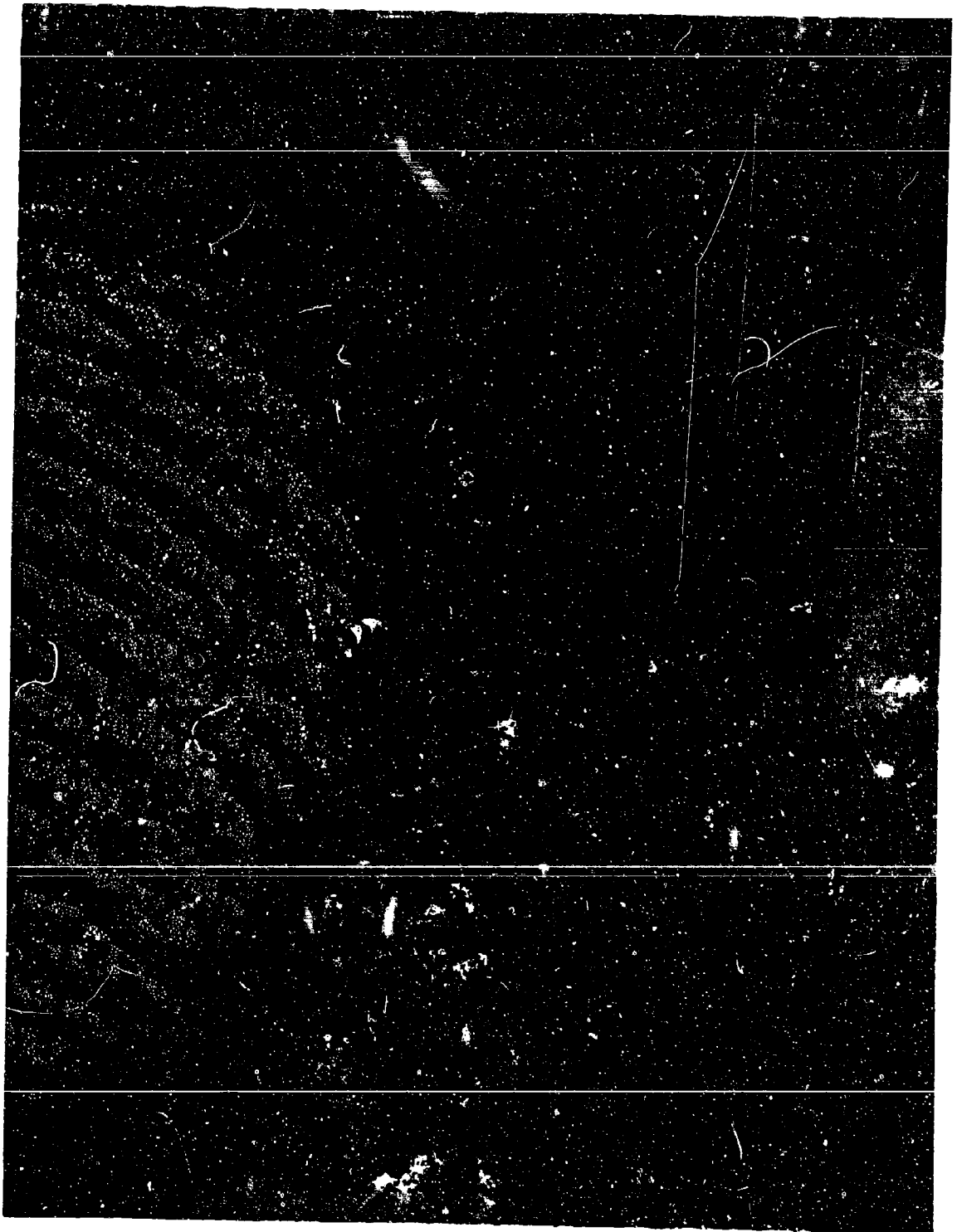


Figure 22. Negative Plate Containing .15% BC-720 at 120 Cycles 200X

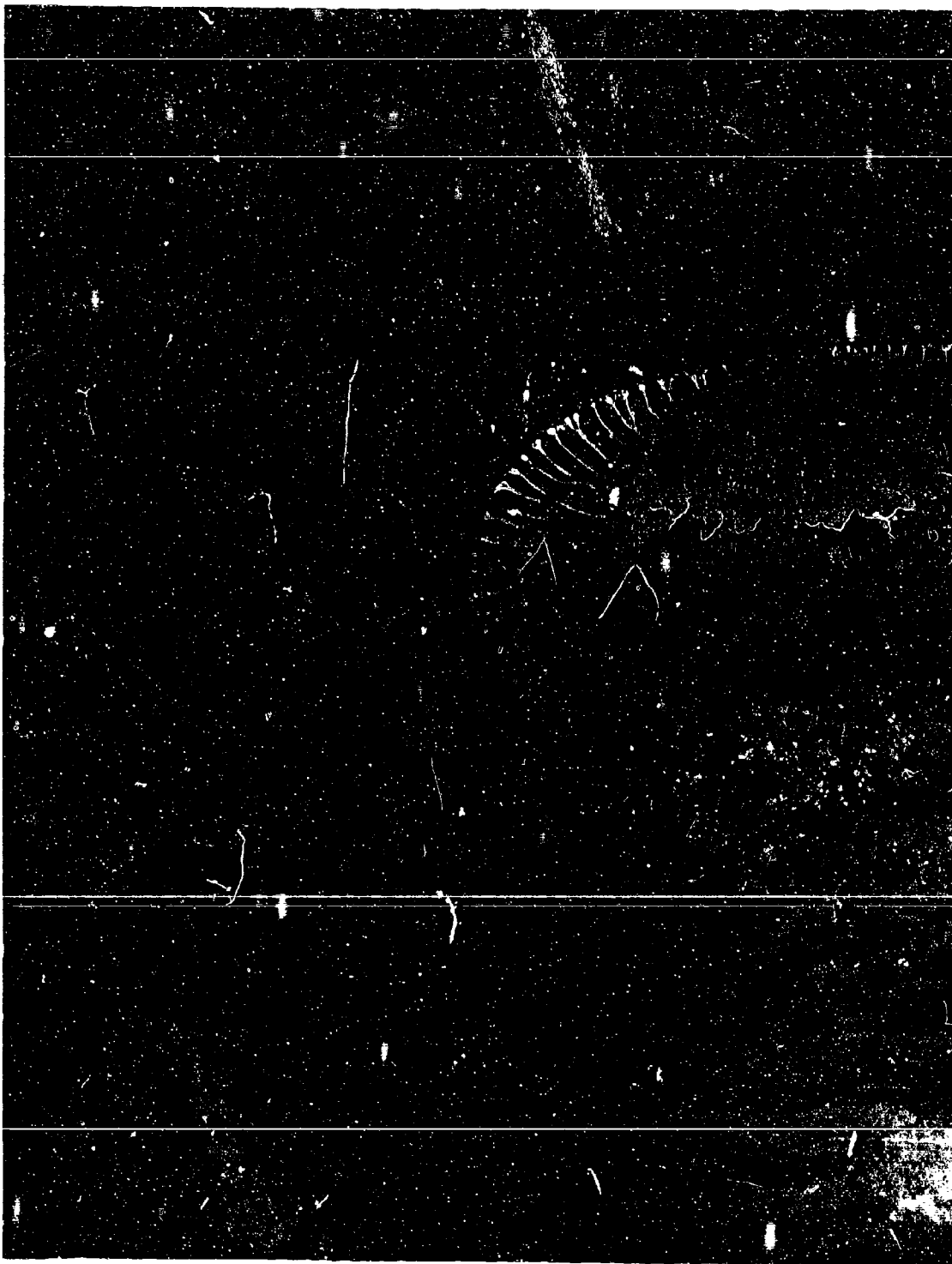


Figure 23. Negative Plate Containing 1% BC-720 at 108 Cycles

200X

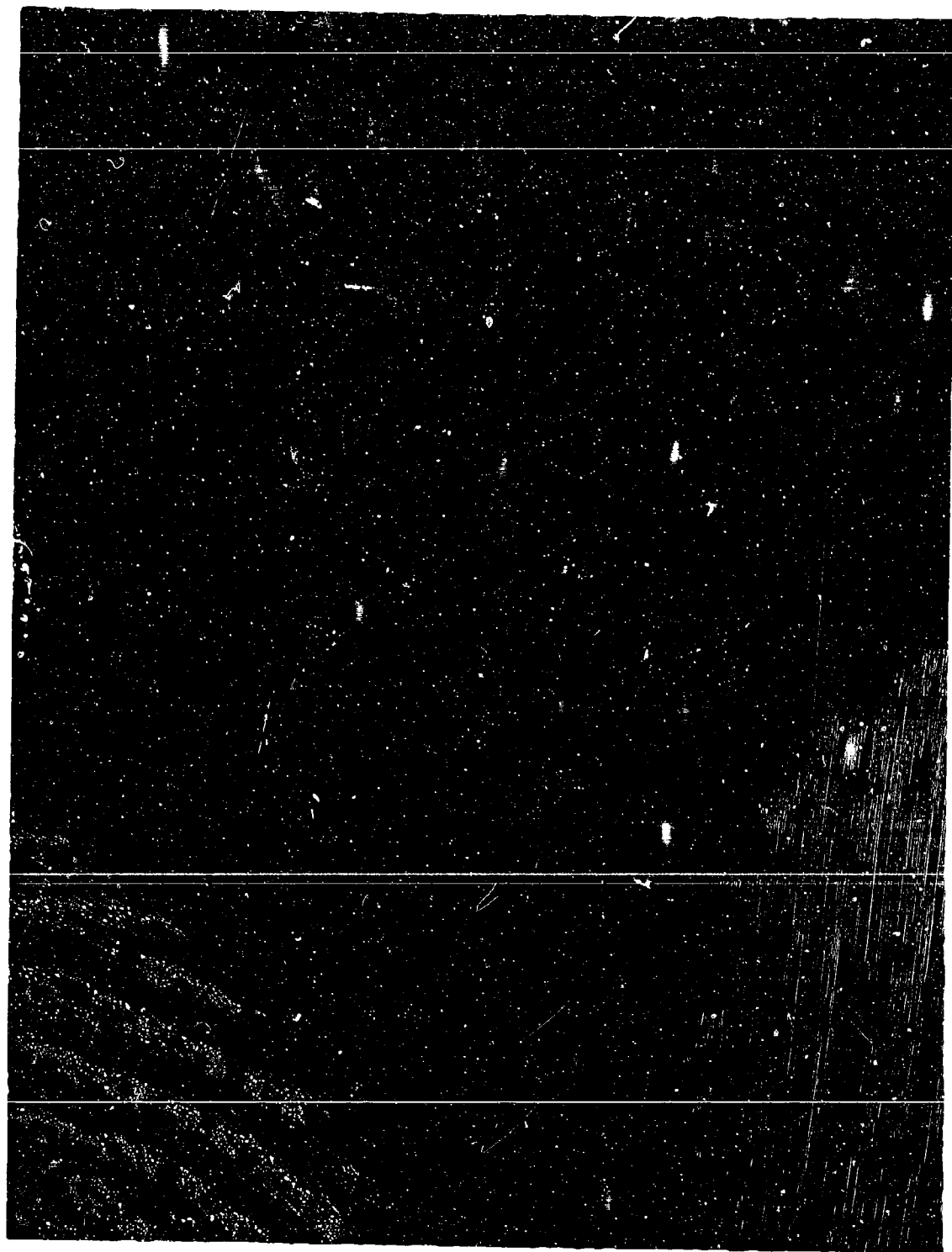


Figure 24. Negative Plate Containing .15% 840 at 168 Cycles

200X

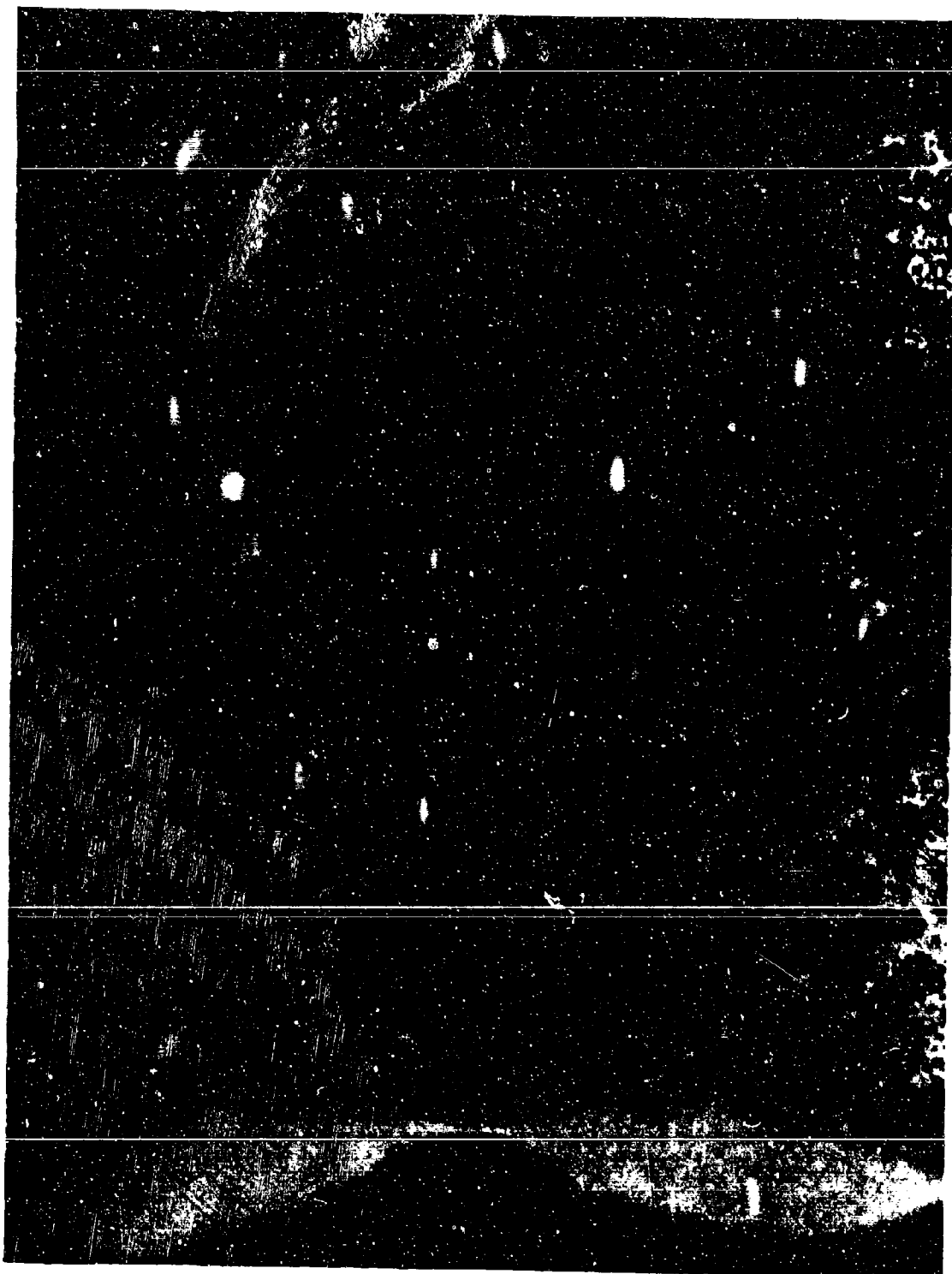


Figure 25. Negative Plate Containing 1% BC-840 at 144 Cycles

200X

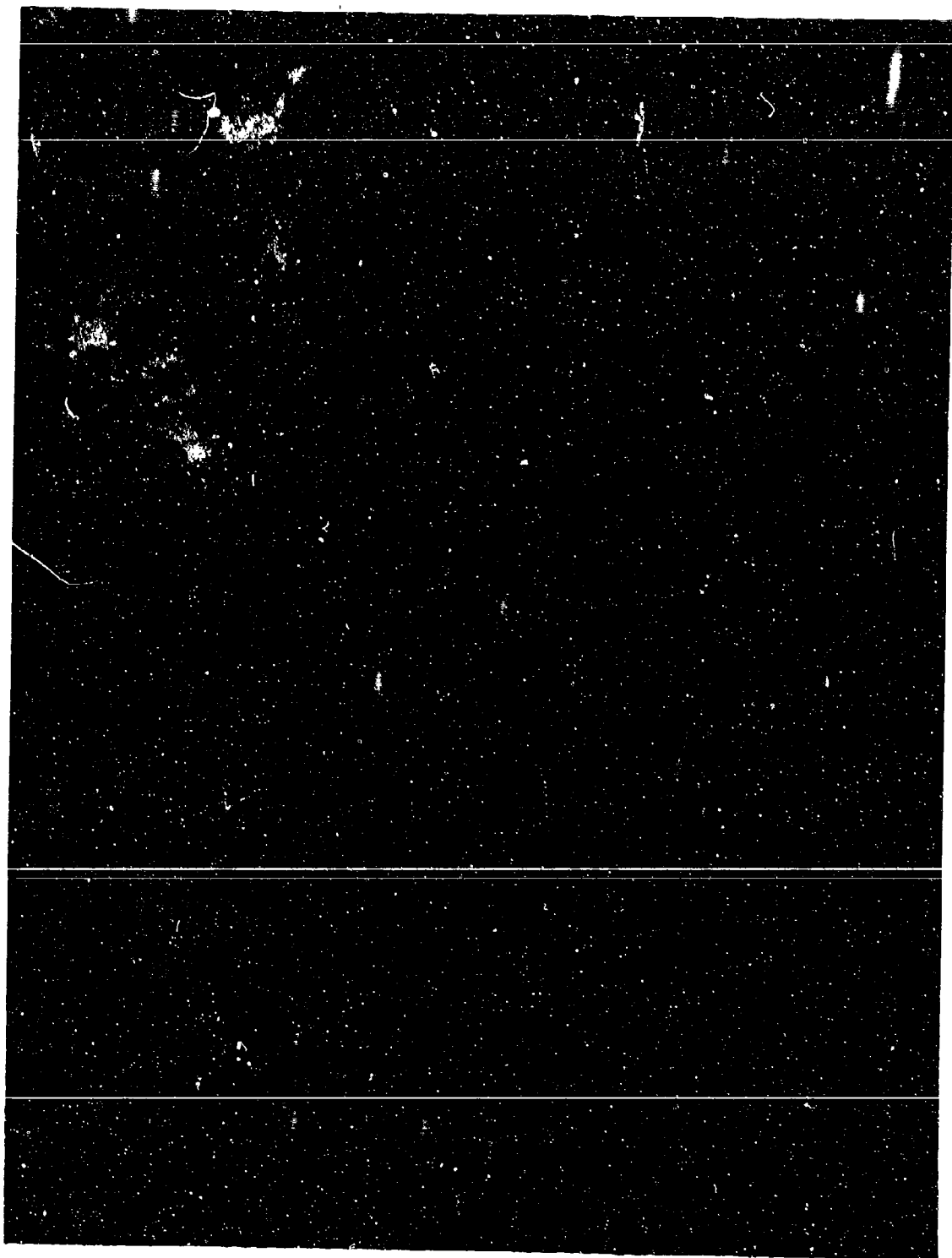


Figure 26. Negative Plate Containing .5% BC-610 at 168 Cycles.
Control Cell

200X



Figure 27. Negative Plate Containing .15% BC-610 at 76 Cycles at 40°F
-88- 200X

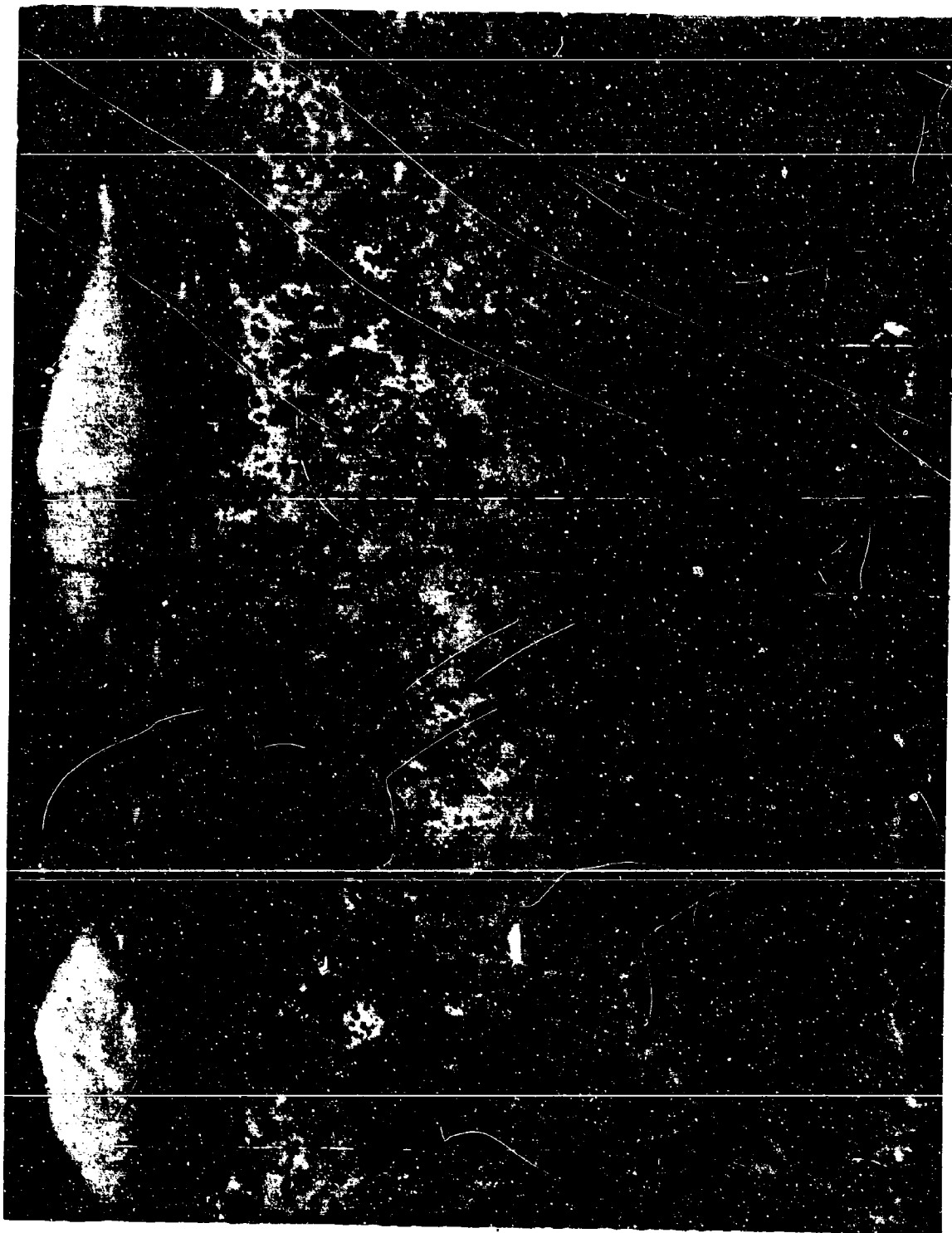


Figure 28. Negative Plate Containing .6% BC-610 at 52 Cycles at 40°F.
-89- 200X

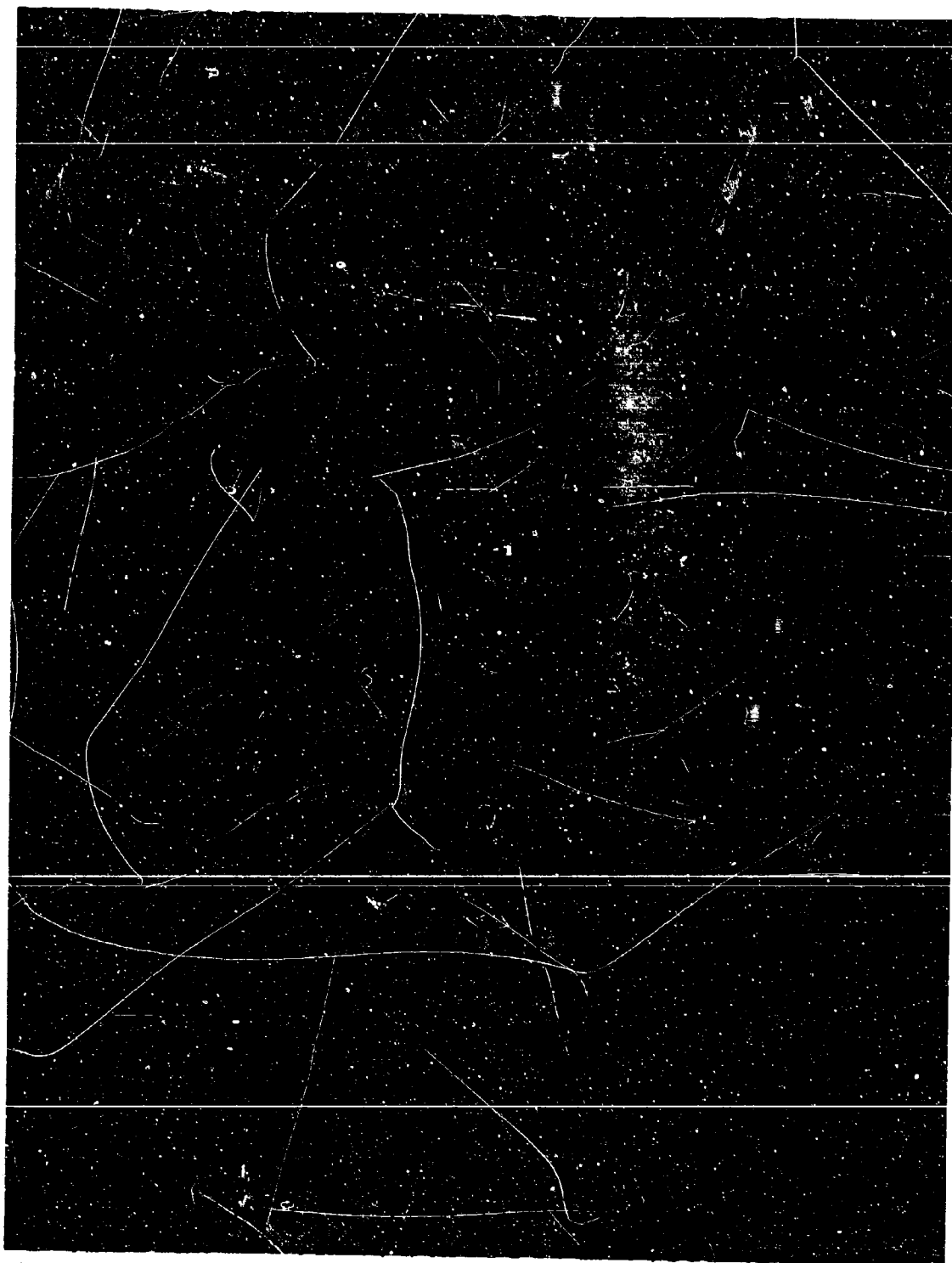


Figure 29. Negative Plate Containing 1% BC-610 at 58 Cycles at 40°F
200X

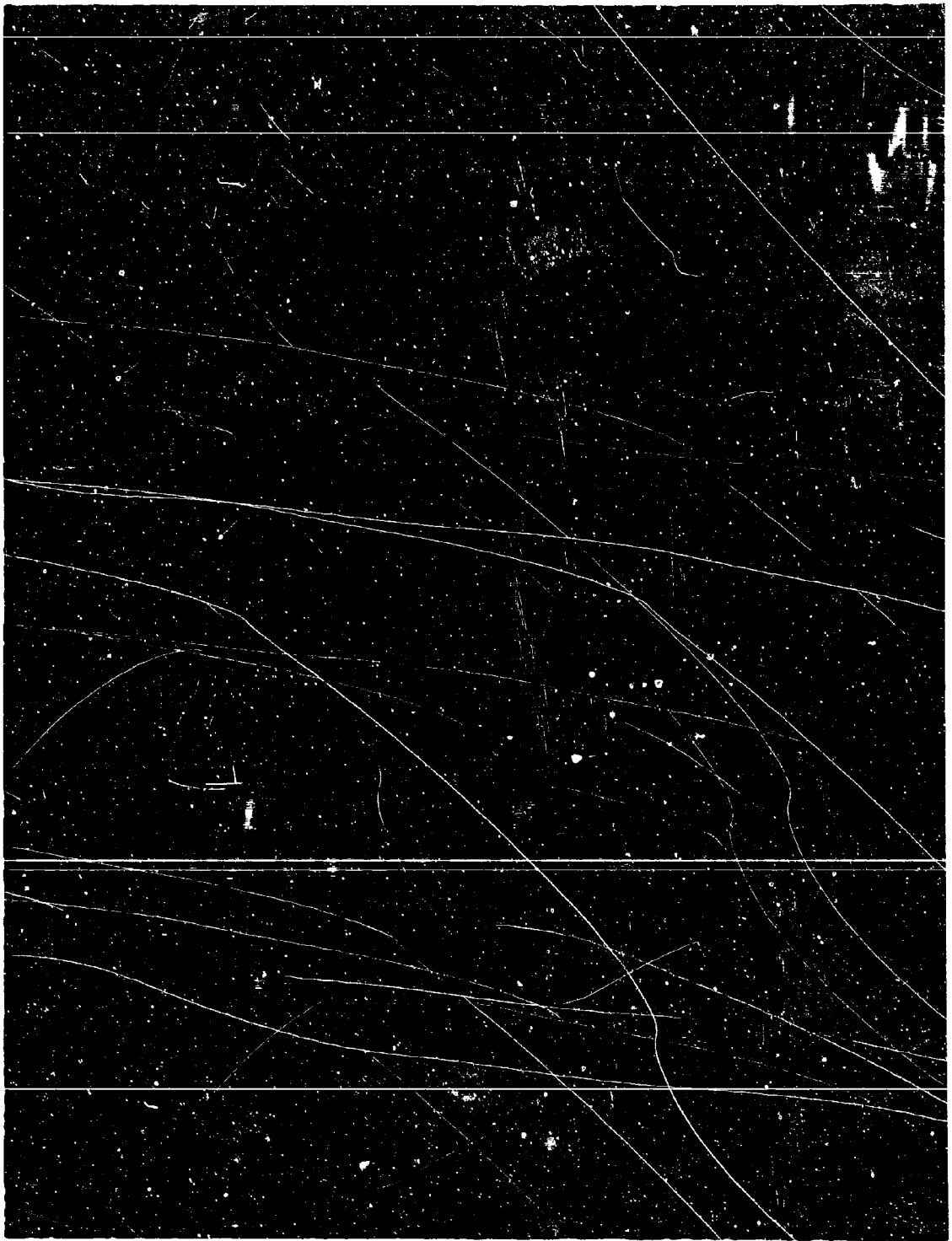


Figure 30. Negative Plate Containing .15% BC-610 at 110 Cycles at 100°F
200X

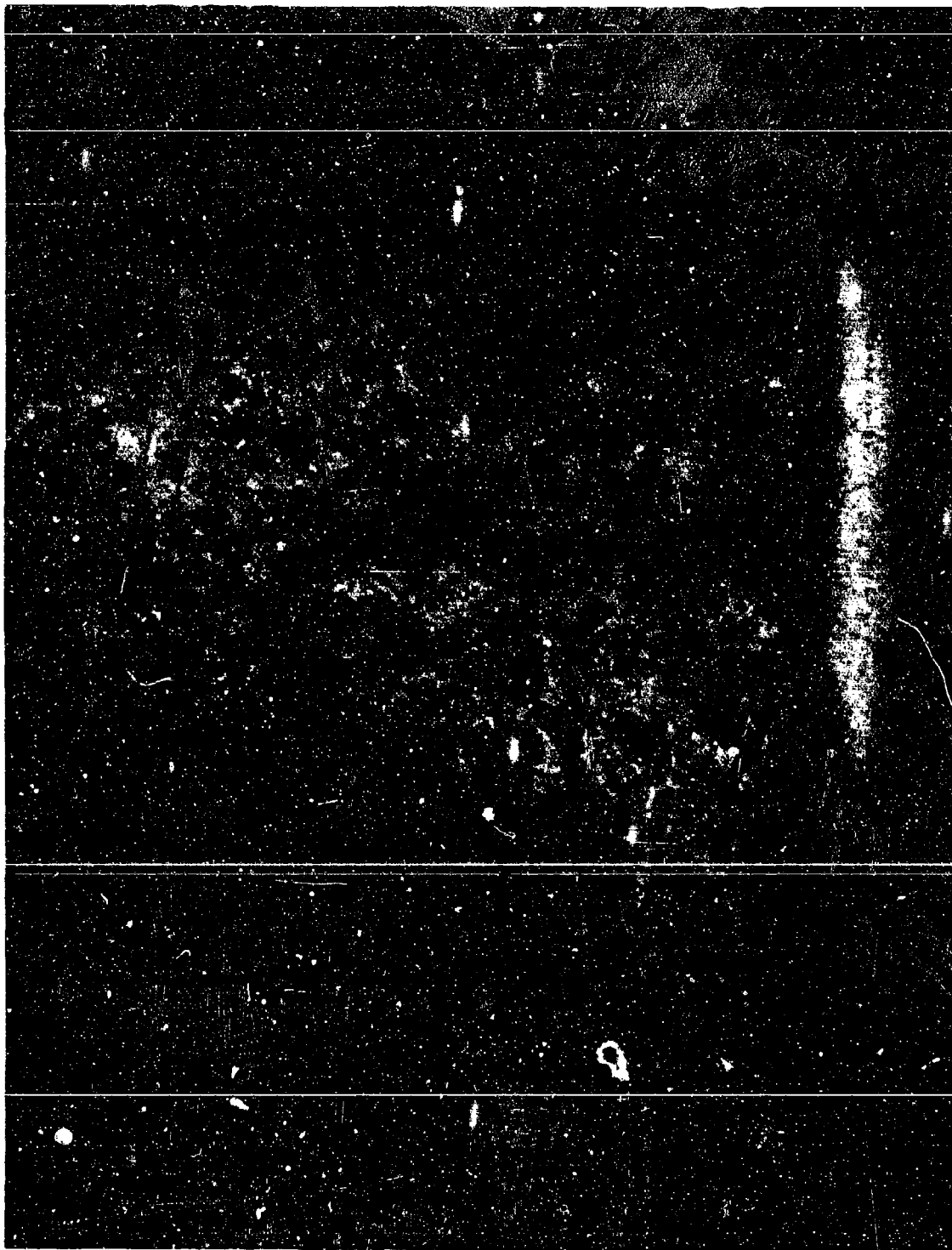


Figure 31. Negative Plate Containing .6% BC-610 at 121 Cycles at 100°F
200X

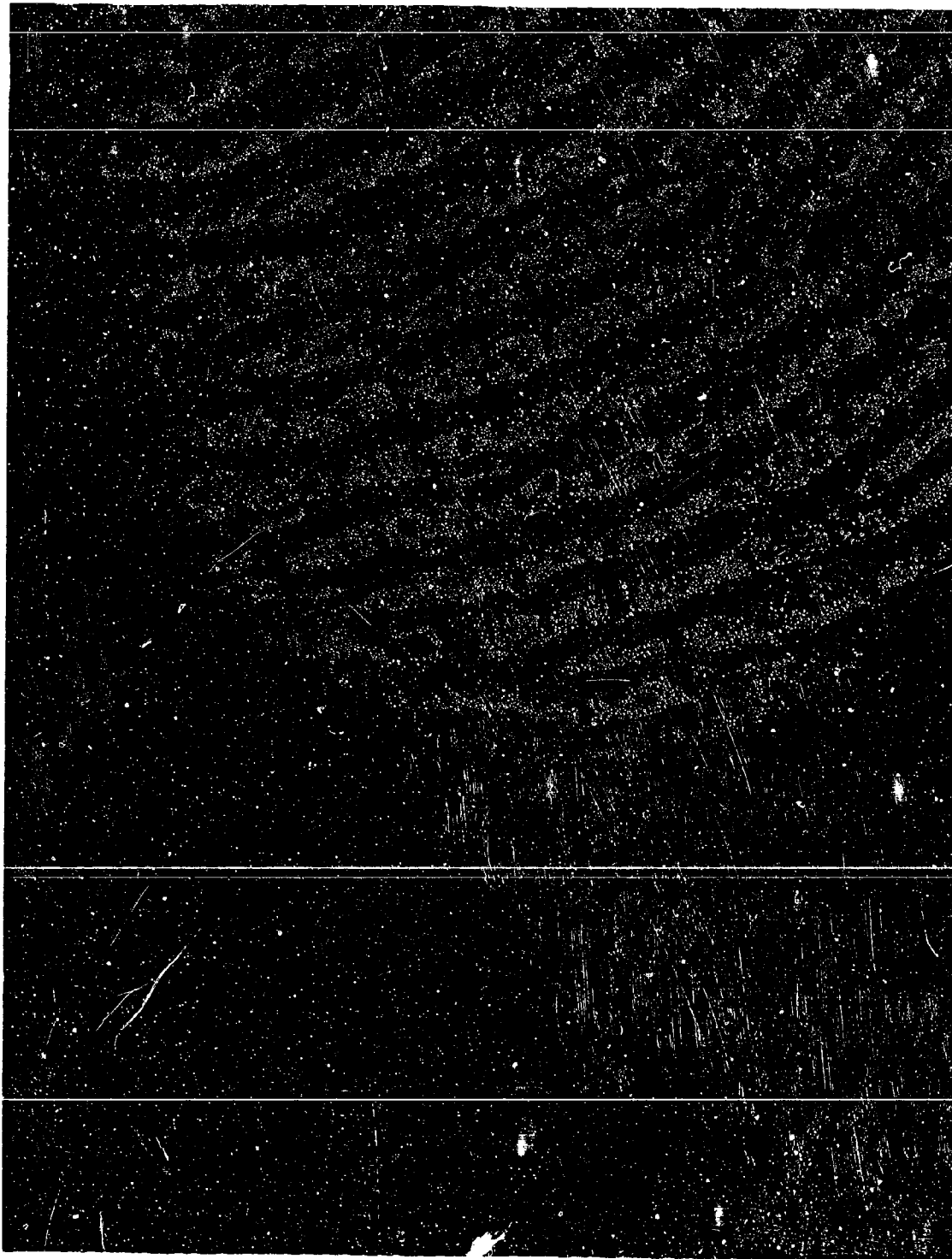


Figure 32. Negative Plate Containing 1% BC-610 at 124 Cycles at 100°F
200X

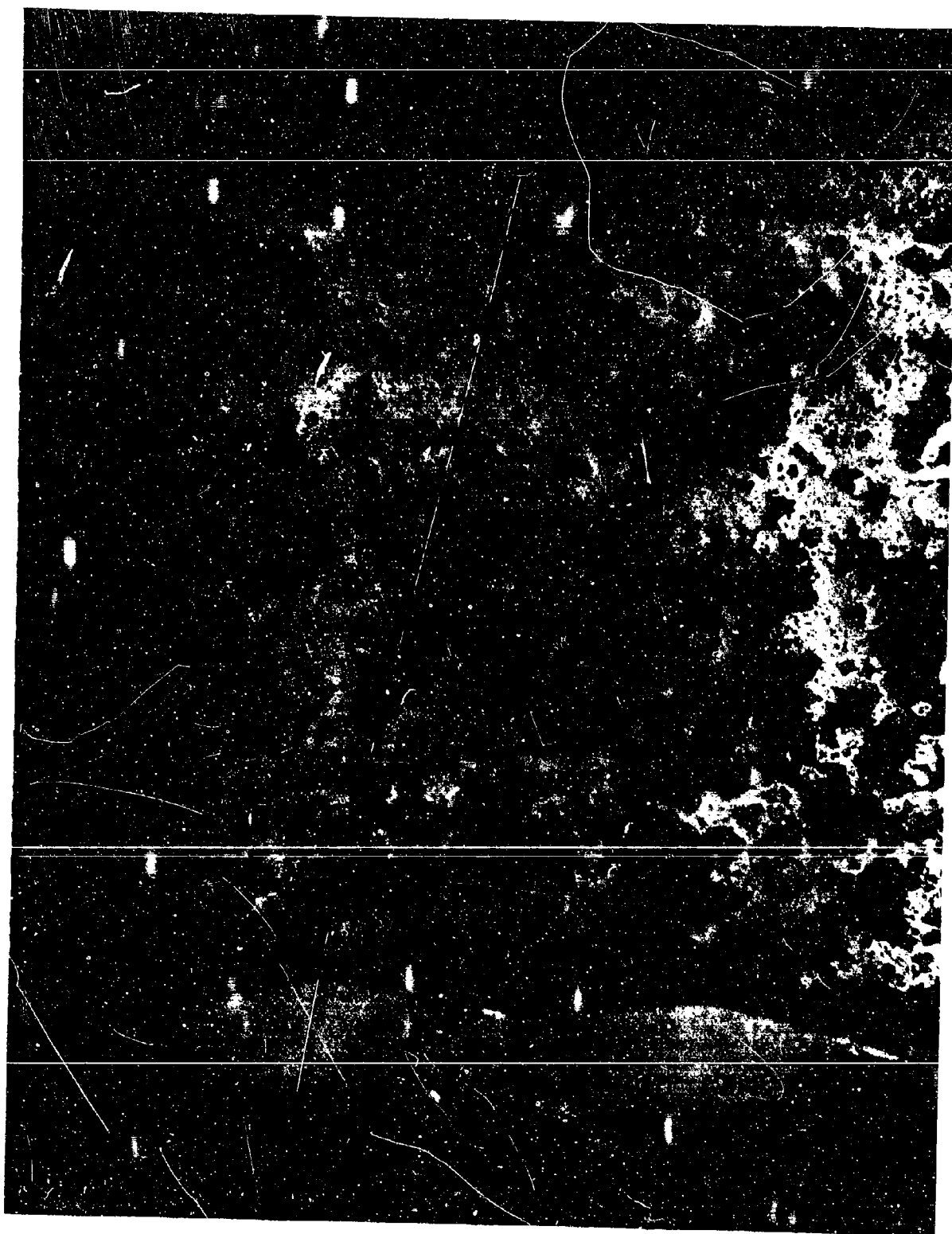


Figure 33. Negative Plate Containing .1% FC-95 at 150 Cycles

200X

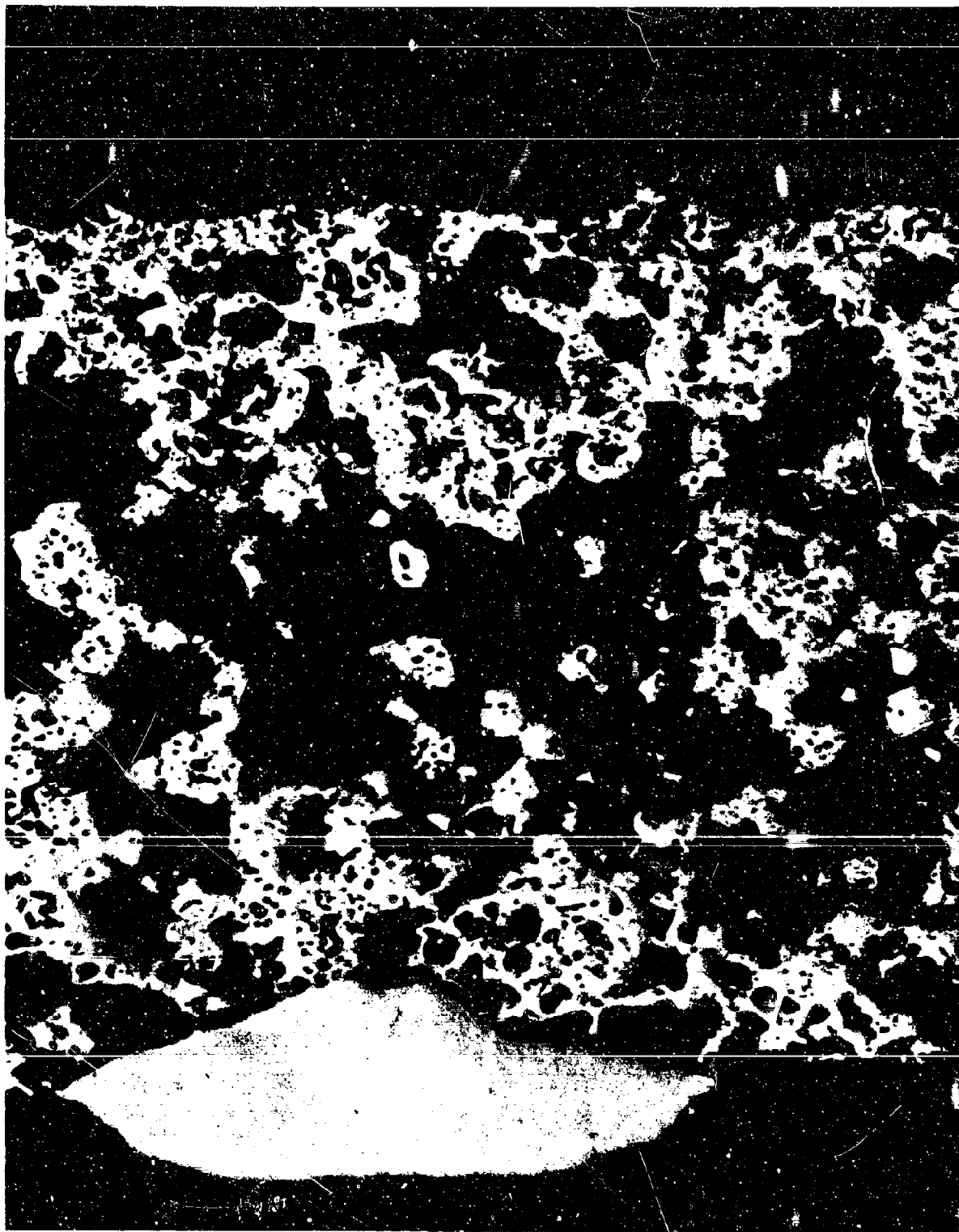


Figure 34. Negative Plate Containing .6% FC-95 at 152 Cycles

200X

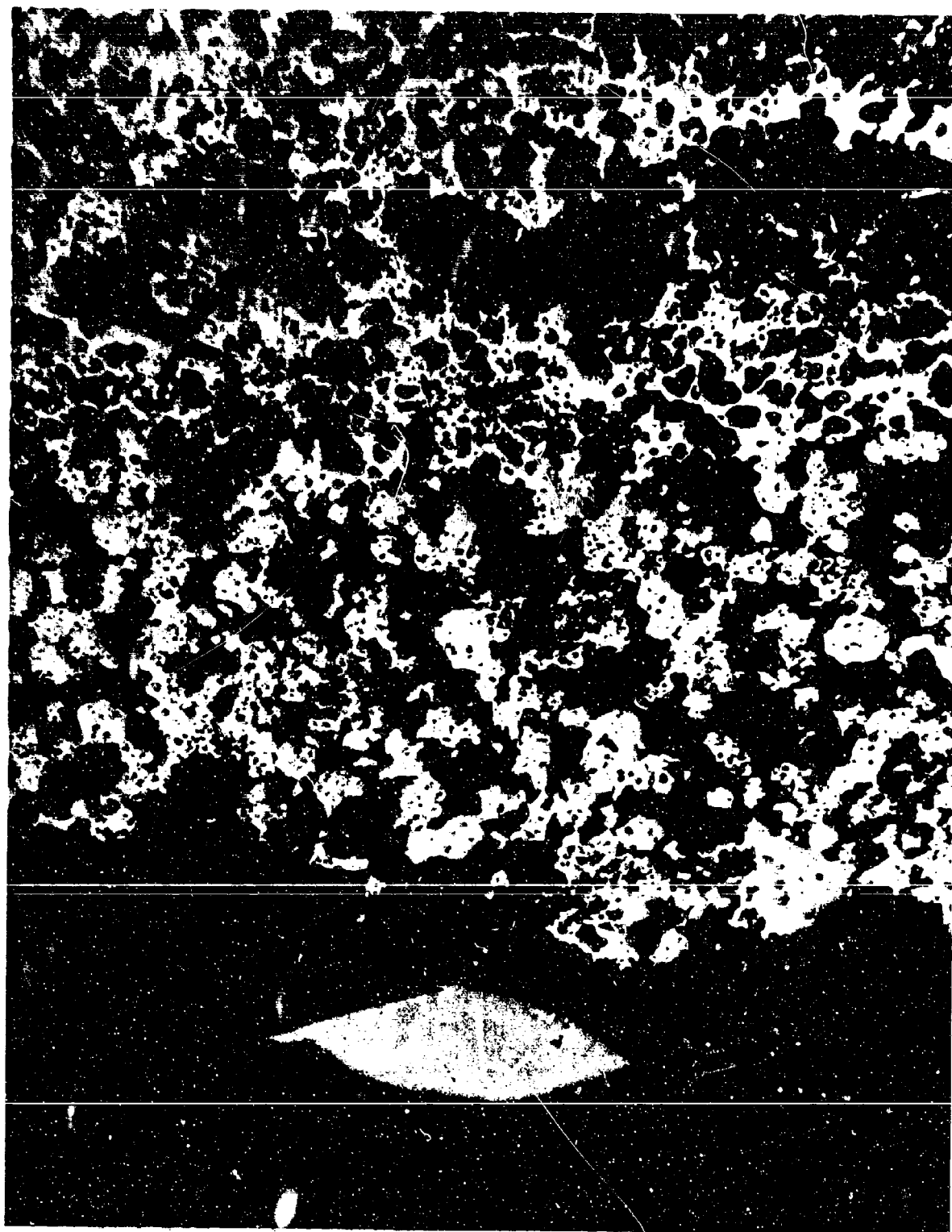


Figure 35. Negative Plate Containing 1% FC-95 at 168 Cycles

200X

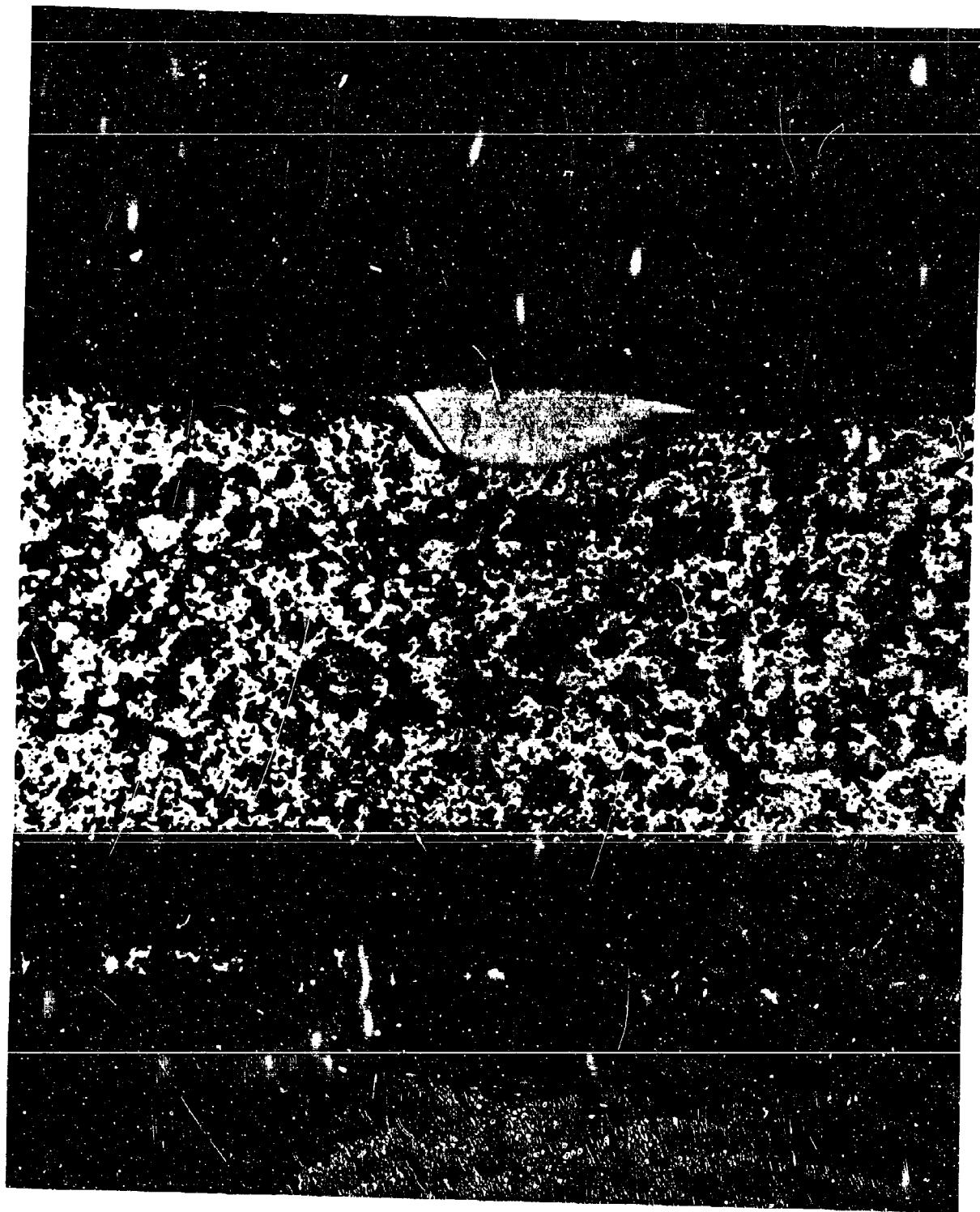


Figure 36. Negative Plate Containing 1% Carbowax with a Molecular Weight Range of 6000 after 132 Cycles

100X

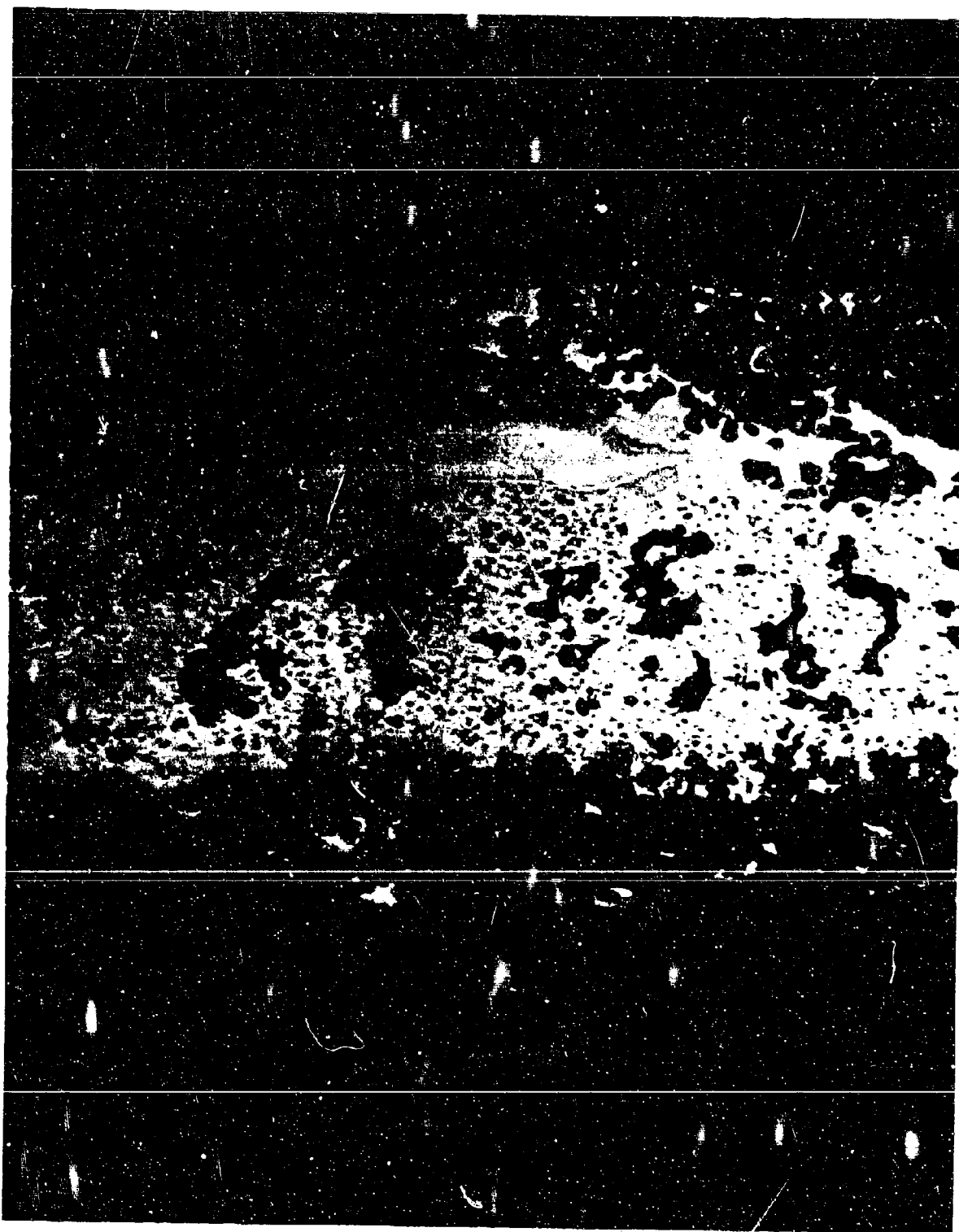


Figure 37. Negative Plate Containing 1% Carbowax with a Molecular Weight Range of 1000 after 200 Cycles

100X

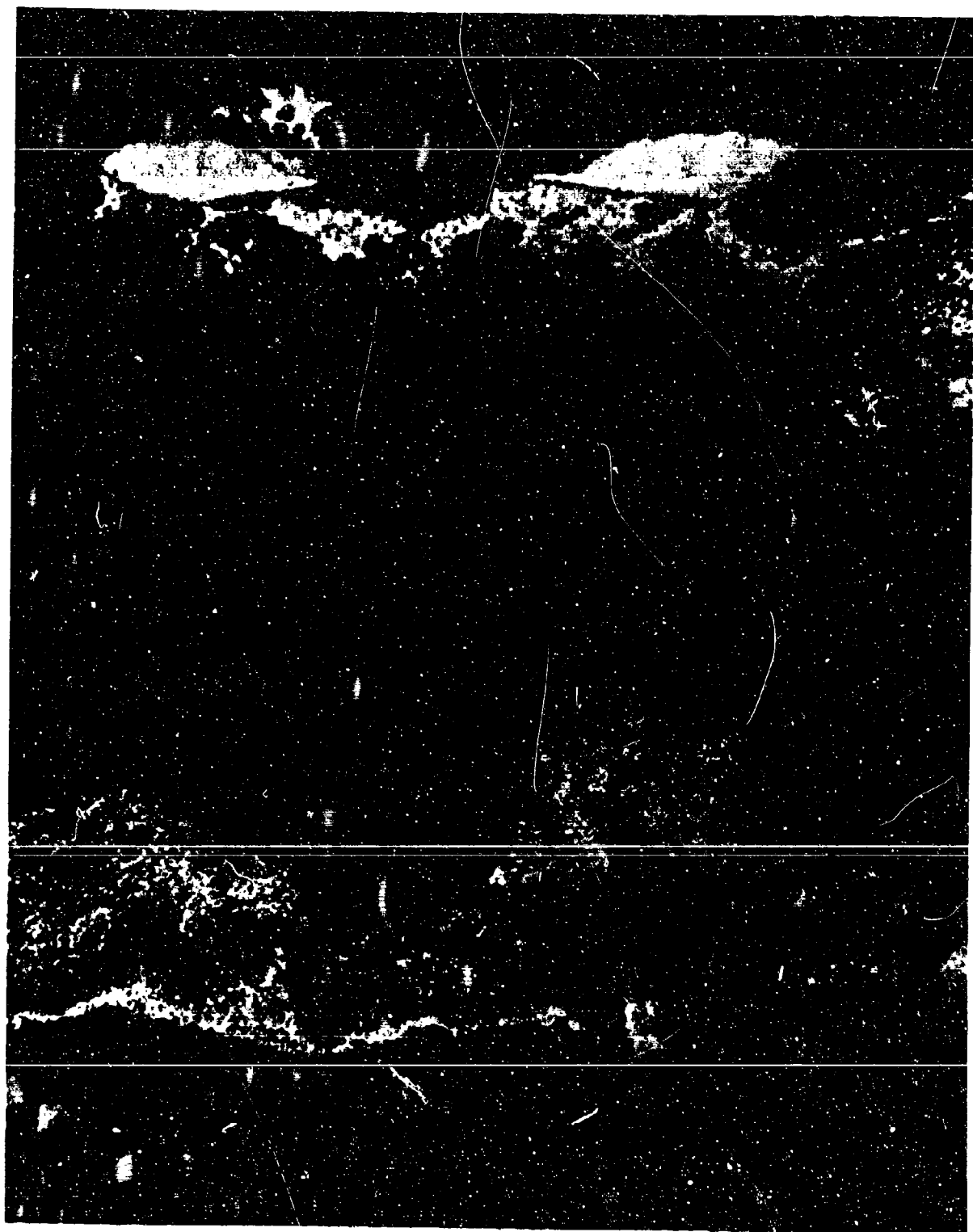


Figure 38. Negative Plate Containing 1% Carbowax with a Molecular Weight Range of 200 after 100 Cycles

100X

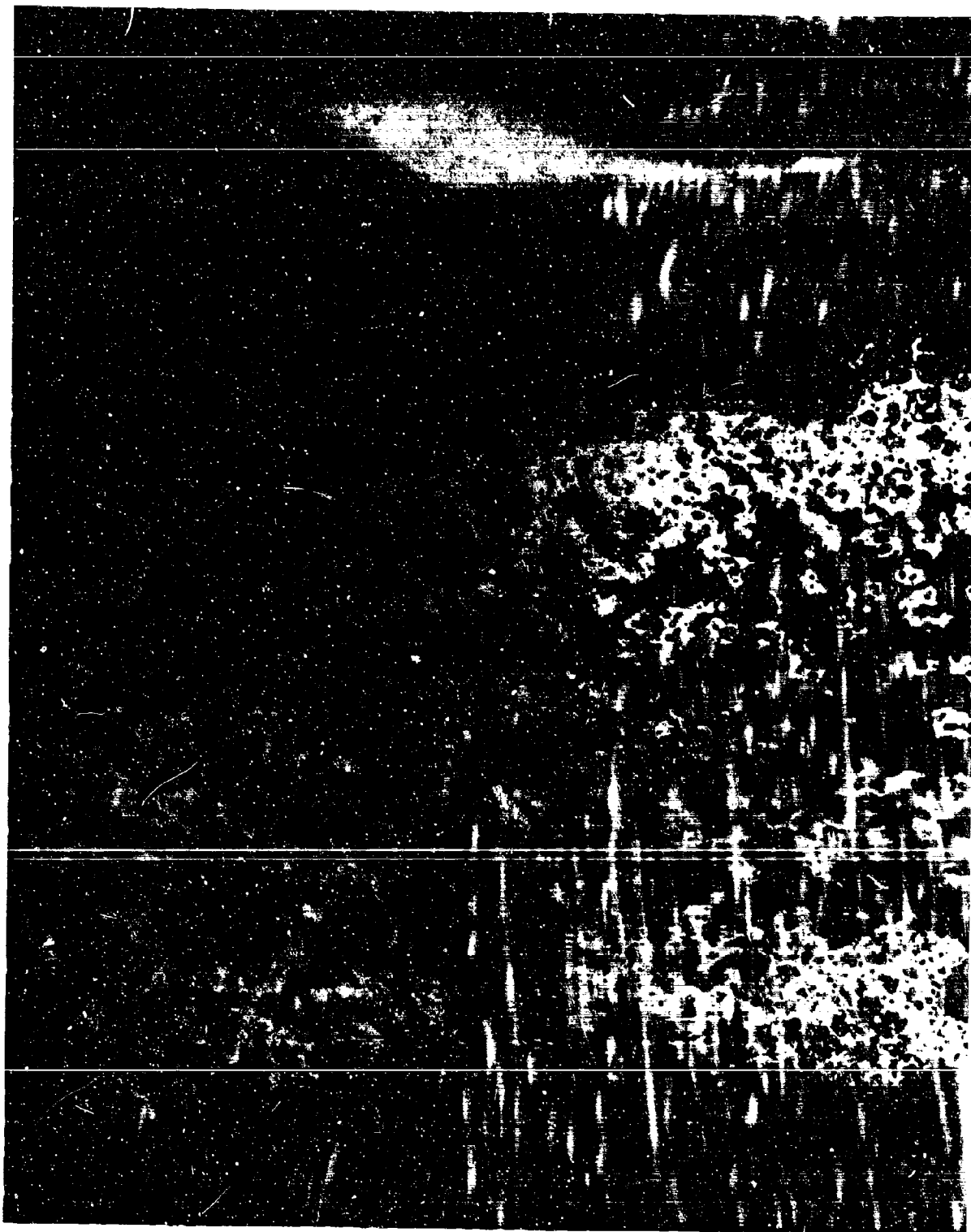


Figure 39. Negative Plate Containing 1.1% LSA After 108 Cycles 200X

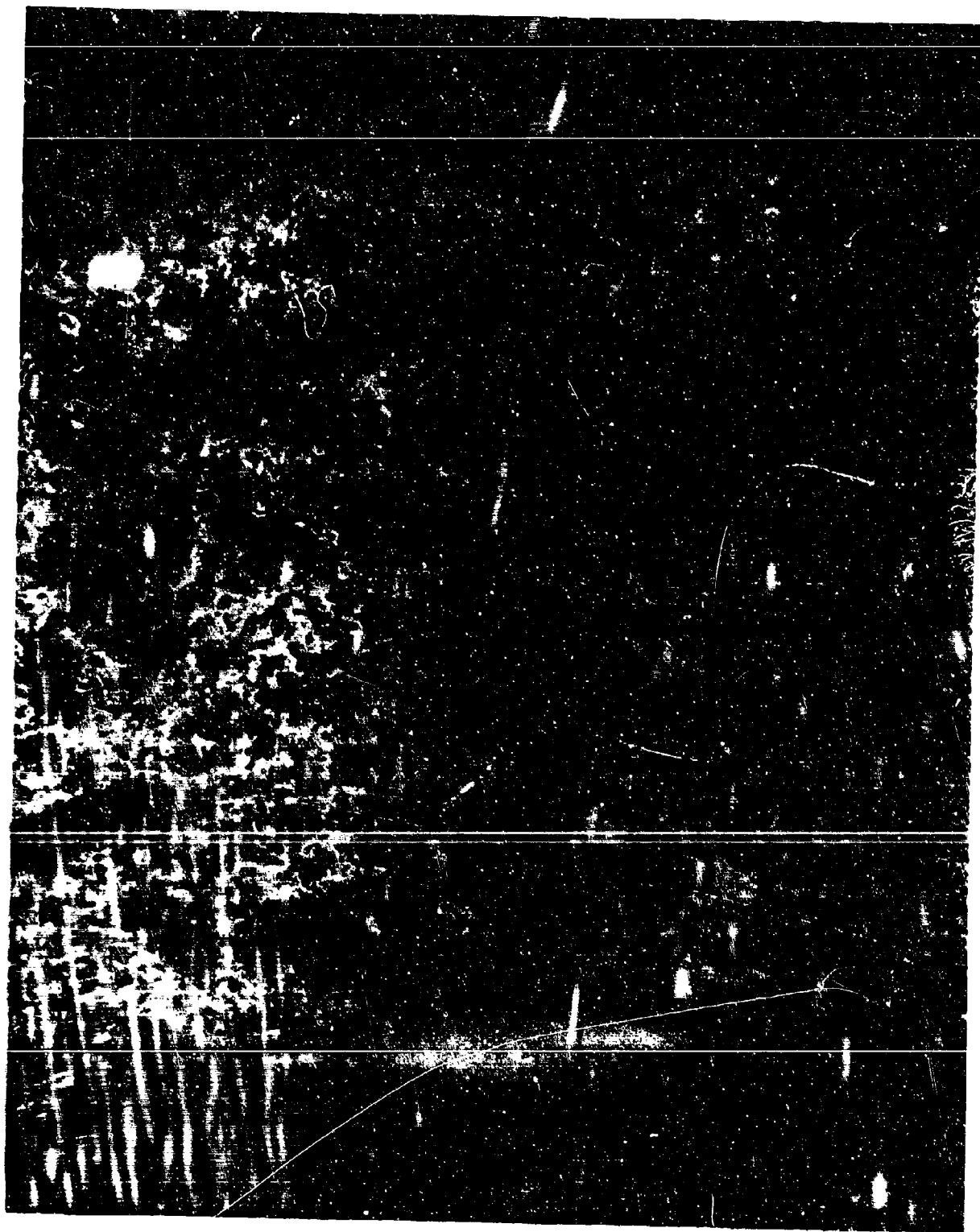


Figure 4C Negative Plate Containing 1.1% LSA and 5% ZnSO_4 after 96 Cycles 200X

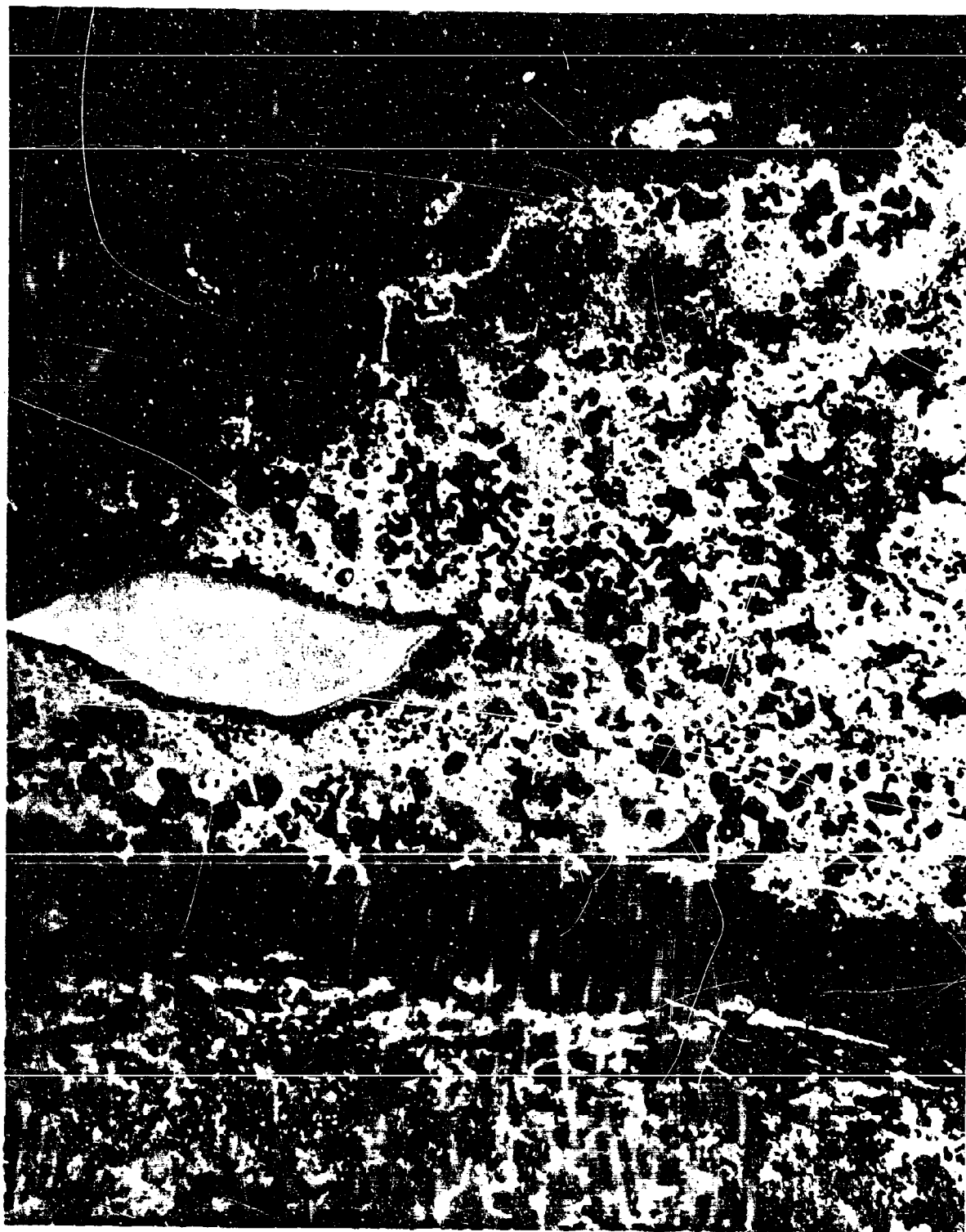


Figure 41. Negative Plate Containing .0008% Pb after 202 Cycles 200X



Figure 42. Negative Plate Containing .028% Pb after 214 Cycles 200X

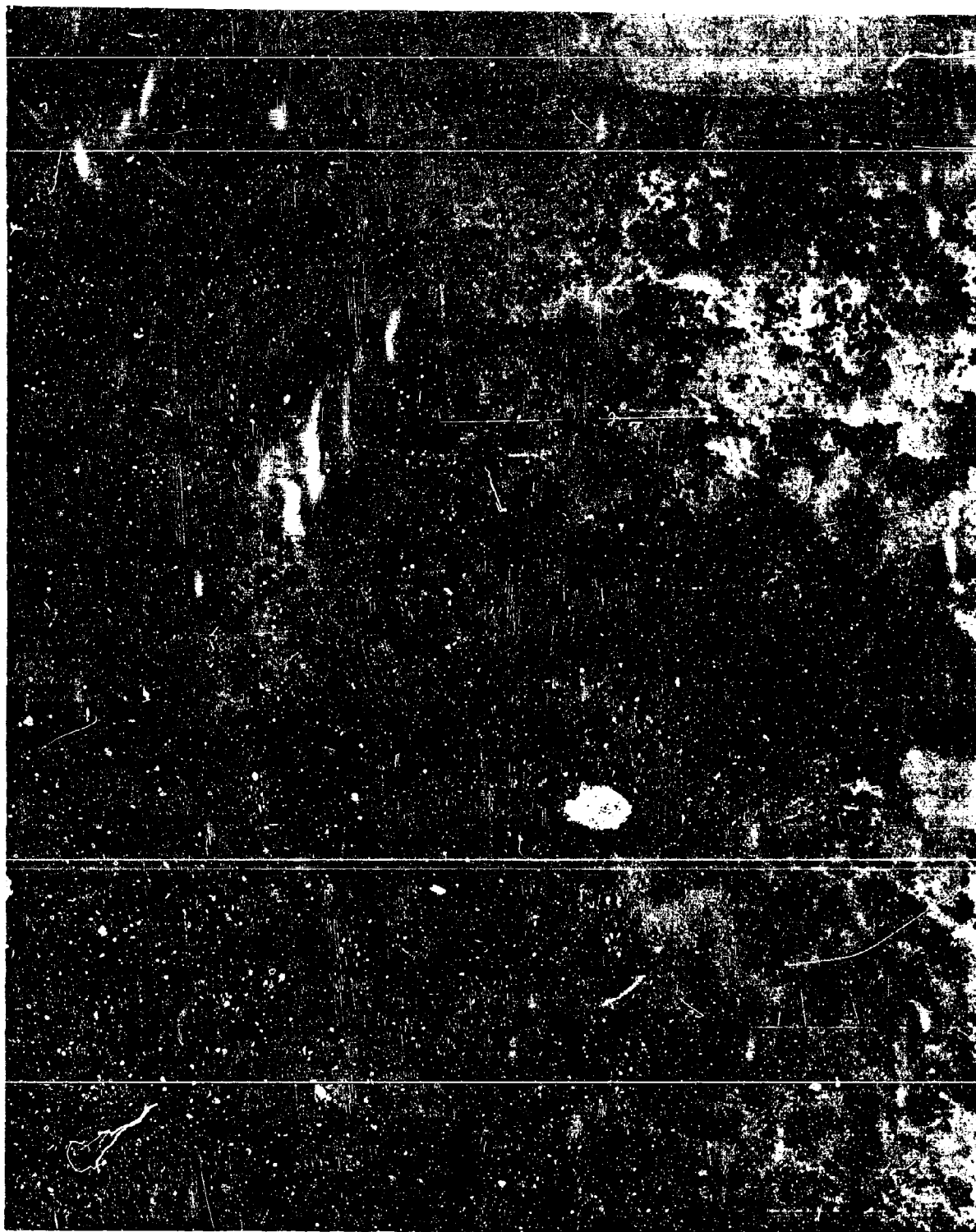


Figure 43. Negative Plate Containing 1.02% Pb after 221 Cycles 200X



Figure 44. Negative Plate Containing 2.4% Pb after 214 Cycles

200X

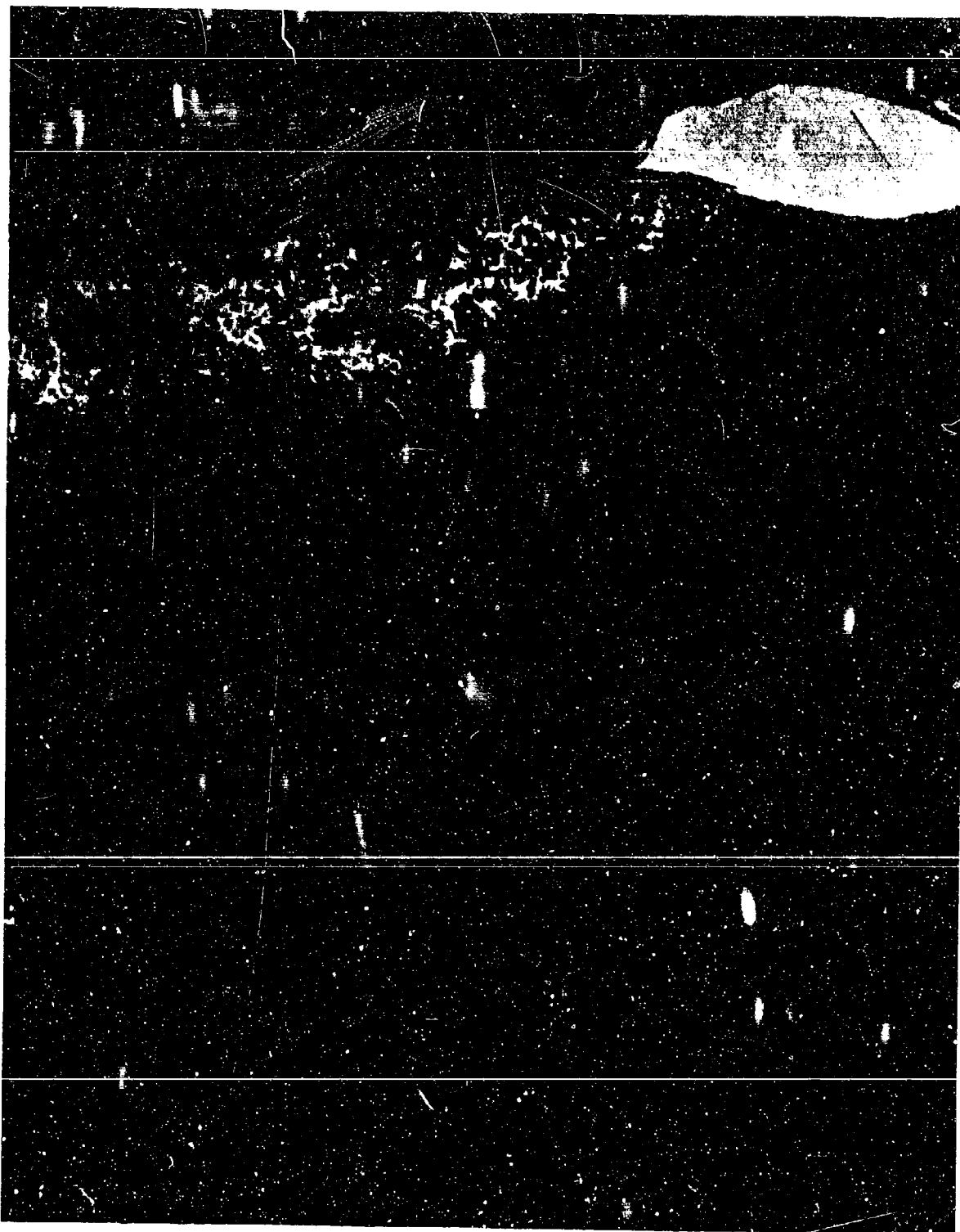


Figure 45. Negative Plate Containing .0006% Fe after 178 Cycles 200X



Figure 46. Negative Plate Containing .0086% Fe after 168 Cycles 200X

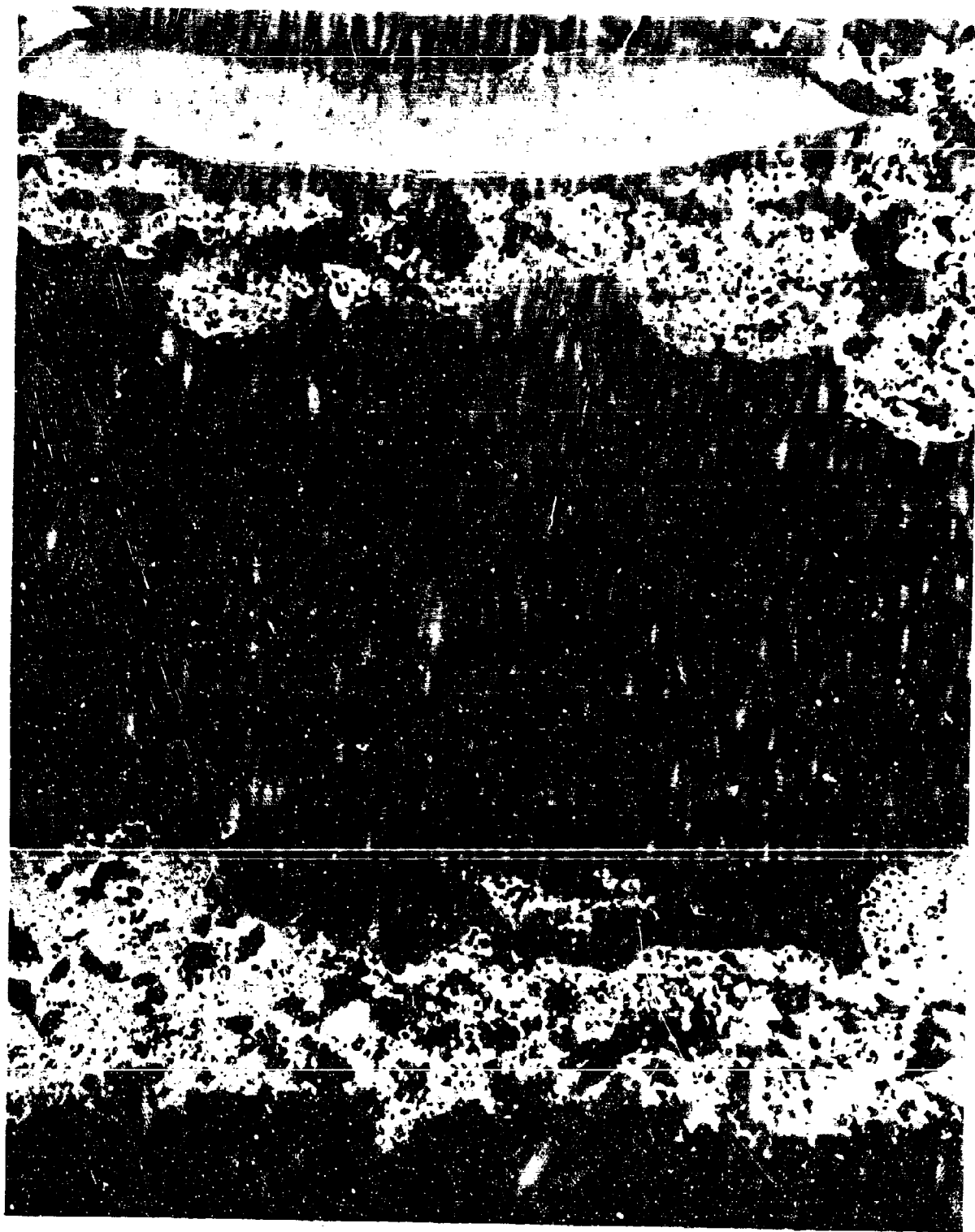


Figure 47. Negative Plate Containing .0092% Fe after 120 Cycles 200X

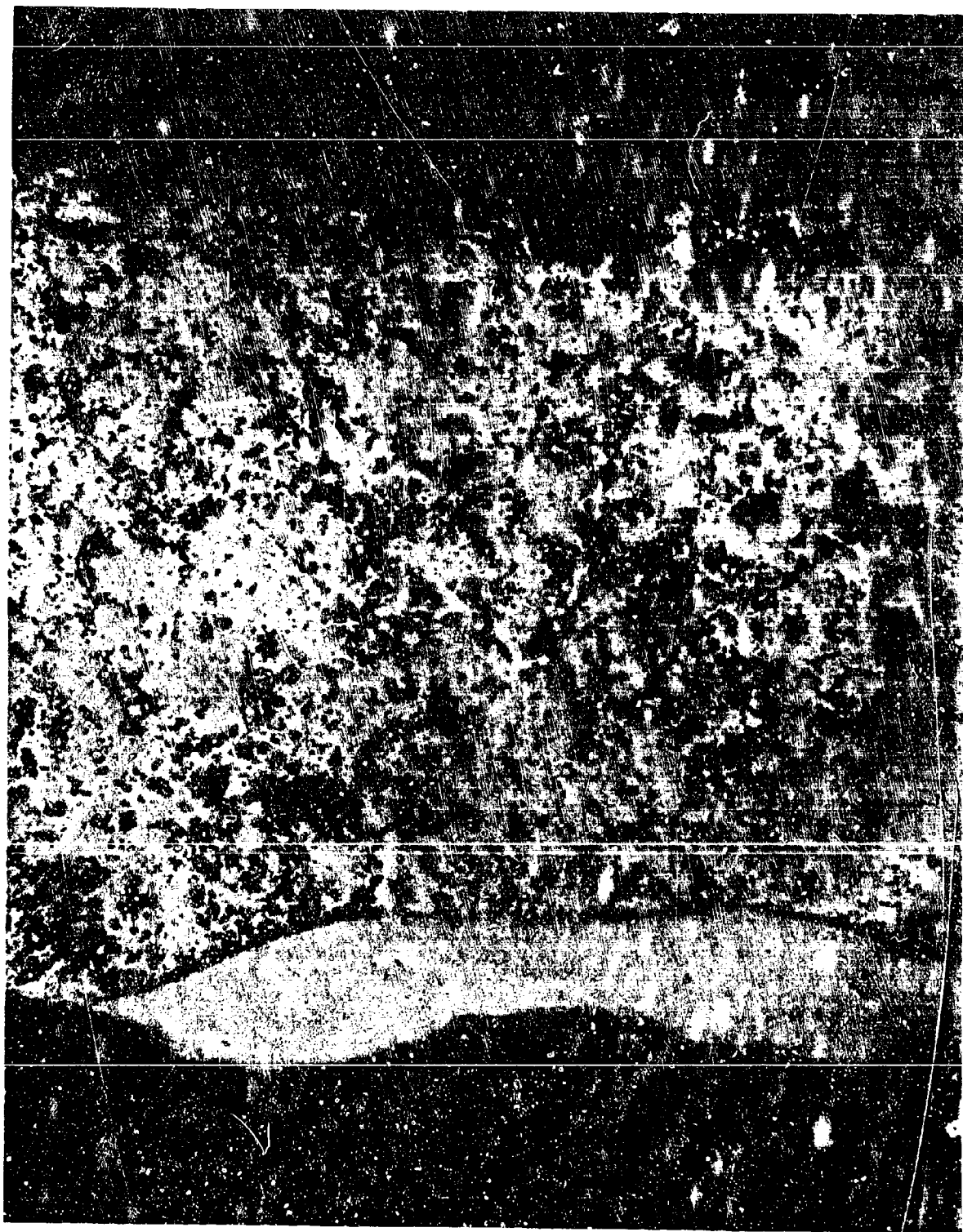


Figure 48. Negative Plate Containing .26% Pb and .010% Fe after 192 Cycles

200X

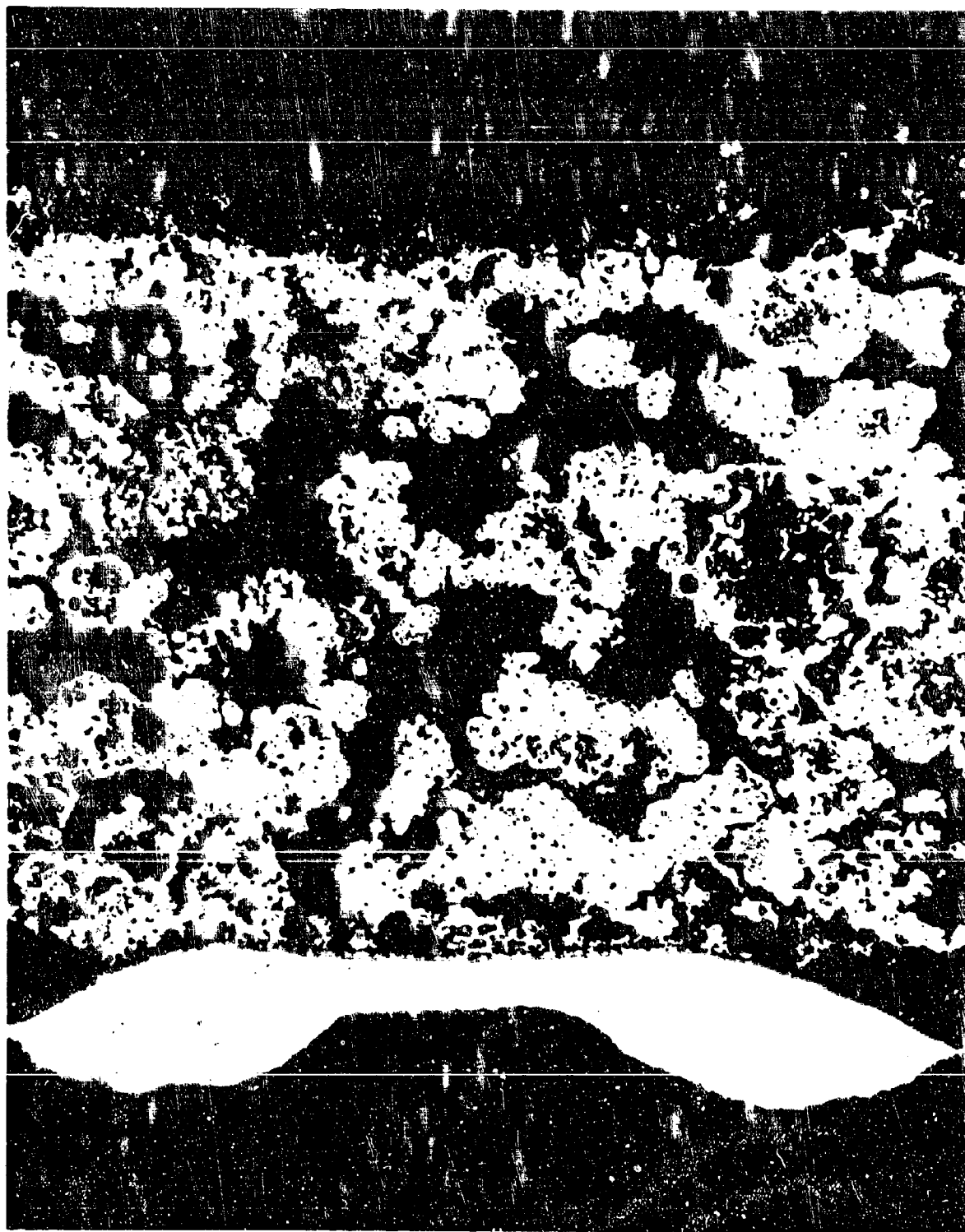


Figure 49. Negative Plate Containing .07% Al and .0010% Fe after 156 Cycles

200X



Figure 50. Negative Plate Containing .9% Al and .0008% Fe after 167
Cycles

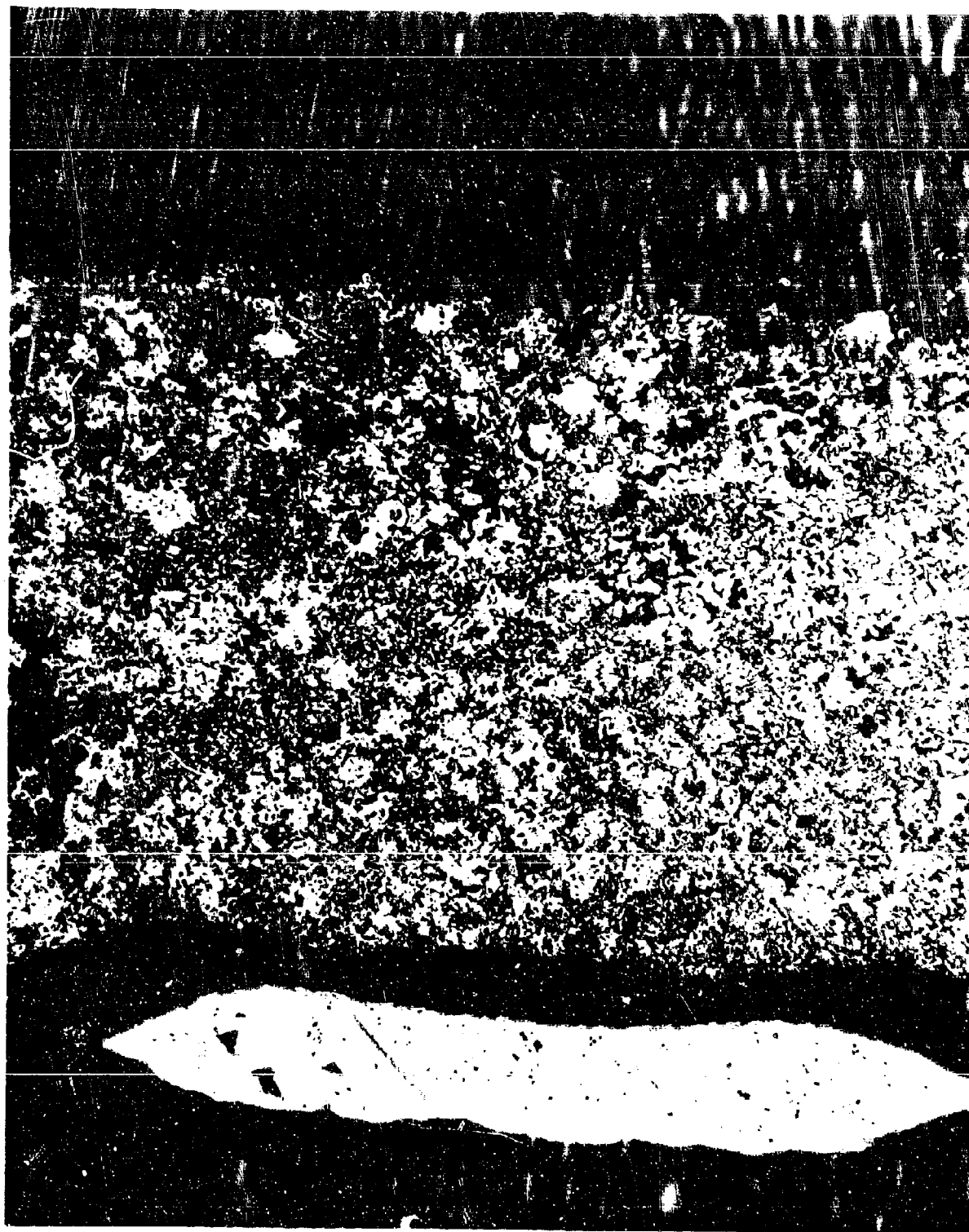


Figure 51. Negative Plate Containing .25% Pb after 221 Cycles 200X



Figure 52. Negative Plate Containing .3% Al after 1/0 Cycles 200X



Figure 53. Negative Plate Containing Kadox 15 after 170 Cycles 200X

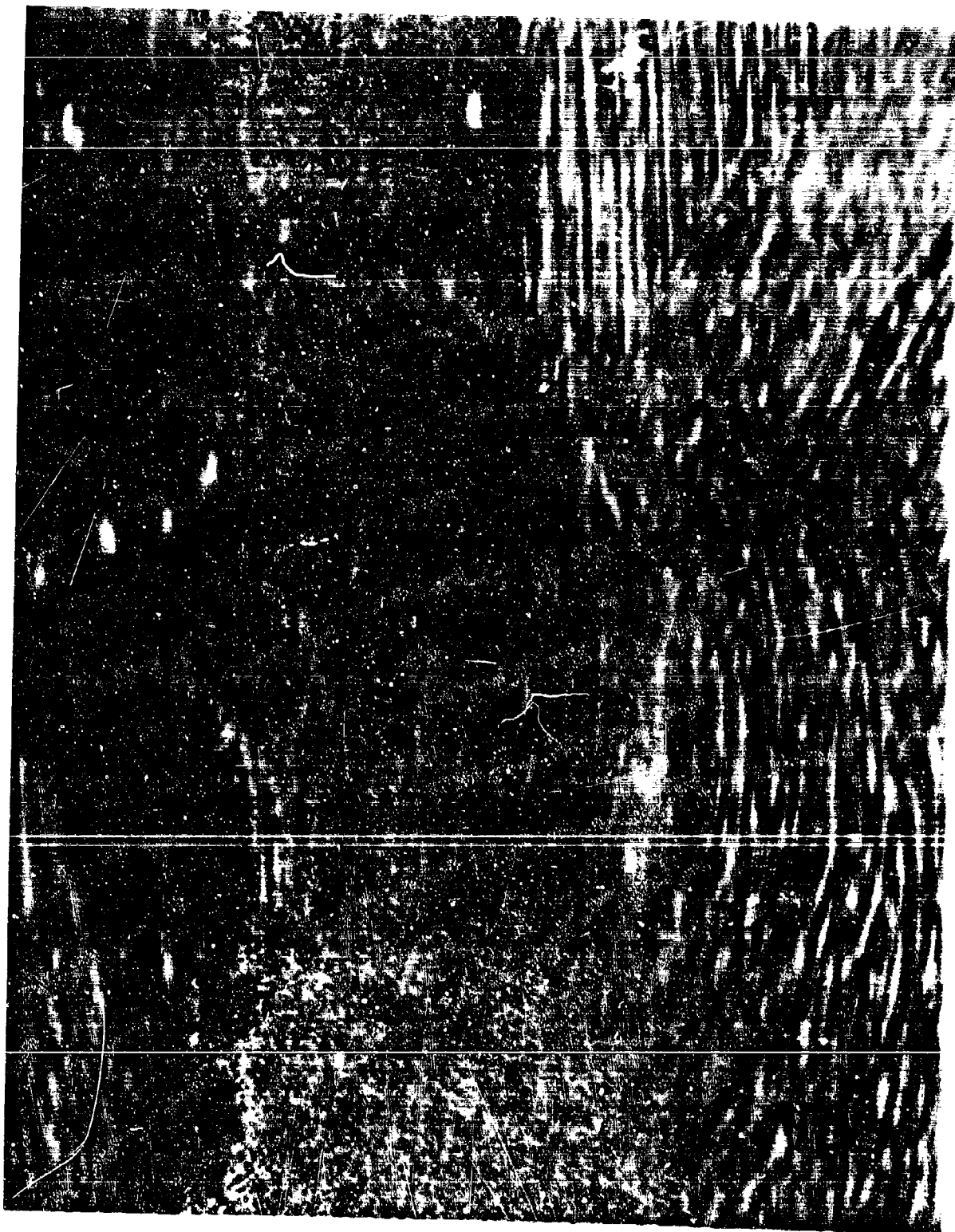


Figure 54. Negative Plate Containing Zinc Dust after 168 Cycles 200X



Figure 55. Negative Plate Containing Zinc Flake after 204 Cycles 100X

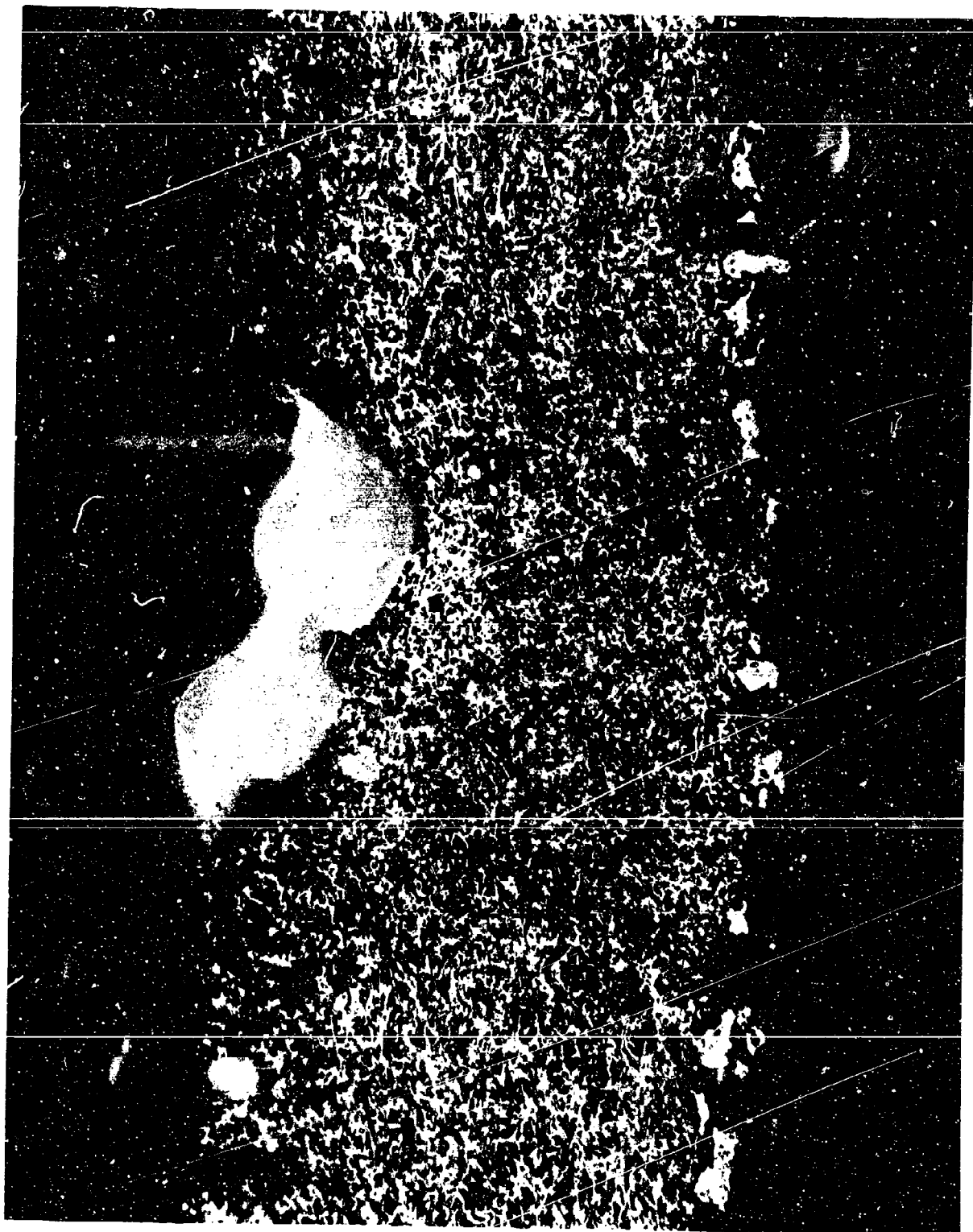


Figure 56. Negative Plate of Electrodeposited Zinc after 96 Cycles 200X

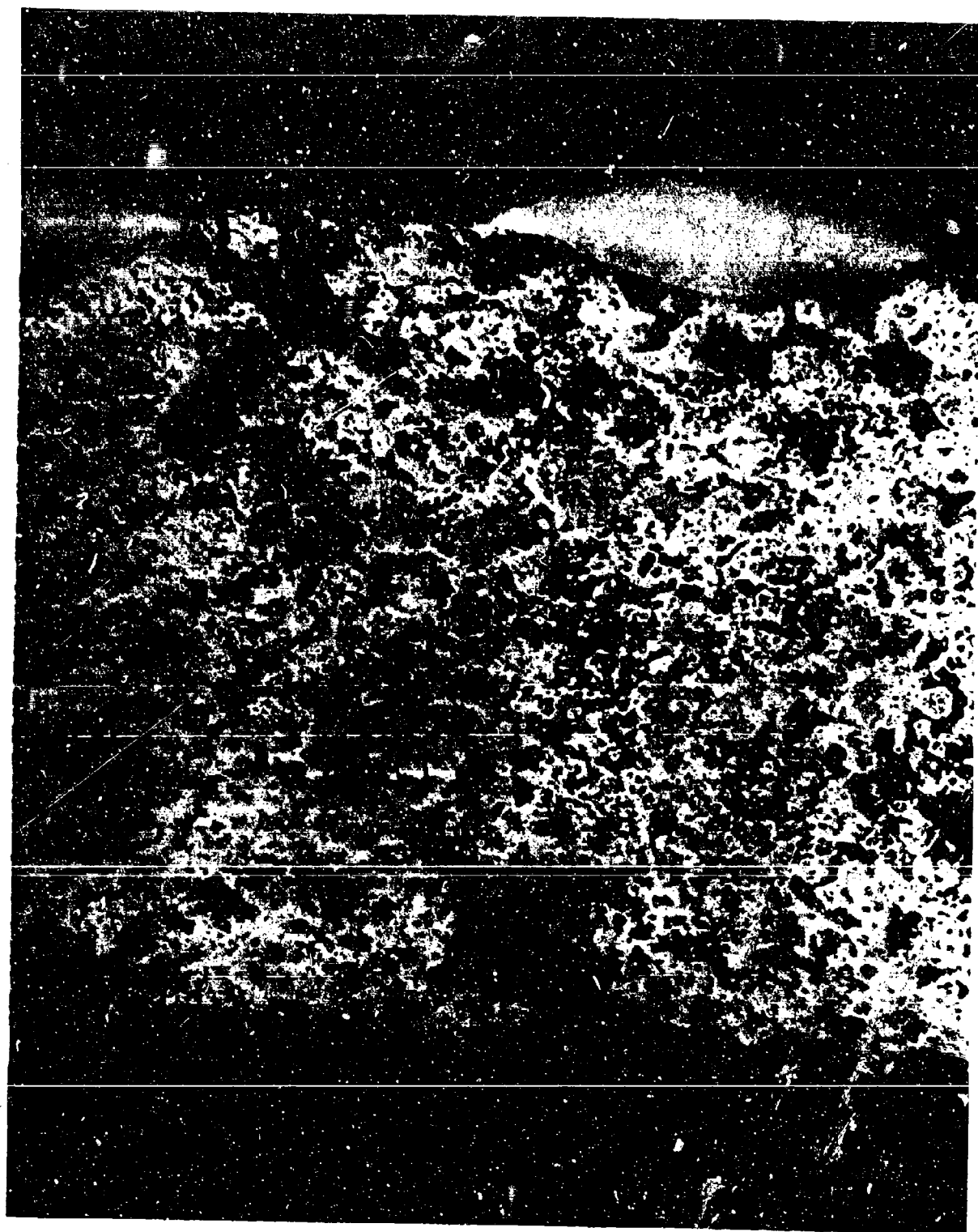


Figure 57. Negative Plate Containing 1% CaO after 156 Cycles

200X

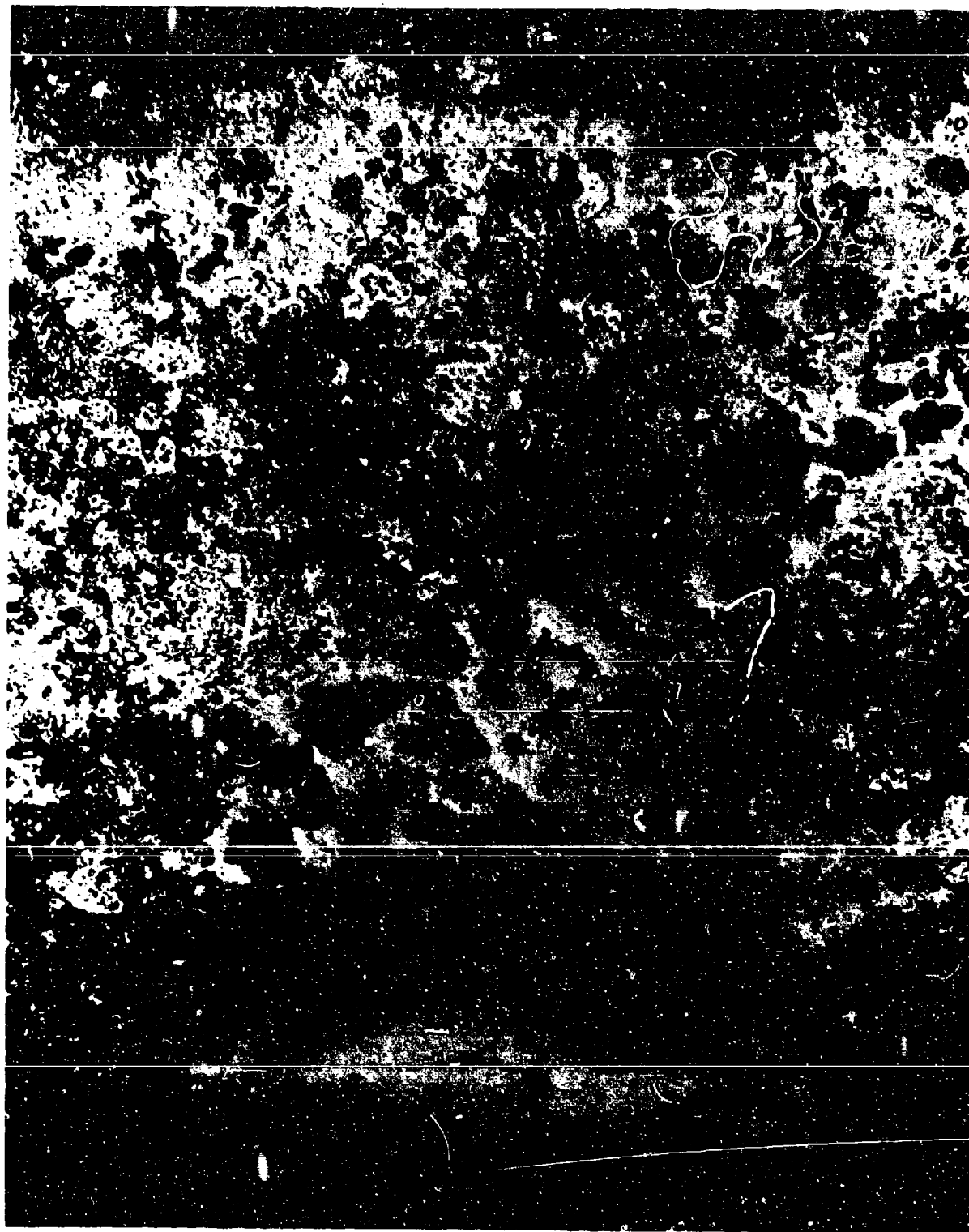


Figure 58. Negative Plate Containing 3% CaO after 96 Cycles

200X



Figure 59. Negative Plate Containing 5% CaO after 156 Cycles

200X

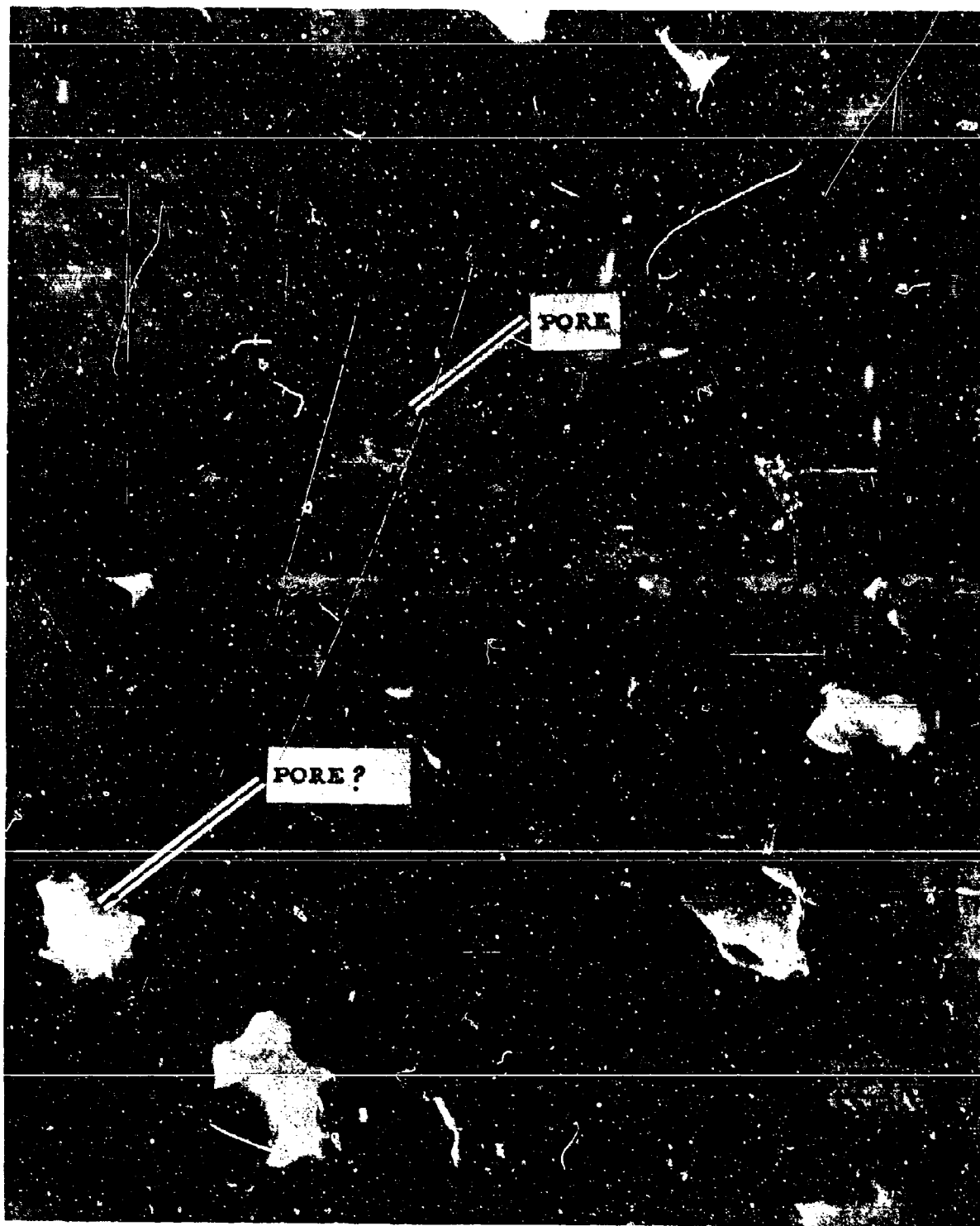


Figure 60. Electronmicrograph of the Surface of VF WP Millipore Material at 150,000 X

100X

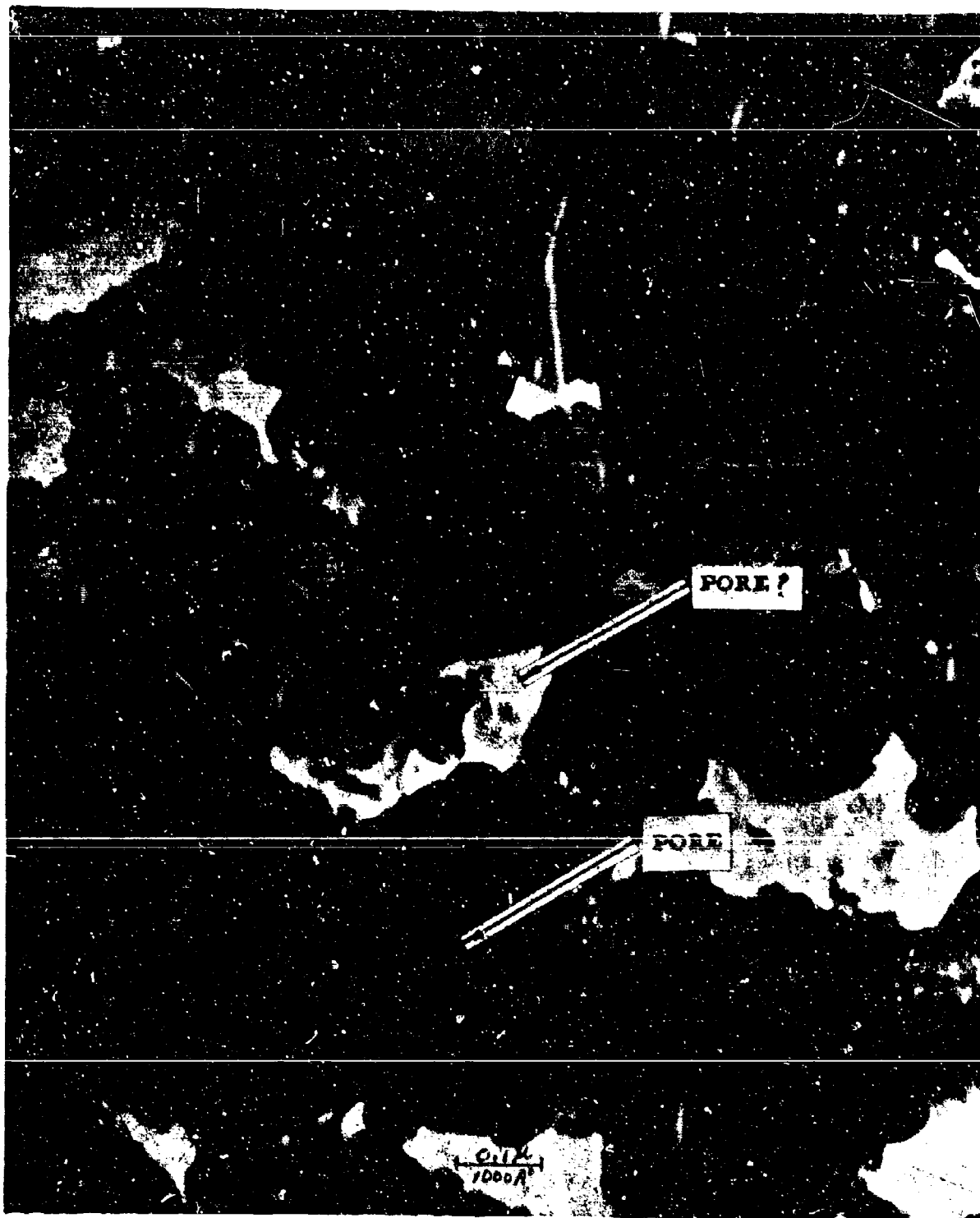


Figure 61. Electronmicrograph of the Surface of VM WF Millipore Material at 150,000 X

100X

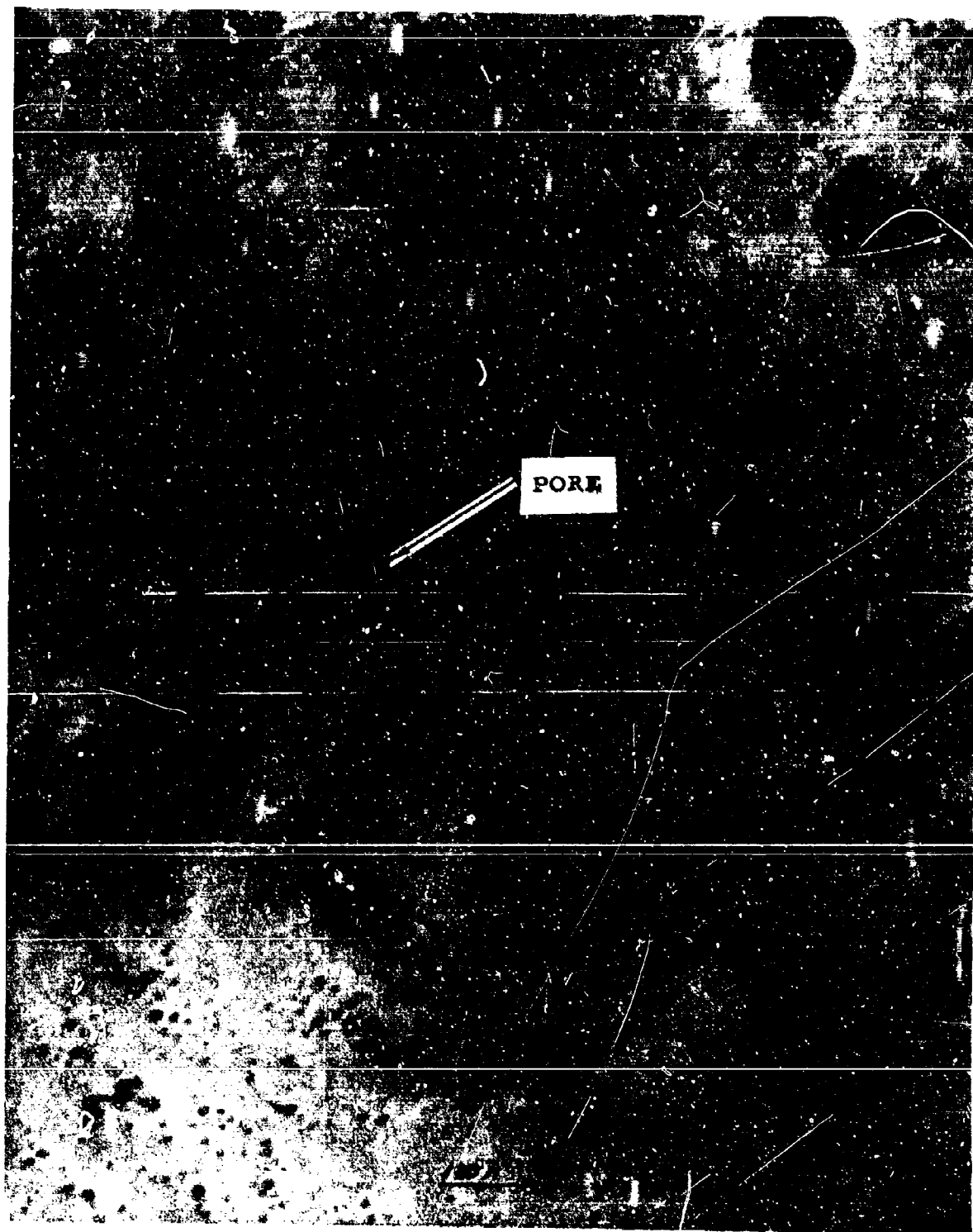


Figure 62. Electronmicrograph of the Surface of Dow Corning Porous Glass at 300,000 X

100X

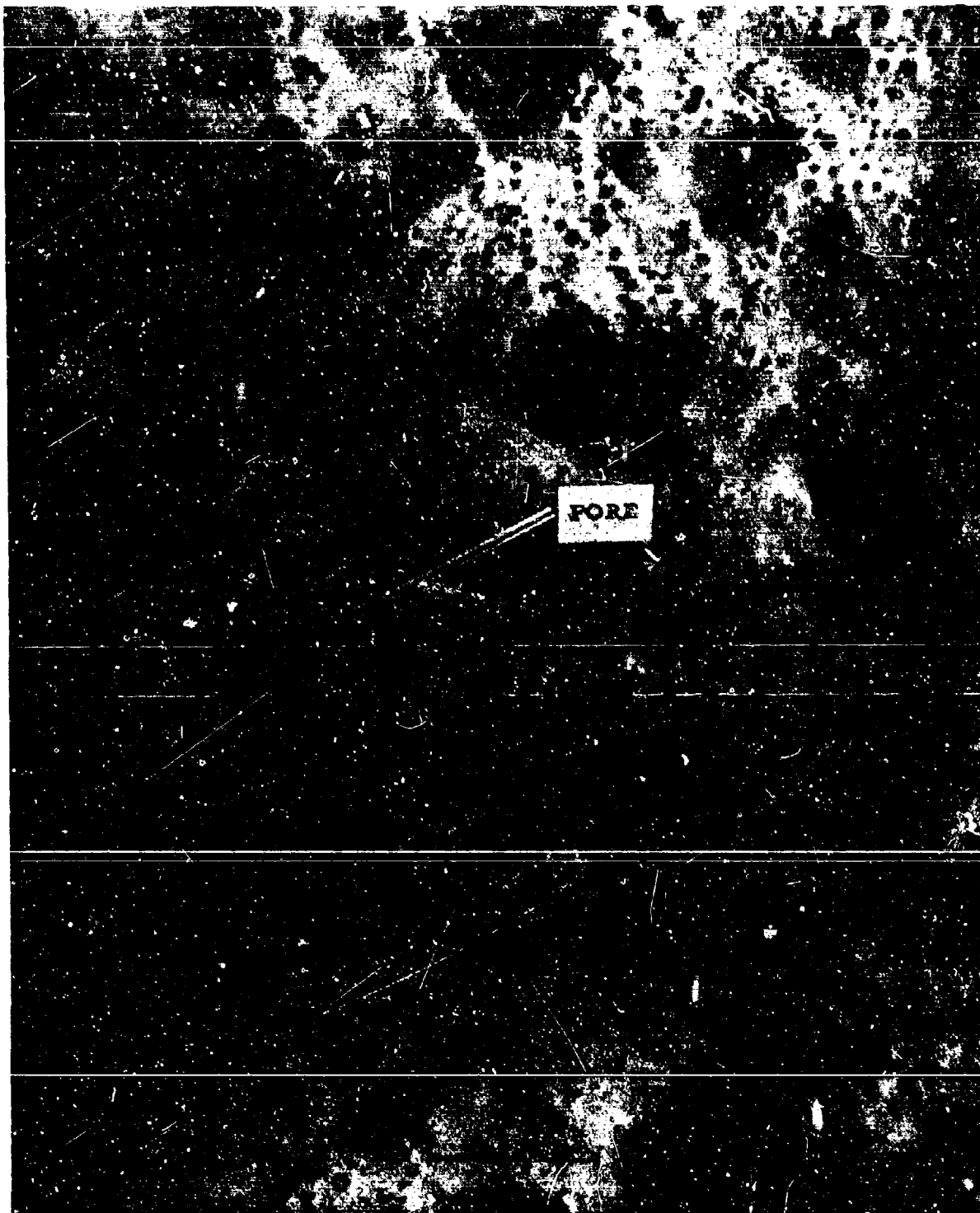
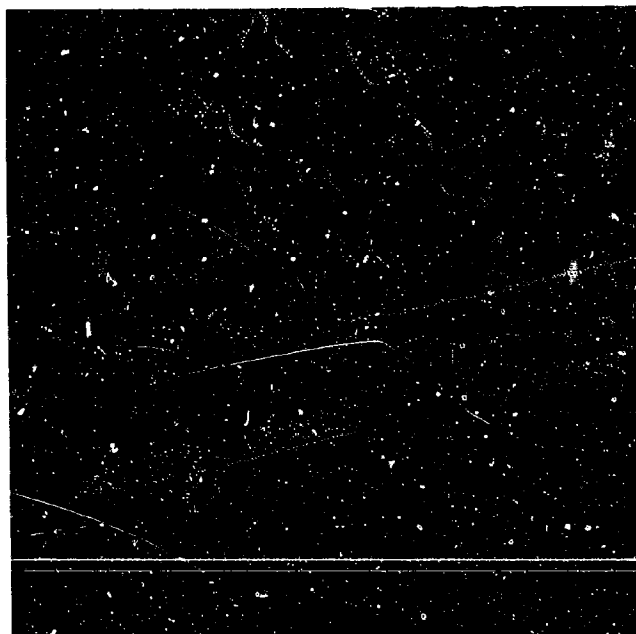


Figure 63. Electronmicrograph of the Surface of 2.2XH Membrane Material
by RAI at 61,000 X 100X



Figure 64. Electronmicrograph of the Surface of Dow Corning Porous Glass at 300,000 X



10.14
μm

Figure 65. Electronmicrograph of the Surface of 2.2XH Membrane Material
by RAI at 51,000 X 100X

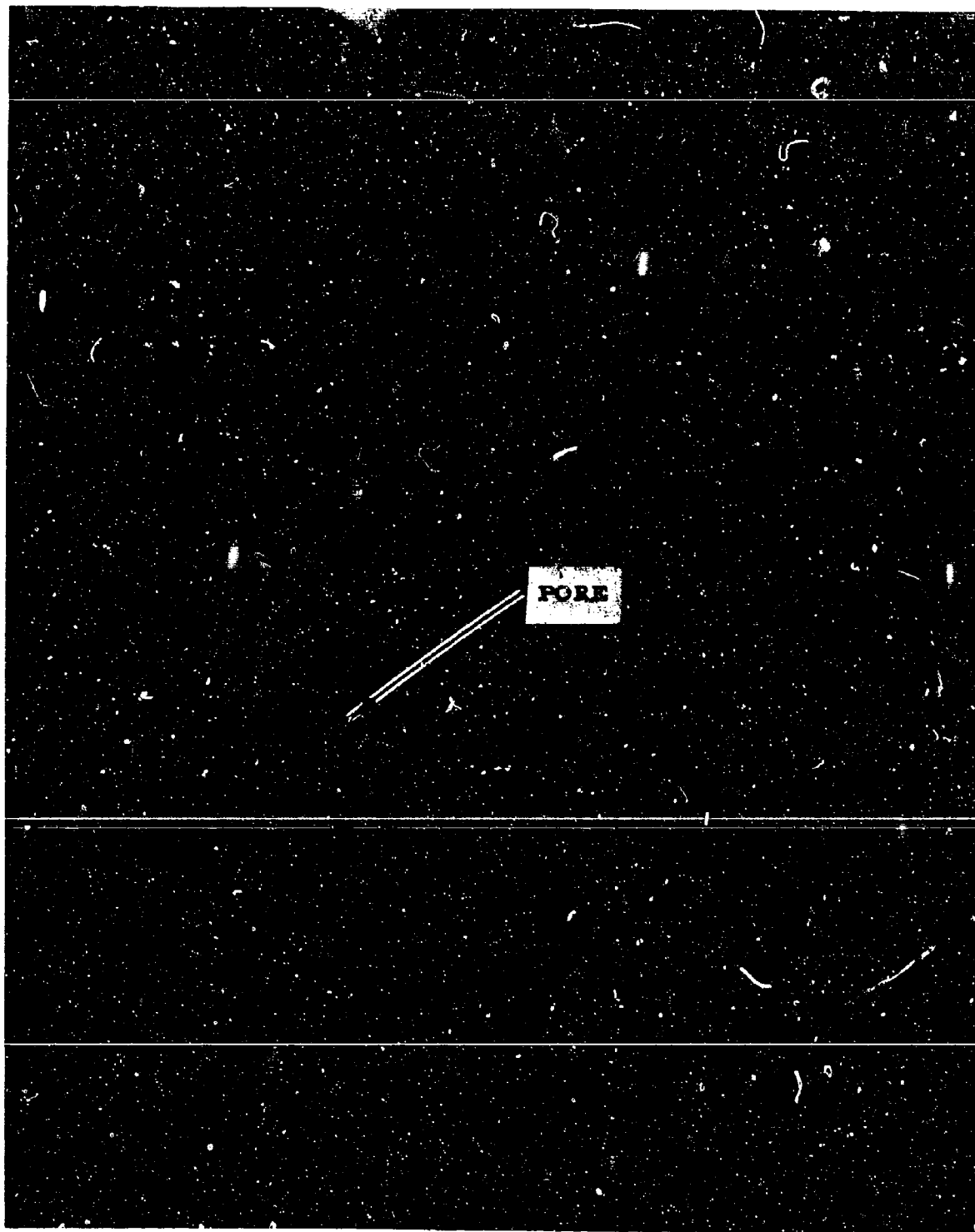


Figure 66. Electronmicrograph of Surface of 2.2XH Membrane Material by RAI at 300,000 X 100X

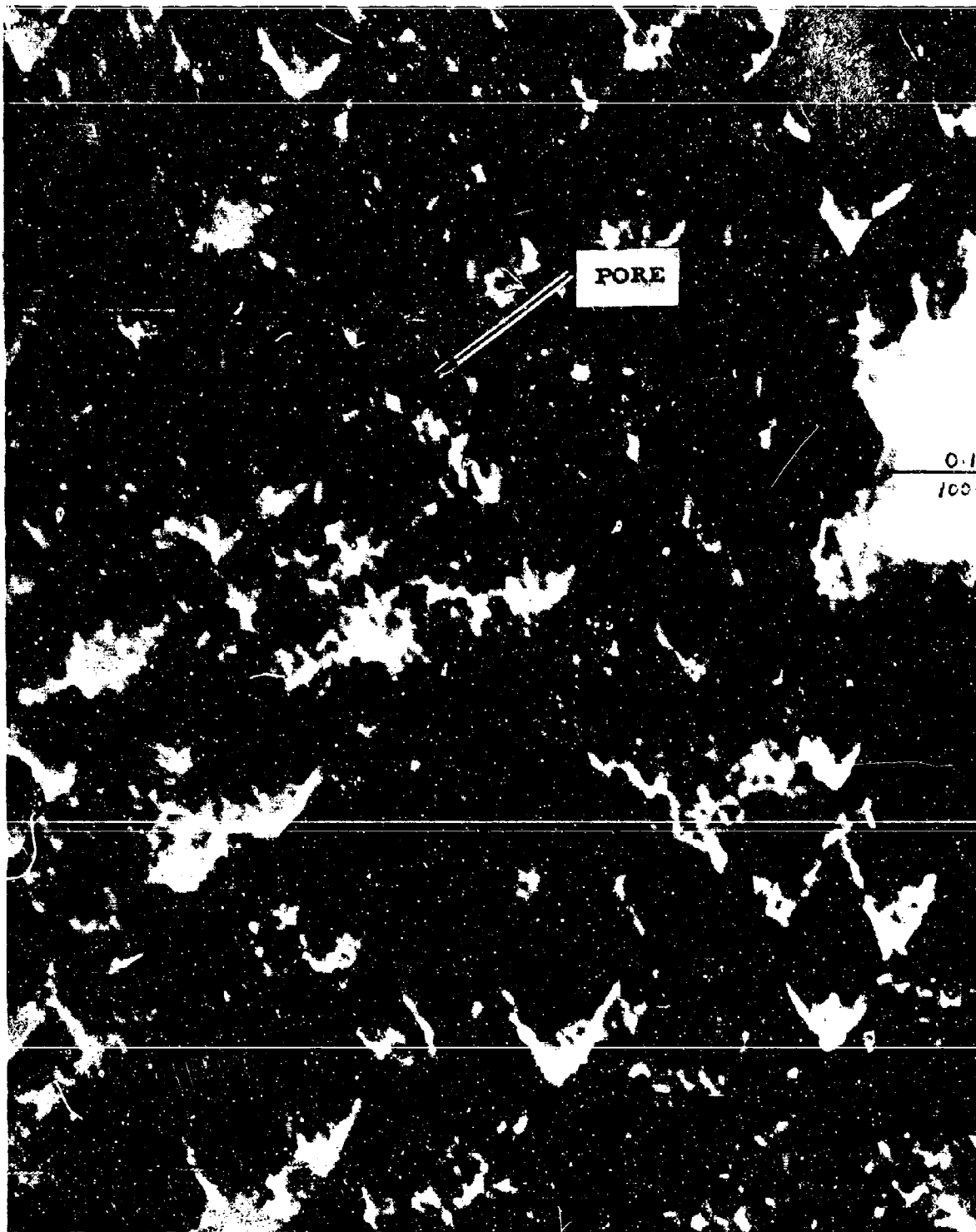


Figure 67. Electronmicrograph of Surface of 2.2XH Membrane Material by RAI at 300,000 X 100X



Figure 68. Negative Plate with a 2:1 Construction after 184 Cycles 100X



Figure 69. Negative Plate with a 3:1 Construction After 204 Cycles 100X

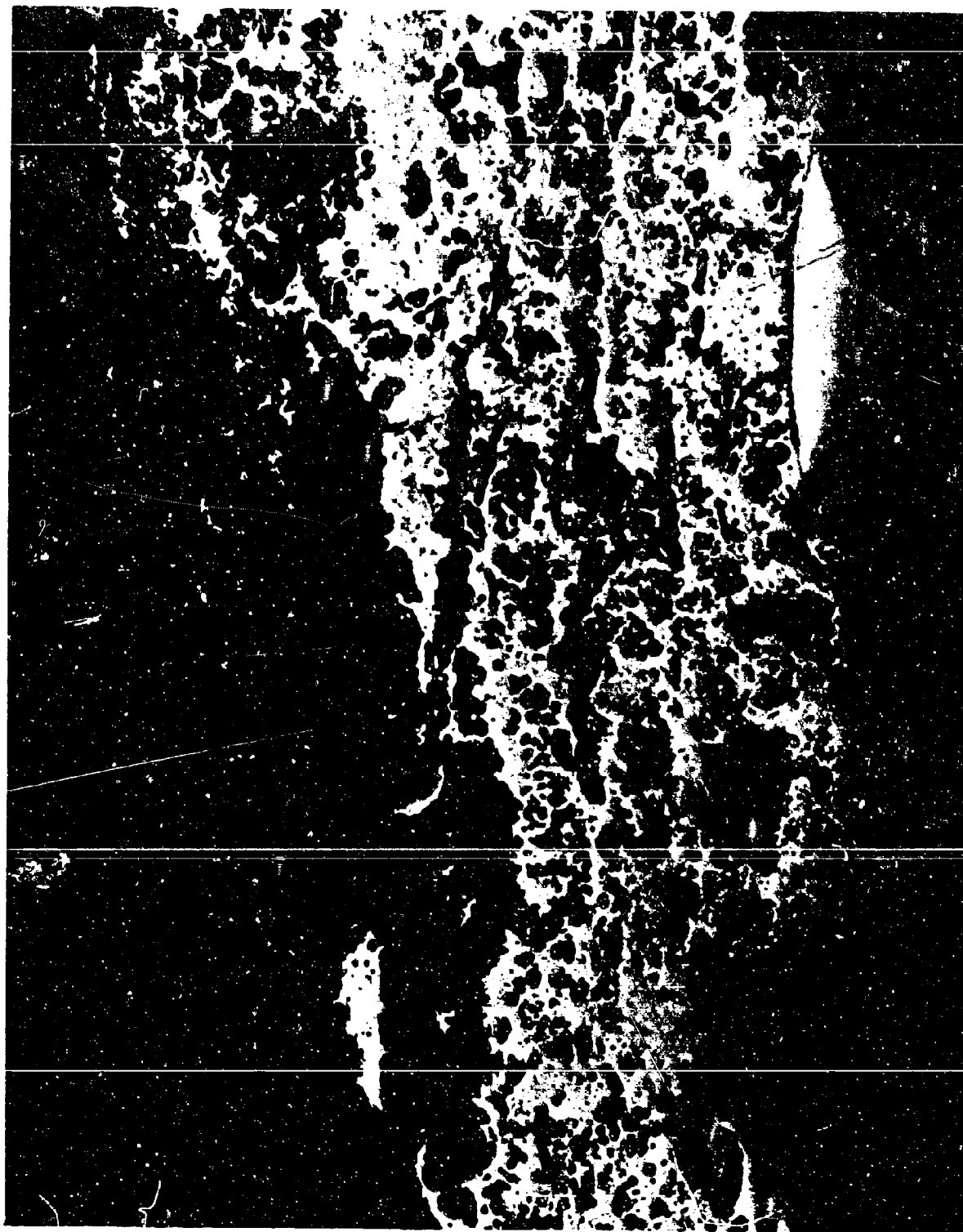
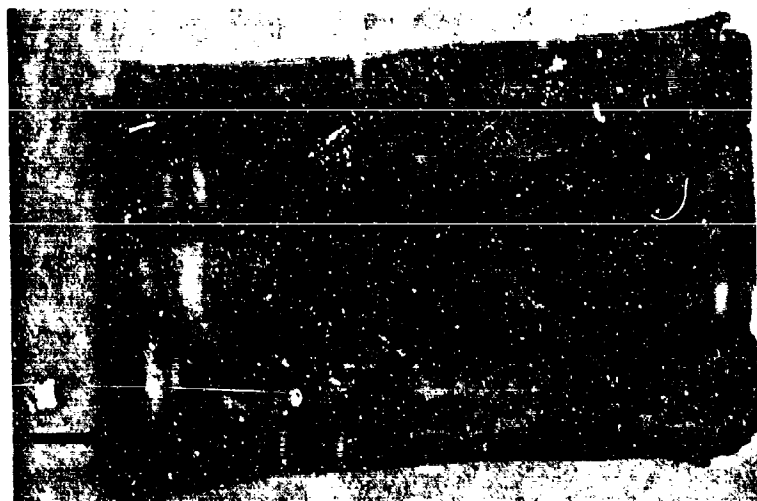
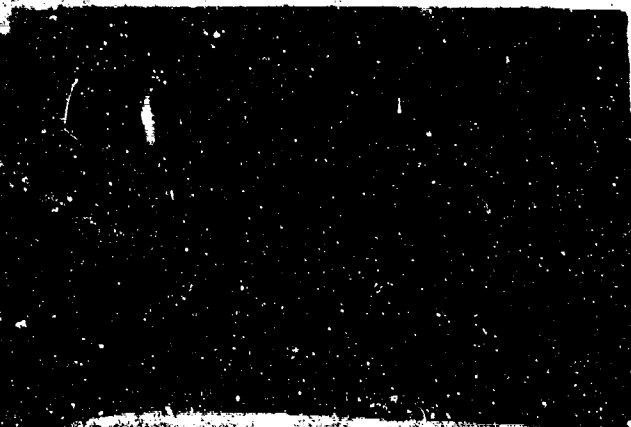


Figure 70. Negative Plate with a 4:1 Construction after 220 Cycles 100X



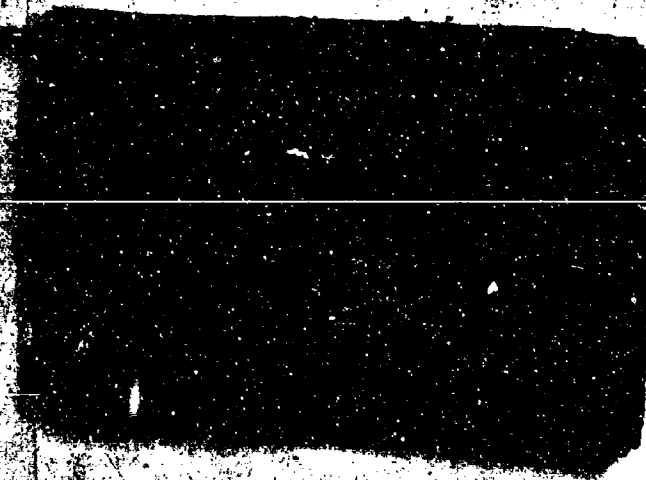
SRAI #4

132 cycles 60% depth



4FSC

312 cycles 40% depth



3RAI #4

276 cycles 40% depth

Figure 71. Appearance of the Negative Material After Cycle Failure in the Separator Test

100X

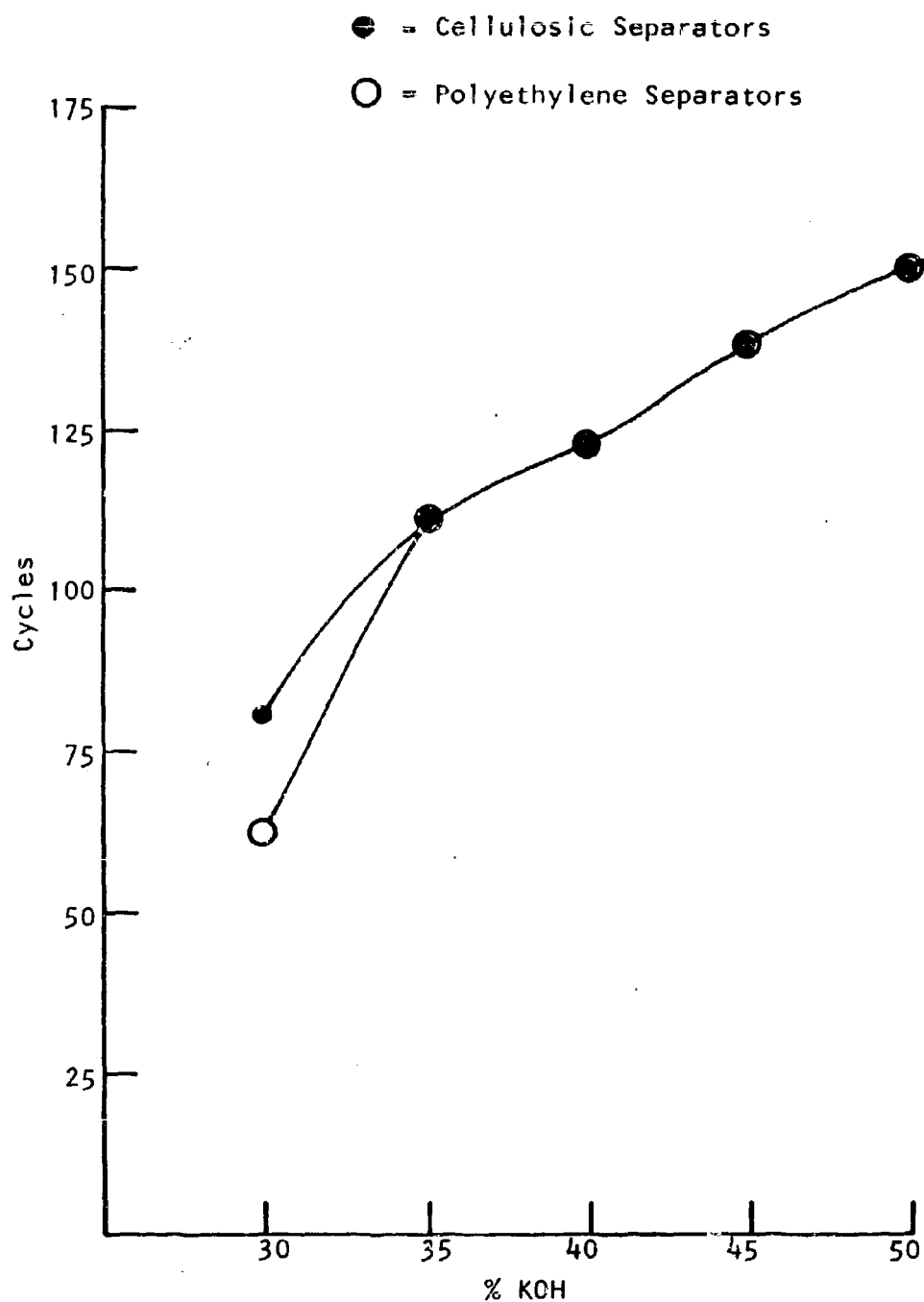


Figure 72. Comparison of Cycle Life of Separators in Various KOH Concentrations

60% DOD

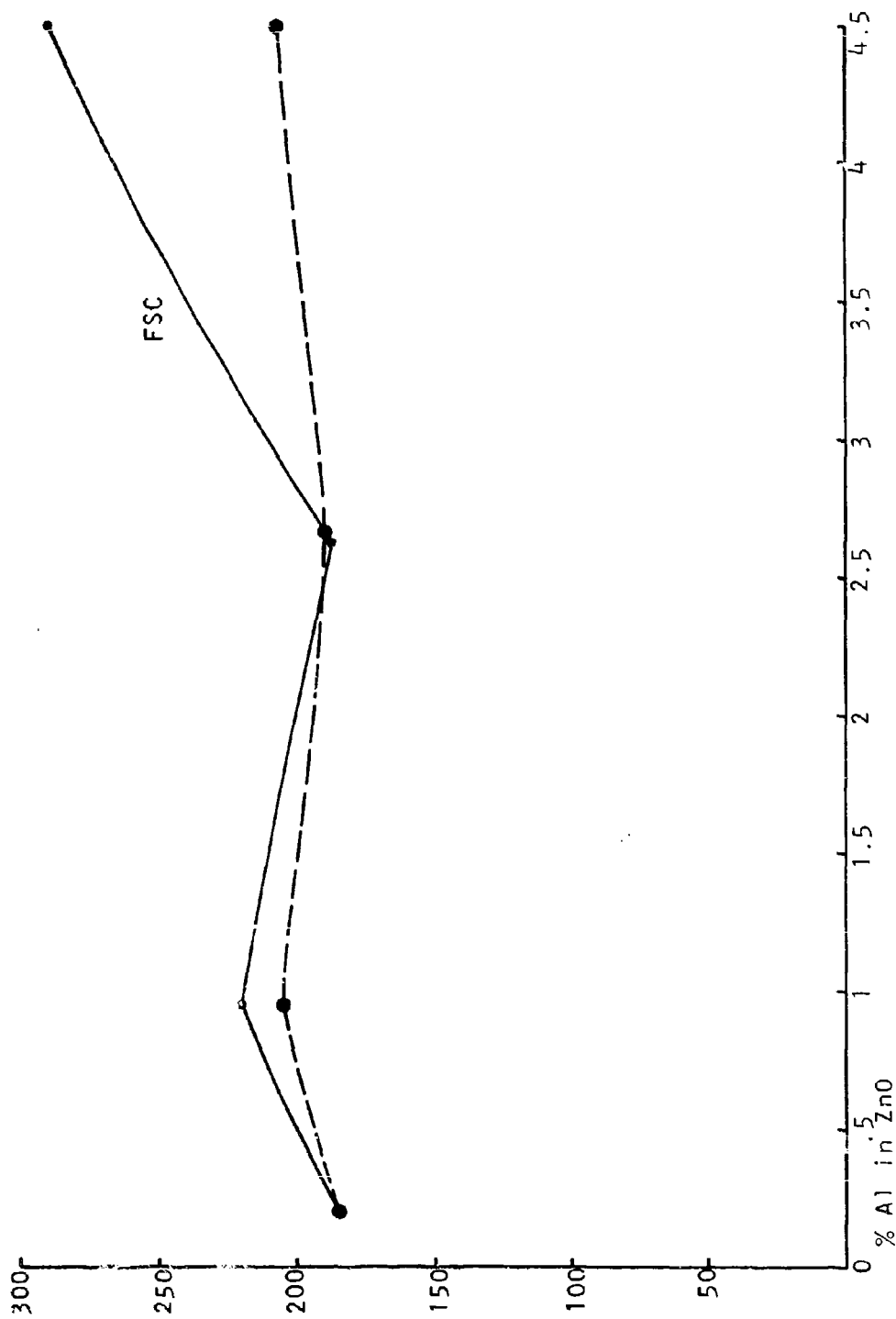


Figure 73. Comparison of Cycle Life of Percent Aluminum in Zinc Oxide in Separators

60% DOD

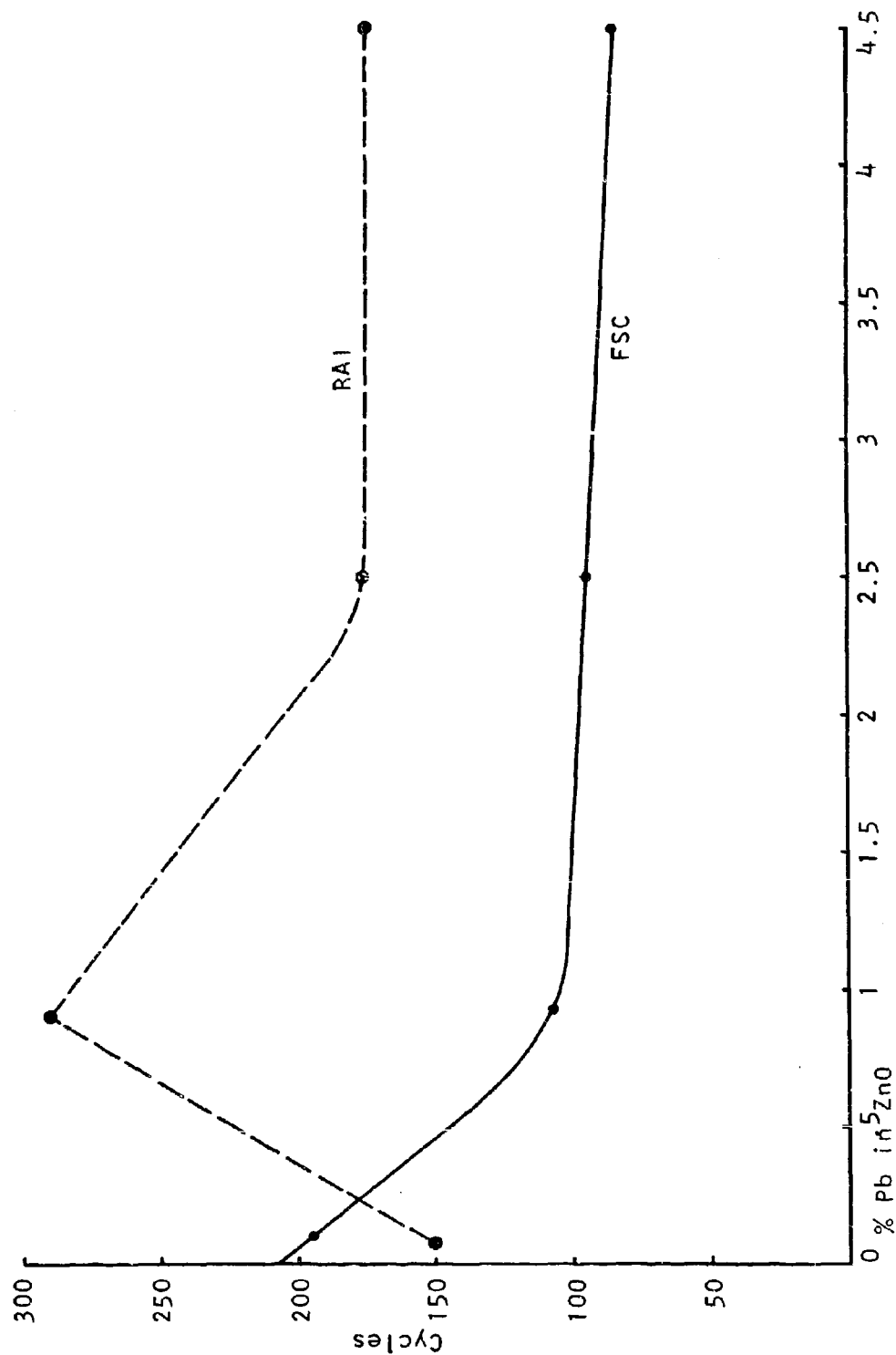


Figure 74. Comparison of Cycle Life of Percent Lead in Zinc Oxide in Separators

APPENDIX I

PREPARATION AND CHARACTERIZATION OF SPECIAL
ZINC OXIDES FOR EVALUATION IN
SILVER OXIDE-ZINC SECONDARY BATTERIES

Purchase Order D-R115475
Under Contract No. AF33(625)-3487

PREPARATION AND CHARACTERIZATION OF SPECIAL
ZINC OXIDES FOR EVALUATION IN
SILVER OXIDE-ZINC SECONDARY BATTERIES

Final Technical Report

Covering the Period

15 October 1966 to 15 October 1968

Dated

October 1968

Prepared by

D. O. Carpenter

G. E. Snow

FOREWORD

This report was prepared by The New Jersey Zinc Company, Palmerton, Pennsylvania on Delco-Remy Division of General Motors Corporation Purchase Order D-R115475 under Air Force Contract No. AF33(615)-3487. The work was directed by Drs. C. E. Barnett and L. J. Reimert.

NOTICE

Foreign announcement and distribution of this report is not authorized. Release to the Clearinghouse for Federal Scientific and Technical Information, CFSTI (formerly OTS) is not authorized. The distribution of this report is limited because it contains technology identifiable with items on the Strategic Embargo Lists excluded from export or re-export under U. S. Export Control Act of 1949 (63STAT.7), as amended (50 USC APP 2020.2031), as implemented by AFR 400-10.

This report is being published and distributed prior to Air Force review. The publication of this report, therefore, does not constitute approval by the Air Force of the findings or conclusions contained herein. It is published for the exchange and stimulation of ideas.

TABLE OF CONTENTS

I. Introduction.....	Page 1
II. Sample Characterization Tests.....	1
A. Air Permeability Particle Size.....	1
B. Nitrogen Adsorption Surface Area.....	2
C. Electron Micrographs.....	2
D. Qualitative Spectrographic Analysis.....	2
E. Special Tests for:	
1. High Electrical Conductivity ZnO.....	3
2. Zinc Dust Samples.....	3
F. Delco-Remy's Electrode Evaluation Procedure.....	4
III. Description of Samples Prepared and Characterized.....	4
A. General Descriptions.....	4
1. Types of ZnO.....	4
2. Particle Size and Morphology of ZnO.....	5
3. Purity and Electrical Conductivity of ZnO.....	5
B. Descriptions of Exploratory Samples.....	7
1. French Process Zinc Oxides of Varying Particle Size.....	7
2. Impurity-doped French Process Zinc Oxides.....	9
A. Survey of Common Impurities.....	9
B. Various Levels of Fe and Pb Impurities....	12
C. Al- and In-Doped Zinc Oxides.....	14
3. High Surface Area Wet Process Zinc Oxides.....	16
A. Wet Process Zinc Oxide from Basic Zinc Carbonate.....	16
B. Wet Process Zinc Oxide from Zinc Chloride.	18
4. Acicular American Process Zinc Oxide.....	20
C. Types of Zinc Dust.....	22
1. Zinc Dust (High Purity).....	22
2. Flaked Zinc Dust.....	22
3. Blue Powder.....	22

TABLE OF CONTENTS (Contd.)

D. Samples Prepared for More Extensive Electrode Evaluation.....	Page 24
IV. Summary of Delco-Remy Electrode Evaluation Results.....	26
V. Appendix - Electron or Optical Micrographs.....	27

LIST OF TABLES

Table 1	ZnO Variables Investigated.....	Page 1
Table 2	Characterization Data for French Process Zinc Oxides of Varying Particle Size.....	8
Table 3	Super-Purity French Process Zinc Oxide.....	10
Table 4	Characterization Data for Impurity-doped French Process Zinc Oxides.....	11
Table 5	Characterization Data for French Process ZnO Doped with Various Levels of Fe and Pb Impurities.....	13
Table 6	Characterization Data for Al- and In-Doped ZnO.....	15
Table 7	Characterization Data for Wet Process Zinc Oxides from Basic Zinc Carbonate.....	17
Table 8	Characterization Data for Wet Process Zinc Oxides from Zinc Chloride.....	19
Table 9	Characterization Data for Acicular American Process Zinc Oxide.....	21
Table 10	Characterization Data for Zinc Dust Samples.....	23
Table 11	Characterization Data for Samples Selected for More Extensive Electrode Evaluations.....	25
Table 12	Effect of Particle Size of French Process Zinc Oxides on Zinc Electrode Performance.....	28
Table 13	Effect of Impurity Doping of French Process Zinc Oxides on Zinc Electrode Performance.....	29
Table 14	Effect of Fe Impurity Doping Level of French Process Zinc Oxides on Zinc Electrode Performance.....	30
Table 15	Effect of Pb Impurity Doping Level of French Process Zinc Oxides on Zinc Electrode Performance.....	31
Table 16	Effect of Al- and In-Doping of French Process Zinc Oxides on Zinc Electrode Performance.....	32
Table 17	Effect of High Surface Area Wet Process Zinc Oxides on Zinc Electrode Performance.....	33

LIST OF TABLES (Contd.)

Table 18	Effect of ZnO Particle Morphology (Acicular vs. Nodular) on Zinc Electrode Performance.....	Page 34
Table 19	Effect of Variations in Zinc Dust on Zinc Electrode Performance.....	35

LIST OF FIGURES

V. Appendix

Figure 1	Sample No. 243-15-1	French Process ZnO	Electron
2	243-27-1	Calcined French Process ZnO	Electron
3	243-139-2	0.92 Wt. % Al-doped French Process ZnO Calcined 600°C.	Electron
4	243-59-1	Wet Process ZnO from Basic Carbonate	Electron
5	243-79-1	Acicular Wet Process ZnO from $\text{ZnCl}_2 + \text{NH}_4\text{OH}$	Electron
6	243-35-1	Acicular American Process ZnO	Electron
7	243-115-1	Blue Powder Type Zinc Dust	Optical
8	243-119-1	Zinc Dust	Optical
9	243-123-1	Flaked Zinc Dust	Optical

8

ABSTRACT

To permit studying the effect of the starting zinc oxide or zinc dust on the performance of the zinc electrode in silver oxide-zinc secondary batteries, a variety of zinc oxides and three zinc dusts were prepared. The samples were selected to allow investigation of the effects of particle size and purity of French Process zinc oxides, particle morphology of American and Wet Process zinc oxide, and the effects of high surface area wet process zinc oxide.

0

I. Introduction

A variety of zinc oxides and zinc dusts have been prepared and characterized for evaluation (by Delco-Remy) in silver oxide/zinc secondary batteries. The objective of the project was to prepare samples which would permit some assessment (by Delco-Remy) of the influence of the starting material on the ultimate performance of the zinc electrodes. Table 1 shows the variables investigated for three types of zinc oxide.

TABLE 1

ZnO Variables Investigated

<u>Type of ZnO</u>	<u>Variables Investigated</u>			
	<u>Particle Size</u>	<u>Particle Morphology</u>	<u>Purity</u>	<u>Electrical Conductivity</u>
French Process	X		X	X
American Process		X	X	
Wet Process	X	X		

In addition to the above zinc oxides, three zinc dusts of varying purity, particle size and particle shape were prepared.

II. Sample Characterization Tests

All of the samples were characterized by the following tests:

A. Air Permeability Particle Size - The method used is essentially the one described by Pechukas and Gage (Industrial and Engineering Chemistry, Analytical Edition, Vol. 18, Page 370, 1946). The reported results represent the surface mean particle diameter. All samples contain a considerable number of fine and coarse particles. The measurement has been calibrated against absolute methods and gives comparable data.

B. Nitrogen Adsorption Surface Area - This measurement is based on the "BET" theory by S. Brunauer, P. H. Emmett, and E. Teller (Journal American Chemical Society, Vol. 60, Page 309, 1938). In place of the usual BET apparatus, an instrument called the AREA-meter, manufactured by Ströhlein and Company, Düsseldorf, Germany, and distributed by the Fisher Scientific Company, is employed. This measurement yields a single-point BET plot, instead of the usual four-point plot. The measured areas are slightly higher than those obtained by standard methods but these differences are not considered serious, especially in view of the high precision of the measurement. The relation between the surface area and surface mean diameter is given by $S = 6/\rho d_g$ where S is surface area in square meters per gram, ρ is density (gm/cc), and d_g is the surface mean diameter in microns.

C. Electron Micrographs - The pigments are well dispersed and mounted in a thin nitrocellulose supporting membrane, with isopropyl acetate as the solvent. The electron micrographs in the report are at 25,200X magnification. This magnification clearly indicates particle morphology but is low enough to assure a representative number of particles in the field.

D. Qualitative Spectrographic Analysis - The procedure for qualitative spectrographic analysis for impurities in a zinc oxide matrix was developed by The New Jersey Zinc Company and is described in a paper by G. W. Standen (Industrial and Engineering Chemistry, Vol. 16, Page 675, November 15, 1944). The results, based on well-defined standards, are reported as follows:

<u>Standard %</u> <u>(Approximate Range)</u>	<u>Reporting Designation</u>
10-100	vs (very strong)
10	s (strong)
1	m (medium)
0.1	w (weak)
0.01	f (faint)
0.001	vf (very faint)
0.0001	xf (extremely faint)
	Trace

With some samples quantitative information with respect to the content of certain impurities was considered to be potentially important. Such samples were analyzed using standard chemical techniques available in the literature.

E. Special Tests for:

1. High electrical conductivity zinc oxides.

Changes in electrical conductivity were measured by a "Dry Powder Resistivity" (DPR) test developed at NJZ. In this test the ZnO powder is compressed in a glass tube and the resistance measured with an electrometer. Resistivity is computed from the sample dimensions and can be in the range of from 10^1 to 10^{10} ohm-cm. Factors such as compacting procedure, temperature, and humidity are important variables, especially for high resistivity samples. The measurement is a satisfactory quality control guide for high conductivity zinc oxides.

2. Zinc dust samples.

Due to the relatively large size of the particles, optical micrographs (1000X) were used to show particle shape instead of electron micrographs. The latter, even at minimum magnification, do not give results representative of the samples.

The particle sizes were measured by the Coulter Counter method. See A.S.T.M. Special Technical Publication No. 234, pg. 245, by R. H. Berg for a description of the method. To avoid the problem of rapid settling of zinc dust, 25 vol. % glycerine was added to the electrolyte.

For the flaked zinc dust sample, the average flake thickness was determined by the covering area method. For test purposes, the particles are rendered hydrophobic by treatment with stearic acid. The flakes are floated on water and the area covered by a given weight of sample is measured. See "Powder Metallurgy" by John Wolffe, American Society for Metals (1942), pg. 127 for a more detailed description of the test.

F. Delco-Remy's Electrode Evaluation Procedure - The cells were constructed with four layers of separator material so as to restrict the mode of failure to the zinc electrode. Except for two samples, the cells were charged to initial capacities of 25 a.h. A 2-hr. cycle (35 min. discharge, 85 min. charge) involving 60% depth of discharge was used for all tests. The electrodes were considered to have failed when recycling reduced the capacity to less than 15 a.h.

III. Description of Samples Prepared and Characterized

A. General Descriptions

1. Types of ZnO - There are two main commercially used methods of manufacture of zinc oxide. French (or Indirect) Process zinc oxide is obtained by heating zinc metal and burning the vapor in air. American (or Direct) Process zinc oxide manufacture involves smelting the zinc ore with coal and burning the evolved zinc vapor and liberated gases in air. Due to the source of the zinc, French Process zinc oxide has higher purity than American Process. (See page 372 of "Zinc - The Metal, Its Alloys and

Compounds" by C. H. Mathewson, Reinhold Publishing Corporation, for a description of manufacturing processes).

A third common method of preparing zinc oxide is referred to as the "wet or precipitation" process. A zinc compound, such as zinc carbonate or zinc oxalate, is prepared by wet chemical techniques and then thermally decomposed to zinc oxide. This procedure yields a high surface area, fine particle size zinc oxide. Another wet process procedure involves precipitation of zinc oxide by the action of Na, K or NH_4 hydroxides on zinc chloride water solutions. (Procedures have been described by K. Terada, Institute of Physical Chemical Research of Tokyo, Vol. 16, Page 75, 1931 and in German patent number 481,284 issued January 27, 1927).

2. Particle Size and Morphology of ZnO - French and American Process zinc oxides covering a particle size range of about 0.1μ to 0.5μ can be produced by varying the zinc vapor combustion conditions. By reheating techniques, the particles can be grown to about 3μ , so the overall range is 0.1μ to 3μ . Wet process zinc oxides with about 0.02μ particle size can be prepared.

Zinc oxides with well-crystallized nodular or acicular needle-like particle morphology can be prepared by careful control of the zinc vapor combustion conditions in the American Process. Both particle morphologies can also be obtained for wet precipitation processes. However, wet process zinc oxides are not as well-crystallized as the French or American Process types.

3. Purity and Electrical Conductivity of ZnO - The purity of ZnO can vary considerably depending on the source of zinc and manufacturing conditions. In some cases, specific impurities (generally cationic) are added

to zinc oxide to alter its properties. A brief discussion of some of the factors involved in doping zinc oxide is given below.

Zinc oxide is a well-known n-type (excess electron) semiconductor. The excess electrons arise because the usual preparation techniques yield a zinc oxide non-stoichiometric in the direction of excess zinc. The excess zinc, occupying interstitial lattice positions, ionizes to yield free or quasi-free electrons with significant lifetimes and mobilities. The concentration of free electrons can be changed by incorporating impurities in the zinc oxide lattice. Addition of trivalent metal cations, for example, Al or In, increases the free electron concentration. The structure of zinc oxide is close-packed hexagonal but, since the zinc and oxygen atoms occupy only 44% of the volume, relatively large (0.95 Å) open spaces are available for accommodation of impurities. Impurity promoters of ZnO are divided into the following two groups:

1. Intracrystalline - impurities with ionic radius approximately 0.6 to 0.9 Å which are internal to the crystalline lattice. Such materials give rise to solid solutions.
2. Intercrystalline - impurities are external to the crystalline lattice.

Such classifications can not be regarded as an absolute rule because intra- or intercrystalline occupancy of positions will be at least partially dependent on the preparation procedure.

A relatively common method for impurity additions involves preparation of an intimate blend of an oxide of the dopant with the zinc oxide followed by calcination. This is frequently a preferred procedure when addition of anion impurities is to be avoided. In some cases, the thermally decomposable dopant oxalates or carbonates are also used.

B. Descriptions of Exploratory Samples

1. French Process Zinc Oxides of Varying Particle Size - Four

French Process zinc oxides covering the particle size range 0.13 to 0.40 μ were selected from New Jersey Zinc Company commercial production. Portions of the 0.40- μ sample were reheated to grow the particle size. The sample designated 243-23-1 was heated 1 hr. at 600°C. in 5% H₂-95% N₂ followed by 1/2 hr. at 600°C. in air. The particle size was increased to 0.62 μ . Sample 243-27-1 was heated for the same time in the two atmospheres but at a temperature of 725°C. The particle size was increased to 1.02 μ . This procedure successfully increases the particle size, while avoiding excessive sintering and formation of excess interstitial zinc. Table 2 gives the air permeability particle size, N₂ adsorption surface area, and qualitative spectrographic analysis data for this series of samples. Figure 1 shows an electron micrograph of a typical French Process ZnO and Figure 2 shows a ZnO calcined to increase the particle size.

TABLE 2

Characterization Data for French Process Zinc Oxides of Varying Particle Size

Sample No.	243-7-1	243-11-1	243-15-1	243-19-1	243-23-1*	243-27-1*
Particle Size, μ	0.13	0.24	0.33	0.40	0.62	1.02
Surface Area, M^2/Gm	9.5	5.0	3.7	3.0	1.7	0.95
Spectrographic Analysis Data						
Zn	vs	vs	vs	vs	vs	vs
Si	Trace	f-w	xf-vf	vf	vf	xf-vf
Pb	vf	vf	vf	vf	vf	vf
Cd	xf-vf	vf	xf-vf	xf-vf	xf-vf	xf-vf
Al	xf-vf	xf-vf	xf-vf	xf-vf	xf-vf	xf-vf
Fe	Trace	Trace	Trace	Trace	Trace	xf
B	xf-vf	xf-vf	xf-vf	vf	vf	vf
Cu	xf	xf	xf	xf	xf	xf
Mg	Trace	Trace	Trace	Trace	Trace	Trace
Sb	Trace	Trace	Trace	Trace	Trace	Trace
Ti	--	--	--	--	--	--
Ge	--	--	--	--	--	--
Sn	--	--	--	--	--	--
Mn	--	--	--	--	--	--
Ag	--	--	--	--	--	--
Ga	--	--	--	--	--	--
Bi	--	--	--	--	--	--
In	--	--	--	--	--	--
Electron Micrograph Figure No.	--	--	1	--	--	2

*Samples reheated to increase particle size.

--Not Detected.

2. Impurity-doped French Process Zinc Oxides

A. Survey of Common Impurities - Table 3 gives the characterization data for a special super-purity French Process ZnO made with high purity metal. Table 4 shows the data for ZnO's containing a variety of metallic impurities. The electron micrograph of the sample in Figure 1 is also typical of these doped ZnO's except that the doping procedure causes some increase in the particle size.

Except for the excess zinc-containing sample, the doped samples were prepared by 600°C. calcination in air of an intimate admixture of the zinc oxide and an oxide of each specific metallic impurity.

(1) Fe, Cd, Cu, Sn, Mn, Pb - These samples contain approximately equal mole percentages, rather than equal weight percentages, of added impurities. Since each sample contains an equal number of impurity ions, intercomparisons, as well as individual comparisons with high purity zinc oxide, are possible.

(2) As - Since growth of dendrites is a factor in the failure of zinc electrodes, a sample was doped with As at a level more than adequate to prevent growth of acicular particles in American Process zinc oxide manufacture.

(3) Zn - The n-type semiconducting properties of zinc oxide are generally attributed to the presence of excess interstitial zinc. To study this effect, the excess zinc content of a French Process zinc oxide was increased from a normal value of about 0.002 wt. % to 0.009 wt. % by calcination at 800°C. in a reducing atmosphere.

TABLE 3

Super-Purity French Process Zinc Oxide (Sample 243-31-1)0.33- μ Particle Size3.7-M²/Gm Surface Area

<u>Qualitative Spectrographic Analysis</u>		<u>Chemical Analysis</u>	
Zn	vs		
Si	xf-vf		
Pb	vf	PbO	0.0006%
Cd	xf-vf	CdO	0.0001%
Al	xf-vf		
Fe	Trace	Fe ₂ O ₃	0.0001%
B	--		
Cu	xf	CuO	<0.00005%
Mg	Trace		
Sb	--		
Ti	--		
Ge	--		
Sn	--		
Mn	--		
Ag	--		
Ga	--		
Bi	--		
In	--		
		S as SO ₃	0.002%
		CO ₂	0.021%

TABLE 4

Characterization Data for Impurity-doped French Process Zinc Oxides

Technical Plan Item No.	18	19	20	21	22	23	24	17
Sample No.	243-83-1*	243-87-1	243-91-1	243-95-1	243-99-1	243-103-1	243-107-1	243-111-1
Impurity	--	Sn	Cd	Cu	Fe	Mn	Pb	As
Wt. % Impurity	--	0.13	0.13	0.081	0.07	0.089	0.25	0.027
Mole % Impurity	--	0.09	0.1	0.1	0.1	0.13	0.1	0.03
Air Permeability	--	0.45	0.44	0.44	0.45	0.43	0.42	0.41
Particle Size (μ)	0.43	0.45	0.44	0.44	0.45	0.43	0.42	1.64
N ₂ Adsorption								
Surface Area								
(M ² /G)	2.7	2.6	2.7	2.6	2.7	2.8	2.9	0.43
Qualitative Spectrographic Analysis - Element								
Zn	vs	vs	vs	vs	vs	vs	vs	vs
Pb	vf	vf	vf	vf	vf	vf-f	w-m	vf
Al	xf-vf	xf-vf	xf-vf	vf	vf	vf	vf	vf
Si	xf	vf	xf	vf	vf	f	vf	xf-vf
Sb	xf-vf	xf-vf	xf-vf	xf-vf	Trace	xf-vf	xf-vf	xf-vf
Cd	xf	xf	w-m	xf-vf	xf-vf	xf-vf	xf-vf	xf
Mg	xf	xf	xf	xf	xf-vf	xf	xf	xf
Cu	xf	xi	xf	w-m	xf	vf	xf	Trace
Fe	Trace	Trace	Trace	Trace	w	xf	xf	Trace
Ti	vf-f	vf-f	--	--	f	--	--	--
B	xf	xf-f	xf	xf-vf	xf-vf	xf-vf	xf-vf	vf
Sn	--	m	--	--	--	--	--	--
Mn	--	--	--	--	xf	w-m	xf	--
As	--	--	--	--	--	--	--	w

*Base ZnO calcined under same conditions as items 18-24 but no impurities added.

B. Various Levels of Fe and Pb Impurities - Electrode evaluation results indicated that Fe at 0.07% had a detrimental effect on cycle-life whereas Pb at 0.25% was beneficial. Therefore, additional samples containing these dopants were prepared in an attempt to investigate the concentration dependency of their respective effects. These Fe-doped ZnO's covered the range 0.0003% to 0.01% Fe and the Pb-doped ZnO's 0.028% to 2.5% Pb. Samples were prepared as in Part A, i.e., 600°C. calcination. Since Fe may be present in ZnO as "tramp" material, one sample was prepared as a simple dry blend of the oxides and not calcined. It was also considered that Pb might counteract the detrimental effects of Fe. Thus one sample was doped with both of these impurities.

It should be mentioned that a qualitative X-ray diffraction examination of the samples containing 1% Pb or more indicated that not all of the Pb went into solid solution with the ZnO.

The characterization data for these samples are given in Table 5.

TABLE 5

Characterization Data for French Process ZnO Doped With

Various Levels of Fe and Pb Impurities

Sample No.	243- 127-2(1)	243- 107-4	243- 107-1	243- 107-2	243- 107-3	243- 131-1	243- 131-2A(3)	243- 131-2B	243- 99-1	243- 135-1
N ₂ Adsorption Surface Area M ² /G	2.7	2.7	2.9	3.4	3.5	2.6	3.5	2.6	2.7	2.9
Air Permeability Particle Size (μ)	0.46	0.47	0.42	0.38	0.37	0.46	0.36	0.45	0.45	0.42
Dopant Content Wt. %										
Fe	0.003(2)	0.003(2)	0.003(2)	0.003(2)	0.003(2)	0.0006	0.0086	0.0092	0.07	0.010
Pb	0.008(2)	0.028	0.25	1.02	2.42	--	--	--	--	0.26

Qualitative
Spectrographic
Analysis -

Zn	vs	vs	vs	vs	vs	vs	vs	vs	vs	vs
Pb	vf-f	w	w-m	f-w	m	vf-f	vf-f	f-w	vf	w-m
Si	f-w	f-w	f-w	f-w	f-w	f	f	f	f	f
Fe	vf	vf	vf	vf	vf	vf	vf	vf	w	f
Cu	vf-f	vf-f	vf	vf	vf-f	xf-vf	vf	xf-vf	xf	xf-vf
Al	vf	vf	vf	vf	vf	vf	vf	vf	vf	vf
Cd	xf	xf	xf	xf	xf	xf	xf	xf	xf-vf	xf
Mg	xf	xf	xf	xf	xf	xf	xf	xf	xf-vf	xf
B	xf	Trace	Trace	Trace	Trace	Trace	Trace	Trace	xf-vf	xf
Bi	--	--	--	--	xf	--	--	--	--	--
Mn	Trace	Trace	Trace	Trace	Trace	Trace	Trace	Trace	xf	xf
Sb	Trace	Trace	Trace	Trace	Trace	Trace	Trace	Trace	Trace	Trace

- (1) Base ZnO calcined at 600°C. in air.
 (2) Impurity present in the base ZnO.
 (3) Not calcined.

C. Al- and In-Doped Zinc Oxides - The general methods for development of high conductivity in zinc oxide were described in Part III A-3. The specific procedure for doping with Al^{+3} is described in U. S. Patent 3,089,856 by H. M. Cyr and N. S. Nanovic, assigned to NJZ, and issued May 14, 1963. Details of the procedure for doping with In^{+3} are considered proprietary information.

Two other Al-doped samples were prepared in an attempt to assess the importance of high electrical conductivity vs. the simple presence of Al in the ZnO. These were prepared by the 600°C. air atmosphere calcination of a blend of ZnO and Al_2O_3 . The surface area and electron micrograph data (Figure 3) show that unfortunately very little of the Al formed a solid solution with the ZnO. The many fine particles apparent in Figure 3 are believed to be Al_2O_3 .

The High Conductivity Al-doped ZnO sample (No. 243-41-1) had a particle size of 1.02μ and is therefore appropriate for comparison with the 1.02μ reheated French Process ZnO (No. 243-27-1) shown in Table 2. It should also be noted that normal French Process ZnO's have "Dry Powder Resistivities" of the order of 10^{10} ohm-cm vs. 10^2 to 10^4 ohm-cm for the High Conductivity oxides.

Characterization data for the above samples are given in Table 6.

TABLE 6

Characterization Data for Al- and In-Doped ZnO

Sample No. Amount and Type of Impurity Dry Powder Resistivity Air Permeability Particle Size N ₂ Adsorption Surface Area	High Conductivity		"Low" Conductivity	
	243-41-1	243-45-1	243-139-1	243-139-2
	0.30% Al*	0.48% In	0.07% Al	0.92% Al
	$9.4 \times 10^2 \Omega\text{-cm}$	$3.5 \times 10^3 \Omega\text{-cm}$	--	--
	1.02 μ	2.3 μ	0.46 μ	0.36 μ
	1.3 m ² /g	0.36 m ² /g	2.7 m ² /g	4.4 m ² /g
Qualitative Spectrographic Analysis - Element				
Zn	vs	vs	vs	vs
Si	vf	vf	f	f
Pb	vf	f	f	f
Cd	xf-vf	xf-vf	xf	xf
Al	w-m	vf	w	w-m
Fe	vf	xf	xf-vf	xf-vf
B	vf	vf	--	--
Cu	xf	xf-vf	xf-vf	xf-vf
Mg	xf	xf	xf-f	xf-f
Sb	Trace	Trace	Trace	Trace
Ti	--	--	--	--
Ge	--	--	--	--
Sn	--	f	--	--
Mn	--	Trace	--	--
Ag	--	--	--	--
Ga	--	--	--	--
Bi	--	--	--	--
In	--	m-s	--	--
Electron Micrograph Figure No.	--	--	--	3

*Residual Cl⁻ content-0.02%.

3. High Surface Area Wet Process Zinc Oxides

A. Wet Process Zinc Oxide from Basic Zinc Carbonate - In these preparations, basic zinc carbonate ($5 \text{ ZnO} \cdot \text{CO}_2 \cdot 4 \text{ H}_2\text{O}$) is formed by adding CO_2 gas to a vigorously agitated water dispersion of 0.33μ French Process ZnO . With calcination, the basic zinc carbonate decomposes to yield a voluminous, high surface area, fine particle size ZnO . The time and temperature of calcination determine the particle size and surface area of the ZnO product. Calcination conditions and other characterization data are given in Table 7. Figure 4 is an electron micrograph of a typical wet process ZnO .

In addition to sample characterization tests previously described, the particle size of sample 243-67-2 was measured by the method of X-ray diffraction line broadening. This method involves the measurement of the width of the lines in the X-ray diffraction pattern, and then estimating the particle size from the Scherrer formula. For this sample the estimated size was 0.018μ . Air permeability particle size measurements are not too satisfactory for very fine particle samples. Hence the 0.018μ line broadening size is probably more representative of the actual size than the 0.025μ air permeability value.

TABLE 7

Characterization Data for Wet ProcessZinc Oxides from Basic Zinc Carbonate

Sample No.	243-59-1	243-63-1	243-67-2
Calcination Time and Temperature	1-1/2 hr, 460°C.	1-1/2 hr, 360°C.	4 hr, 310°C.
Air Permeability			
Particle Size	0.052 μ	0.031 μ	0.025 μ
Nitrogen Adsorption			
Surface Area	21.7 m ² /g	33.7 m ² /g	51.0 m ² /g
CO ₂ Content	0.21%	0.23%	0.34%
Qualitative Spectrographic Analysis			
Zn	vs	vs	vs
Al	vf	xf-vf	xf-vf
Si	vf	f	xf
Ti	--	--	--
Fe	vf	vf	xf
Ca	--	--	--
Mg	xf	xf	Trace
Cr	xf	--	--
Ni	xf	--	--
Pb	vf	vf	vf
Mn	xf	--	Trace
B	vf	vi	vf
Mo	--	--	--
Cu	xf-vf	xf-vf	xf
Cd	xf-vf	xf-vf	xf
Sb	xf-vf	xf	Trace
Electron Micrograph Figure No.	4	--	--

B. Wet Process Zinc Oxide from Zinc Chloride - Samples of wet process ZnO were prepared by the reactions of ZnCl_2 with NaOH, KOH, and NH_4OH . The NaOH and KOH reaction products are fine nodular oxides, with NaOH yielding the smaller particle size. The NH_4OH reaction product is acicular.

The NaOH and KOH reactions were carried out by adding a solution of 5.4-M reagent grade ZnCl_2 to a 6.8-M solution of the base at 100°C . under moderate agitation. Two mols of base were used per mol of ZnCl_2 added. The addition time was 4 hr for the NaOH reaction and 3 hr for the KOH. The products were washed by reslurrying in distilled water to remove the residual chloride and dried in air at 110°C . The final dry cake was micropulverized.

No detailed conditions for the $\text{ZnCl}_2 + \text{NH}_4\text{OH}$ reaction are presented, since this is considered proprietary information.

The characterization data are given in Table 8. Figure 5 shows the electron micrograph of the acicular sample from $\text{ZnCl}_2 + \text{NH}_4\text{OH}$.

TABLE 8

Characterization Data for Wet Process

Zinc Oxides from Zinc Chloride				
Sample No.	Method of Preparation	243-71-1 ZnCl ₂ + NaOH	243-75-1 ZnCl ₂ + KOH	243-79-1 ZnCl ₂ + NH ₄ OH
Air Permeability Particle Size		0.092 μ	0.155 μ	0.155 μ
N ₂ Adsorption Surface Area		18.3 M ² /G	10.5 M ² /G	7.1 M ² /G
CO ₂ Content		--	--	--
Cl ₂ Content		0.13%	0.11%	0.43%

Qualitative Spectrographic Analysis

	Zn	Si	Pb	Cd	Al	Fe	B	Cu	Mg	Sb	Ti	Mn	Ca	Cr	Ni
	vs	vs	vs	vs	vs	vs	vs	vs	vs	vs	vs	vs	vs	vs	vs
	w-m	w-m	w-m	w-m	w-m	w-m	w-m	w-m	w-m	w-m	w-m	w-m	w-m	w-m	w-m
	vf-f	vf-f	vf-f	vf-f	vf-f	vf-f	vf-f	vf-f	vf-f	vf-f	vf-f	vf-f	vf-f	vf-f	vf-f
	vf	vf	vf	vf	vf	vf	vf	vf	vf	vf	vf	vf	vf	vf	vf
	vf	vf	vf	vf	vf	vf	vf	vf	vf	vf	vf	vf	vf	vf	vf
	xf	xf	xf	xf	xf	xf	xf	xf	xf	xf	xf	xf	xf	xf	xf
	xf-f	xf-f	xf-f	xf-f	xf-f	xf-f	xf-f	xf-f	xf-f	xf-f	xf-f	xf-f	xf-f	xf-f	xf-f
	vf	vf	vf	vf	vf	vf	vf	vf	vf	vf	vf	vf	vf	vf	vf
	xf-vf	xf-vf	xf-vf	xf-vf	xf-vf	xf-vf	xf-vf	xf-vf	xf-vf	xf-vf	xf-vf	xf-vf	xf-vf	xf-vf	xf-vf
	f	f	f	f	f	f	f	f	f	f	f	f	f	f	f
	vf	vf	vf	vf	vf	vf	vf	vf	vf	vf	vf	vf	vf	vf	vf
	xf	xf	xf	xf	xf	xf	xf	xf	xf	xf	xf	xf	xf	xf	xf
	xf-vf	xf-vf	xf-vf	xf-vf	xf-vf	xf-vf	xf-vf	xf-vf	xf-vf	xf-vf	xf-vf	xf-vf	xf-vf	xf-vf	xf-vf
	--	--	--	--	--	--	--	--	--	--	--	--	--	--	--
	5	5	5	5	5	5	5	5	5	5	5	5	5	5	5

Electron Micrograph Figure No.

5

4. Acicular American Process Zinc Oxide - American Process (A.P.)

ZnO with acicular particle morphology can be obtained by careful control of the Zn combustion conditions, as previously mentioned. Since the impurities (water-soluble salts and sulfur) present in A.P. ZnO might affect electrode performance, an attempt was made to "purify" the acicular A.P. ZnO by a washing procedure.

This is accomplished by dispersing 240 gm of acicular A.P. zinc oxide in one liter of distilled water at room temperature. Aqua ammonia is added to increase the pH from 6.9 to 9.1. After 1/2 hr of mild agitation, the zinc oxide is filtered out, dried at 110°C., and micropulverized to break up particle aggregates.

Table 9 and Figure 6 give the characterization data for this sample.

TABLE 9

Characterization Data for Acicular American Process Zinc Oxide

Sample No.	243-35-1
Method of Preparation	Washed A.P.
Air Permeability Particle Size	0.26 μ
N ₂ Adsorption Surface Area	4.7 m ² /g
Chemical Analysis: % Cl ₂	--
% S as SO ₃	0.04 (0.22*)
% H ₂ O-Sol. Salts	0.11 (0.50*)
% PbO	0.068 (0.08*)

Qualitative Spectrographic Analysis

Zn	vs
Si	w-m
Pb	w
Cd	w
Al	f
Fe	f
B	vf-f
Cu	vf-f
Mg	vf
Sb	vf
Ti	f-w
Mn	vf

*Impurity of typical acicular A.P. ZnO.

Electron Micrograph Figure No. 6

C. Types of Zinc Dust

1. Zinc Dust (High Purity) - Zinc dust is prepared by condensation of refined zinc vapor in an inert atmosphere; hence the metallic content is high and the iron content low. (See J. N. Pomeroy and J. E. Crowley, ACS Monograph No. 142,318 (1959) for more information on zinc dust manufacturing processes).

2. Flaked Zinc Dust - The flaked zinc dust was prepared by ball milling a portion of the above type zinc dust of product in a varnolene dispersion. This milling treatment causes some "flattening" of the zinc particles. The varnolene residue is removed by repeated washing with acetone. The washing and drying occasions some oxidation, which decreases the metallic zinc content. Steel balls used for the milling cause some increase in iron contamination.

3. Blue Powder - The Blue Powder sample is a by-product of the vertical retort zinc smelting process. It is collected by water scrubbing the condenser exhaust gases. Due to the method of collection and drying, considerable oxidation of the zinc occurs. The iron impurity content tends to be high because at this stage in the vertical retort process the metal has not been refined.

The characterization data for these samples is given in Table 10 and Figures 7-9.

TABLE 10

Characterization Data for Zinc Dust Samples

<u>Sample No.</u>	<u>Description</u>	<u>Average Particle Size</u>	<u>% Metallic Zinc</u>	<u>% Total Zinc</u>	<u>% Iron</u>
243-115-1	Blue Powder	10.5 μ	57.2	83.5	0.14
243-119-1	Zinc Dust	5.3 μ	95.7	98.8	0.0001
243-123-1	Flaked Zn Dust	*	91.1	97.4	0.003

Spectrographic Analysis

Element	Sample No.	
	243-115-1	243-119-1 243-123-1
Si	s	f-w w
Al	m-s	vf vf
Mg	m-s	xf xf
Ti	m	vf vf
Cd	w-m	w w
Ca	w-m	-- --
Pb	w	w-m w-m
Mn	f-w	-- --
Sn	f-w	-- vf
B	f	xf --
Cu	vf-f	vf vf
Cr	vf-f	xf-vf xf-vf
V	vf-f	-- --
Sn	vf	-- --
Sb	vf	xf-vf xf-vf
Bi	xf	xf xf

*Average flake thickness = 2.5 μ Optical Micrograph
Figure No.

7

8

9

D. Samples Prepared for More Extensive Electrode Evaluation

Delco-Remy selected the following samples for more extensive electrode evaluation tests:

<u>Sample No.</u>	<u>Description</u>	<u>Quantity Prepared</u>
243-41-2	High Conductivity Al-doped ZnO	25 lb
243-107-5	0.25% Pb-doped ZnO	25 lb
243-123-2	Flaked Zn-Dust	25 lb
243-41-3	High Conductivity Al-doped ZnO	75 lb
243-107-6	0.25% Pb-doped ZnO	75 lb

Characterization data for these samples are given in Table 11. The electrode evaluations are still in progress.

TABLE 11

Characterization Data for Samples Selected for More Extensive Electrode Evaluations

Sample No. Description	243-41-2 High Conductivity Al-doped	243-41-3 High Conductivity Al-doped	243-107-5 Pb-doped ZnO 600°C. Calcination	243-107-6 Pb-doped ZnO 600°C. Calcination	243-123-2 Flaked Zinc Dust
Quantity Prepared	25 lb	75 lb	25 lb	75 lb	25 lb
Particle Size, μ	1.04	1.08	0.42	0.42	*
Surface Area, m^2/g	1.3	1.2	2.5	2.5	--
Impurity	0.27% Al	0.29% Al	0.24% Pb	0.25% Pb	0.08% Pb 0.002% Fe 96.7% Tot. Zn
Dry Powder Resistivity (ohm-cm)	3.2×10^3	5.8×10^3	--	--	--
Qualitative Spectro- graphic Analysis					
Zn	vs	vs	vs	vs	vs
Cd	xf	Trace	xf	xf	w
Pb	xf-vf	xf	w-m	w-m	w
Fe	vf	vf	xf	xf	vf-f
Si	f	vf	xf-vf	xf	vf-f
B	Trace	--	Trace	--	vf-f
Al	w	w-m	vf	xf-vf	vf
Cu	xf-vf	xf	xf-vf	xf	xf-vf
Mg	vf	xf	xf	xf	xf
Mn	xf	Trace	--	--	Trace
Sb	Trace	Trace	Trace	Trace	Trace

*Average flake thickness - 2.5μ

IV. Summary of Delco-Remy Electrode Evaluation Results

This section contains a brief summary of the electrode performance data obtained by D-R on the smaller samples. No attempt will be made to electrochemically interpret the results or judge their significance. The evaluation procedure employed by D-R has been described in section II of this report.

Table 12 covers the effect of French Process ZnO particle size on cell life. The results are not conclusive but they do indicate decreased performance for excessively large particle size ZnO.

Table 13 gives the effects of relatively high levels of metallic impurities. Many of these impurities are present at low levels in commercial French Process ZnO. Of those listed in the table, Fe and Pb were considered of interest. The Fe had a definite detrimental effect, whereas Pb appears to be beneficial.

Table 14 shows the detrimental effect of Fe at various concentrations from 0.003 to 0.07%. The data suggest that Fe levels should be kept as low as possible.

Table 15 gives results for various levels of Pb. The data indicate a generally high performance for Pb-doped ZnO but do not clearly define the concentration effects. A comparison of sample 243-135-1 with 243-131-2B (Table 14) suggests that Pt might possibly compensate for the adverse effects of Fe.

Table 16 shows the influence of Al-impurity added under two conditions; (a) controlled activation to yield high electrical conductivity, and (b) simple 600°C. air atmosphere calcination which yields low electrical conductivity. A high conductivity In-doped ZnO is also shown. Nothing

definite can be said about the effects of Al. However, the results do show that both of the high conductivity samples perform quite satisfactorily in comparison with an undoped oxide (243-27-1) of similar particle size.

Table 17 covers the effect of particle size, but in this case very fine particle size ZnO's prepared by wet processes were evaluated. The results do not indicate any advantage for ZnO's with particle sizes less than normal French Process ZnO.

In Table 18, the performances of nodular and acicular ZnO's of similar particle size are compared. The American Process acicular ZnO was very poor and the wet process sample no better than nodular French or wet process ZnO's. These results have not clearly established the effects of particle morphology. Delco-Remy have noticed that upon cell failure the acicular ZnO's tend to exhibit less electrode erosion than the nodular oxides.

Table 19 compares 3 types of zinc dust samples. The normal Zn-dust and flaked Zn-dust performed satisfactorily in comparison with the ZnO's. However, the Blue Powder, possibly because of its particle size or Fe content, failed completely.

V. Appendix

Electron or optical micrographs of samples.

TABLE 12

Effect of Particle Size of French Process Zinc Oxides on Zinc Electrode Performance

(Cycles to failure at 60% depth of discharge)

Sample No. *	Description	Particle Size, μ	Surface Area, M^2/Gm	Cycles to Failure
	Delco-Remy Control (Kadox 15 - Fine particle size French Process ZnO)			130
243-7-1	French Process ZnO	0.13	9.5	108
243-11-1	French Process ZnO	0.24	5.0	96
243-15-1	French Process ZnO	0.33	3.7	106
243-19-1	French Process ZnO	0.40	3.0	132
243-23-1	Sample 243-19-1 calcined at 600°C. to increase particle size	0.62	1.7	96
243-27-1	Sample 243-19-1 calcined at 725°C. to increase particle size	1.02	0.95	80

*For more sample information see Table 2.

TABLE 13
Effect of Impurity Doping of French Process Zinc Oxides
on Zinc Electrode Performance

(Cycles to failure at 60% depth of discharge)
(Impurity added by 600°C. air atmosphere calcination of
dry blend of ZnO plus impurity oxide)

Sample No.*	Description	Impurity Level** Wt. %	Particle Size, μ	Surface Area, M^2/Gm	Cycles to Failure
	Delco-Remy Control				130
243-31-1	Super-Purity ZnO		0.33	3.7	124
243-83-1	Base ZnO for samples below		0.43	2.5	156
243-87-1	Sn-Impurity	0.13	0.45	2.6	132
243-91-1	Cd-Impurity	0.13	0.44	2.7	120
243-95-1	Cu-Impurity	0.08	0.44	2.6	132
243-99-1	Fe-Impurity	0.07	0.45	2.7	0
243-103-1	Mn-Impurity	0.089	0.43	2.8	130
243-107-1	Pb-Impurity	0.25	0.42	2.9	200
243-111-1	As-Impurity	0.027	0.41	2.9	80
243-49-4	Zn-Impurity	0.009	1.64	0.43	156

*For more sample information see Tables 3 and 4.

**Except for sample 243-111-1, samples all contain about 0.1 mole % impurity.

TABLE 14
Effect of Fe Impurity Doping Level of French Process Zinc Oxides
on Zinc Electrode Performance

(Cycles to failure at 60% depth of discharge)
(Impurity added by 600°C. air atmosphere calcination of
dry blend of ZnO plus impurity oxide)

Sample No.(1)	Wt. % Fe	Particle Size, μ	Surface Area, M^2/Gm	Cycles to Failure
243-127-2(2)	0.0003(3)	0.46	2.7	202
243-131-1	0.0006	0.46	2.6	178
243-131-2A(4)	0.0086	0.36	3.5	168
243-131-2B	0.0092	0.46	2.6	120
243-99-1	0.07	0.45	2.7	0

(1) For more sample information see Table 5.

(2) Base ZnO calcined at 600°C. in air.

(3) Impurity present in the base ZnO.

(4) Not calcined.

TABLE 15
Effect of Pb Impurity Doping Level of French Process Zinc Oxides
on Zinc Electrode Performance

(Cycles to failure at 60% depth of discharge)
(Impurity added by 600°C. air atmosphere calcination of
dry blend of ZnO plus impurity oxide)

Sample No. (1)	Wt. % Fe	Wt. % Pb	Particle Size, μ	Surface Area, M^2/Gm	Cycles to Failure
243-127-2(2)	0.0003(3)	0.0008(3)	0.46	2.7	202
243-107-4	0.0003(3)	0.028	0.47	2.7	214
243-107-1	0.0003(3)	0.25	0.42	2.9	221
243-107-2	0.0003(3)	1.02	0.38	3.4	197
243-107-3	0.0003(3)	2.42	0.37	3.5	214
243-135-1	0.010	0.26	0.42	2.9	192

(1) For more sample information see Table 5.

(2) Base ZnO calcined 600°C. in air.

(3) Impurity present in the base ZnO.

TABLE 16

Effect of Al- and In-Doping of French Process Zinc Oxides

on Zinc Electrode Performance

(Cycles to failure at 60% depth of discharge)

Sample No.*	Description	Impurity	Particle Size, μ	Dry Powder		Cycles to Failure
				Resistivity ohm-cm		
	Delco-Remy Control (Kadox 15 - Fine Particle Size French Process ZnO)	--	--	--		130 (170)
243-27-1	French Process ZnO Calcined to Increase Particle Size	--	1.02	High		80
243-41-1	High Conductivity Al-doped	0.3% Al	1.02	9.4×10^2		150 (170)
243-139-1	Low Conductivity Al-doped. Prepared by 600°C. Calcination of ZnO + Al ₂ O ₃ Blend.	0.07% Al	0.46	High		156
243-139-2	Same preparation as 243-139-1	0.92% Al	0.36	High		168
243-45-1	High Conductivity In-doped	0.48% In	2.3	3.5×10^3		135

*For more sample information see Table 6.

TABLE 1/
Effect of High Surface Area Wet Process Zinc Oxides

on Zinc Electrode Performance					
(Cycles to failure at 60% depth of discharge)					
Sample No. *	Description	Particle Size, μ	Surface Area, M^2/Gm	Cycles to Failure	
	Delco-Remy Control (Kadox 15 - Fine particle size French Process ZnO)			130	
243-7-1	French Process ZnO	0.12	9.5	108	
243-75-1	Wet Process ZnO prepared from $ZnCl_2$ + KOH	0.16	10.5	126	
243-71-1	Wet Process ZnO prepared from $ZnCl_2$ + NaOH	0.092	18.3	132	
243-59-1	ZnO prepared by decomposition of $ZnCO_3$ at 460°C.	0.052	22	148	
243-63-1	ZnO prepared by decomposition of $ZnCO_3$ at 360°C.	0.031	34	148	
243-67-2	ZnO prepared by decomposition of $ZnCO_3$ at 310°C.	0.025	51	135	

*For more sample information see Tables 7 and 8.

TABLE 18

Effect of ZnO Particle Morphology (Acicular vs. Nodular)

on Zinc Electrode Performance

(Cycles to failure at 60% depth of discharge)

Sample No *	Description	Particle Size, μ	Surface Area, M^2/Gm	Cycles to Failure
	Delco-Remy Control (Kadox 15 - Fine particle size French Process ZnO)			130
243-7-1	Nodular French Process ZnO	0.12	9.5	108
243-79	Acicular Wet Process prepared from $ZnCl_2$ + NE_4OH	0.15	7.1	122
243-11-1	Nodular French Process ZnO	0.24	5.0	96
243-35-1	Washed Acicular American Process ZnO	0.26	4.7	12

*For more sample information see Tables 2 and 9.

TABLE 10
Effect of Variations in Zinc Dust on Zinc Electrode Performance

(Cycles to failure at 60% depth of discharge)			
Sample No.*	Description	Particle Size, μ	Cycles to Failure
	Delco-Remy Control (Kadox 15 - Fine particle size French Process ZnO)		130
243-119-1	Fine particle size Zinc Dust 95.7% Metallic Zn 0.0001% Fe	5.3	168
243-123-1	Flaked Zinc Dust (243-119-1) 91.1% Metallic Zn 0.003% Fe, 0.078% Pb	**	204
243-115-1	Blue Powder 57.2% Metallic Zn 0.14% Fe	10.5	0

*For more sample information see Table 10.

**Average flake thickness = 2.5 μ

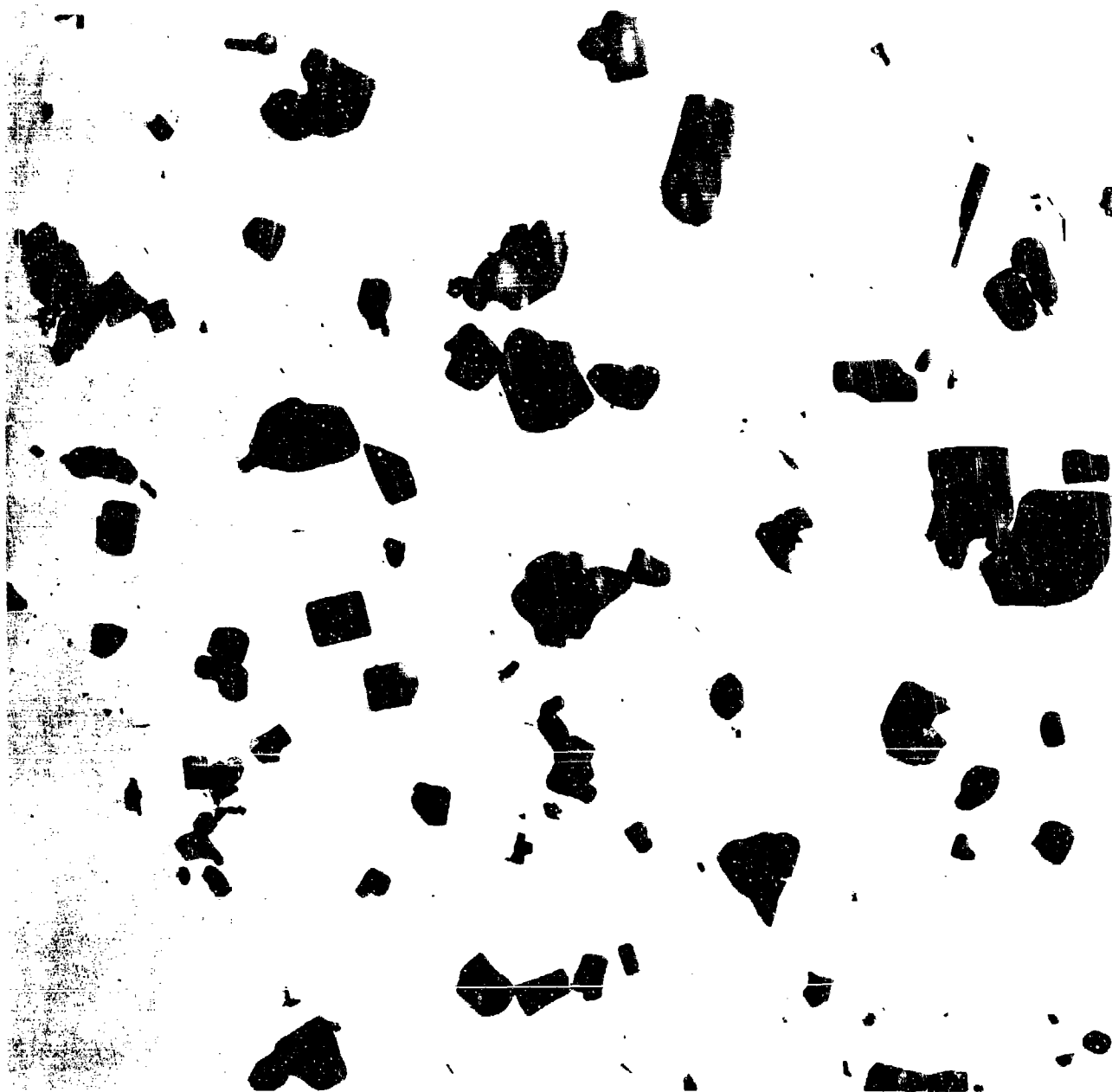


Figure 1. Sample No. 243-15-1 - French Process ZnO
Particle Size = 0.33μ
Surface Area = $3.7 \text{ m}^2/\text{g}$
Magnification = 25,200X
(See Tables 2 and 12 for more information.)

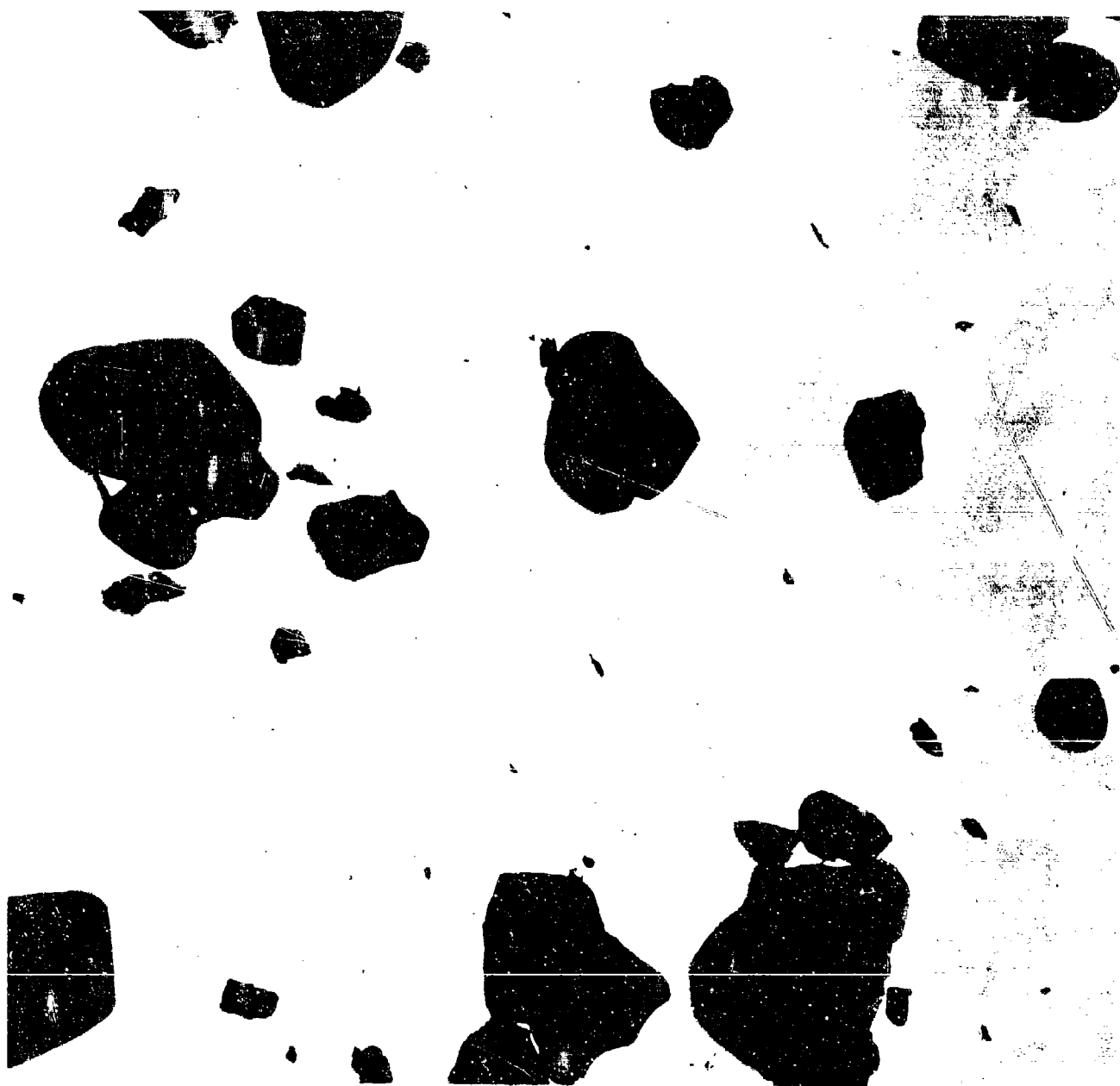


Figure 2. Sample No. 243-27-1 - Calcined French Process ZnO
Particle Size = 1.02μ
Surface Area = $0.95 \text{ m}^2/\text{g}$
Magnification = 25,200X
(See Tables 2 and 12 for more information.)

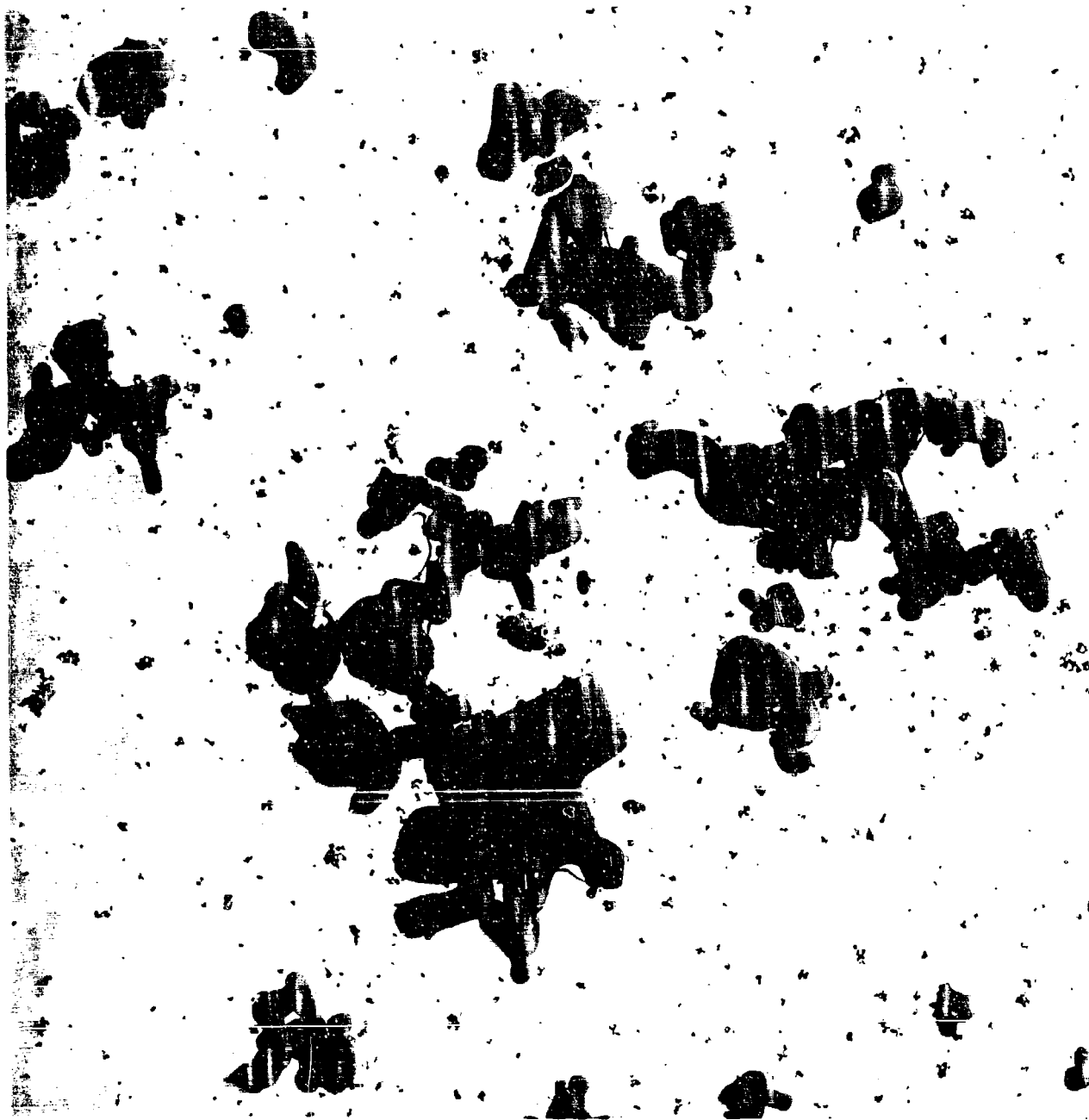


Figure 3. Sample No 243-139-2 - 0.92 Wt. % Al-doped French Process ZnO
Calcined 600°C. in Air
Particle Size = 0.36 μ
Surface Area = 4.4 m²/g
Magnification = 25,200X

(See Tables 6 and 16 for more information.)

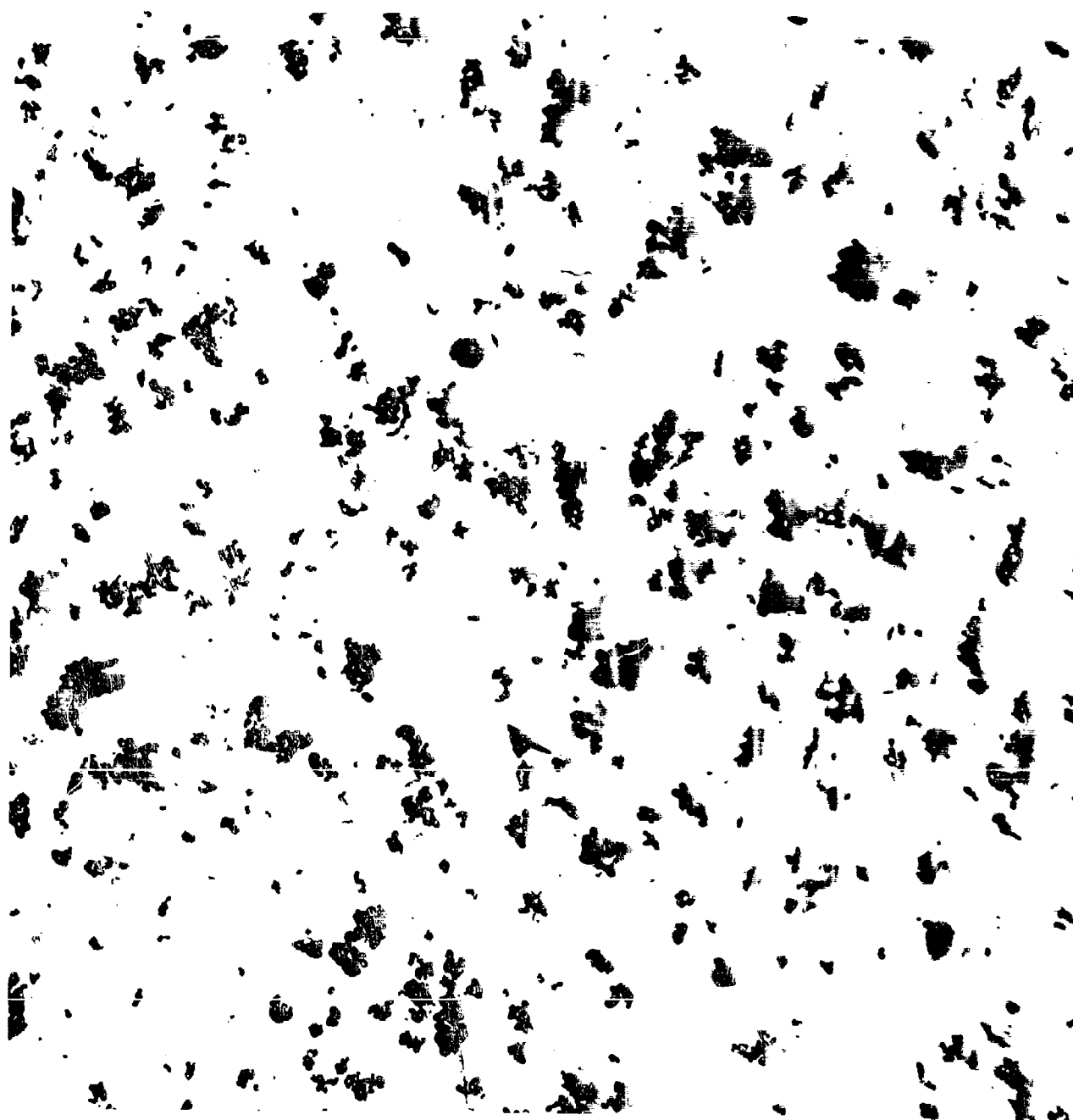


Figure 4. Sample No. 243-59-1 - Wet Process ZnO from Basic Zinc Carbonate
Particle Size = 0.052μ
Surface Area = $21.7 \text{ m}^2/\text{g}$
Magnification = $25,200\times$
(See Tables 7 and 17 for more information.)



Figure 5. Sample No. 243-79-1 - Acicular Wet Process ZnO from $\text{ZnCl}_2 + \text{NH}_4\text{OH}$

Particle Size = 0.155μ

Surface Area = $7.1 \text{ m}^2/\text{g}$

Magnification = 25,200X

(See Tables 8 and 18 for more information.)



Figure 6. Sample No. 243-35-1 - Acicular American Process ZnO
Particle Size = 0.26μ
Surface Area $\sim 4.7 \text{ m}^2/\text{g}$
Magnification = 25,200X
(See Tables 9 and 16 for more information.)

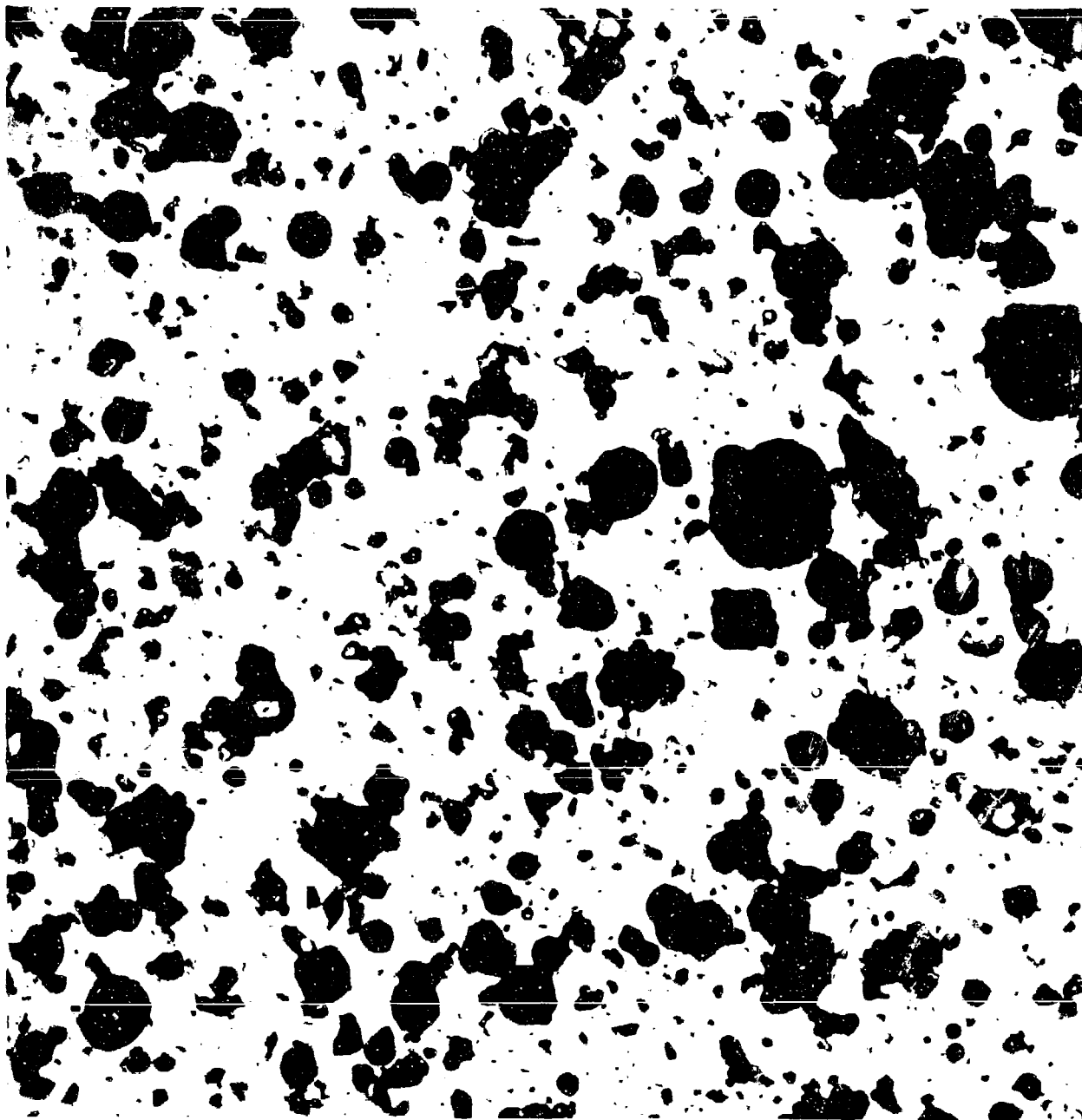


Figure 7. Optical Micrograph - Sample No. 243-115-1 -
Blue Powder Type Zn-Dust
Particle Size = 10.5 μ
Magnification = 1,000X
(See Tables 10 and 19 for more information.)

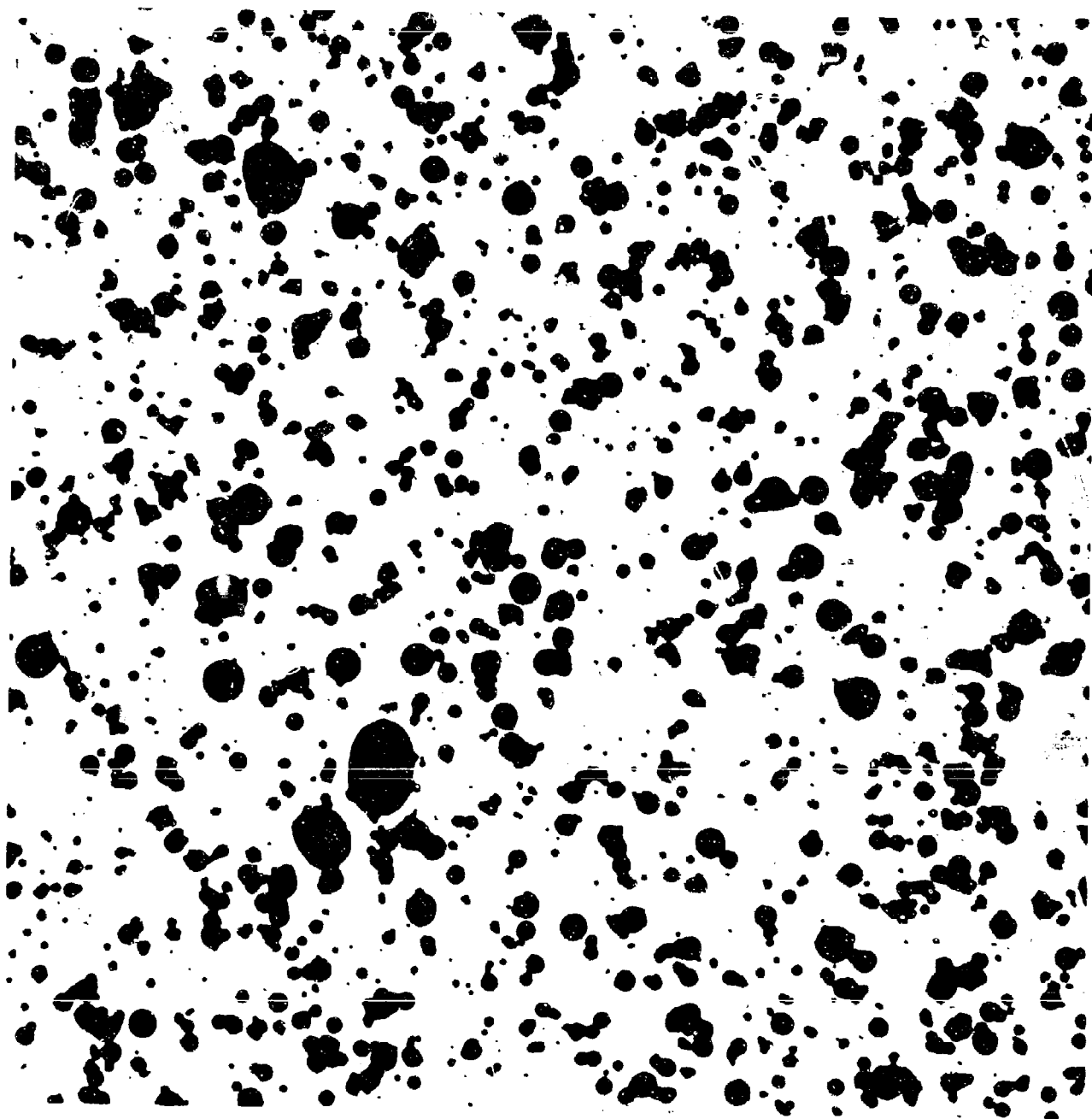


Figure 8. Optical Micrograph - Sample No. 243-119-1 - Zinc Dust
Particle Size = 5.3μ
Magnification = 1,000X
(See Tables 10 and 19 for more information.)



Figure 9. Optical Micrograph - Sample No. 243-123-1 -
Flaked Zinc Dust

Average Flake Thickness = 2.5μ

Magnification = 1,000X

(See Tables 10 and 19 for more information.)

APPENDIX II

ADSORPTION OF ORGANIC MATERIALS ON ZINC ELECTRODES

ADSORPTION OF ORGANIC MATERIALS ON ZINC ELECTRODES

Final Progress Report

Covering the Period

15 October 1966 to 14 October 1968

Purchase Order DR-120111

Under Contract AF 33(615)-3487

Prepared by

Dewitt A. Payne

Hiroyasu Tachikawa

Allen J. Bard

The University of Texas

Austin, Texas

Introduction

Our original objective was to determine whether simple alcohols, glycols and other organic structures related to Emulphogene could be adsorbed on a zinc electrode in strong alkaline media, and if so, to measure the extent of their adsorption. Additionally we wanted to study how adsorption affected the electrochemical processes.

A summary of our results follow; details are given in the sections on Results and Discussion. We found that simple compounds desorbed at potentials too positive to affect the zinc reaction. More complex organics, and Emulphogene, which did adsorb could not be measured quantitatively due to slow establishment of equilibrium conditions required for quantitative measurements. We established with a reasonable degree of certainty that the polyethylene oxide end of Emulphogene is closest to the electrode surface, and in particular that the oxygen atoms in the polyethylene oxide chain are closest to the surface. Some similar compounds, such as methyl cellulose, exhibit strong adsorption similar to Emulphogene.

The secondary objective of our study was to determine how adsorption of Emulphogene-like compounds affects the electrochemical process. Our original thinking was that this would not be too hard to do, but we soon found out that electrochemical processes at zinc in alkaline media were not as well understood as we had originally thought. This required us to spend a large amount of time on a study of the basic electrochemistry of the zinc-zinc (II) reaction before we could determine how it was altered by adsorption.

Particular emphasis was placed on a study of the zinc-zinc amalgam system since battery plates are normally amalgamated, and amalgamation removes contribution to the reaction kinetics from crystallization processes. All our latest evidence leads us to believe that the mechanism of the reaction involves two successive one-electron transfers, with the E^0 for the Zn (II), Zn (I) electron transfer being more negative than E^0 for Zn (I), Zn(Hg) with rate constants for both electron transfers of the same order of magnitude. This mechanism is very similar to the mechanism proposed by Farr and Hampson¹ for the zinc metal electrode.

Our studies of the effects of adsorption on the electrochemical processes suffered from lack of quantitative adsorption measurements. Also, it required so much time to study the unperturbed system, that by the time we began to get a reasonable understanding of the unperturbed system there was no time left for a careful study of its behavior upon addition of surfactants. About the only qualitative observation it was possible to make was that addition of Emulphogene caused a lowering of the apparent rate constant.

Experimental

The potential-step chronocoulometric instrument is similar in most respects to that described in the literature² (Figure 1). Additions have been made to the basic circuitry to allow for partial compensation for solution resistance to improve the overall rise-time. A fraction of the output of the current measuring amplifier is fed back to the potentiostat.³ The potential step is generated by adding in a new control potential by means of a high speed mercury wetted relay. The integrator, current-measuring amplifier, and the potentiostat are Philbrick SP656 chopper-stabilized, operational amplifiers. The follower and other control amplifiers are Philbrick P65AU differential operational amplifiers.

This instrument is particularly useful for both qualitative and quantitative studies of adsorption by being able to measure directly the charge on the electrode. By stepping from one potential to another in the case where no Faradaic reaction occurs at either potential and integrating the current that flows as a result of this change, the difference in charge between the two potentials can be readily observed. Following this procedure it is possible to easily determine the shape of the q vs. E curve. To determine the curve exactly it is necessary to know the absolute value of the charge at some potential on the curve. This can be determined by holding the potential constant, changing the area of the electrode, and integrating the charging current.

If there is adsorption of a material on the electrode surface, the shape of the q vs. E curve will vary with the concentration of the material in solution.

In the event there is a Faradaic reaction involving a non-adsorbed species at the potential stepped to, it is still possible to determine a charge value. This may be done by plotting Q vs. $t^{1/2}$ and extrapolating back to $t = 0$. The intercept on the Q axis is the difference in charge between the two potentials.

The automatic capacitance bridge was based on the circuit designed by Kowalski and Srzednicki^{4,5}. The published circuit⁵ contains an error. The error is corrected in the circuit diagram in this report (Figure 2). The transistors used in our circuit are all RCA SK3004. Potential is applied with respect to ground from a high impedance source to post A. Post C is attached to the input of a current measuring amplifier.

For purposes of calibration, test runs were made with both instruments on a .1 M solution of potassium chloride utilizing a hanging drop mercury electrode. Water was purified in a Barnstead still from basic permanganate. Reagent grade KCl was used without further purification. Mercury was triple-distilled quality. Drop sizes of 0.018 cm² for differential capacity measurements, and 0.032 cm² for potential step measurements were reproducibly obtained from a Metrohm micrometer electrode obtained from Brinkmann Instruments.

Computer programs for data processing were modified versions of programs supplied to us by David Mohilner. They are given in Appendix I.

The gas chromatograph uses were a F&M scientific model 609 with temperature programming and a flame ionization detector. A seven foot, one-quarter inch diameter column was used, packed with Borapak and operated at a temperature of 150°C. Propylene oxide was extracted from the KOH solution with hexane. The above conditions gave a complete separation of the hexane and propylene oxide peaks with the propylene oxide peak appearing first, so that we were able to use the maximum sensitivity to detect the propylene oxide.

Several different rotating zinc disk electrodes have been constructed which differ in electrode area and purity of the zinc metal. The most useful electrode (Figure 3) is made by sealing 0.020" zinc wire, 99.9% pure, in a Teflon rod 0.5" in diameter. The other end of the rod is drilled out to accept a 0.25" steel shaft which makes contact with the zinc wire. The shaft is then mounted in two ball bearings and is driven by a Motomatic E-150 servomotor. The rotator may be set to rotate at any speed from zero to 10,000 rpm.

A Lippmann capillary electrometer was used to obtain electrocapillary data. The capillary is drawn from 1/2 millimeter capillary tubing and attached to a mercury reservoir which in turn is connected to a pressurizing system. Coarse pressure adjustment is obtained by filling the system from a tank of water pumped nitrogen. Excess nitrogen is released through a fine needle valve. When the approximate pressure is reached, the system is closed and final adjustment is made with a large brass bellows in the system.

The capillary was calibrated with 0.1 N KCl solution using a 0.1 N calomel reference electrode with no liquid junction. The data were from Devanathan and Peries⁶ that was used to calibrate the capillary. The KCl solution was purified with activated charcoal and then electrocapillary curves were measured until there was agreement over the whole curve between our measured data and the data from the literature to at least 0.1 dyne/cm. KOH solutions were purified with charcoal before addition of Emulphogene. Conductivity water from a Branstead still was used to prepare solutions.

We obtained from Eagle-Picher 99.9999% pure zinc metal and an electrode was constructed by casting the metal in a pyrex capillary under 10^{-6} mm Hg vacuum. When the glass had cooled, it was broken away from the resulting metal rod, a length of which was sealed in a teflon sleeve and made into a rotating disk electrode similar to the one previously described. The rates of the electrode reactions at the zinc and zinc amalgam electrodes were made with the instrument and cell previously described using both chronocoulometry and chronoamperometry.

The mercury hanging drop electrodes as well as the hanging drop amalgam electrodes were formed by a Metrohm micrometer electrode obtained from Brinkmann Instruments.

Samples of Emulphogene BC-420, BC-610, BC-720 and BC-840 were obtained from General Aniline and Film Corporation. Klucel-HA was obtained from the Western Company. Other chemicals were obtained from the regular chemical companies and were used without further purification. Solutions were prepared from conductivity water prepared by distilling previously deionized water from basic permanganate in a Barnstead still.

An addition to our instrumentation was a Princeton Applied Research HR-3 lock-in amplifier with a type G preamp. This instrument has allowed us to

perform phase selective ac polarography which in turn allowed us to obtain much more useful kinetic information from an ac experiment.

A different method of preparation of zinc amalgam was used to increase storage life of the amalgam. A weighed quantity of mercury was placed in a cell which was then evacuated on a high vacuum line to below 10^{-5} mm Hg pressure. The cell was then filled with purified helium and opened. While the cell was open, a rapid stream of helium flowed through the cell. A carefully measured piece of 99.9% pure zinc wire which had been cleaned and lightly amalgamated by dipping for a few seconds in mercuric chloride solution was then added to the mercury and the cell was closed and re-evacuated and was allowed to stand for a day with occasional agitation. This amalgam was then used in the Kemula electrode with fresh amalgam used for each day's experiments. The amalgam is never exposed to air; whenever the cell is opened, it is attached to a source of helium which flows over the surface. The cell is stored under vacuum. Amalgam prepared in this fashion has remained stable for a period of several weeks. Potential steps were always carried out on fresh drops which were not allowed to stand for more than a few seconds.

Results

Adsorption on Zinc Amalgam and Mercury Electrodes

One of the techniques employed in investigating adsorption involved determining the differential capacity (Cde) of the electrode in the background electrolyte alone (e.g., 1 M KOH) as a function of potential, E, using the apparatus for automatic Cde-determination. The compound under study was then added and appreciable decrease of Cde was taken as an indication of adsorption. Typical curves are shown in Figures 4 and 5. Of particular interest is the potential range of about -1.4 to -1.9 V vs Ag/AgCl, which represents the zone of stability of a zinc amalgam electrode in 1 M KOH. Adsorption of various simple organic compounds chemically related to Emulphogene, including straight chain alcohols through n-heptane, propylene oxide, and propylene glycol, were studied by differential capacity measurements. In all these cases especially strong adsorption was not observed in the region of zinc electrode stability. Even at concentrations approaching solution saturation the cathodic desorption

peaks for these compounds were relatively broad and they were all desorbed at potentials more positive than the zinc reaction potential.

A number of more complex compounds were found that did exhibit strong adsorption behavior. Among these were Triton X-100, methyl cellulose, Klucel HA (a cellulose derivative) and two different molecular weight polyethylene oxides (Table I). Some complex organics which did not exhibit strong adsorption behavior were gum arabic, a nonionic polyacrylamide surfactant and gelatine. The Cde curve of a mercury electrode in a solution containing Emulphogene is radically different from the curve obtained in a solution containing compounds like simple alcohols or glycols. Specifically, decreases in Cde from the pure solution are obtained at much lower concentrations of Emulphogene than of simpler compounds. Also, the cathodic desorption peak occurs at more negative potentials and over a much narrower potential range for Emulphogene than for simple related compounds. Addition of simple compounds related to Emulphogene did not cause lowering of differential capacity curves at zinc amalgam or zinc electrodes, while addition of Emulphogene to solutions caused a lowering of the differential capacity at all these electrodes (Figs. 6 and 7).

Although qualitative evidence of adsorption was obtained from the differential capacitance measurements, rigorous quantitative determination of the extent of adsorption can only be obtained by electrocapillary measurements⁷ or by direct analysis of a solution before and after adsorption occurs.

An attempt was made to make quantitative measurements of the extent of adsorption of Emulphogene BC-720 on mercury in 1 M KOH by electrocapillary measurements. A difficulty arises, however, in measurements such as these with very strongly adsorbed substances. To determine the extent of adsorption, as measured by the surface excess, Γ , one must determine, with a high degree of precision, the surface tension, σ , at various potentials and concentration of adsorbate, allowing sufficient time for equilibrium to be established at the electrode-solution interface. Then, by thermodynamics (Lipmann equation)⁸

$$\Gamma = (d\sigma/d\ln a)_E$$

Since it is necessary to make at least some of these measurements with less than saturation surface coverages where very strong adsorption occurs, this

requires one to work at very low concentrations of surface active material.⁹ At these low concentrations equilibrium is established so slowly because of slow mass transfer of the surface active substance from the bulk solution to the mercury surface in the capillary, that it is nearly impossible to obtain a sufficient number of points to properly define the curve in a finite amount of time. If one were able to allow a very long time for equilibration, other problems would then crop up. Trace contaminants would also have sufficient time to equilibrate and distort results. Also, the capillary is attacked by the alkali solution and its calibration is altered by an unknown and time variable factor. It was discovered that even after allowing the electrode to equilibrate for as much as 30 minutes at one potential at low concentrations of Emulphogene the surface tension was not constant and points on the curve showed a great deal of scatter. The first time measurements were attempted the scatter was so bad that nothing at all was learned from them. Measurements were made on a second set of solutions and results that were more self consistent with less scatter were obtained (Fig. 8). However, after running a series of solutions with different Emulphogene concentrations, a test run was made on pure KOH and pressure readings were found to be different by better than 10%. Also, less than 20 points were obtained for any one curve due to the time factor, and 20 points are not nearly enough to insure reasonably accurate quantitative results.

However, some general trends in the behavior of mercury electrodes in solutions containing Emulphogene were observed. Emulphogene BC-720 is definitely adsorbed at mercury electrodes since the surface tension at a given potential is lower in a solution containing Emulphogene than in a solution which does not contain Emulphogene (Fig. 8). Also, addition of Emulphogene to a solution causes the electrocapillary maximum (e.c.m.), which corresponds to the potential of zero charge (p.z.c.), to shift to more negative potentials. This adsorption and shifting occur at extremely low concentrations of the additive, 10% by weight.

Direct measurement of adsorption requires the determination of adsorbate in a solution before and after an amount of metal of known surface area is added. In this case complications arose because of the alkalinity of the solution and of the difficulty of accurate quantitative analysis of low

concentrations of Emulphogene and related compounds. Furthermore, difficulties in determining the surface area of the electrode material (zinc powder), maintaining the potential of the material and prevention of corrosion of the electrode material in the alkaline solutions occur. Preliminary experiments failed to uncover a suitable spectrophotometric method. While gas chromatographic procedures, particularly with low molecular weight materials (e.g., propylene oxide) appeared more promising, reliable results were not obtained. In retrospect we feel that direct measurements for these compounds on zinc will be difficult. Perhaps a radiotracer method with carbon-14 tagged compounds would be more successful.

Kinetics of the Zinc-Zinc (II) Reaction

Several different techniques were used in our study of the kinetics of the zinc-zinc amalgam system, including potential step chronocoulometry, rotating disc voltammetry and a.c. and d.c. polarography.

Measurements of the rate of the zinc reaction were made at a mercury or amalgam drop electrode using the chronocoulometric technique with large potential steps.¹⁰ In this technique a potential step is applied to the hanging drop electrode, and the total number of coulombs which pass, Q , are recorded as a function of time, t . The equation governing the variation of Q with t is ¹⁰:

$$Q = \frac{A}{\lambda^2} (\exp y^2 \operatorname{erfc} y + \frac{2y}{\sqrt{\pi}} - 1) \quad (1)$$

where

$$K = nFAk_a^0 [C_0 e^{-\alpha n f(E-E^0)} - C_R e^{(1-\alpha)n f(E-E^0)}] \quad (2)$$

$$y = \lambda t^{1/2}$$

$$\lambda = k_a^0 \left[\frac{e^{-\alpha n f(E-E^0)}}{\sqrt{D_0}} + \frac{e^{(1-\alpha)n f(E-E^0)}}{\sqrt{D_R}} \right] \quad (4)$$

$$f = F/RT$$

A plot of Q vs \sqrt{t} becomes linear for $y > 5$, and shows an intercept on the \sqrt{t} axis, $\sqrt{t_1}$, such that

$$\lambda = \sqrt{\pi}/2\sqrt{t_1} \quad (6)$$

and allows the determination of λ . A plot of $\ln \lambda$ vs E in regions where one or the other terms in (4) are negligible shows a slope of $-\alpha n f$ or $(1-\alpha) n f$, and allows determination of α . However, we have recently altered our method of data analysis. Originally, we had plotted Q vs $t^{1/2}$ and performed a linear extrapolation to Q equal zero. It was found, however, that this technique could lead to significant systematic error. Therefore, we wrote a computer program to perform an iterative analysis of the data according to the complete theory by selecting an approximate λ , calculating theoretical values of Q at the appropriate values of t and comparing these values of Q to the measured values and then altering λ until an optimum fit was obtained. The criterion used for optimization was the minimization of the sum of the squares of the differences between Q calculated and Q measured. This technique gave results which were much more consistent than the previous technique, and hence more trustworthy. Using this technique, we have obtained the following results from a careful series of experiments at different concentrations of hydroxide (Fig. 9):

$$\alpha n_{\text{cathodic}} = .66$$

$$\beta n_{\text{anodic}} = .35$$

$$k_a^0 = 1.06 \times 10^{-3}$$

$$E^0 = 1.216 + \frac{RT}{2F} \ln [\text{OH}^-]^4 \text{ vs } \text{H}_2; \text{H}^+$$

$$\frac{\partial k_a^0}{\partial [\text{OH}^-]} = 0$$

Conventional dc polarographic studies were performed using a dropping mercury electrode only on the cathodic process. Data analysis followed that of Israel and Meites¹¹ (Fig. 10). Amalgam forming reactions are very susceptible to distortion from spherical diffusion¹² particularly over the time scale of the polarographic experiment which was from 5 to 11 seconds. Hence, it is not unusual that dc polarography gave somewhat different results from potential step measurements which were performed on a much shorter time scale and were less likely to be distorted from theoretical planar electrode behavior.

Our results from dc polarography were:

$$\alpha n = 1.0$$
$$k_a^0 = 5 \times 10^{-4}$$

E^0 was the same and there was no dependence of the rate constant on hydroxide concentration.

AC polarography is even more strongly affected by departures from planarity and there is no adequate theory which includes contributions both from drop growth and geometry.¹² However, a theory for the simple charge transfer reaction at a stationary spherical electrode has been developed.¹² It is extremely difficult to apply, but it does predict that the behavior of the phase angle of the ac current with frequency and potential should be unaffected. Our measurements of the phase angle at various potentials and different drop times do not agree with those predicted by simple theory. In particular we found that the phase angle appears to be different at different drop times (Fig. 11). Analysis of one $\cot \theta$ vs E curve by conventional methods¹³ gives

$$\alpha n = .7$$
$$\beta n = .5$$
$$k_a^0 = 6 \times 10^{-4}$$

The results of our studies on solid electrodes, zinc metal and amalgamated zinc metal, are almost certainly distorted by adsorption from solution of trace organic impurities. This is not a major problem with hanging drop and dropping mercury electrodes, since it is possible to obtain a fresh electrode surface for each experiment with these, and the electrode does not remain in the solution for a long period of time allowing trace contaminants time to diffuse to it. Furthermore, for anodic studies, the current requirements for potential step experiments are prohibitive, while dc measurements such as at a rotating disk electrode (r.d.e.) are complicated by the fact that the surface of the electrode is rapidly being altered by dissolution. A number of experiments were performed with r.d.e.'s and stationary electrodes to get a qualitative feel for the dissolution process at the solid electrode.

The dissolution of zinc metal electrodes, both stationary and rotating, in the potential range cathodic to passivation appears to be limited by diffusion from solution. Rotating disk polarograms show a leveling off of the current as the potential is made more anodic (Fig. 12). The current on the plateau is still rotation rate dependent and a plot of limiting current, i vs square root of rotation rate, $\omega^{1/2}$ is linear (Fig. 13). Stationary potential scan experiments exhibit a limiting current peak which varies approximately with the square root of scan rate. If the electrode potential is made somewhat more anodic, the current observed drops sharply (Fig. 13). It is not possible to observe stable intermediate values of the current. At a stationary electrode, the current falls to zero. At an r.d.e. a current dependent on rotation rate is observed, but its value is somewhat less than $1/5$ of the current before "passivation". Scanning the potential back in a cathodic direction causes the current to suddenly go back up to its original level, but not until a potential slightly more cathodic than the passivation potential. In the case of stationary electrodes when the scan direction is reversed the current jumps back in an anodic direction. If the scan is continued, the current potential behavior is nearly identical to what it would have been if the scan had been reversed at a potential just before passivation (Fig. 14).

Amalgamated electrode behavior is quite similar except that no leveling off of the pre-passivation oxidation current is observed (Fig. 15). If the potential of the amalgamated zinc r.d.e. is made sufficiently anodic, however, another rotation rate dependent oxidation wave is observed at about 0.5 volts vs. sat. Ag/AgCl (Fig. 15). This wave has a definite limiting current plateau whose value is about the same as the level the current reached just before passivation. The surface of a solid zinc r.d.e. permanently dulls after passivation, even when the electrode is made cathodic. An amalgamated zinc r.d.e. remains bright until the potential of the second wave is reached, whereupon it dulls. If the potential of the amalgamated electrode is then made more negative, so that it is off the second oxidation wave, the surface becomes shiny again.

A platinum ring, amalgamated zinc disk electrode was constructed to

further study the anodic wave.¹⁴ The potential of the platinum ring was held at 0 volts and the potential of the disk was scanned from -1.5 volts in the positive direction. When the potential of the disk reached -0.5 volts, the current at the ring started to increase rapidly in the anodic direction. This observation generally means that a product is being formed at the disk which can be further oxidized at the ring potential.¹⁵ Unfortunately, it was only possible to perform one experiment before the electrode deteriorated and we were unable to construct another electrode which did not show appreciable solution leakage around the electrode.

Effects of Adsorption on the Electrochemical Processes at Metal and Amalgam Electrodes

Extensive quantitative measurements of the effects of various adsorbants, particularly Emulphogene, on the electrochemical processes at the various zinc electrodes were not attempted due to our lack of quantitative knowledge of the adsorption behavior of these compounds. The primary effect of addition of Emulphogene was to cause the oxidation and reduction processes to occur at potentials farther away from the standard potential (Fig. 1). In the case of the reduction process at the amalgamated or amalgam electrode, it is possible to cause the process to shift so far cathodic as to be lost in the current from hydrogen evolution. There appeared to be little or no alteration of the limiting current for the anodic or cathodic processes at the amalgam electrode. The potential at which passivation occurred was not altered for the solid electrodes. Potential step experiments at the amalgam electrode indicated that the rate constant was made considerably smaller by addition of Emulphogene, but that the charge transfer coefficient was not significantly altered.

Discussion

Adsorption of Zinc Amalgam and Mercury Electrode

Since we did not find any simple compound chemically related to Emulphogene which exhibited similar adsorption behavior, the obvious conclusion is that it is the very complexity of Emulphogene which causes its extremely

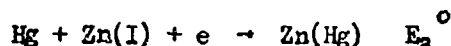
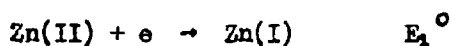
strong adsorption. It has been well established that the polyethylene oxide chain is the part of the molecule which adsorbs, since pure polyethylene oxide has been shown to be a beneficial additive of about the same magnitude as Emulphogene¹⁶ and our differential capacity measurements of polyethylene oxides and similar polymers give results nearly identical to Emulphogene. Unfortunately, because we were unable to make quantitative measurements of the extent of adsorption of any of these compounds, good quantitative correlations involving structure and extent of adsorption cannot be made. However, the qualitative results were quite informative. One does not expect adsorption of a neutral species to shift the position of the e.c.m. unless it displaces an adsorbed ionic species.¹⁶ Neither potassium nor hydroxide ions are adsorbed, however. Parsons¹⁷ has reported, though, that when a molecule with a significant net dipole moment is adsorbed with the dipole nonparallel to the electrode surface, it can shift the e.c.m. and the p.z.c. cathodic or anodic depending on whether the negative or positive end of the dipole is closest to the surface. This is attributed to the image charge effect; when a charge or dipole is brought close to a metal surface, there is an attraction generated between the metal and the charge. The magnitude of this force is calculated by assuming the existence of a charge or dipole of opposite sign or orientation on the other side of the surface and the same distance away. In other words a "mirror image" of the charge or dipole. This image charge has all the other properties of a real charge. Hence, if there are a number of charges or dipoles adsorbed, then at any given potential the surface of the metal has a different charge density than if there were no adsorption. With particular reference to our case, if a molecule with a dipole moment was adsorbed so that the negative end of the dipole was closest to the electrode surface, then the electrode would be more positively charged at any given potential. Hence, the p.z.c. and the e.c.m. would be shifted in a cathodic direction.

Since we know that the polyethylene oxide chain is adsorbed and since it could have a dipole moment with the negative end closest to the surface if all the oxygen atoms in the molecule were closest to the surface, we will make the assumption that this is indeed the case. The image charge effect could also help explain why the adsorption of the long chain molecules is so strong and why desorption occurs over such a narrow potential range. The

image charge created by one oxygen atom would also attract the oxygen atoms on either side of it in the chain. Thus, the adsorption of each oxygen atom in the chain would reinforce the adsorption of all the others. The forces of coulombic attraction thus generated would be quite strong. For simple molecules the similarly oriented dipoles of the individual molecules would tend to repel each other and there would be no reinforcement. In the polymer, however, the chemical binding takes care of this repulsion and the monomers are forced to be close to each other. The adsorption of one polymer chain would cause the charge of the electrode to become more positive making it easier for another chain to adsorb. This effect can be reversed when the potential and charge density of the electrode is made sufficiently negative so that the coulombic attraction starts to become repulsion. Then when one chain desorbs the charge becomes even more negative and so on. Hence desorption would occur over a very narrow potential range. Methyl cellulose has a large number of ether type linkages similar to Emulphogene and hence it was expected that its differential capacity curves would be similar to those of Emulphogene.

Kinetics of the Zn, Zn (II) Reaction

The study of kinetics at amalgam electrodes was initiated when it was found that the zinc-zinc amalgam system was not as well understood as a cursory examination of the literature would indicate. Our interpretation of the results of our potential step experiments were completely at odds with nearly all mechanisms previously published in the literature.^{18, 19} Potential step results are consistent only with a consecutive electron transfer mechanism:



where E_1° is more negative than E_2° both rate constants are the same order of magnitude, and there are possible preceding and intervening chemical reactions. The apparent rate constant shows no variation with the hydroxide concentration. Contrary to statements in previous reports,¹⁸ we have found that neither branch of a $\log \lambda$ vs E curve shows hydroxide concentration dependence. Only the standard potential of the overall reaction is changed when the hydroxide concentration is changed (Fig. 9). This makes our results consistent with the

general behavior of other studies.^{18, 19} The principal reason for concluding from the potential step results that the reaction involves consecutive electron transfers is that αn and βn add up to considerably less than two.²⁰ In this finding we are at odds with other researchers.^{18, 19} However, determination of α and β by most methods is highly dependent on the choice of mechanism used to formulate a model for evaluation of experimental data. Farr and Hampson¹ do propose a consecutive electron transfer mechanism for the solid electrode which is very similar to our proposed mechanism, but they do not feel that this mechanism also applies to the amalgam electrode.¹⁹

Because the mechanism elicited from the potential step data was at odds with previously proposed ones, we turned to a.c. polarography to provide additional evidence to confirm or disprove our model. Although a.c. polarographic currents are very susceptible to spherical diffusion effects in amalgam forming reactions,¹² it has been shown that the phase angle of the current should be independent of time even with amalgam-amalgam formation for a quasi-reversible single two electron step.¹² Hung and Smith²¹ have shown that for a consecutive electron transfer reaction where E_1^0 is much less than E_2^0 and charge transfer kinetics are important, the phase angle at constant potential should vary with time. The lock-in amplifier system allowed us to measure phase angle with high accuracy. We observed that there is a significant change in the phase angle with time.

The appearance of an apparently diffusion controlled limiting current for metallic zinc oxidation is hard to explain. Diffusion control by hydroxide ion at the particular concentrations used and using the geometric area of the electrode should cause a much higher limiting current. Other workers²²⁻²⁴ have also noted apparent diffusion control in that chronopotentiograms give anodic transition times which show constant $ir^{1/2}$ behavior, and potential sweeps have a limiting current peak which gives some evidence of diffusion controlled behavior. Other researchers²⁴ have theorized that this limiting current is caused by film formation at the electrode surface which results in slower diffusion through the film. Our observation that there is rotation rate dependence of the current even in the passivated region throws considerable doubt on this hypothesis since it is well known that surface effects of that nature are not rotation rate dependent.²⁵ A possible explanation for this behavior is some sort of potential dependence of the active area of the electrode.

If the active area of the electrode becomes much smaller as its potential is made more anodic, a limiting current which was rotation rate dependent would be observed. Much more work needs to be done in this area. The problems involved, however, are enormous, chief among them being that at the current densities involved, the electrode surface is rapidly altered, making reproducibility and theoretical calculations difficult.

Amalgamated zinc r.d. electrodes do not show the limiting current behavior of non-amalgamated electrodes. This indicates, perhaps, that the limiting behavior of the non-amalgamated electrode is due to the crystalline nature of the pure zinc metal electrode. Passivation of amalgam electrodes appears to depend on the concentration of zinc in the amalgam. At low concentrations of zinc passivation is not observed. However, at high zinc concentrations, such as with an amalgamated electrode, passivation is observed.

Effects of Adsorption on the Electrochemistry of Zinc

The presence of a neutral organic adsorbate may have several effects on the electrode process. It may change the transport processes of the reaction species, reduce the effective electrode area, change the charge distribution on the electrode, change the charge transfer reaction and change the chemical reactions before and after the discharge. There is at present no adequate general theory of the effect of adsorbed neutral substances on electrode reactions.

It has been observed that adsorption may affect the charge transfer rate of a reaction without affecting the diffusion limiting current. The normal rate equation must be multiplied by a factor $f(\Gamma)$ where Γ is the amount adsorbed and:

$$\begin{array}{ll} 0 < f(\Gamma) < 1 & \text{when } \Gamma > 0 \\ f(\Gamma) = 1 & \text{when } \Gamma = 0 \end{array}$$

The reaction could also be affected by changes in the potential at the outer Helmholtz plane due to changes in the structure of the double-layer caused by the organic adsorbate. The charge transfer coefficient, α , might also be affected.

The primary effect of Emulphogene on the electrochemistry of zinc, whether amalgamated or not, seems to be to lower the apparent rate constant without affecting the magnitude of the limiting current.

Conclusion

Some of the difficulties we experienced were in themselves revealing in achieving a start on rationalization of structure effects. It seems to us that the special properties of Emulphogene are due to its structure containing a large number of closely spaced polar groups. Methyl cellulose and Klucel HA have structures similar to Emulphogene and exhibit similar behavior.

Certain criteria for the selection of possible additives can now be put forward. It must be very strongly adsorbed. If the molecule desorbs at potentials more positive than -1.4 V. vs SCE, it will have no effect on the reaction. Differential capacity curves on mercury are relatively easy to measure, and if the compound does not adsorb on mercury, it is unlikely that it will be adsorbed more strongly than hydroxide ion on zinc. The adsorbing groups should be similar to the hydroxide ion so that they will compete with hydroxide for reactive sites. Finally, the adsorbing groups should be very closely spaced and not sterically hindered from adsorbing close to each other.

One possibility along these lines is a polysulfide molecule. Model sulfide compounds with only one sulfide atom per molecule such as thiourea exhibit strong adsorption and also shift the electrocapillary maximum in a negative direction. It is possible that a polymer analogous to Emulphogene with sulfur atoms replacing the oxygen atoms would exhibit beneficial effects. However, it is more likely that such a molecule containing nothing but sulfur atoms would adsorb too strongly and block the reaction completely. It would be interesting to test polymers containing varying proportions of sulfur and oxygen atoms if such could be obtained. Another possibility would be to increase the dipole moment of polyethylene oxide by attaching electron donating groups to the carbon atoms in the chain. Care would have to be taken to insure that these groups did not adsorb more strongly than the oxygen atoms or else the positive end of the dipole would then be adsorbed causing an anodic shift in the p.z.c.

Table I. Adsorption of Various Substances on a Hanging
Drop Mercury Electrode in 1 M KOH

Compound Added	Conc.	Cde at Various Potentials			E _{desorption}
		-1.40	-1.50	-1.60	
BC-420	10 ⁻⁵ %	10μf/cm ²	13μf/cm ²	22μf/cm ²	-1.75V
BC-610	4 x 10 ⁻⁴ %	10μf/cm ²	11μf/cm ²	12μf/cm ²	-1.75V
BC-720	4 x 10 ⁻³ %	-	-	14μf/cm ²	-1.72V
BC-840	10 ⁻² %	8μf/cm ²	8.5μf/cm ²	10μf/cm ²	-1.78V
Carbowax #301	.1%	-	-	-	-1.8V
Carbowax #701	.1%	-	-	-	-1.8V
Triton X-100	.01%	7.8μf/cm ²	8.3μf/cm ²	9.4μf/cm ²	-1.78
Klucel-HA	.1%	9.2μf/cm ²	10.5μf/cm ²	17μf/cm ²	-1.65
Methyl Cellulose	.1%	9.2μf/cm ²	9.7μf/cm ²	14μf/cm ²	-1.67
Gum Arabic	.1%	22.2μf/cm ²	24.4μf/cm ²	28μf/cm ²	-

Literature Cited

1. J. P. G. Farr and N. A. Hampson, *J. Electroanal. Chem.* **13** (1967) 433-441.
2. (a) E. R. Brown, D. E. Smith and Glenn L. Scowen, *Anal. Chem.* **40** (1968) 1411-1423.
(b) F. C. Anson and D. A. Payne, *J. Electroanal. Chem.* **13**, 35 (1967).
3. G. Lauer and R. A. Osteryoung, *Anal. Chem.* **38**, 1106 (1966).
4. Z. Kowalski and J. Szrednicki, *J. Electroanal. Chem.* **8**, 399 (1964).
5. R. G. Barradas and E. M. L. Valeriete, *Ibid.* **12**, 67 (1966).
6. M. A. V. Devanathan and P. Peries, *Trans. Faraday Soc.* **50**, 1236 (1954).
7. P. Delahay, "Double Layer and Electrode Kinetics," Interscience (1965) 30.
8. .. Delahay, *Op. Cit.*, p. 25.
9. *Ibid.*, p. 119.
10. J. H. Christie, G. Lauer and R. A. Osteryoung, *J. Electroanal. Chem.*, **7**, 60 (1964).
11. L. Meites and Y. Israel, *J. Am. Chem. Soc.*, **83**, 4903 (1961).
12. J. R. Delmastro and D. E. Smith, *Anal. Chem.* **37**, 572 (1965).
13. D. E. Smith, "Electroanalytical Chemistry," (A. J. Bard, ed.) Dekker (1966) Chap. 1, pp. 26-34.
14. D. A. Payne, H. Tachikawa and A. J. Bard, Delco-Remy Engineering Report, "Silver-Zinc Electrodes and Separator Research," AF 33(615)-3487, D-R 120111, Tenth Quarterly Technical Progress Report.
15. B. Miller and R. S. Visco, *J. Electrochem. Soc.* **115**, 251 (1968).
16. J. A. Keralla, Delco-Remy Technical Report AFAPL-TR-68-115 (Sept. 1968).
17. R. Parsons, *Proc. Royal Soc.*, 261A, 79 (1961).
18. H. Gerischer, *Z. Physik, Chem.*, **202**, 302 (1953).
19. J. P. F. Farr and N. A. Hampson, *J. Electroanal. Chem.* **18**, 407 (1968).
20. R. M. Hurd, *J. Electrochem. Soc.* **109**, 327 (1962).
21. H. L. Hung and D. E. Smith, *J. Electroanal. Chem.* **11**, 425 (1966).
22. T. P. Dirkse, Delco-Remy Technical Report AFAPL-TR-68-115, App. 1, p. 12 (Sept. 1968).
23. I. Sanghi and W. F. K. Wynne-Jones, *Proc. Indian Acad. Sc.* **47A**, 49 (1958).
24. I. Sanghi and M. Fleischmann, *Electrochimica Acta*, **1**, 161 (1959).
25. K. J. Vetter, "Electrochemical Kinetics," Academic Press (1967), p. 247.

List of Figures

- Fig. 1 Block Diagram of the Potential Step Apparatus
- Fig. 2 Circuit Diagram of the Automatic Double Layer Capacitance Bridge
- Fig. 3 Diagram of Zinc Rotating Disk Electrode
- Fig. 4 Differential capacity vs Potential* Stationary Mercury Drop,
Area 0.018 cm^2 , 1 N KCl
Line 1 $.00137 \text{ M n-butanol}$
Line 2 $.0219 \text{ M n-butanol}$
Line 3 $.1096 \text{ M n-butanol}$
- Fig. 5 Differential capacity vs Potential Mercury Drop, 0.018 cm^2 area
 5 M KOH , 30 Hz
Line 1 $0\% \text{ BC-420}$
Line 2 $2 \times 10^{-3}\% \text{ BC-420}$
- Fig. 6 Differential Capacity vs Potential 1 M KOH , $0.1\% \text{ Zn Amalgam Drop}$
 0.018 cm^2 area, 100 Hz
Line 1 $0\% \text{ BC-420}$
Line 2 $2 \times 10^{-6}\% \text{ BC-420}$
Line 3 $10^{-5}\% \text{ BC-420}$
Line 4 $2 \times 10^{-4}\% \text{ BC-420}$
- Fig. 7 Differential Capacity vs Potential Pure Zinc Electrode,
Area 0.002 cm^2 , 1 M KOH
Line 1 $0\% \text{ BC-720}$
Line 2 $2 \times 10^{-3}\% \text{ BC-720}$
Line 3 $4 \times 10^{-3}\% \text{ BC-720}$
Line 4 $10^{-2}\% \text{ BC-720}$
Line 5 $2 \times 10^{-2}\% \text{ BC-720}$
- Fig. 8 Pressure vs Potential for a Capillary Electrometer
 1 M KOH , Mercury Electrode Potential vs 1 M KOH , Hg/HgO
Line 1 $0\% \text{ BC-720}$
Line 2 $10^{-7}\% \text{ BC-720}$
Line 3 $10^{-6}\% \text{ BC-720}$
Line 4 $10^{-5}\% \text{ BC-720}$
Line 5 $10^{-4}\% \text{ BC-720}$
Line 6 $4 \times 10^{-4}\% \text{ BC-720}$
- Fig. 9 Log Λ vs Potential from Chronocoulometry
— 0.16 M KOH , 3.84 M KF
- - - 0.32 M KOH , 3.68 M KF
- . - 0.96 M KOH , 3.04 M KF
- . . - 1.76 M KOH , 2.24 M KF
- Fig. 10 Log $(i/i_d - i)$ vs Potential for Zincate Reduction at a Dropping
Mercury Electrode. $t = 5 \text{ sec}$, $.96 \text{ M KOH}$, 3.04 M KF

*All potentials vs sat. Ag, AgCl unless otherwise noted.

- Fig. 11 Co Tangent of the Phase Angle of ac Current vs Potential for
Zincate Reduction at a Dropping Mercury Electrode
.96 M KOH, 3.04 M KF
Line 1 $t = 5$ sec.
Line 2 $t = 10$ sec.
- Fig. 12 Current vs Potential for a Rotating Zinc Disk Electrode
2.5 M KOH, .002 cm² geometric area
200 radians/second rotation rate.
- Fig. 13 Current vs Square Root of Rotation Rate 1 M KOH, Zinc Metal
Rotating Electrode .002 cm² Area.
Potential set at -1.25 volts vs sat. Ag, AgCl
- Fig. 14 Current vs Potential for a Stationary Zinc Metal Electrode
5 M KOH, .02 cm² geometric area, scan rate 50 mV/second
- Fig. 15 Current vs Potential for Rotating Amalgamated Zinc Electrode
4 M KOH, .002 cm² area
Line 1 500 rpm rotation rate
Line 2 1000 rpm
Line 3 1500 rpm
- Fig. 16 Current vs Potential for Rotating Amalgamated Zinc Electrode
4 M KOH, .002 cm² area
1500 rpm
Line 1 0% BC-720
Line 2 $2 \times 10^{-3}\%$ BC-720
Line 3 $2 \times 10^{-2}\%$ BC-720

A1 Potentiostat SP656
 A2 Current Measuring Amplifier SP656
 A3 Integrator SP656
 A4 Follower P65AU
 R 100K ohm
 e_1 is the product of the current through
 the cell times the value of R_m
 e_2 is the integral of e_1 vs time multiplied
 by $1/R_i C_i$ from the time that C_i is
 unshorted

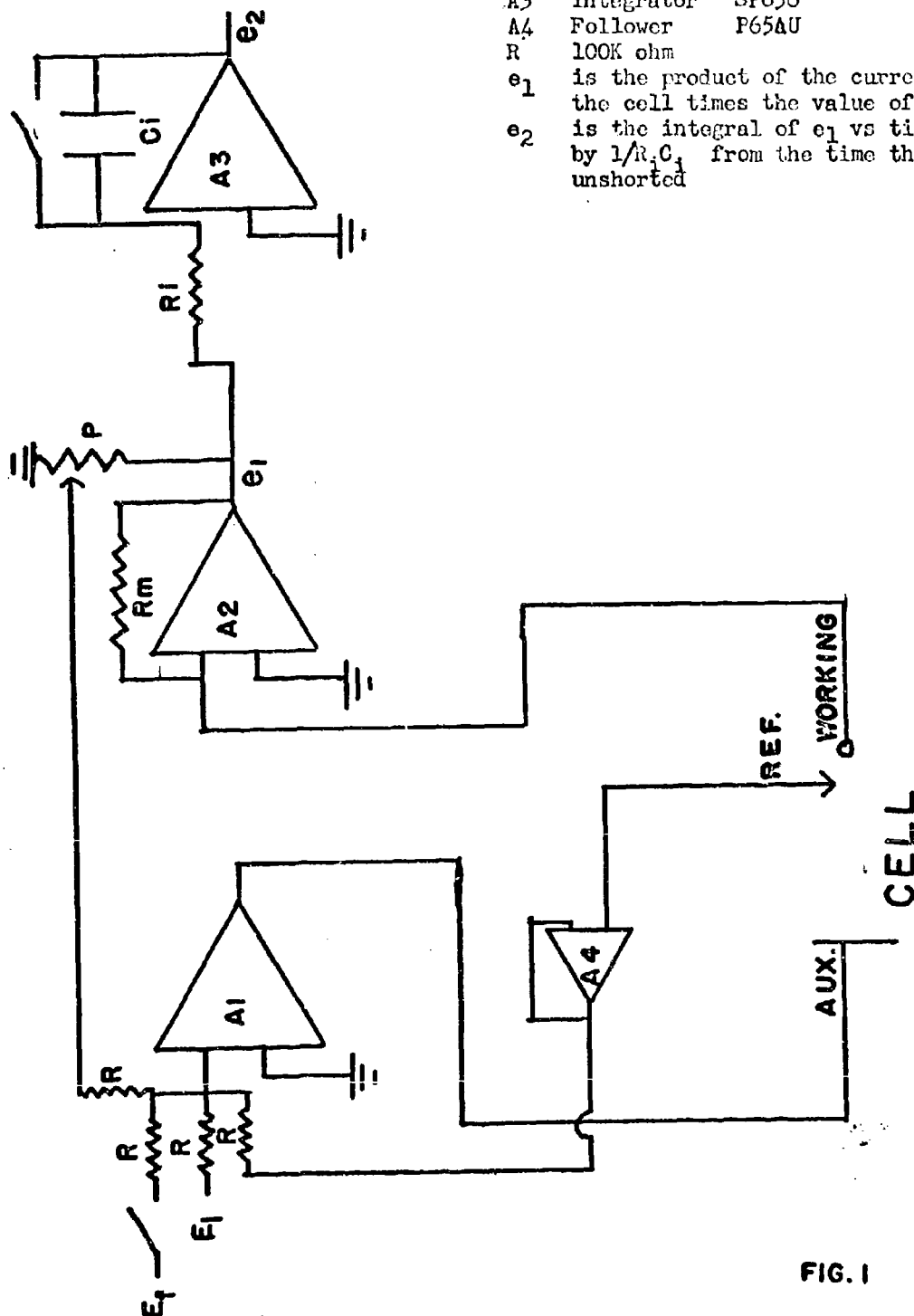


FIG. 1

FIG2

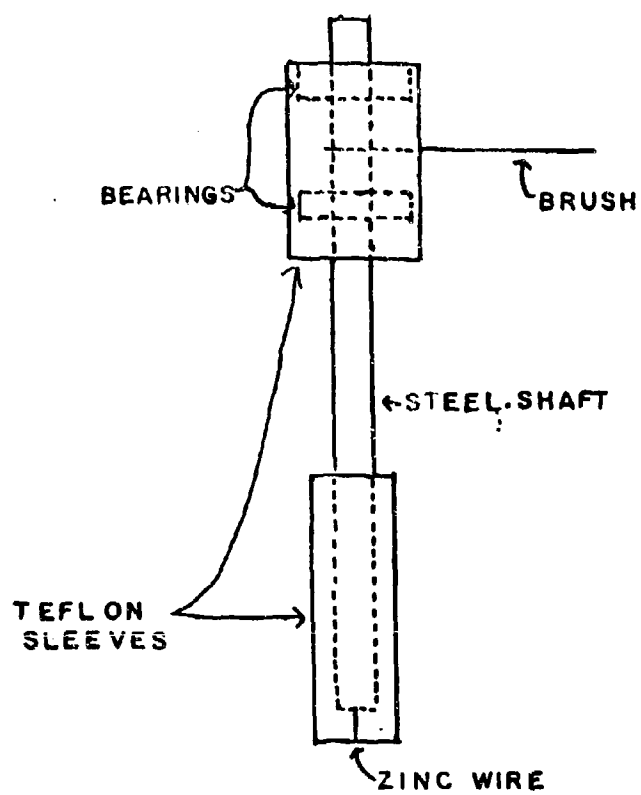


FIG.3

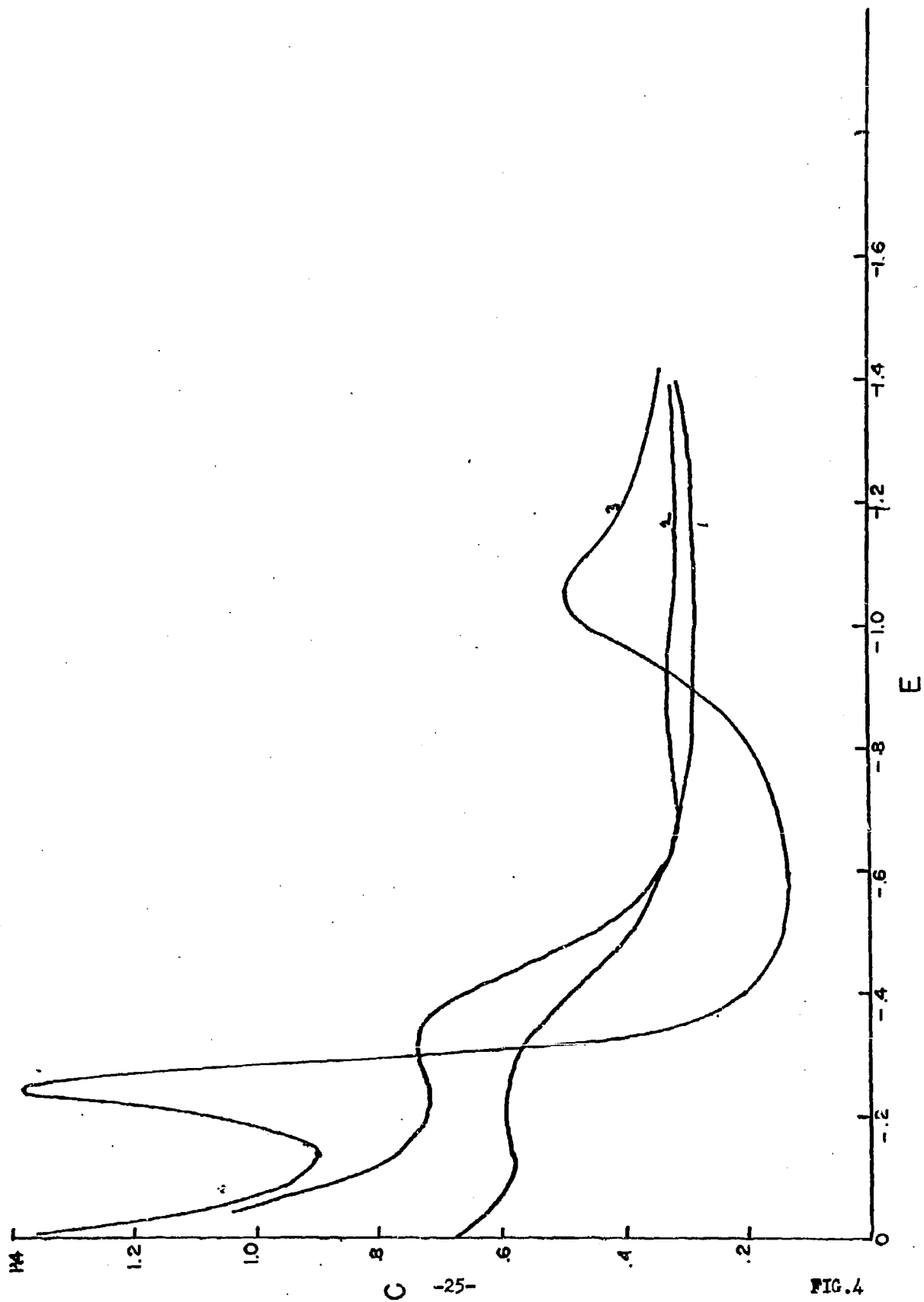


FIG. 4

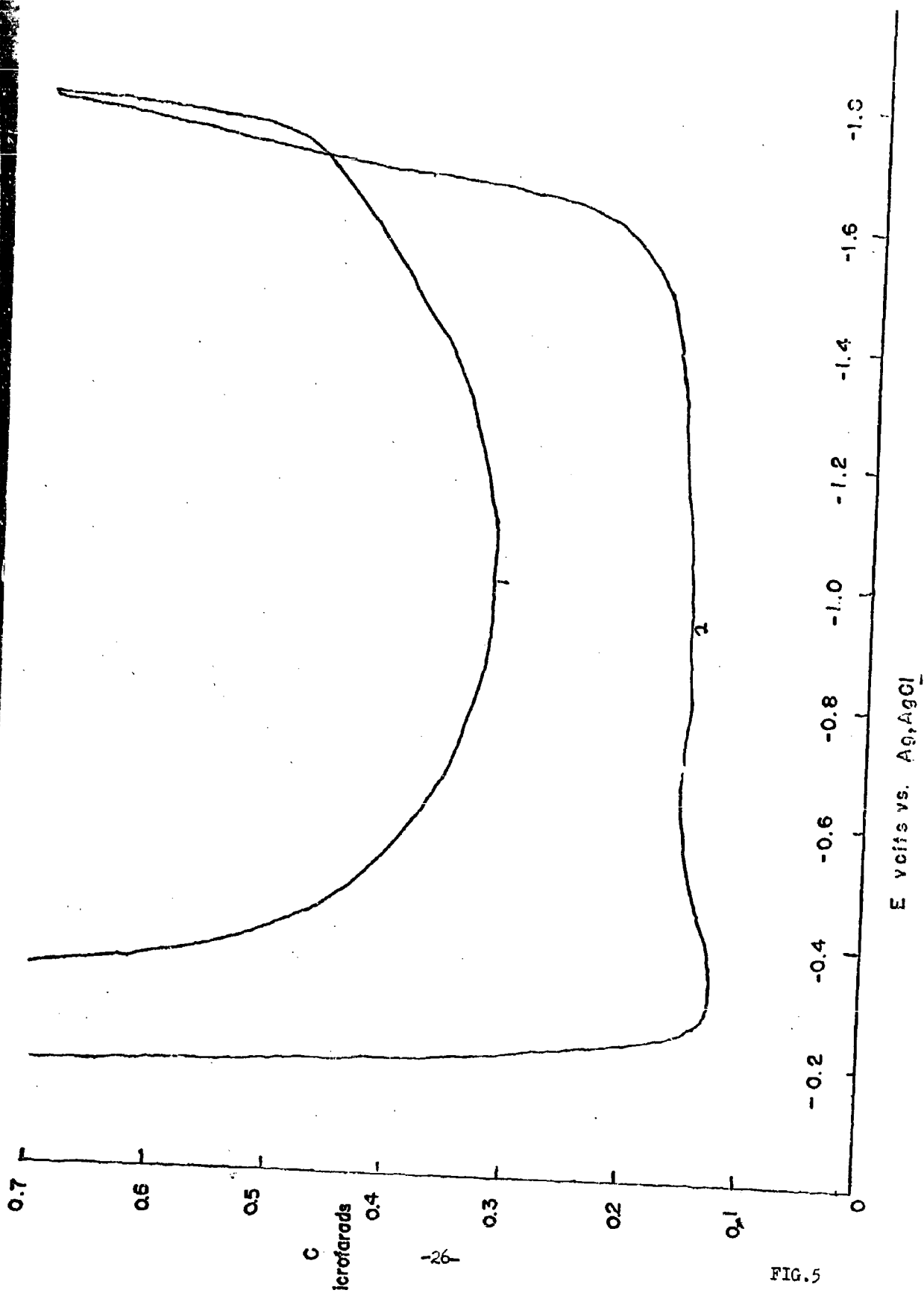


FIG. 5

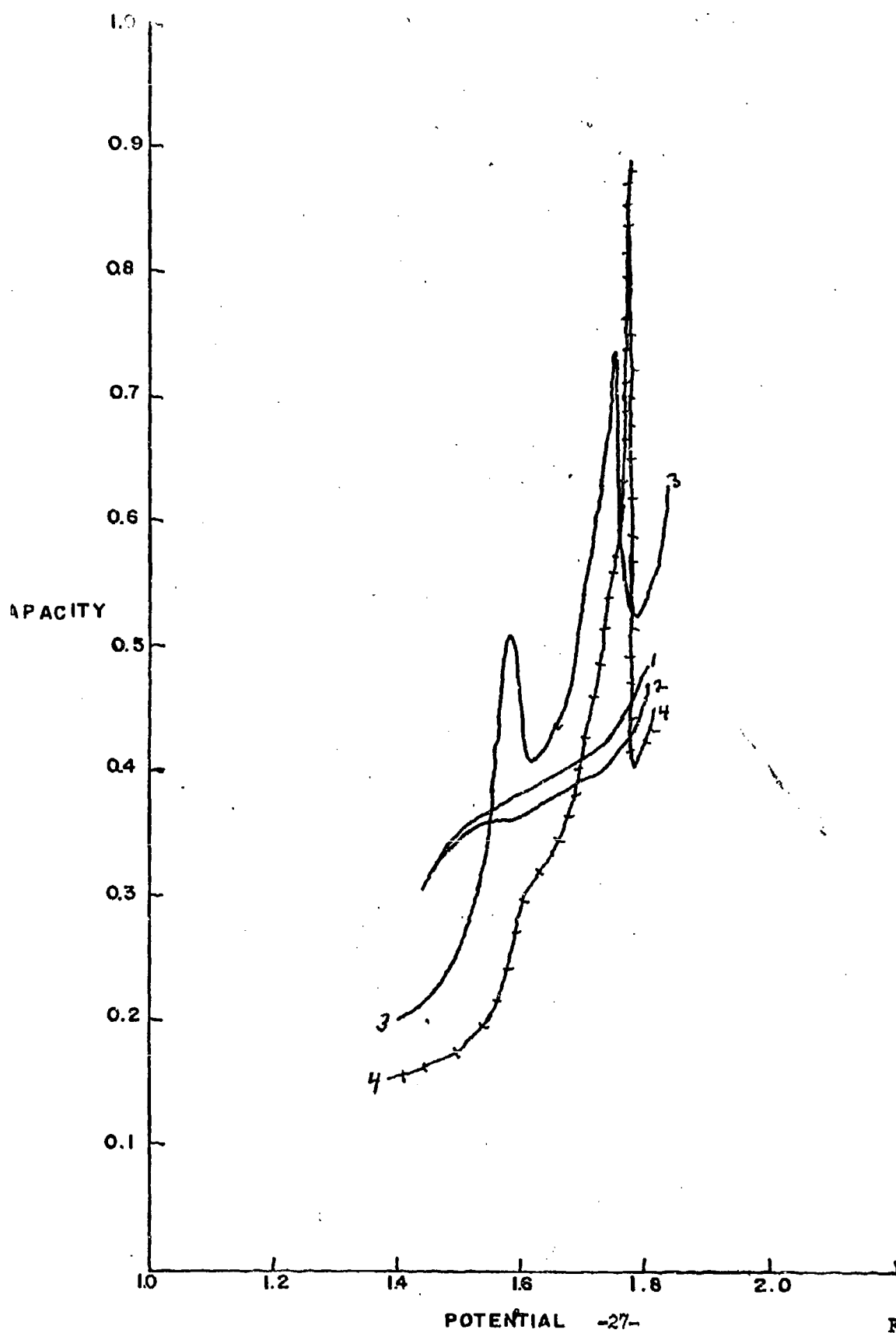


FIG.6

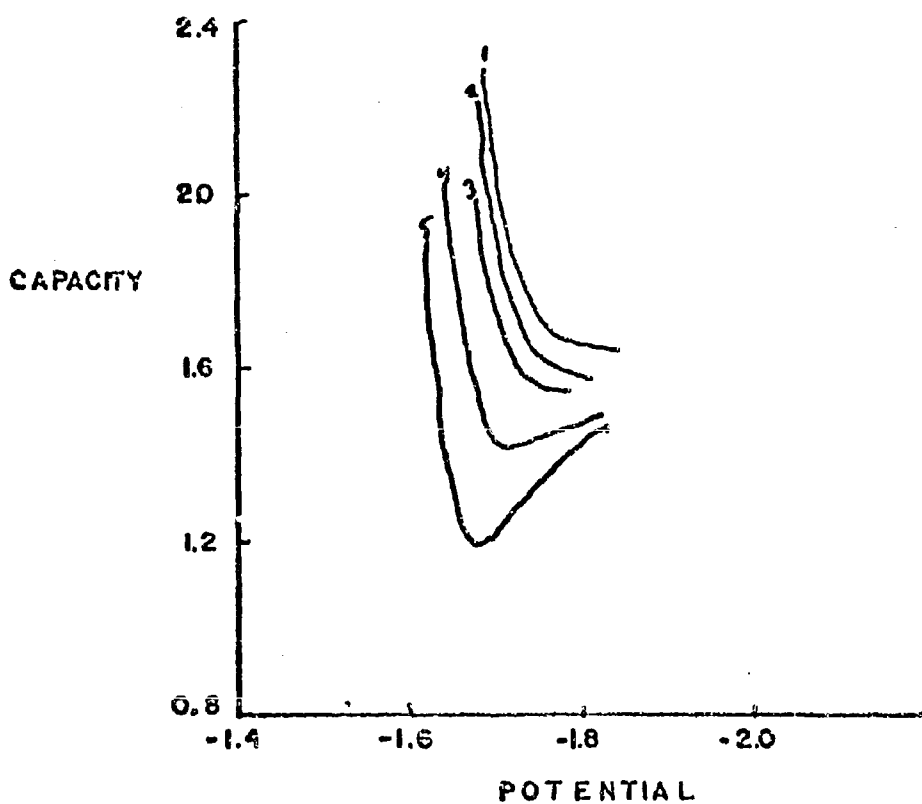


FIG.7

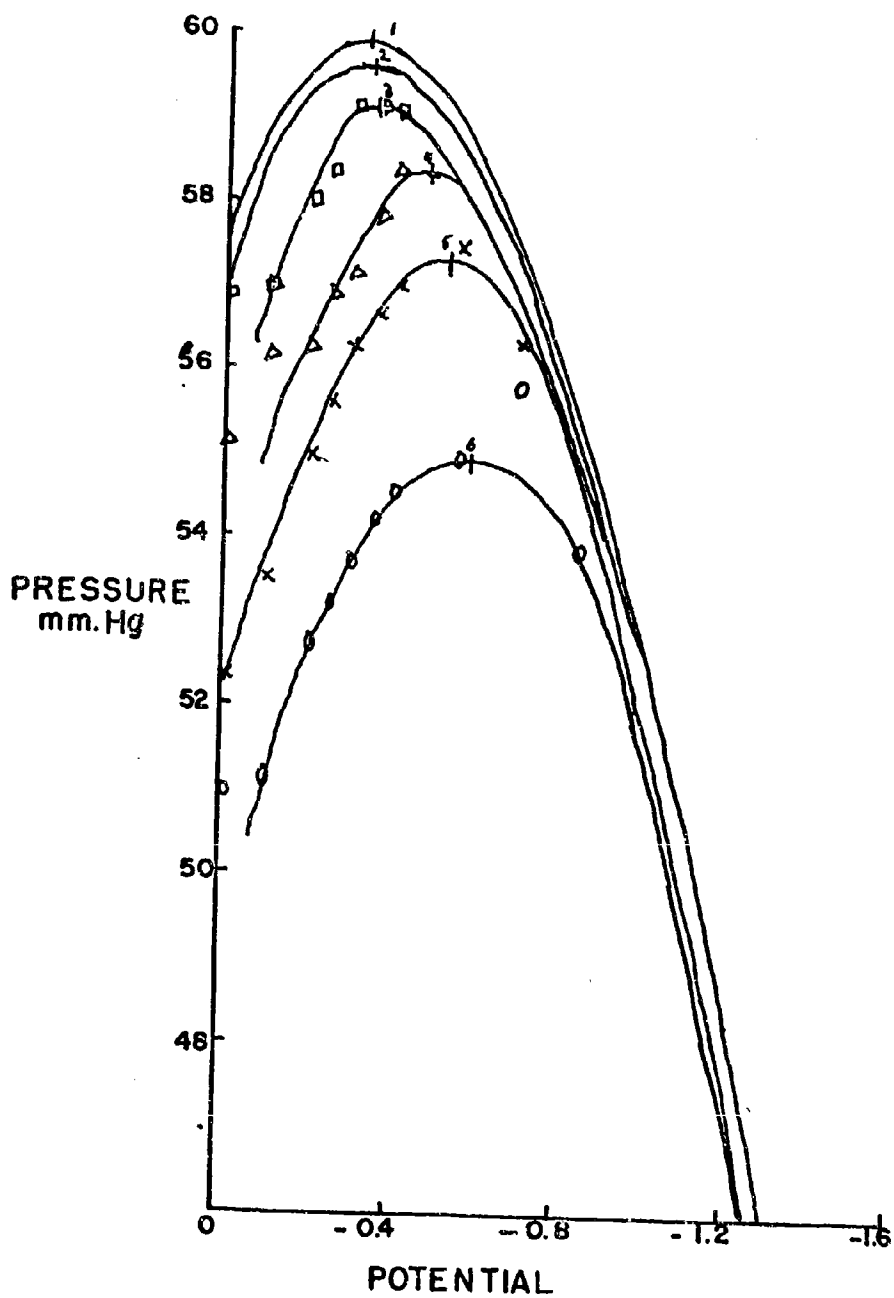
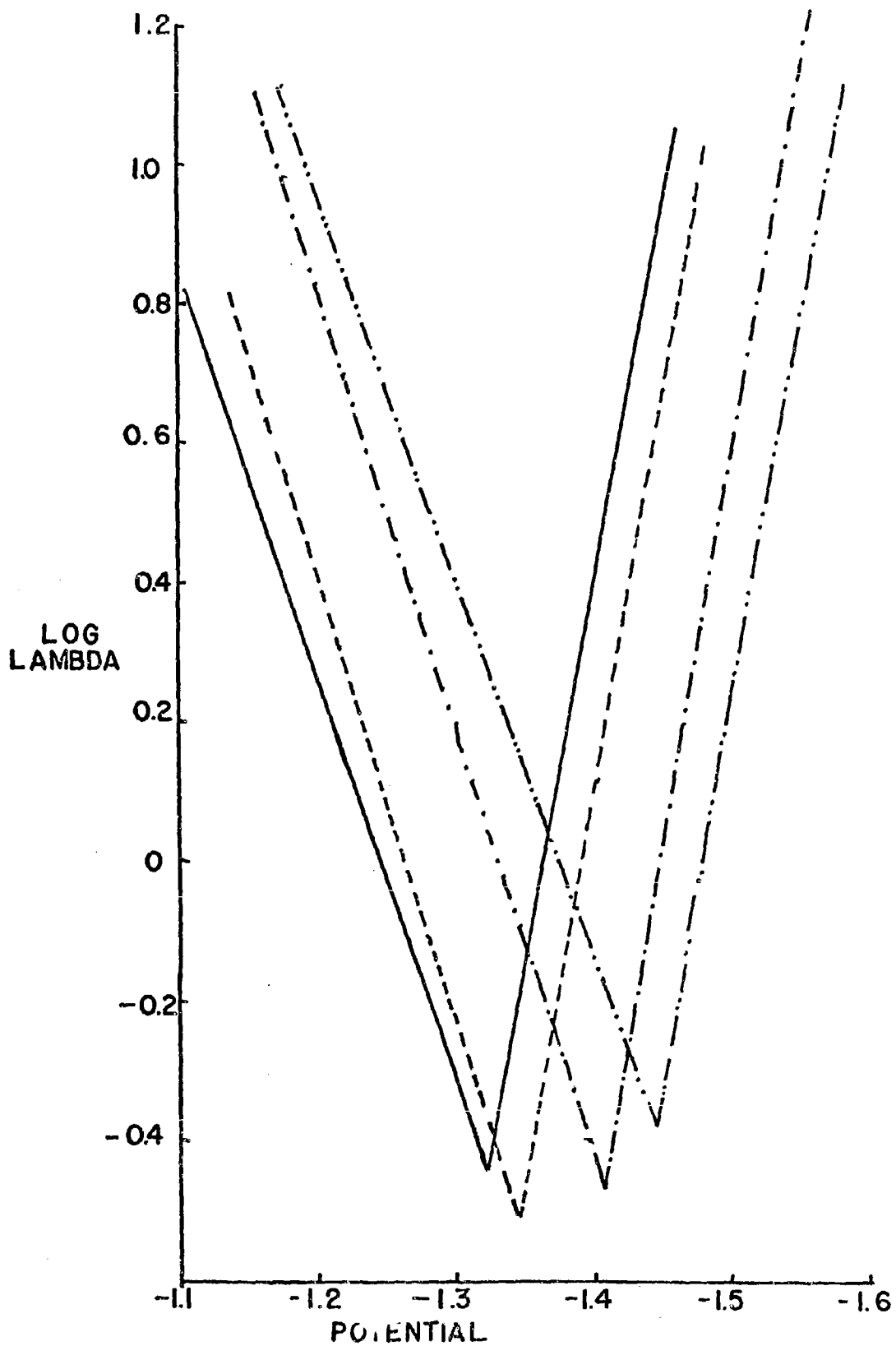
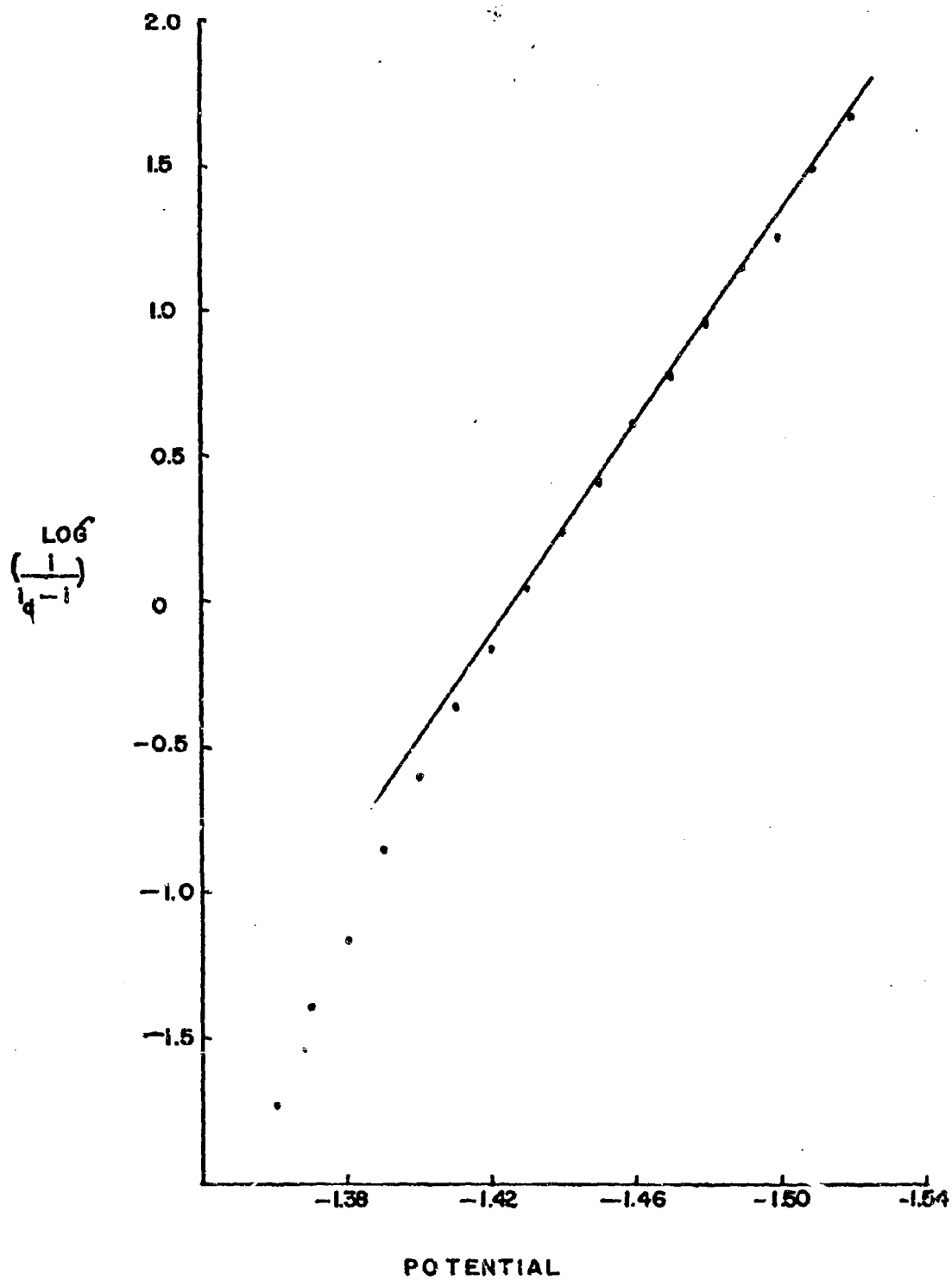
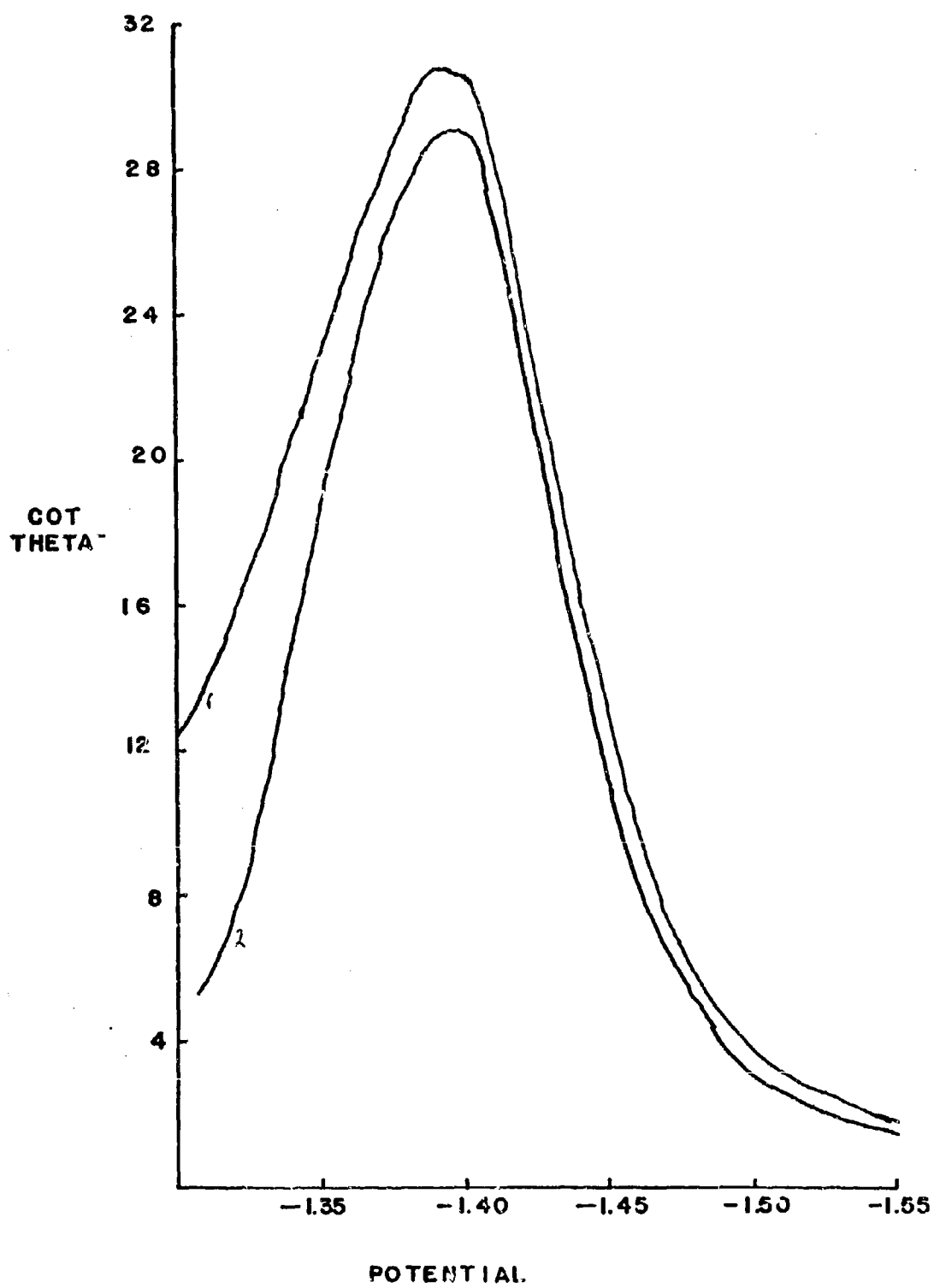


FIG.8







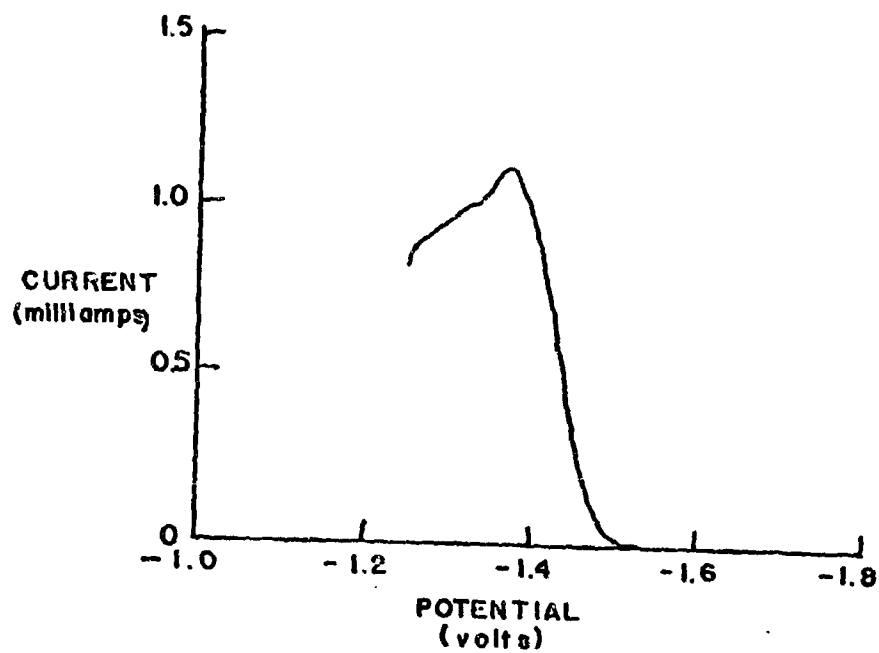
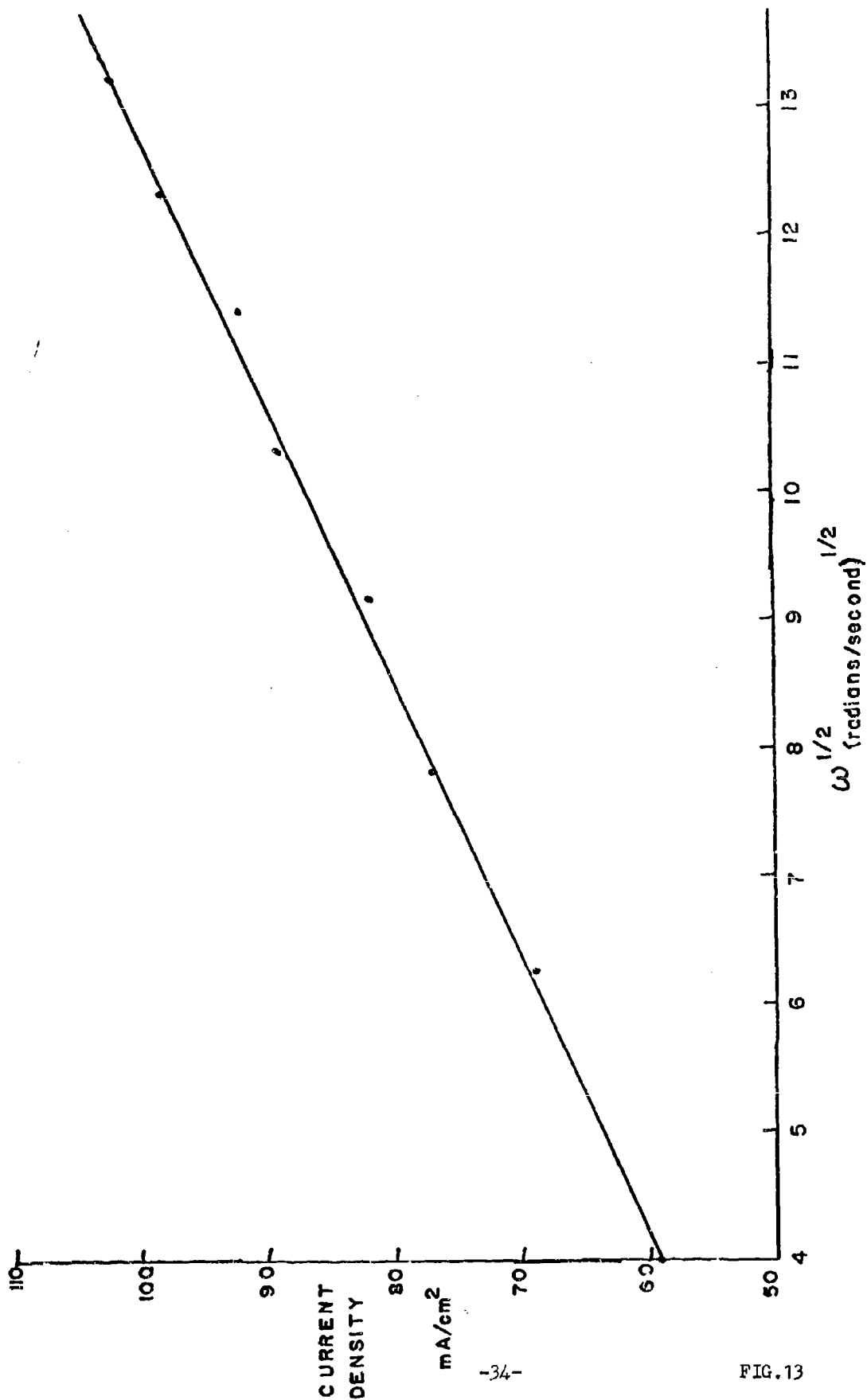
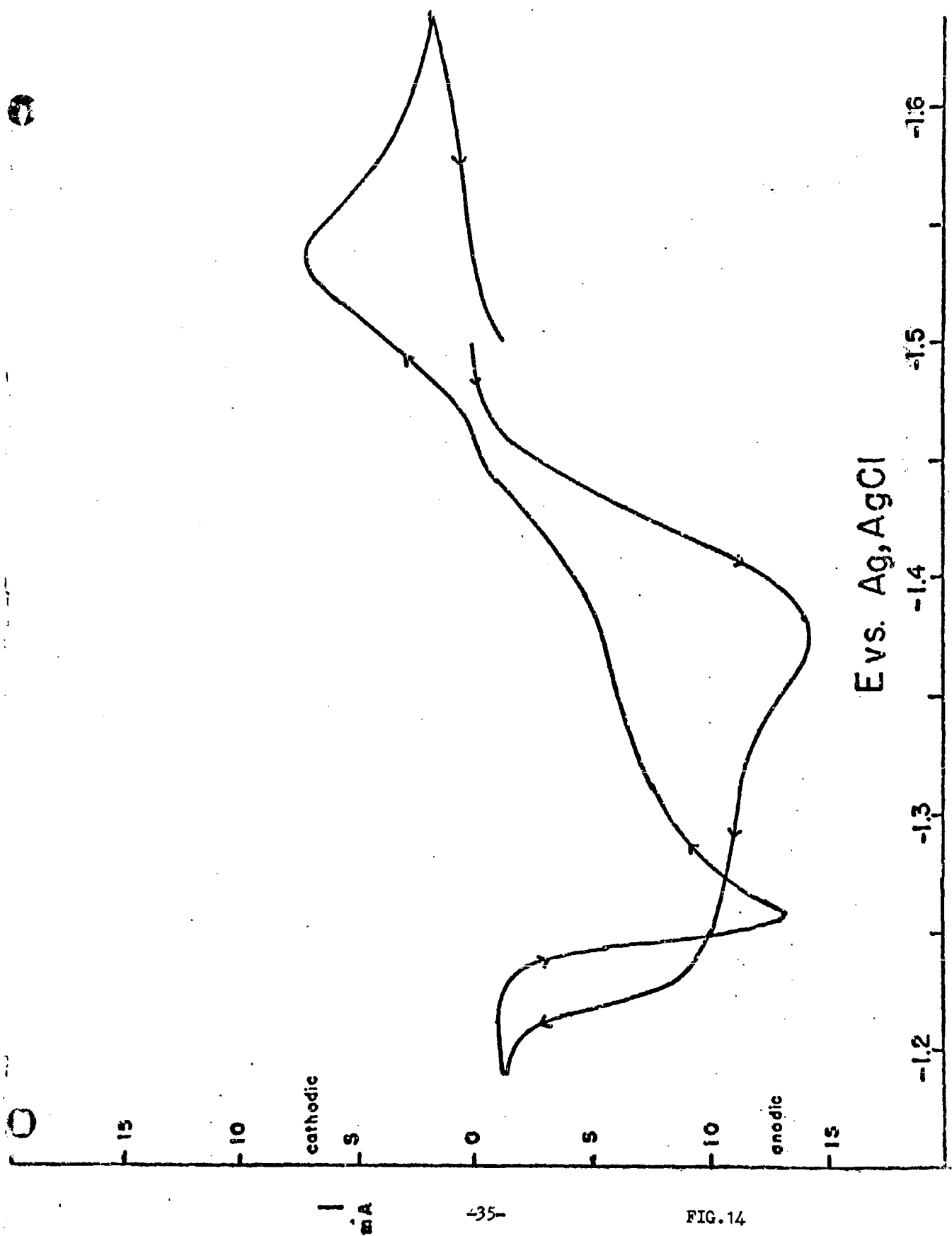


FIG. 12





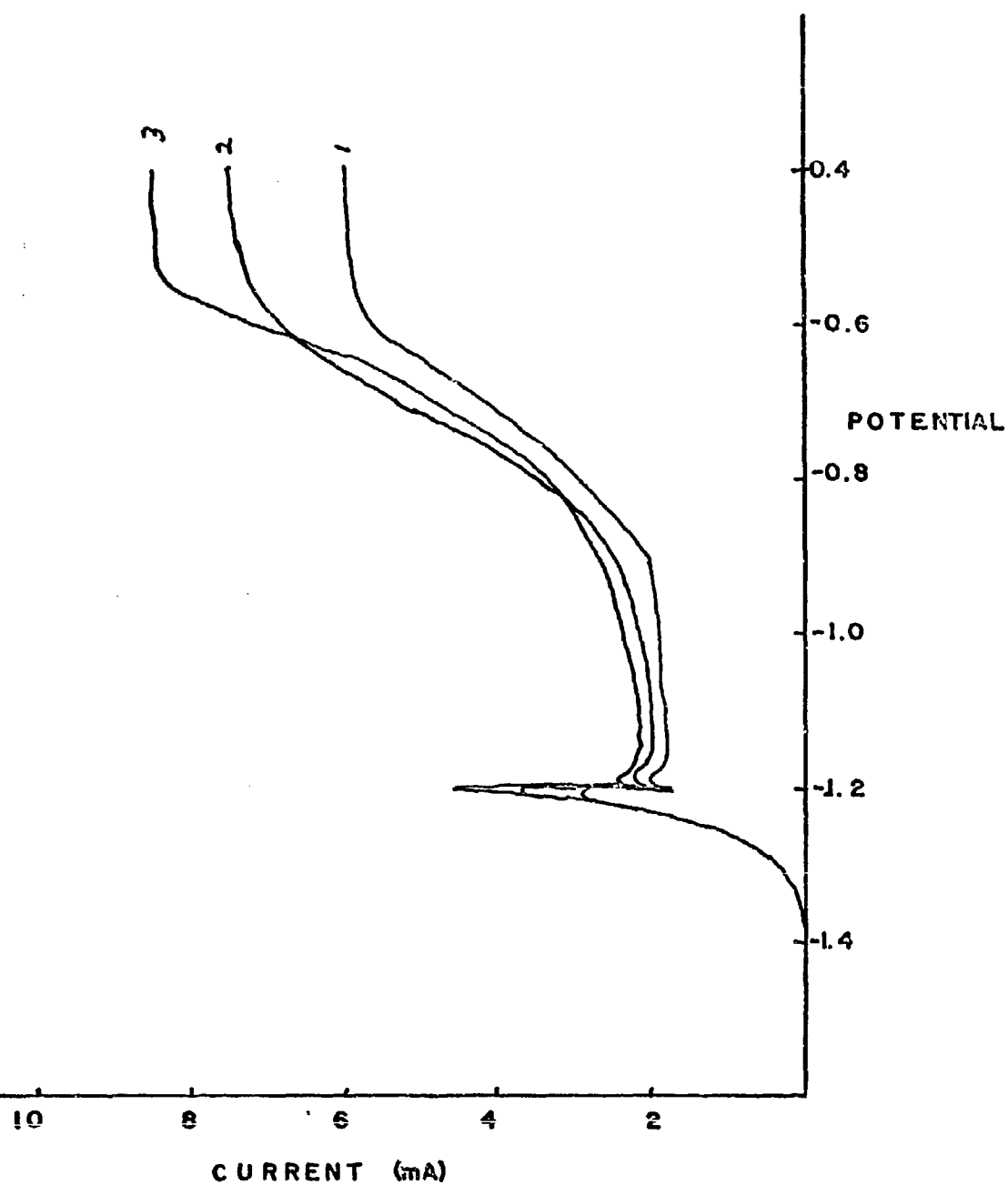


FIG.15

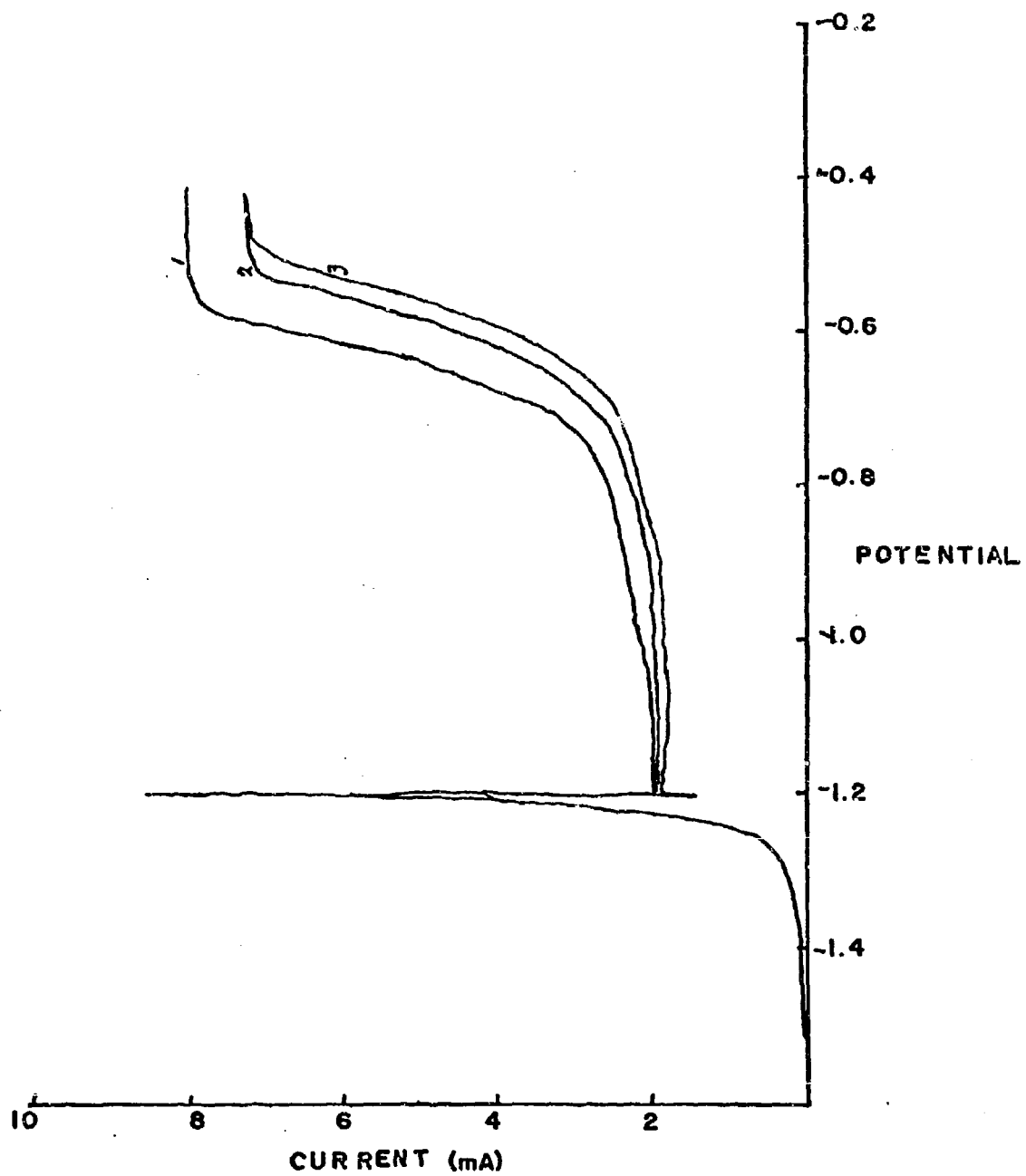


FIG.16

APPENDIX I. Computer Programs Used in Treatment of Data

A. Program SEFILS3

Program SEFILS3 is a Chippewa Fortran (CDC 6600) program which takes raw electrocapillary data, smooths it and calculates the charge on the electrode. The program requires subroutines CUBFIT, VIPRAB, TABLE, HUNTER, and QCAL.

Input format:

Card 1 number of curve families right justified in the first 5 columns.

Card 2 number of EMF's for which smoothed surface tension and charge are desired right justified in first five columns (max. 50).

Card 3ff Master EMF set F10.4

Card xx Surface tension F7.2, EMF F7.4 beginning in column 24, concentration E11.4 beginning in column 47, and the number of points on the curve I3 right justified ending in column 71.

Remainder of cards in curve punch only surface tension and EMF as above format.

Each new curve in a family must have a new xx card and each new family begins with a new Card 2.

Output format:

Error statements are fairly obvious.

For each curve the output consists first of the smoothed value of the surface tension in E18.10 format and then the EMF and the concentration, the rest of the line gives indications as to how each point was calculated. Then the charge, EMF, and concentration are printed out with some other numbers.

B. Program QGRAL

Program QGRAL calculates the charge from differential capacity data. It requires a slightly modified subroutine CUBFIT, the variables are passed through COMMON rather than in the cell.

Input:

Card 1 Number of points in the curve right justified in column 5.
The number of the point equal to the potential of zero charge.

In both programs EMF's are stacked in order with the most negative first.

Card 2ff EMF columns 1-10 Capacity columns 11-20.

Output:

Charge EMF Capacitance


```

PROGRAM SEFILS3 (INPUT,OUTPUT)
DIMENSION EMF(50),SURF(50),SFIT(50),X(4),Y(4),CHIEFE(50),
1 SFIT2(50)
IDCARD=35
5201 FORMAT (2I5)
5203 FORMAT(F10.4)
5204 FORMAT(F7.2,16X,F7.4,16X,E11.4,11X,I3)
5205 FORMAT(E18.10,1X,F7.4,16X,E11.4,6X,I5,2I3,I2,I3)
5206 FORMAT(1X,5HCURV+,I3,28H WIS NOT 69TT5D 85YON4 POINT,I3)
5207 FORMAT (1X,5HCURVE,I3,22H WAS NOT FITTED AT ALL,I2)
      READ 5201,NFAM
      DO 5241 N=1,NFAM
      READ 5201,NECHFOKU-VES
      DO 5211 I=1,NECHF
5211 READ 5203,CHIEFE(I)
      DO 5241 K=1,KURVES
      READ 5204,SURF(1),EMF(1),CONC,NEMF
      DO 5212 I=2,NEMF
5212 READ 5204,SURF(I),EMF(I)
      CALL VLPRAB (EMF,SURF,SFIT,NEMF,KOUNT,MJ)
      IF (MJ-5) 1,5272,5272
1 IF (KOUNT) 5271,5272,5219
5271 KOUNT =-KOUNT
      PRINT 5206,K,KOUNT
      MARK =0
      DO 5273 I=1,KOUNT
5273 PRINT 5205,SFIT(I),EMF(I),CONC,KOUNT,I,K,MARK,IDCARD
      CALL GCAL (SFIT,EMF,KOUNT,K,CONC)
      GO TO 5241
5272 PRINT 5207,K,MJ
      GO TO 5241
5219 DO 5242 I=1,NECHF
      Z=CHIEFE(I)
      CALL TABLE (Z,EMF,NEMF,J)
      IF (J-51) 5224,5225,5224
5224 MARK=0
      PRINT 5205,SFIT(J),EMF(J),CONC,KOUNT,I,K,MARK,IDCARD
      SFIT2(I)=SFIT(J)
      GO TO 5242
5225 CALL HUNTER (Z,EMF,NEMF,J)
      IF (J-52) 5226,5227,5226
5226 IF (J-(NEMF-1)) 5232,5227,5227
5227 DO 5231 M=1,4
      MM=M+NEMF-4
5231 X(M)=SFIT(MM)
      GO TO 5240
5232 IF (J-3) 5233,5233,5235
5233 DO 5234 M=1,4
      X(M)=EMF(M)
5234 Y(M)=SFIT(M)
      GO TO 5240
5235 DO 5236 M=1,4
      MM=M+J-3
      X(M)=EMF(MM)
5236 Y(M)=SFIT(MM)

```

5240 CALL CUBFIT (X,Y,A,B,C,D)
S=A*Z*Z*Z+E*Z*Z+C*Z+D
MARK=1
PRINT 5205,S,Z,CONC,OUNT,I,K,MARK,1DCARD
SFIT2(1)=S
5242 CONTINUE
CALL UCAL (SFIT2,CHIEFL,NECHIF,K,CONC)
5241 CONTINUE
END

```

SUBROUTINE CUBFIT (X,S,A,B,C,D)
DIMENSION X(4),Y(4),S(4),DEN(4)
Y(1)=S(1)
Y(2)=-S(2)
Y(3)=S(3)
Y(4)=-S(4)
BA=X(2)-X(1)
CA=X(3)-X(1)
DA=X(4)-X(1)
CB=X(3)-X(2)
DB=X(4)-X(2)
DC=X(4)-X(3)
DEN(1)=BA*CA*DA
DEN(2)=BA*CB*DB
DEN(3)=DC*CA*CB
DEN(4)=DC*DA*DB
GB=X(2)
GC=X(3)
GD=X(4)
J=1
A=0.
B=0.
C=0.
D=0.
8001 WA=GB+GC+GD
WE=GB*GC+GB*GD+GC*GD
WI=-Y(J)/DEN(J)
A=A+WI
WI=Y(J)*WA/DEN(J)
B=B+WI
WI=-Y(J)*WE/DEN(J)
C=C+WI
WI=Y(J)*GB*GC*GD/DEN(J)
D=D+WI
GO TO (8002,8003,8004,8005),J
8002 GB=X(1)
J=2
GO TO 8001
8003 GC=X(2)
J=3
GO TO 8001
8004 GD=X(3)
J=4
GO TO 8001
8005 CONTINUE
RETURN
END

```

```

SUBROUTINE VLPRAB (X,Y,YFIT,NPTS,KOUNT,J)
DIMENSION X(50),Y(50),YFIT(50)
J=1
1  X4S=0.
   X3S=0.
   X2S=0.
   X1S=0.
   X2YS=0.
   XYS=0.
   YS=0.
   SI=0.
   GO TO (2,3,25,25),J
2  L=1
   M=4
   INT=4
   GO TO 4
3  L=INT-2
   M=INT+1
   INT=INT+1
4  DO 5 I=L,M
   YS=Y+Y(I)
   XYS=XYS+X(I)*Y(I)
   X1S=X1S+X(I)
   X2=X(I)*X(I)
   X2YS=X2YS+X2*Y(I)
   X2S=X2S+X2
   X3S=X3S+X2*X(I)
   SI=SI+1.
5  X4S=X4S+X2*X2
15 DELTA=X4S*(SI*X2S-X1S*X1S)-X3S*(SI*X3S-X2S*X1S)+X2S*(X3S*X1S-
1  X2S*X2S)
   A=X2YS*(SI*X2S-X1S*X1S)/DELTA-XYS*(SI*X3S-X2S*X1S)/DELTA+
1  YS*(X3S*X1S-X2S*X2S)/DELTA
   IF (A) 6,12,12
6  B=-X2YS*(SI*X3S-X2S*X1S)/DELTA+XYS*(SI*X4S-X2S*X2S)/DELTA-
1  YS*(X4S*X1S-X3S*X2S)/DELTA
   C=X2YS*(X3S*X1S-X2S*X2S)/DELTA-XYS*(X4S*X1S-X3S*X2S)/DELTA+
1  YS*(X4S*X2S-X3S*X3S)/DELTA
   GO TO (7,8,8,25),J
7  L=1
   M=INT-2
   J=2
   GO TO 9
8  L=KOUNT-1
   M=INT-2
9  DO 10 I=L,M
10 YFIT(I)=A*X(I)*X(I)+B*X(I)+C
   IF (NPTS-INT)22,22,11
11 KOUNT=INT
   GO TO 1
12 IF(NPTS-INT)16,16,13
13 INT=INT+1
   K=INT
14 YS=Y+Y(K)
   XYS=XYS+X(K)*Y(K)

```

```

X1S=X1S+X(K)
X2=X(K)*X(K)
X2S=X2S+X2
X2YS=X2YS+X2*Y(K)
X3S=X3S+X2*X(K)
SI=SI+1.
X4S=X4S+X2*X2
GO TO 15
16 GO TO (17,18,19,25),J
17 KOUNT =0
RETURN
18 J=3
K=KOUNT-3
GO TO 14
19 IF(K-1)20,20,21
20 KOUNT =-KOUNT
RETURN
21 K=K-1
GO TO 14
22 GO TO (23,23,23,24),J
23 J=4
KOUNT=KOUNT+1
L=NPTS-1
M=NPTS
GO TO 9
25 J=J+5
24 CONTINUE
RETURN
END

```

```

SUBROUTINE TABLF(A,ARRAY,NPT,J)
DIMENSION ARRAY(50)
DO 1 I=1,NPTS
IF (ARRAY(I)-X)1,2,1
1 CONTINUE
J=51
GO TO 3
2 J=1
3 CONTINUE
RETURN
END
SUBROUTINE MONIE- (A,ARRAY,NPT,J)
DIMENSION APRAY(50)
DO 1 I=1,NPTS
IF (ARRAY(I)-X)1,3,3
1 CONTINUE
J=52
GO TO 4
3 J=1
4 CONTINUE
RETURN
END

```

```

SUBROUTINE QCAL (SURF,EMF,NEMF,K,CONC)
  DIMENSION SURF(50),EMF(50),A(4),B(4)
5304  FORMAT(E18.10,1X,F7.4,16X,E11.4,11X,2I3)
  DO 5312 M=1,4
    X(M)=EMF(M)
5312  Y(M)=SURF(M)
    CALL CUBFIT(X,Y,A,B,C,D)
    Q=(-3.*A*EMF(1)*EMF(1)-2.*B*EMF(1)-C)/10.
    J=1
    PRINT 5304 ,Q,EMF(1),CONC,J,K
    Q=(-3.*A*EMF(2)*EMF(2)-2.*B*EMF(2)-C)/10.
    J=2
    PRINT 5304 ,Q,EMF(2),CONC,J,K
    L=NEMF-3
    DO 5314 I=2,L
      J=I+1
      DO 5313 M=1,4
        MM=M+I-1
5313  X(M)=EMF(MM)
        Y(M)=SURF(MM)
        CALL CUBFIT(X,Y,A,B,C,D)
        Q=(-3.*A*EMF(J)*EMF(J)-2.*B*EMF(J)-C)/10.
5314  PRINT 5304 ,Q,EMF(J),CONC,J,K
        J=NEMF-1
        Q=(-3.*A*EMF(J)*EMF(J)-2.*B*EMF(J)-C)/10.
        PRINT 5304 ,Q,EMF(J),CONC,J,K
        J=NEMF
        Q=(-3.*A*EMF(J)*EMF(J)-2.*B*EMF(J)-C)/10.
        PRINT 5304 ,Q,EMF(J),CONC,J,K
      RETURN
    END

```

```

PROGRAM QGRAL (INPUT,OUTPUT)
COMMON X,Y,A,B,C,D
DIMENSION EMF(50),CAP(50),CAPFIT(50),X(4),Y(4)
GRAL(ARG)=(A*ARG**4)/4.+B*ARG**3/3.+C*ARG*ARG/2.+D*ARG
READ 1,NEMF,NOFLZ
1 FORMAT(2I5)
DO 2 I=1,NEMF
2 READ 3, EMF(I),CAPFIT(I)
3 FORMAT(2F10.4)
DO 4 M=1,4
MM=NOFLZ+M-1
X(M)=EMF(MM)
4 Y(M)=CAPFIT(MM)
CALL CUBFIT
RESULT=GRAL(EMF(NOFLZ+1))-GRAL(EMF(NOFLZ))
PRINT 5,RESULT,EMF(NOFLZ+1),CAPFIT(NOFLZ+1)
5 FORMAT(1X,E12.5,F7.4,16X,E11.4)
SUM=RESULT
RESULT=GRAL(EMF(NOFLZ+2))-GRAL(EMF(NOFLZ+1))
SUM=SUM+RESULT
PRINT 5,SUM,EMF(NOFLZ+2),CAPFIT(NOFLZ+2)
N=NOFLZ+1
L=NEMF-3
DO 7 I=N,L
DO 6 M=1,4
MM=I+M-1
X(M)=EMF(MM)
6 Y(M)=CAPFIT(MM)
CALL CUBFIT
RESULT=GRAL(EMF(I+2))-GRAL(EMF(I+1))
SUM=SUM+RESULT
7 PRINT 5,SUM,EMF(I+2),CAPFIT(I+2)
RESULT=GRAL(EMF(NEMF))-GRAL(EMF(NEMF-1))
SUM=SUM+RESULT
PRINT 5,SUM,EMF(NEMF),CAPFIT(NEMF)
DO 8 M=1,4
MM=NOFLZ+M-4
X(M)=EMF(MM)
8 Y(M)=CAPFIT(MM)
CALL CUBFIT
RESULT=GRAL(EMF(NOFLZ-1))-GRAL(EMF(NOFLZ))
PRINT 5,RESULT,EMF(NOFLZ-1),CAPFIT(NOFLZ-1)
SUM=RESULT
RESULT=GRAL(EMF(NOFLZ-2))-GRAL(EMF(NOFLZ-1))
SUM=SUM+RESULT
PRINT 5,SUM,EMF(NOFLZ-2),CAPFIT(NOFLZ-2)
I=NOFLZ-1
DO 10 M=1,4
MM=I+M-4
X(M)=EMF(MM)
10 Y(M)=CAPFIT(MM)
CALL CUBFIT
RESULT=GRAL(EMF(I-2))-GRAL(EMF(I-1))
SUM=SUM+RESULT
PRINT 5,SUM,EMF(I-2),CAPFIT(I-2)

```



```
IF(I-4)11,12,11
11 I=I-1
   GO TO 9
12 RESULT=GRAL(EMF(1))-GRAL(EMF(2))
   SUM=SUM+RESULT
   PRINT 5,SUM,EMF(1),CAPFIT(1)
   SUM=0.
   PRINT 5,SUM,EMF(NOFEZ),CAPFIT(NOFEZ)
   END
```

8

APPENDIX III

SURFACE AREA STUDIES OF ZINC ELECTRODES

SURFACE AREA STUDIES OF ZINC ELECTRODES

Summary Report

March 25, 1968

T. P. Dirks

Calvin College

3

SURFACE AREA STUDIES OF ZINC ELECTRODES
Summary Report

INTRODUCTION

In the development of zinc electrodes for use in alkaline battery systems, the surface area exposed to the electrolyte is of considerable importance. However, no convenient method is available to measure the surface area of battery electrodes of the type produced by Delco-Remy. These are porous electrodes made by the electrolytic reduction of zinc oxide.

The purpose of the work described here was to develop a method for measuring the surface area of such electrodes. The approach was to determine the time required to passivate a zinc electrode and then relate this time to the surface area.

It is generally agreed that as the zinc electrode discharges (is anodized) a solid product is formed. This product dissolves readily in the KOH electrolyte. When this dissolution is no longer possible, the discharge product deposits on the electrode and forms a film which passivates the electrode. If the anodization is carried out at a high current rate, the dissolving of the discharge product may not take place to an appreciable extent and this product then deposits on the electrode directly. It has been observed that the zinc may become covered with a blue film. This film may be the passivating layer. The color of this film suggests that it is about 500 Å. thick. Thus, if the anodization can be carried out so rapidly that no dissolution of the discharge product takes place, then the number of coulombs passed before passivation tells us the amount of discharge product formed on the

Q

electrode. Assuming a thickness of 500 Å for the film or layer, we can then calculate the surface area, or at least a relative surface area.

Sheet zinc electrodes were used as reference standards for surface area measurements. KOH concentrations ranging from 1% to 40% were used and runs were made at 0°, 15°, and 25°C.

EXPERIMENTAL

The sheet zinc electrodes were zinc strips 1.5 x 0.5 inches and 0.02 inches thick. These strips were degreased in ethylene dichloride and then given a slight etch with dilute HCl. Following this they were rinsed thoroughly, dried, and then painted with polystyrene cement so that only an area 0.5 x 0.5 inches was exposed to the electrolyte. They were then stored until ready for use.

The circuit consisted of a 28 volt battery in series with variable resistors to reduce the current to the proper level. A switch turned on the current and an electric timer at the same time.

The cell was a jar 6 x 5 x 3 inches holding about 350 ml of the KOH solution. Two nickel oxide electrodes, 4 x 4 inches, were placed on either side of the cell. A piece of zinc wire served as a reference electrode. The test zinc electrode was placed between the two nickel oxide electrodes. A vacuum tube volt meter was used to measure the potential between the test electrode and the reference electrode. When this potential rose suddenly to more than 2 volts the current and timer were turned off and the electrode

was considered to be passivated.

RESULTS

Effect of Pre-treatment.

During the time the sheet zinc electrodes were stored it is possible that they acquired a small amount of oxide coating. This had to be removed before the electrode could be anodized. Three kinds of pretreatment were used:

- 1- the electrodes were immersed in the electrolyte for 5 minutes, then treated cathodically at about 35 ma. for one minute, and then allowed to remain on open circuit for another 5 minutes before anodization.
- 2- the electrodes were placed in the electrolyte for 5 minutes and then anodized.
- 3- the electrodes were abraded with a 3/0 silicon carbide paper, rinsed with distilled water and allowed to remain in the KOH solution for 5 minutes before the run was started.

These electrodes were all anodized in 10% KOH at 25°C. The results are shown on Figure 1. There appears to be no significant difference. The same results are obtained regardless of the method of pretreatment. In subsequent work, pretreatment #1 was used.

It is likely true that the surface area was not exactly the same after the three types of pretreatment. Abrading should alter the surface area while cathodic current and immersion in the electrolyte would remove surface oxide films by reduction or by dissolving.

Any such differences, however, are within the experimental uncertainty of the method being used. Several factors contribute to this uncertainty. The main ones are: (a) lack of reproducibility in exposing exactly a 0.5 x 0.5 inch area to the electrolyte; (b) time lag in switching; and (c) the possibility that some of the discharge product is being dissolved.

Effect of Amalgamation.

Another factor to be considered is that commercial zinc battery electrodes are amalgamated. Evidence is available that amalgamation has the effect of increasing the surface area of the zinc electrode. Consequently, several sheet zinc electrodes were amalgamated by dipping them for 30 seconds in a solution containing 50 gms. of HgCl_2 per liter. These were then anodized and compared with non-amalgamated electrodes. The results are shown on Figure 2. It is obvious from Figure 2 that this method cannot distinguish between the surface area of amalgamated and non-amalgamated electrodes, if there is such a difference. Thus in using this method to compare the surface area of porous zinc electrodes with that of sheet zinc electrodes we need not take into account the fact that our sheet zinc electrodes are not amalgamated while the porous electrodes are.

Effect of Surfactants.

Delco-Remy electrodes as currently produced contain about 0.1% of an Emulphogene. This material is a surfactant which has increased the cycle life of the zinc electrodes. The reason for this improvement is as yet not known. Consequently, a few runs were made to determine whether this surfactant would alter the effective

surface area of the electrode as determined by this method.

An excess of Emulphogene BC-610 was added to 10% KOH (the solubility of the Emulphogene is very low). The results of the passivation times are given on Figure 3 together with similar results obtained in 10% KOH containing no Emulphogene. Apparently, the Emulphogene makes no difference in the surface area measurement by this method. Consequently, in making comparisons between Delco-Remy electrodes and sheet zinc electrodes, it is not necessary to make any allowance for the presence or absence of Emulphogene.

Effect of KOH Concentration and Temperature

In view of the assumed mechanism for the passivation of the zinc electrode, both temperature and KOH concentration should have an effect on the passivation times. The rate of dissolution of the discharge product is undoubtedly a function of the temperature. The solubility limit is a function of the KOH concentration. Consequently, at low temperatures and low KOH concentrations the dissolution of the discharge product should be minimized. Then the coulombs needed to passivate the electrode should be a direct measure of the amount of material needed to cover the surface of the zinc electrode with a passivating layer.

Passivation times were measured in a concentration range of 1 to 40% KOH and at 0°, 13°, and 25°C. Figures 4, 5, and 6 give the results obtained at each temperature. These results are what would be expected. More coulombs are needed to passivate the zinc electrode as the KOH concentration increases, although the difference between 10 and 20% KOH is not great. The curve in 1% KOH

at 0°C is almost parallel to the base. This suggests that the same number of coulombs are required to passivate the electrode regardless of the current used. That is, the rate of dissolution of the discharge product is approaching zero.

The results are presented differently on Figures 7, 8, 9, and 10. Here the effect of temperature is more clearly seen. As would be expected, more coulombs are needed to passivate the electrode as the temperature increases. This is because the rate of dissolution of the discharge product increases with increasing temperature.

Delco-Remy Electrodes.

Having obtained data about passivation times for sheet zinc electrodes under a variety of conditions, the next step was to determine passivation times for Delco-Remy porous electrodes under some of these same conditions. These electrodes could not be painted with polystyrene cement to expose only a limited surface area to the action of the electrolyte. Consequently, a 0.5 x 0.5 inch section of the electrode was used. This was cut from the upper corner where the lug or tab was attached. In this way, the lug could be used for electrical connection to the active material.

In making these runs several experimental difficulties were encountered. First of all, a considerably higher current was required to give passivation times comparable with those obtained for the sheet zinc electrodes. This higher current rate was more difficult to control and maintain constant throughout the run. Secondly, these electrodes behaved somewhat differently than did the sheet zinc electrodes. For the latter, the voltage rose very abruptly at passivation. There was no difficulty in determining

from the voltage change when the electrode had become passive. The porous electrodes showed a gradual increase in voltage during anodic treatment. The voltage did not rise abruptly. Consequently, it was difficult to determine from the voltage change just when the electrode had become passive. A rather arbitrary standard was finally adopted. The electrode was considered to have become passivated when its voltage showed that it had been polarized to the extent of 4 volts. This, admittedly, is arbitrary and is partly responsible for the rather poor reproducibility encountered in measuring these passivation times.

A third difficulty was encountered in cutting and handling these porous electrodes. During these processes some active material was lost from the electrode area that was to be tested. This also contributed to the lack of reproducibility.

In addition to these experimental difficulties there is another consideration. This method we are describing uses the amount of anodic coulombs as a measure of surface area. This means that only the surface area which is zinc can be measured. It can undergo anodic oxidation. Any surface area which is an oxidized form of zinc, e.g., zinc oxide, zinc hydroxide, zinc carbonate, will not be measured by this method because it cannot be further oxidized. However, if these materials should dissolve in the electrolyte and then expose zinc, this exposed zinc could be oxidized and would be included in any calculated area. This method, then, does not measure total surface area but rather it measures the area available for electrochemical oxidation. And this is not necessarily the area that would be measured, e.g., by the BET method using gas adsorption.

The above considerations are mentioned to help in interpreting the results that were obtained.

The procedure used was as follows. The electrode was placed in the electrolyte at open circuit for five minutes. It was then given a cathodic treatment for one minute at a low current density. Hydrogen was being evolved at the electrode by the end of this minute. Following this the electrode was left on open circuit for another five minutes and then anodized.

After measuring the time to passivation, this time was compared with the time to passivation for a sheet zinc electrode. For example, if the time to passivation for a porous electrode was 10 seconds, then reference was made to sheet zinc electrodes passivated under the same conditions of KOH concentration and temperature, Figures 3-10. From these curves one reads the number of coulombs required to passivate a sheet zinc electrode in 10 seconds. The ratio of this number of coulombs to the number of coulombs required to passivate the porous electrode in 10 seconds under the same conditions is considered to be also the ratio of the surface areas of the two types of electrodes.

These ratios were determined under several conditions and are summarized in Table I

TABLE I
RATIO OF AREA OF DELCO-REMY ELECTRODES TO THAT OF SHEET ZINC

<u>% KOH</u>	<u>Temp, °C</u>	<u>Ratio</u>
40	25	7:1
10	25	10:1
10	13	10:1
10	-3	13:1
1	-3	28:1

The uncertainty of the ratios given in this Table is about $\pm 20\%$. It appears to decrease somewhat at lower temperatures and at lower KOH concentrations. It is obvious that the ratio obtained depends on the conditions under which the measurements are made. The ratio increases as the temperature is lowered and as the KOH concentrations are decreased. These are the same conditions under which one would expect the rate of dissolution of the discharge reaction product to be less. Thus, it seems that the less the interference of the dissolving of the discharge product, the higher is the ratio of apparent surface area of porous zinc electrodes to sheet zinc electrodes. This might suggest that the best ratio or the most realistic ratio is the one determined in 1% KOH at 0°C . However, this is merely a guess until an independent method is available which will determine the surface area of the electrochemically active zinc in these porous electrodes. Certainly, a surface area ratio of 30:1 seems more realistic than a ratio of 7:1. Until an independent method is used to determine what the surface area ratio is, this method cannot very well be used to determine such a ratio. If such an independent method would tell us the ratio, then we could select the conditions under which this coulombic method gives the same ratio, and use the method for determining surface area ratios for zinc electrodes. The method is fairly simple and with further work the uncertainty could probably be reduced to about $\pm 10\%$.

Surface Area of Failed Electrodes.

Attempts were also made to determine the relative surface area of Delco-Remy porous zinc electrodes which had been removed from cells. These cells had been cycled until failure, and failure

was due to loss of zinc electrode capacity. These electrodes were treated the same way as the fresh zinc electrodes were, and the same difficulties were encountered in making time-to-passivation measurements.

In addition to this there was an added difficulty. This had to do with selecting a representative sample. In most electrodes there was no active material left on the grid in the vicinity of the lug. The active material on these electrodes had, during cycling, been redistributed away from the top of the electrode towards the bottom of the electrode. We were limited to the use of a 0.5 x 0.5 inch segment of the electrode. We eventually selected a sample from the center of the electrode. However, this was not necessarily a representative sample. This certainly had a higher surface area of active material than did a similar sized section near the lug (where there was no active material). Because of this the surface area measurement on such a segment will tell us only the relative surface area of that section and will tell us little, if anything, about the surface area of the total electrode compared to that of a fresh electrode.

These surface area measurements were also made under several conditions and the relative surface areas so determined are given in Table II.

TABLE II

RELATIVE SURFACE AREA OF FAILED ZINC ELECTRODES COMPARED TO
SHEET ZINC ELECTRODES

<u>%KOH</u>	<u>Temp. °C</u>	<u>Ratio</u>
40	25	9:1
10	-3	14:1
1	-3	25:1

The uncertainty in these measurements was about $\pm 7\%$.

Comparing these results with those in Table I it appears that there is not a great deal of difference. The differences are within the experimental uncertainties of each other. The value for the failed electrodes is higher under two conditions, but lower under the third. Thus we may conclude that this method of measurement shows no difference between the relative surface area of a fresh Delco-Remy porous zinc plate and a similar plate which has been cycled to failure. However, as noted earlier, this measurement was made on a segment of the electrode. There were other areas on the grid of these failed electrodes that had no active material. Thus, because the active material still remaining on the grid had a surface area equal to that of a fresh electrode, it is obvious that the total surface area of a failed electrode is less than that of a fresh electrode. To what extent it is less can only be judged by noting what fraction of the grid has no active material on it.

Kinetic Interpretations.

The primary purpose of the work described in this report was to evaluate this method as a means to determine surface areas of zinc electrodes. However, these results can be treated in other ways as well. Because current and time were measured, these values can be used to test various limiting conditions for the electrode reaction.

The times involved in these measurements were rather short and hence it is possible that these electrode reactions were limited and controlled by diffusion of solution species. One common way to check this is to plot current vs. $t^{-\frac{1}{2}}$. If the results show a linear relationship between these two values, then it is likely that

the electrode reaction is diffusion controlled.

Not all of our measurements were amenable to such treatment because the range of time or the range of currents used at a given temperature and in a given KOH concentration were too narrow. Figure 11 is an i vs $t^{-1/2}$ plot for some of the results we obtained where the spread in time and current was sufficiently broad to make the plot meaningful, and where a sufficient amount of data was available. The relationship is reasonably linear. This suggests strongly that these electrode reactions were diffusion controlled. The results do not allow us to infer which ion is the controlling one. It may be diffusion of OH^- ions to the electrode or the diffusion of zincate ions away from the electrode. It may be that both processes are equally significant.

Solution Rates.

If one accepts as valid the general outline for the anodic zinc reaction given earlier in this report, then the results we have obtained may be able to give us an indication of the rate at which the discharge reaction product dissolves under various conditions.

The coulombs-time data given, e.g., on Figure 4 generally show that the number of coulombs accepted by the electrode during electrolytic oxidation increases with increasing passivation times. The increased time allows more of the discharge reaction product to dissolve. Thus more coulombs are needed so that the electrode surface will be covered with undissolved reaction product. The results in 1% KOH at 0°C , however, show no such positive slope. This suggests that under these conditions the rate of dissolution of the reaction product is so slow that all the coulombs accepted by the electrode

are used to coat the surface of the electrode. Thus the number of coulombs needed to bring about passivation is independent of the time allowed for passivation. If this be so, then the number of coulombs required for passivation in 1% KOH at 0°C gives us a direct measure of the surface area (this will be treated later), and of the amount of reaction product needed to coat the surface of the sheet zinc electrodes. The amount required for covering the surface of the sheet zinc electrodes then is 0.1 coulomb.

Later work under these same conditions but over a wider time range showed that at 0°C in 1% KOH the plot of coulombs vs. time also shows a positive slope, Figure 12. The line, however, does extrapolate to 0.1 coulomb for the electrode. This then will be assumed to be the amount of charge needed to cover the surface of the 0.5 x 0.5 inch area of the sheet zinc electrodes. This amounts to $0.1/2 \times 96500$ or 5.2×10^{-7} moles of zinc oxide or hydroxide. Any additional zinc compound produced during the time to passivation is assumed to have dissolved in the electrolyte.

The rate of dissolution of the zinc reaction product may then be calculated as follows. From Figure 3 a value of 3.8 coulombs is obtained for a passivation time of 10 seconds. Of this, 0.1 coulomb was needed to coat the electrode surface and 3.7 coulombs, the remainder, then represents the amount of discharge product that dissolved or diffused away in the 10 seconds. The 3.7 coulombs corresponds to 19×10^{-6} moles of reaction product. This amount dissolved over a period of 10 seconds which, on a linear basis, corresponds to 19×10^{-7} moles per second as a rate of dissolving. This same procedure has been followed for calculating the dissolution rates under other conditions. The results are summarized in Table III, and on Figure 13.

TABLE III

RATE OF DISSOLUTION OF ZINC ELECTRODE DISCHARGE PRODUCT

MOLES PER LITER PER SECOND $\times 10^{+7}$			
temp % KOH	-3 °C	13 °C	25 °C
1	1	1	2
10	7	8	19
20	10	11	20
30		28	32
40	20	31	35

The results on Figure 13 are given as rate of dissolution per square centimeter of electrode surface.

The dissolution rates are what would be expected. They increase with increasing temperature and with increasing KOH concentration. Whether they are real or not depends on the validity of the assumptions made in calculating them. There is no other way known to us at the moment for checking these results nor are we aware of any other such measurements having been made.

The solubility of the discharge product was studied in still another way. After an electrode became passive it was assumed to be covered with a film or layer of the discharge reaction product, probably zinc hydroxide. This product is soluble in the KOH solution and when it has dissolved the electrode should again be electrochemically active. After being passivated the electrode was allowed to remain on open circuit in the electrolyte for a period of time. It was then treated anodically and the time to passivation

was again measured. When the time to passivation was about the same as that for a fresh electrode in the same solution, the electrode was considered to be electrochemically active.

One such series of trials was carried out in 10% KOH at 25° using sheet zinc electrodes. It was found that when the electrode remained on open circuit for at least 10 seconds, it had regained its electrochemical activity. For periods of less than 10 seconds the electrode showed some semblance of passivity, i.e., time to passivation was shorter than for a fresh electrode.

A similar experiment was carried out under the same conditions using Delco-Remy porous zinc electrodes. With this electrode it was found necessary to leave the electrode on open circuit at least 3 minutes before electrochemical activity was regained. This added time reflects the increased surface area and the greater congestion in the pores of the electrode. The ratio of these two open circuit times is $3 \times 60/10$ or 18:1, which is considerably larger than the surface area ratio shown in Table I for these same conditions.

No further work was possible in this area because of time limitations. Until more such work is done no significant conclusions can be drawn from these data.

Dimensions of Surface Film.

It was pointed out earlier that 0.1 coulomb or 5.2×10^{-7} moles of reaction product are required to form the passivating layer over the surface of the electrode. If this film is zinc hydroxide then the weight of the film is $99.4 \times 5.2 \times 10^{-7} = 5.2 \times 10^{-5}$ grams. The handbook density for this substance is given as 3 gm/cc.

This, of course, may not be the density of the actual material in the passivating layer. However, assuming that it is, then the volume of the layer is 1.7×10^{-5} cc. For a surface area of 0.5 x 0.5 inch, this gives a value of 1000 Å for the thickness of the film. This assumes a roughness factor of 1. A roughness factor of 2 to 3 is a more realistic figure and this would give a film thickness of 300 to 500 Å. This may or may not be a realistic value. If the thickness of the film could be determined by an independent method then this could be used to calculate the roughness factor for the sheet zinc surface.

The experimental difficulty involved is in actually observing the passivating film. It dissolves readily in the KOH electrolyte. Furthermore, if removed from the electrolyte, the film may undergo changes in composition.

An alternate way of getting some indication of the thickness of the passivating film is to assume that during passage of current there is film formation and film dissolution, with the latter process being slower than the former. Then, the film gradually thickens as the current is passed and when it has reached a certain thickness the electrode is passivated.

The rate of growth of the film = $k \times i$. The thickness of the film, x , is

$$X = \frac{1 \times t \times 99.4}{2 \times 96,500 \times 3 \times 1.6} \text{ cm.} \quad (1)$$

Where i = current

t = time

99.4 = mol. wt. of Zn(OH)_2

2 = mol. wt./equiv. wt. for Zn(OH)_2

3 = density of Zn(OH)_2

1.6 = surface area of the sheet zinc electrodes

96,500 = the Faraday

The rate of dissolution of the film, k_d , is constant at a given temperature in a given KOH concentration. This is expressed as moles/sec. To change this value to a corresponding film thickness we change this to a corresponding weight and volume and divide by the density.

$$X' = \frac{k_d \times t \times 99.4}{3 \times 1.6} \text{ cm.} \quad (2)$$

The thickness at any time X_t then is $X - X'$ or

$$X_t = \frac{1 \times t \times 99.4}{2 \times 96,500 \times 3 \times 1.6} - \frac{k_d \times t \times 99.4}{3 \times 1.6}$$

or

$$X_t = \frac{t \times 99.4}{3 \times 1.6} \left[\frac{1}{193,000} - k_d \right] = 20.6 t \left[\frac{1}{193,000} - k_d \right] \quad (3)$$

For equation (3) we have values for i and t and estimated values for k_d .

An attempt has been made to solve equation (3) for the thickness of the layer from the time-current data we have obtained. However, the two terms in the brackets, i.e., $1/193,000$ and k_d are so nearly equal in value, that the difference between them is less than the experimental uncertainty in either one. Consequently, this approach has to be abandoned for the calculation of the thickness of the passivating film until more precise data become available.

T. P. Dirkse

T. P. Dirkse

March 28, 1955

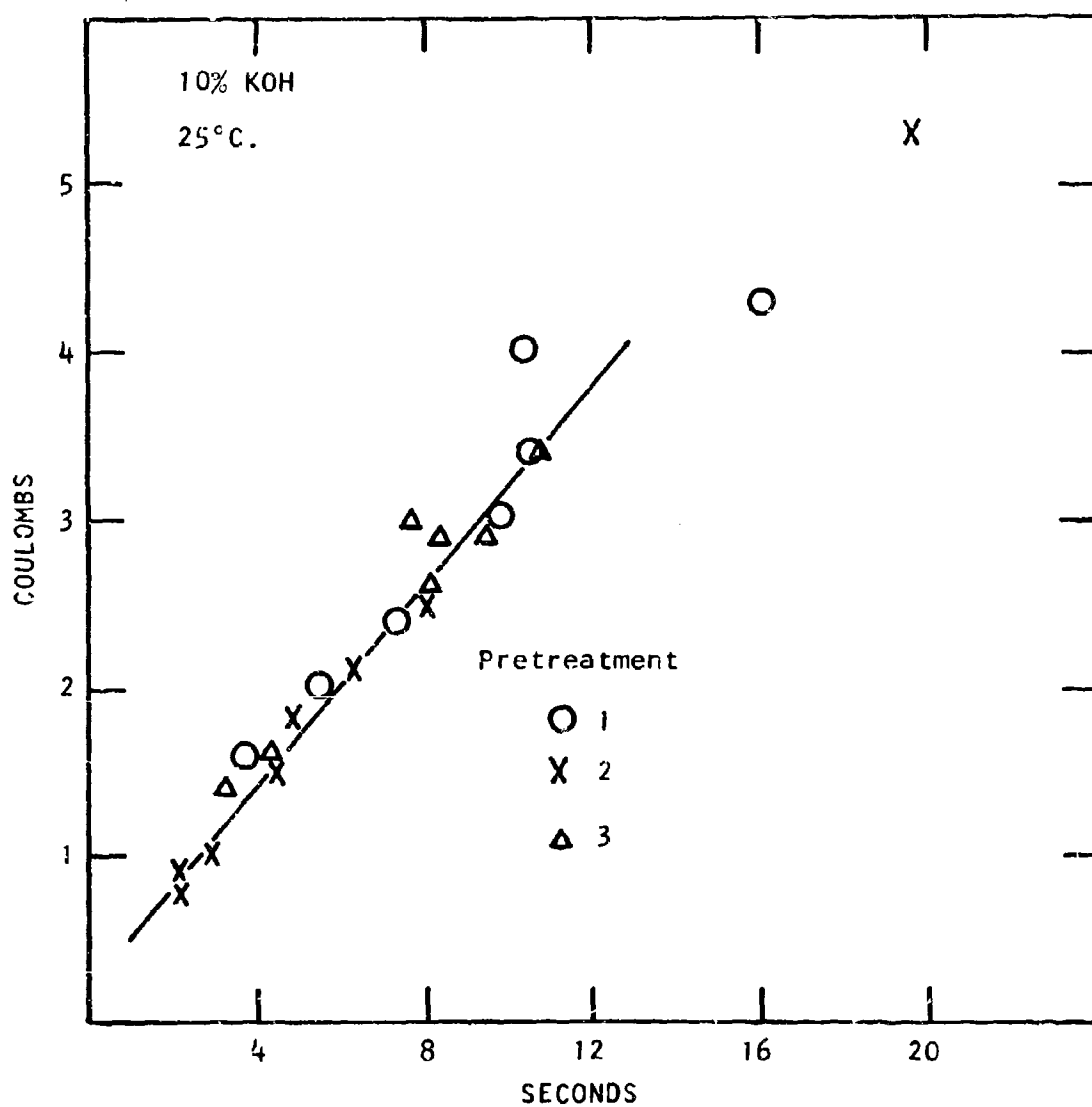


Figure 1 Passivation times for sheet zinc electrodes as a function of the method of pretreatment.

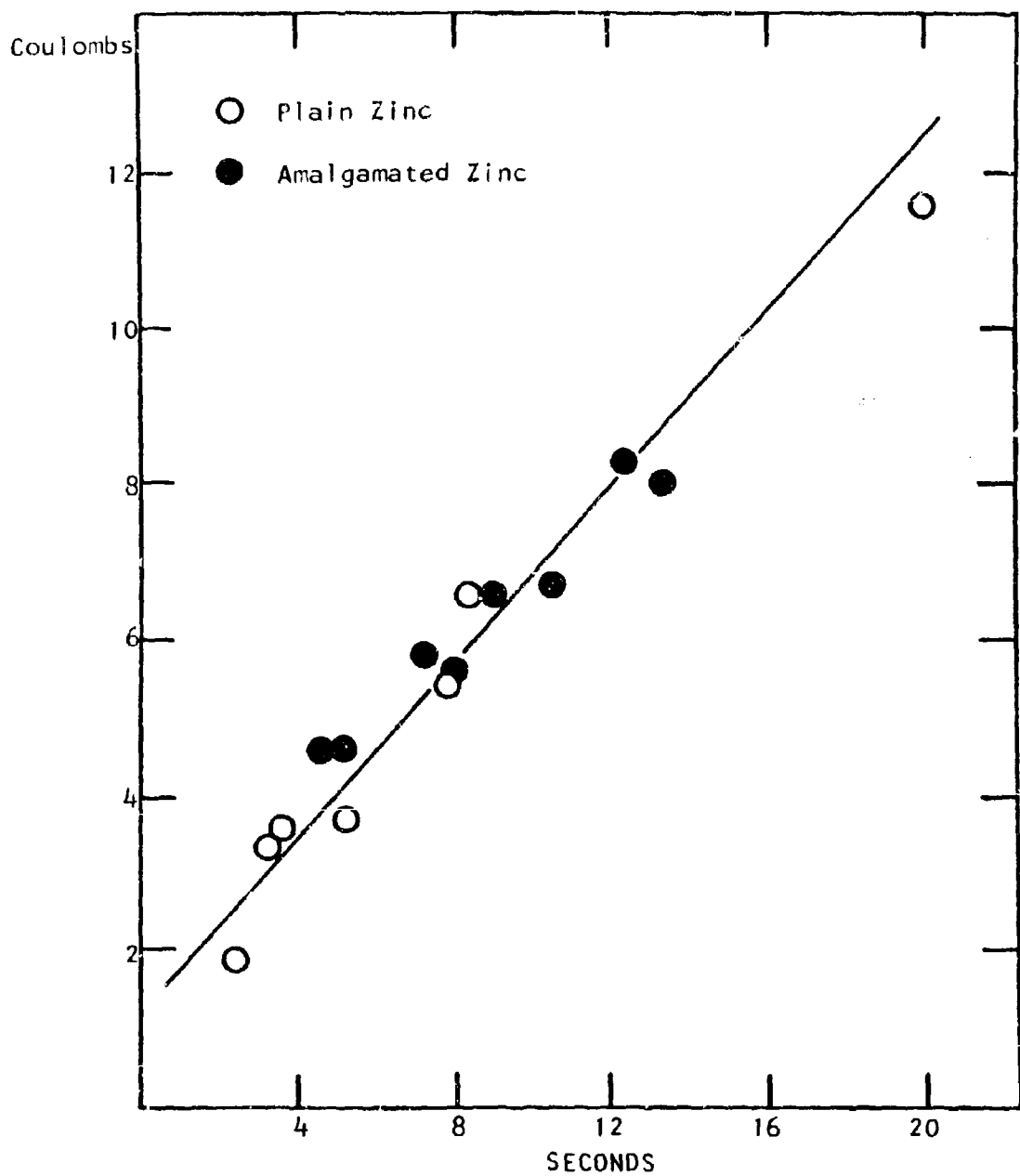


Figure 2 Effect of amalgamation on passivation times for sheet zinc electrodes in 40% KOH at 25°C.

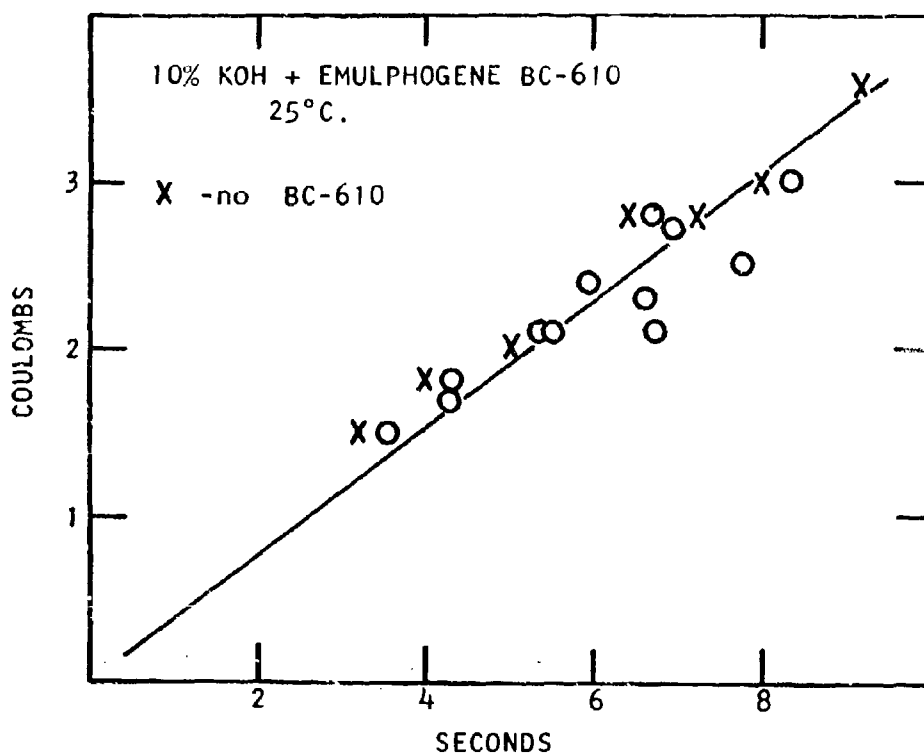


Figure 3 Effect of amalgamation on the passivation times for sheet zinc electrodes.

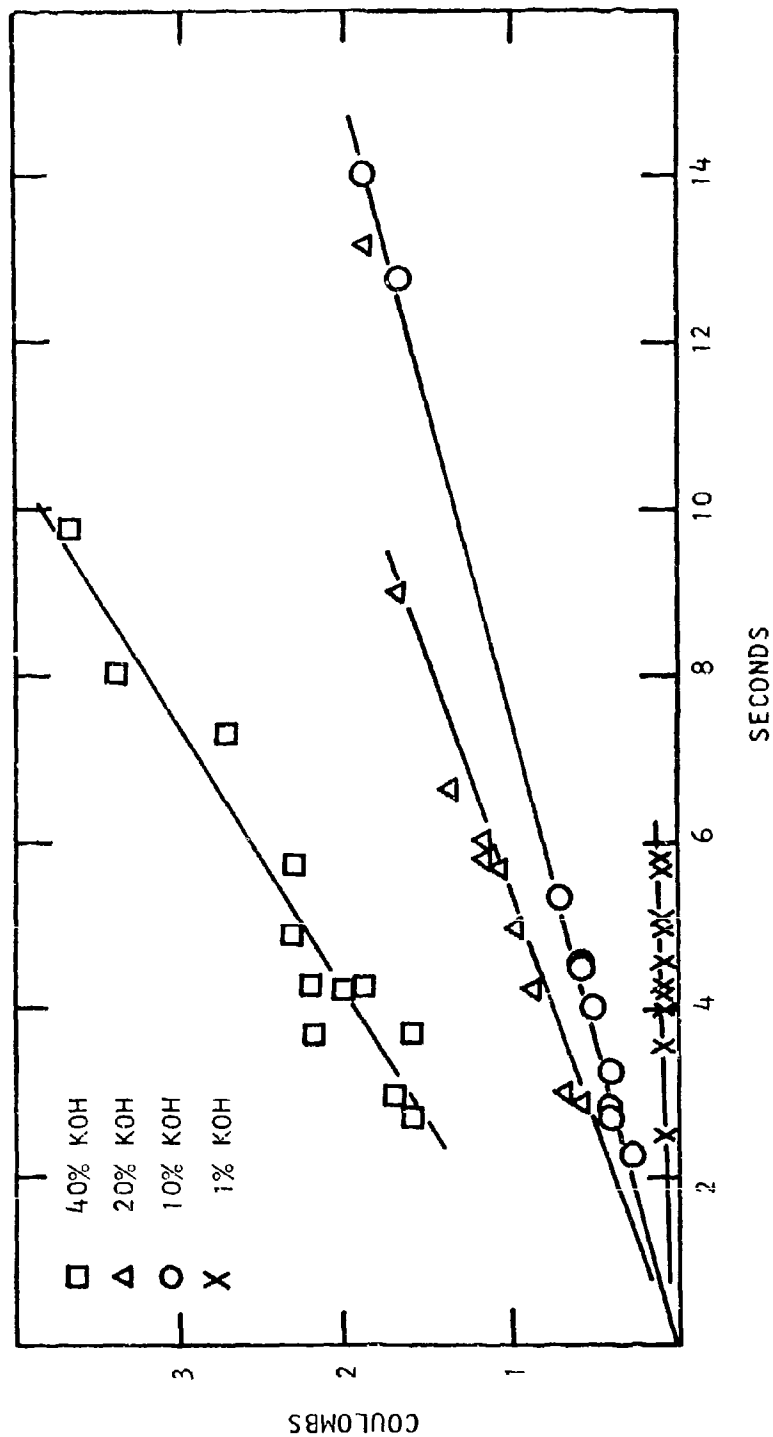


Figure 4 Passivation times for zinc electrodes at 0°C.

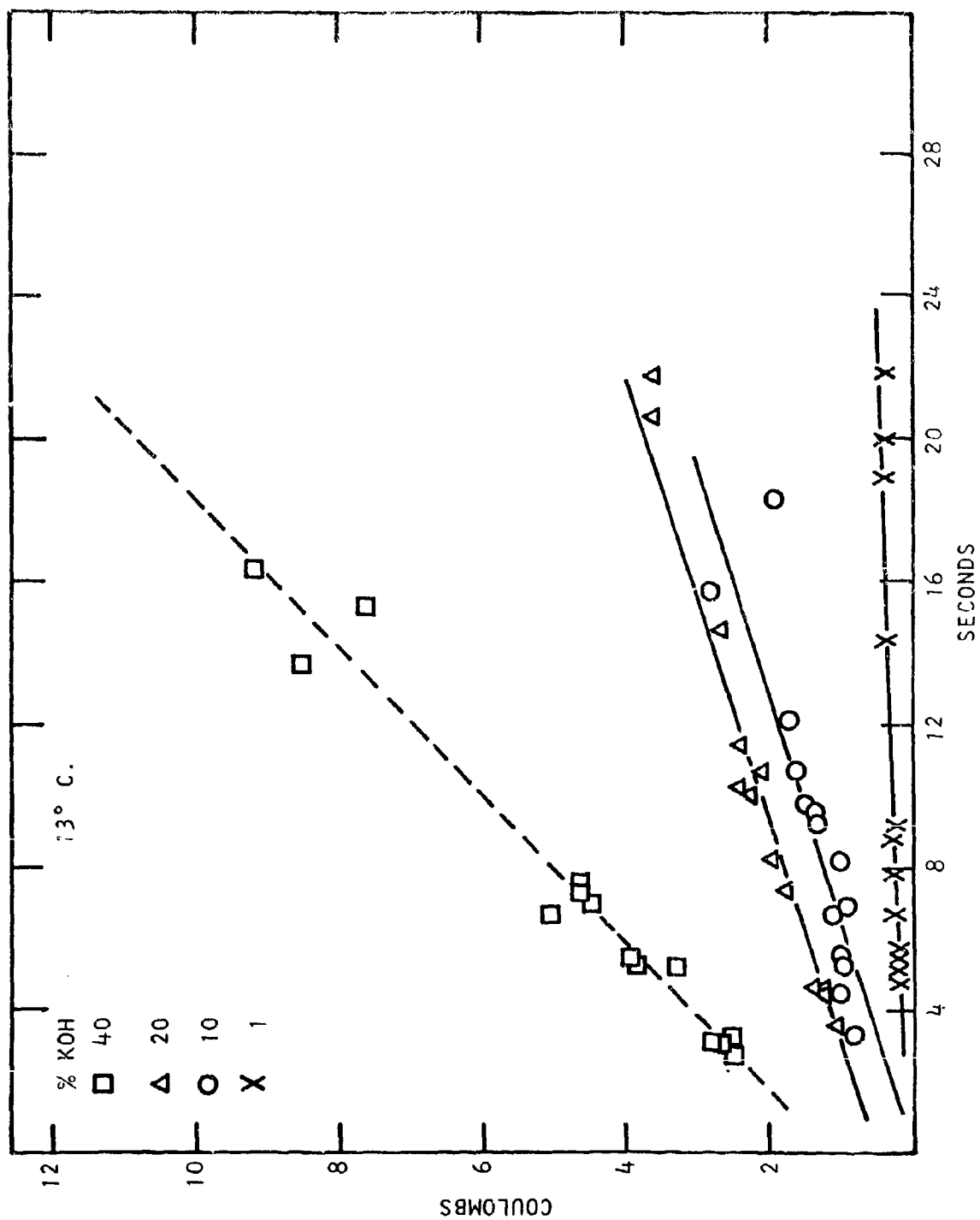


Figure 5 Passivation times for sheet zinc electrodes at 13°C.

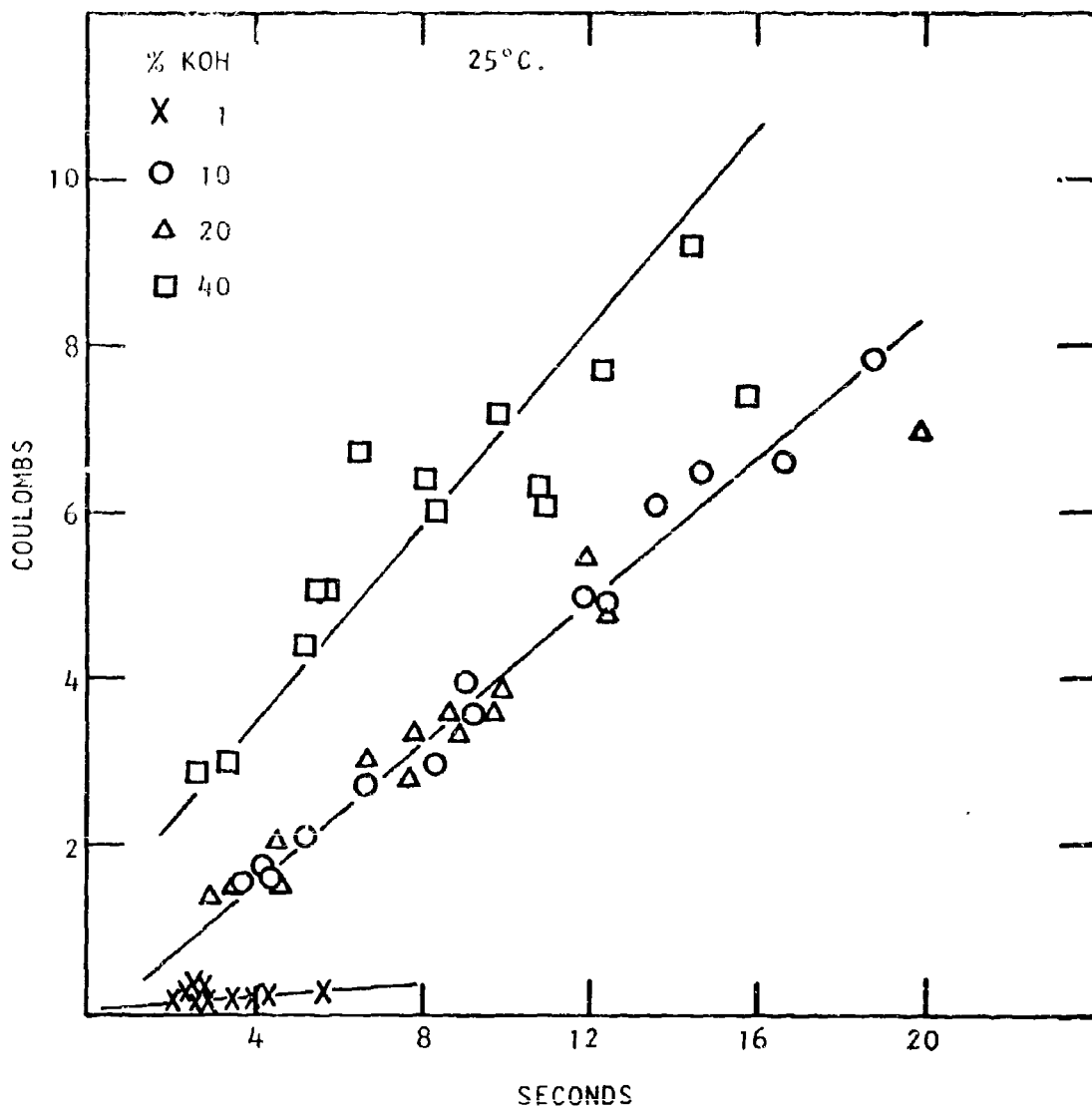


Figure 6 Passivation times for sheet zinc electrodes at 25°C.

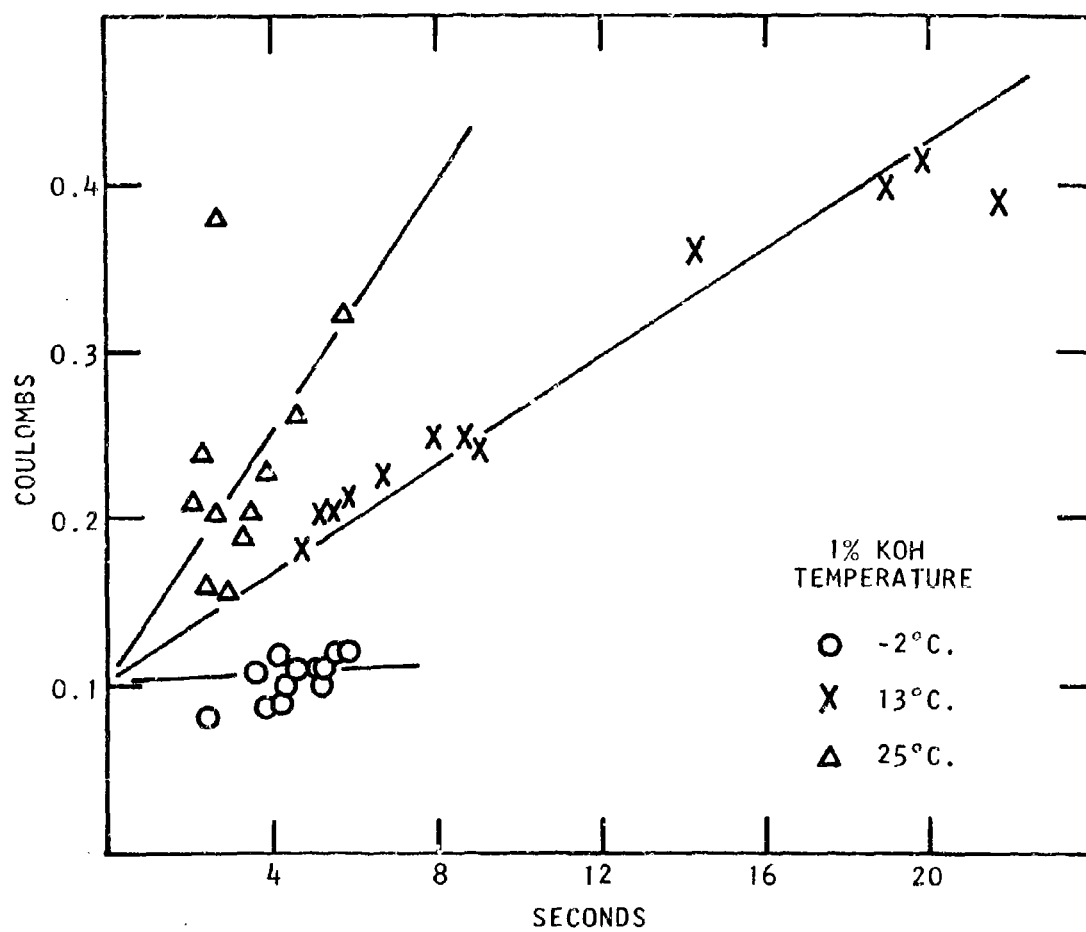


Figure 7 Passivation times for sheet zinc electrodes in 1% KOH

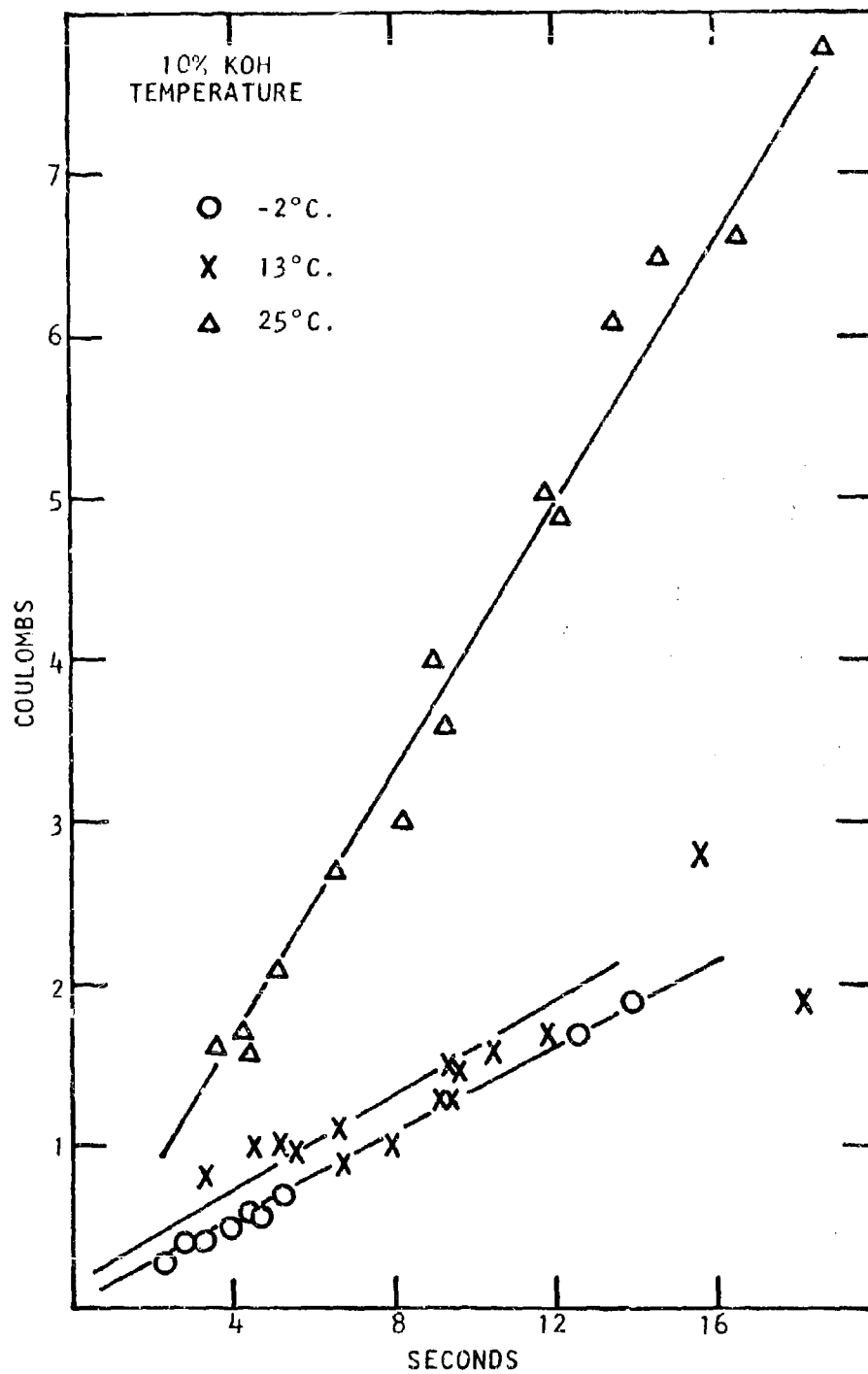


Figure 8 Passivation times for sheet zinc electrodes in 10% KOH.

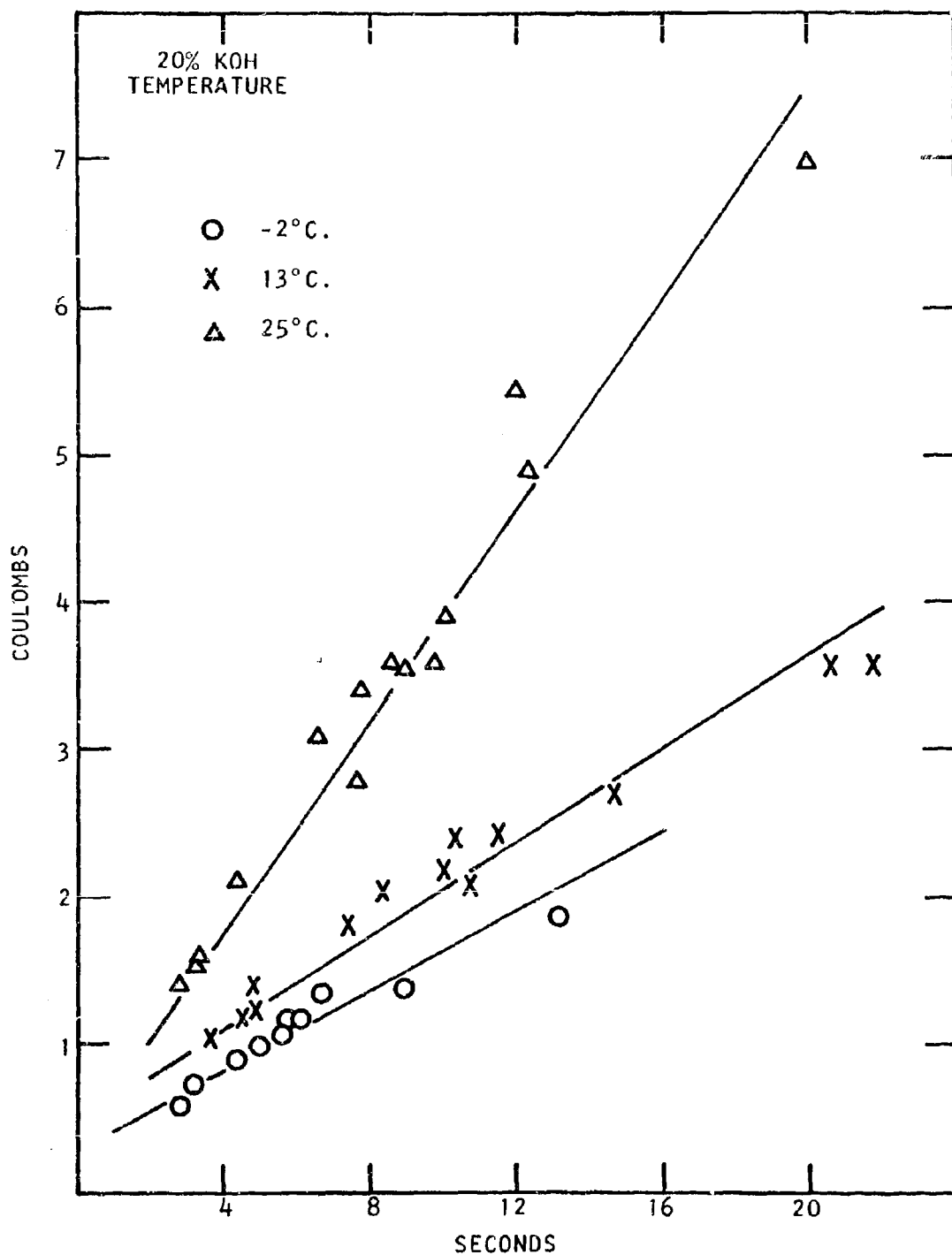


Figure 9 Passivation times for sheet zinc electrodes in 20% KOH

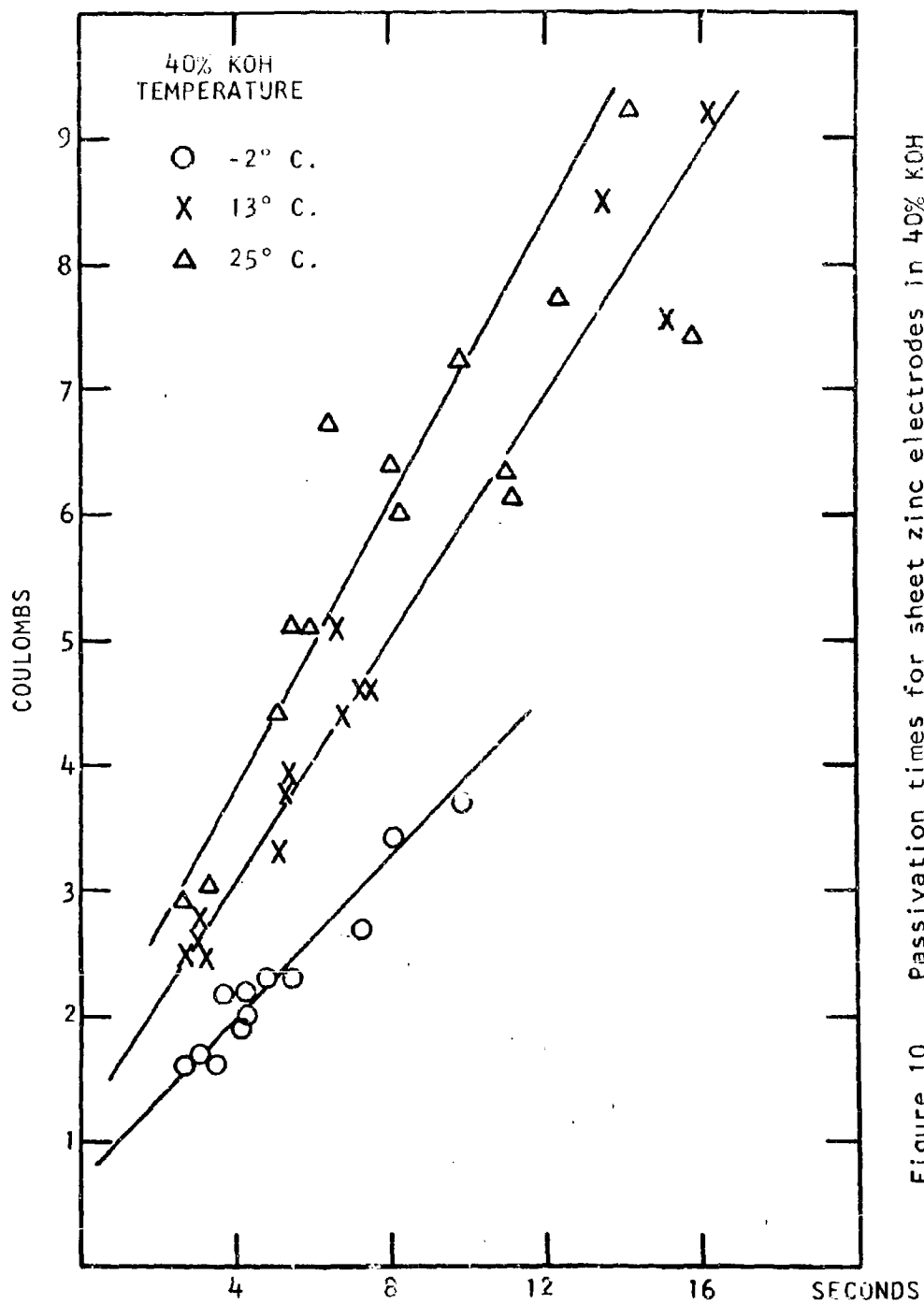


Figure 10 Passivation times for sheet zinc electrodes in 40% KOH

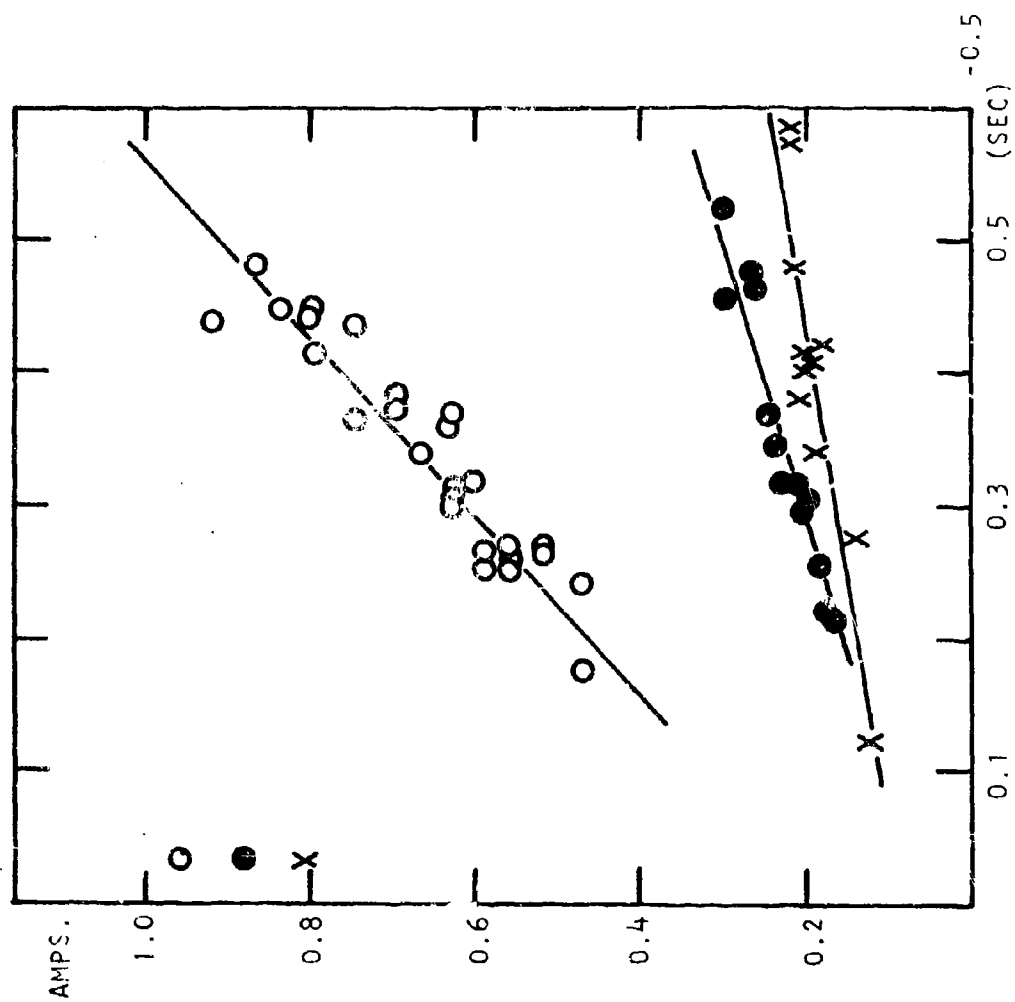


Figure 11 Current vs. $t^{-1/2}$ plots for sheet zinc electrodes

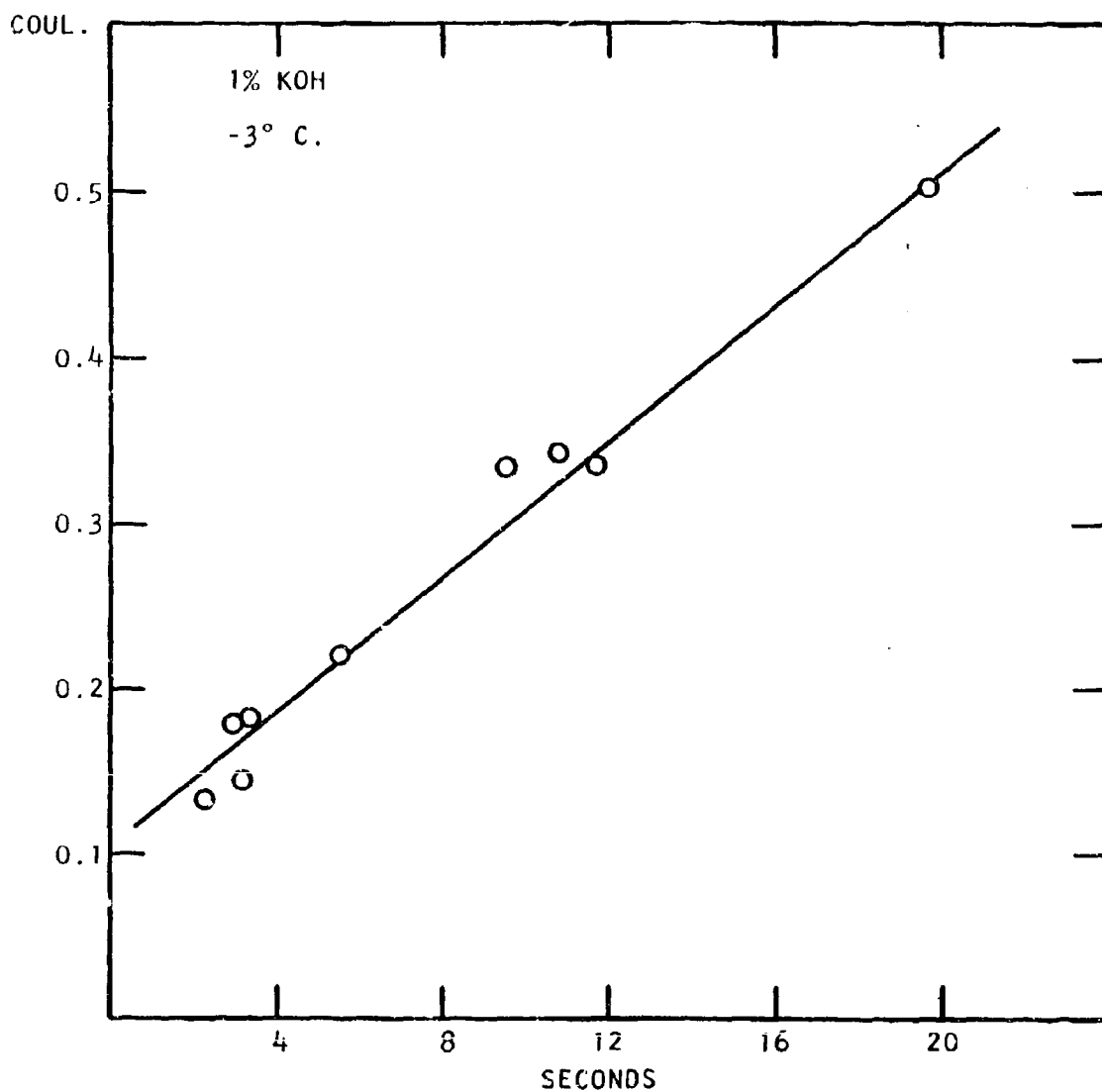


Figure 12 Time-to-passivation data for sheet zinc electrodes

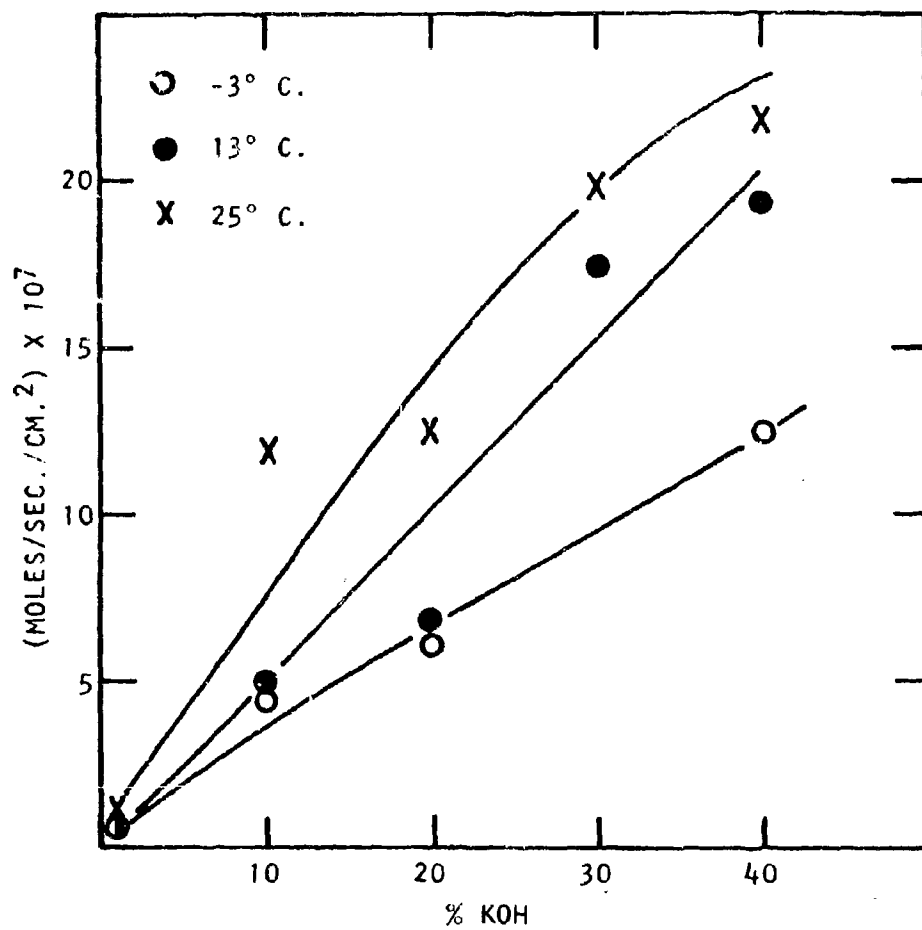


Figure 13 Calculated dissolution rates for the zinc discharge reaction product.

APPENDIX IV

A LITERATURE SURVEY ON THE SOLUBILITY
OF ZnO IN OTHER DIVALENT METAL OXIDES
AND OF Zn(OH)_2 IN OTHER DIVALENT METAL
HYDROXIDES

In the search for a possible host lattice for ZnO and Zn(OH)_2 , the only compounds considered are those containing a divalent cation. This limitation immediately eliminates compounds of the alkali metals, lanthanides, actinides, and other metals which do not normally show the +2 oxidation state.

The compound ZnO has a hexagonal (Wurtzite) lattice with the following cell parameters: $a = 3.24 \text{ \AA}$, $c = 5.19 \text{ \AA}$ ⁽¹⁾. Among the commonly occurring metal oxides only beryllium oxide, BeO , has a hexagonal structure. Its lattice parameters are: $a = 2.69 \text{ \AA}$, $c = 4.3 \text{ \AA}$ ⁽²⁾. Even though the difference between these sets of parameters is somewhat greater than 15%, BeO and ZnO do appear to form a solid solution on which conductivity and X-ray diffraction measurements were made ⁽³⁾. No other information on phase relationships between BeO and ZnO is available in the literature.

Diadochy, rather than isomorphism, is the primary criterion in solid solution formation, so that a hexagonal compound may form a solid solution with a non-hexagonal one if the ionic sizes are correct ⁽⁴⁾. Substitution of one cation for another in a particular lattice is often possible if the difference in the ionic sizes is less than about 15%. Using this criterion and Pauling's

-
1. C. W. Bunn, Pr. phys. Soc., **47**, 835 (1935).
 2. W. M. Lehman and M. Haase, Z. Kryst., **65**, 537 (1927).
 3. I. D. Tretyak and M. A. Emchik, Pitannya Fiz. Tverd. Tila L'vivs'k Derzh. Univ., **1964**, 80 (Ukrain).
C. A., **62**: 12560f
 4. B. Mason, Principles of Geochemistry, 2nd ed., J. Wiley and Sons, Inc., New York, 1958, p. 85.
-

empirical values for crystal radii⁽⁵⁾, the following ions may be diadochic in side structures:

Zn	0.74 Å	Mn	0.80 Å
Co	0.74	Cr	0.84
Ni	0.72	Pd	0.86
Fe	0.76	Cu	0.69

This is born out also by the fact that in minerals the Zn ion is often replaced by Mn, Fe, Co, or Cu.

The crystal structures and cell parameters of the oxides of these metals are as follows:

- CrO , probably cubic, parameters not determined⁽⁶⁾
MnO , cubic, $a = 4.47 \text{ Å}$ (7)
FeO , cubic, $a = 4.27 \text{ Å}$ (8)
CoO , cubic, $a = 4.25 \text{ Å}$ (9)
NiO , cubic, $a = 4.17 \text{ Å}$ (10)
CuO , monoclinic, $a = 4.65$, $b = 3.41$, $c = 5.11 \text{ Å}$, $\beta = 99^\circ 29'$ (11)
PdO , tetragonal, $a = 3.02$, $c = 5.31 \text{ Å}$ (12)

L. Pauling, The Nature of the Chemical Bond, 3rd ed., Cornell University Press, Ithaca, N. Y., 1960, p. 518.

H. Lux, L. Eberle, and D. Sarre, Ber., 97 (2), 503 (1964).

H. Ott, Z. Krist., 63, 222 (1926).

V. M. Goldschmidt, Ber., 60, 1285 (1927).

H. P. Walmsley, Phil. Mag., 7, 1101 (1929)

J. Brentano, Proc. Phys. Soc. London, 37, 184 (1925)

G. Tunell, E. Posnjak, and C. J. Ksanda, Z. Krist., 90, 120 (1935).

W. J. Moore, and L. Pauling, J.A.C.S., 63, 1393 (1941).

The compound CrO has not been well characterized. It is not affected by pure water but is readily oxidized by atmospheric oxygen ⁽¹³⁾. The most stable and the most easily prepared appear to be the oxides of Co, Ni, Cu, and Pd.

No references were found in the literature (up to Dec., 1966) on solid solution formation between ZnO and CrO . ZnO does form solid solutions with the other six oxides listed above. In addition, ZnO forms solid solutions with BeO (see p. 1 of this report), and with MgO , CdO , and SnO .

Some aspects of the phase relations among these compounds are given in the following references:

14. R. Rigamonti, Gazz. Chim. Ital., **76**, 474 (1946) C. A., **41**, 71911
Formation of solid solutions of ZnO in MgO , NiO , CoO , MnO and CdO .
Preparation, X-ray data, cell parameters, and limits of solubility are discussed.
15. R. Isomatsu, and S. Kitagawa, Doshisha Daigaku Rikogaku Kenkyu Hokoku, **5**, (2), 67 (1964)
C. A., **62**, 10167a
Phase diagram of the system ZnO - FeO is determined by X-ray diffraction.
16. J. Robin, Compt. Rend., **235**, 1301 (1952)
C. A., **47**, 4719i
Preparation of mixed Co and Zn oxides, determination of phase diagrams.
17. E. Hayek, Monatsh., **66**, 197 (1935)
C. A., **30**, 39¹
Mixed crystals of SnO with various oxides including ZnO are prepared by precipitation from solution.

13. H. Lux, and E. Pröschel, Z. anorg. Chem., **257**, 73 (1948)

18. G. Natta, and L. Passerini, Gazz. Chim. Ital., 59, 139 (1929)

C. A., 25, 633

Formation of solid solutions among the oxides of Ca, Cd, Mn, Co, Ni, and Zn.

19. J. A. Hedvall, Z. anorg. allgem. Chem., 103, 249 (1918)

C.A., 13, 3098⁵

Formation of solid solutions of NiO with ZnO and other metal oxides.

20. H. Kedesdy, and A. Drukalsky, J.A.C.S., 76, 5941 (1954)

C.A., 49, 15599c

Formation of NiO-ZnO solid solutions, structure and X-ray data are given.

21. T. Ando, and R. Umemoto, Ceram. Abstr., 1952, 151 (in J. Am. Ceram. Soc.,

35, no. 8)

C.A., 47, 6669g

Describes formation of ZnO-CoO solid solution from ZnO and CoCO_3 in a CO_2 atmosphere.

22. V. D. Balarev, Annuaire fac. sci.-phys. et math. Chemie, 47, 3 (1952)

C.A., 48, 7976e

Fusion of ZnO with CuO may indicate the existence of a eutectic in this system.

23. G. Yamaguchi, and H. Miyabe, Kogyo Kagaku Zasshi, 63, 562 (1960)

C.A., 57, 9278h

Composition and lattice constants are given for various solid solution phases in the ternary system ZnO-CoO-MgO.

The following references are less directly related to this problem but may be of interest:

24. V. P. Chalyi, and O. I. Shor, Ukrain. Khim. Zhur., 27, 7 (1961)

C.A., 55, 17325g

A thermographic study of hydroxide mixtures. Dehydration gives solid solutions of NiO and ZnO, depending on concentrations.

25. C. Frondel, Am. Mineral., 25, 534 (1940)

C.A., 35, 711¹

Discusses exsolution growths of ZnO in MnO.

26. H. P. Rooksby, Trans. Brit. Ceram. Soc., 56, 581 (1957)

C.A., 52, 17871c

Distortion of the NiO structure by ZnO substitution.

27. O. Schmitz-Dumont, K. Brokopf, and K. Burkhardt, Z. anorg. allgem.

Chemie, 295, 7 (1958)

C.A., 53, 1915g

Absorption spectra of solid solutions of CoO and ZnO.

Information available in the literature suggests only two possible host lattices for Zn(OH)_2 , namely Ni(OH)_2 and Co(OH)_2 . Zn(OH)_2 occurs at at least five different phases, two of which have been characterized rather well. The α -form is hexagonal, with lattice parameters $a = 3.11$ and $c = 7.8 \text{ \AA}$ (28). The ϵ -form is rhombic with $a = 5.16$, $b = 8.53$, and $c = 4.92 \text{ \AA}$ (29). Co(OH)_2 occurs in two forms. It is blue when freshly made, but changes to the more stable pink form on standing. It is slightly soluble in alkaline solutions, and is easily oxidized by atmospheric oxygen. Co(OH)_2 has a trigonal structure with $a = 3.19$ and $c = 4.66 \text{ \AA}$ (30).

28. W. Feitknecht, Ang. Chem., 52, 202 (1939)

29. R. B. Corey, and R.W.G. Wyckoff, Z. Krist., 86, 8 (1933)

30. G. Natta and A. Reina, Atti Linc. Mem., 4, 51 (1926)

Ni(OH)_2 is more stable toward oxidizing agents. It also has a trigonal structure with $a = 3.07$ and $c = 4.60 \text{ \AA}$ (31).

The following references deal with the phase relations between the hydroxides of An, Co, and Ni.

32. W. Feitknecht and W. Lotmar, Helv. Chim. Acta, **18**, 1369 (1935)

C.A., **30**, 2077⁴

Solid solution formation in mixed precipitates of Zn, Ni, and Co hydroxides.

Structure and composition of crystals is given.

33. G. Natta and L. Passerini, Gazz. Chim. Ital., **58**, 597 (1928)

C.A., **23**, 1556

Discussion of solid solutions of Zn(OH)_2 with Co(OH)_2 and Ni(OH)_2 .

34. Th. v. Hirsch, Z. Physik. Chem., **43**, 227 (1964)

C.A., **63**, 2451g

An investigation of coprecipitation and mixed crystal formation between Co and Zn hydroxide, and others.

35. W. Lotmar and W. Feitknecht, Z. Krist., **93**, 368 (1936)

C.A., **30**, 6260²

Changes in ionic distances in Zn, Ni, and Co hydroxide solid solutions.

Two miscellaneous references were found which deal with the phase relationships between ZnO and Zn(OH)_2 .

36. G. F. Hüttig, and H. Möldner, Z. anorg. Chem., **211**, 368 (1933)

C.A., **27**, 3415.

A discussion of the relative stability of Zn(OH)_2 with respect to ZnO in H_2O .

-
31. G. Natta, Atti. accad. Lincei, **2**, 495 (1926)

37. R. Scholder, and G. Hendrich, Z. anorg. allgem. Chem., 247, 76
(1939)

C.A., 33, 5271⁹

Phase relations in the system of $\text{ZnO-Na}_2\text{O-H}_2\text{O}$.

APPENDIX V

SIZES OF ZINCATE ION AND SOLUBLE
SILVER SPECIES IN KOH

Dr. J. J. Lander

Sizes of Zincate Ion and Soluble Silver Species in KOH

In an attempt to achieve a better understanding of concentrated KOH solutions, available data from the literature have been treated as discussed herein. It is of interest to achieve a better understanding of battery strength KOH solutions as a firm basis for further studies on zincate ion and the soluble silver species. For example, it would be desirable to have a separator material which would allow free migration and diffusion of KOH and yet screen out the passage of zincate ion and soluble silver species. In order for this to be achievable, a sufficient difference in ionic (or molecular) diameters would have to exist between K^+ and OH^- on the one hand and zincate and soluble silver on the other. If an appreciable difference were to be found, then it would make sense to try to develop separator materials with a pore size large enough to admit free diffusion of KOH, but small enough to block zincate ion and silver. Conversely, if ionic (or molecular) sizes of KOH (K^+ , OH^-) were to be found to be nearly equivalent to zincate and silver sizes, then attempts to develop separator materials to achieve the desired end on a pore size basis would be useless, and different approaches would have to be found.

The work herein reported may be regarded as a first approach to the problem and is incomplete in the sense that data for the several separate ions have not been achieved except in terms of upper and lower limits; however, data in the existing literature can be treated to obtain molecular volumes for hydrated KOH in battery strength solutions.

Partial Molal Volumes

As a first step in the procedure, the density data* for KOH solutions up to 50% by weight (68°F) were used to calculate the volumes of solutions containing 1000 grams of water. The data are shown in Table 1.

TABLE I
Volumes of KOH Solutions (68°F)

Weight % KOH	Density	Volumes of Solutions Containing 1000 gm. H ₂ O (c.c.)	Weight KOH Grams	Molality n ₂
0	0.997	1003	0	0
2	1.016	1004	20	0.36
6	1.053	1010	65	1.16
10	1.090	1022	112	2.00
16	1.147	1037	190	3.39
24	1.226	1074	317	5.65
30	1.288	1110	430	7.66
40	1.396	1193	668	11.9
50	1.512	1322	1000	17.8

From these data, the solution volume may be plotted against the molality, as in Figure 1. The tangent to the curve at any value of molality provides data for the calculation** of the partial molar volume. As an example, from the tangent at 40% by weight, the volume of KOH in solution is calculated to be 20.5 c.c. This may be compared with 27.4 c.c. calculated for the molar volume from the handbook value of 2.044 gm. per c.c. for the density of solid KOH.

From the molar volume, the volume per molecule of KOH in solution may be calculated, using Avagadro's number

$$\frac{20.5}{6.023 \times 10^{23}} = 3.41 \times 10^{-23} \text{ c.c.}$$

or $3.41 \times 10^{-23} \times 10^{24} = 34.1 \text{ cubic Angstroms.}$

*JACS, Apr. 1941, p. 1088.

**See, for example, "Textbook of Physical Chemistry," Glasstone, 2nd Ed. p. 239, D. VanNostrand Co., Inc. 1946.

If the molecule is treated as a sphere, the molecular diameter is calculated to be

$$d^3 = \frac{6 \times 34.1}{\pi} = 65$$

$$d = 4 \text{ \AA}$$

On this basis, the diameter of either the K^+ or the OH^- ion would be less than 4 \AA .

From the shape of the curve, it is evident that the molar volume of the KOH gets progressively smaller as the concentration of solution decreases. Thus at $n_2 = 2$ (10% by weight KOH), the molar volume is calculated from the tangent to be 12 c.c. per mole. Evidently, KOH solutions are quite non-ideal, and the molecular volumes of dissolved KOH and water are far from being additive. Just how far they are from being additive is described in Figure 2 where the volume per mole for KOH solutions is plotted against the mole fraction of KOH. These data were calculated from Table I.

The deviation from ideality means, of course, that the ions from dissolved KOH are more-or-less hydrated in solution. As a consequence, the molecular volume and diameter previously calculated for KOH in 40% solutions may be considered to be effective values for KOH stripped of waters of hydration, and therefore, not representative of the real situation in solution. While Figure 2 says that there is a good deal of solute-solvent interaction, the data of the figure do not provide quantitative means of determining how much water is tied up by dissolved KOH as water of hydration.

Degree of KOH Hydration

A very thorough review of the literature has not yet been made in terms of ionic hydration numbers in strong KOH solutions; however, some information is available for comparison with the treatment which will be made below. For example, G. Yagil has found a hydration number of 3 for OH^- ion in concentrated KOH and NaOH solutions (JACS 85 (16), 2376-80, 1963) by means of reaction rate studies. In good agreement with Ackermann (CA 55, 13054 a) who studied hydration number of 4 for K^+ ion in concentrated KOH solutions (11.36% and 18.81% KOH, by weight) using X-ray diffraction (Norelco Report 5, 111, 1958). The latter

article also contains reference to theoretical means of calculation of hydration numbers. Textbook values (Glasstone, "Textbook of Physical Chemistry, p. 921, 2nd Ed. D. VanNostrand and Co., New York, 1946) of hydration numbers for K^+ ion in KCl solutions of 5.4 and 10.5 are given.

At any rate, a treatment which enables calculation of hydration numbers of KOH as a function of concentration is proposed, hereby, which is believed to be novel and which indicates that hydration numbers depend substantially on concentration.

The concept and treatment of data are very simple.

Determination of molecular weights from freezing point depression, boiling point elevation, vapor pressure reduction, etc., are all commonly used techniques, and any standard elementary physical chemistry text provides the theoretical basis for making such determinations. Furthermore, the same texts discuss solutions of strong electrolytes, where 100% ionization is assumed to be the case. The major problem seems to be that such experimental data are good only for relatively dilute solutions (1 to 2 molal, or less).

When freezing point depression data, boiling point elevation data, and vapor pressure lowering data for KOH solutions are examined, it is apparent that the quantities involved are substantially larger than those which can be calculated on the basis of the simple theory, assuming 100% ionization, as concentration increases beyond 1 or 2 molal. It is suggested, therefore, that this result occurs simply because of the hydration of ions (and/or molecules), and that comparison of the actual data with that calculated as theoretical based on 100% ionization (From Raoult's Law) can provide a means of determining the extent of hydration. What this means is: because of hydration, the water of hydration becomes a component of the solute* and, consequently, the real concentration of a solute becomes appreciably larger than that calculated from the straight molal quantities of each component originally added in making up the solution.

The vapor pressure lowering relationship is chosen to illustrate the method of data treatment. In Figure 3 are shown the measured values of vapor pressure of water for solutions of KOH up to 50% by weight at 68°F. (International Critical Tables, Vol. III, p. 373). On the same graph are shown

*See, for example: "Ionic Sizes," Stern and Amis, Chem. Rev. 59, Feb. 1959, p. 23.

values of the vapor pressure calculated from Raoult's Law based on 100% ionization (this latter curve is different from the one shown in Figure 24, Second Quarterly Report, because Raoult's Law was improperly handled in calculating the theoretical vapor pressure lowering in the earlier report, as pointed out by Professor Dirkse in a private communication dated May 15, 1967).

The tie-lines drawn in the figure indicate that a 3 molal solution behaves like a theoretical 4.5 molal solution, a 5 molal solution behaves like a theoretical 9.3 molal solution, an 8 molal solution behaves like a 21.8 molal theoretical solution, and so forth.

Now, a 9.3 molal solution contains 55.6 moles of water in the ratio 9.3/55.6, so the 5 molal solution behaves as though it contains water in the same ratio.

$$\frac{5.0}{X} = \frac{9.3}{55.6}$$

$$X = 29.9$$

But, inasmuch as the 5 molal solution actually contains 55.6 moles of water, then $55.6 - 29.9 = 25.7$ moles of water have become part of the solute as water of hydration. Therefore, 25.7 moles of water are associated with 5 moles of KOH for a hydration number of 5.14. In similar fashion, a hydration number can be calculated for each concentration of KOH, and the curve described in Figure 38 is obtained. The curve indicates that the number of moles of water associated with one mole of KOH falls off as concentration is increased.

Now we are in a position to calculate the size of the hydrated molecule. Using a 40% by weight solution (11.9 m), from Figure 38 it is seen that 3.6 moles of water are tied up with 1 mole of KOH. Because there are 11.9 moles of KOH in a 40% solution, 42.9 moles of water are hydrated, leaving 12.7 moles of solvent water. If it is assumed that solvent water has the same specific volume as pure water, then the volume of solvent water is

$$12.7 \times 18.1 = 230 \text{ c.c.}$$

But, from Figure 1, an 11.9 molal solution containing 1000 grams of water has a volume of 1190 c.c. Therefore, the volume of hydrated KOH is

$$1190 - 230 = 960 \text{ c.c.}$$

$$\text{or } 960/11.9 = 80.6 \text{ c.c./mole}$$

The value of 80.6 c.c. per mole may be compared with the additive value of 90.9 calculated from the molar volume of solid KOH and that for 3.6 moles of water.

Again, using Avagadro's number, the volume per hydrated molecule for KOH in a 40% solution is

$$\frac{80.6}{6.023 \times 10^{23}} = 13.4 \times 10^{-23} \text{ c.c.}$$

$$\text{or } 13.4 \times 10^{-23} \times 10^{24} = 134 \text{ cubic Angstroms.}$$

If the hydrated molecule is treated as a sphere, the molecular diameter is calculated to be

$$d^3 = \frac{6 \times 134}{\pi} = 255.5 \text{ cubic Angstroms}$$

$$d = 6.35 \text{ A}^\circ$$

For a 4 molal solution (hydration number 5.6), the volume per molecule is calculated to be 187 cubic Angstroms and the spherical diameter to be 7.1 A°. On this basis, the diameter of either the hydrated K⁺ ion or the hydrated OH⁻ ion would be less than 7.1 - 6.35 A°, over the concentration range involved.

The phase diagram for KOH - H₂O solutions indicates formation of the solid compound, KOH·4H₂O, at 44% KOH by weight (-28°F). This is 13.9 molal, for which there are exactly 4 moles of water per mole of KOH available for hydration. At the freezing point, the degree of hydration may be regarded as corresponding perfectly to the available water. It is interesting that the projected curve of Figure 4 lies under 4 waters of hydration for the 44 weight % solution. It would be expected on this basis that the degree of hydration should decrease as temperature increases, and it would be interesting to go through similar calculations for vapor pressure curves at other temperatures, as well as similar treatments of the freezing point depression curves and boiling point elevation curves.

It is interesting, also, that at 4 molal (18.8% by weight) the total hydration obtained by the scheme used in this section is 5.6. This may be compared with a possible expected total of 4.0 + 3.0 = 7.0 from the references quoted at the beginning of this section.

Figure 5 shows the total moles of both bound and free water, calculated from the data of Figure 4, as a function of concentration. The data of this curve corrects the upper curve of Figure 26 in the Second Quarterly Report.

On the basis of the fact that the phase diagram shows the concentration of KOH to be 52.8% by weight (20 m) at a freezing point of 68°F, another point can be located on the curve of Figure 39 for 20 molal and it would correspond, of course, to 55.6 moles of bound water. (This assumes that the vapor pressure of water at the freezing point would be substantially nil). Extrapolation of the actual vapor pressure curve of Figure 3 to zero indicates zero vapor pressure around 20-22 molality for a hydration number of 2.6 - 2.8.

Ion-Ion Association

In the Second and Third Quarterly Reports, some speculation was given to the possibility of ion-ion association in strong KOH solutions, on the basis of Figure 26 in the Second Quarterly Report, and on the basis of the fact that the product of the conductivity and the viscosity divided by the molarity was found to be not a constant at 20°C. Professor Dirkse in a similar calculation (private communication dated May 25, 1967) showed constancy of the function $\eta\lambda/C$ for KOH solutions at 25°C. Consequently, the data were recalculated for 25°C. using the viscosity data given in Table 5, page 155, of "Characteristics of Separators for Alkaline Silver Oxide Batteries - Screening Methods." These data were found to agree exactly with viscosity data given by Hitchcock and McIlhenny (Ind. & Eng. Chem., Vol. 27, p. 466). Data for conductivity at 25°C. were obtained from the resistance values of KOH at 25°C. given in Table 2, pages 149-150 of the Screening Methods reference given above. Table II shows the data and the calculated values of $\eta\lambda/C$.

TABLE II

Data for the Function $\eta\lambda/C$ for KOH Solutions at 25°C

Concentration (Molarity)	η	λ	$\eta\lambda$	$\eta\lambda/C$
0.6	0.91	0.130	0.118	0.198
0.8	0.93	0.170	0.159	0.197

TABLE II (Cont'd.)

Data for the Function $\eta\lambda/C$ for KOH Solutions at 25°C

Concentration (Molarity)	η	λ	$\eta\lambda$	$\eta\lambda/C$
1.0	1.00	0.200	0.200	0.200
1.5	1.02	0.295	0.304	0.204
2.0	1.10	0.360	0.396	0.198
4.0	1.40	0.575	0.805	0.201
6.0	1.83	0.640	1.17	0.195
8.0	2.42	0.620	1.50	0.187
9.0	2.82	0.583	1.64	0.182
10.0	3.30	0.541	1.78	0.178
11.0	4.00	0.505	2.03	0.184
12.0	4.83	0.460	2.22	0.184
13.0	6.20	0.405	2.50	0.193
13.4	7.00	0.387	2.71	0.202
Avg.				$0.193 \pm 3.6\%$

While there is some variation in the values of $\eta\lambda/C$ and, possibly a minimum in the value near 10.0 molar, actually the values lie within an average deviation of $\pm 3.6\%$ which is probably not outside the limits of experimental error.

The point is this: if $\eta\lambda/C$ is truly a constant, then there should be no ion-ion association effects in KOH solutions, even up to 45% by weight, and, consequently, no regard need be given to such possible effects on the values of hydration numbers and ion sizes, as was attempted in the Third Quarterly Report (see text, pps. 4 and 5, and illustration, Figure 2). Again, it may be suggested that a body of such data should be obtained with temperature as a parameter. These data are very interesting in terms of KOH solutions, in view of the existing theory concerning ion-ion association in strong electrolytes. Similar work for solutions (other than KOH) of high-concentration, strong electrolytes is also suggested, in order to check out electrolyte theory in this respect. It seems possible that a good deal of this might be accomplished with data already existing in the literature.

Zincate Ion

A simple technique was used to measure the volume increase of a 45% solution of KOH as increasing amounts of ZnO were

added at 72°F. A 500 c.c. volumetric flask was filled to the calibration mark with 45% KOH. Weighed amounts of ZnO were added and when solution was complete, the increase in the height of the meniscus in the neck of the flask was measured with a centimeter scale. The internal diameter of the neck of the flask was measured, and so, knowing the i.d. and the increase in height of the liquid level, the volume change could be calculated. The results are shown in Figure 6. The shape of the curve is slightly S-like; however, a straight line was drawn through the points and its slope = 20.9 c.c./mole. This may be compared with 14.86 c.c./mole calculated from the handbook value for the density of solid ZnO. Therefore, the oxide occupies more volume when dissolved in 45% KOH at room temperature than it does in the dense solid state.

Treating the ZnO as a dissolved molecule and assuming a spherical configuration, the diameter may be calculated.

$$\frac{20.9 \times 10^{24}}{6.023 \times 10^{23}} = 34.6 \text{ cubic } \text{\AA}^3 = \text{volume/ZnO molecule}$$

$$r^3 = \frac{3}{4} \times \frac{34.6}{\pi} = 8.25$$

$$r = 2.2 \text{ } \text{\AA}$$

$$d = 4.04 \text{ } \text{\AA}$$

This value may be regarded as a value for unionized and unhydrated ZnO. However, as Dirkse's data show the molecule is likely to exist as the $\text{Zn}(\text{OH})_4 \cdot 2\text{H}_2\text{O}$ ion in solutions of strongly alkaline KOH. This is equivalent to $\text{ZnO}_2 \cdot 4\text{H}_2\text{O}$, or a ZnO_2 ion with 4 waters of hydration.

We can estimate a minimum volume for $\text{ZnO}_2 \cdot 4\text{H}_2\text{O}$ in the following way. From the data of Figures 1 and 2 the volume of one mole of bound water in 45% KOH may be calculated to be 13.4 c.c. per mole. Next, using the value of 14.86 c.c./mole for ZnO in the solid crystal and adding $4 \times 13.4 = 53.6$ c.c., we obtain 68.5 c.c. per mole for $\text{ZnO}_2 \cdot 4\text{H}_2\text{O}$ without accounting for the extra oxygen atom. Then,

$$\frac{68.5 \times 10^{24}}{6.023 \times 10^{23}} = 113.4 \text{ cubic Angstroms}$$

$$d^3 = \frac{6 \times 113.4}{\pi} = 217$$

$$d = 6 \text{ } \text{\AA}$$

so, a minimum dimension for a spherical $\text{ZnO}_2 \cdot 4\text{H}_2\text{O}$ ion is 6 \AA diameter, which is not very different from the values $6.4 - 7.1 \text{ \AA}$ calculated previously for hydrated KOH molecules. While 6 \AA is unquestionably slightly too small, it could be concluded that the construction of a separator membrane which would screen out zinc diffusion, yet allow un-inhibited diffusion of KOH, is simply out of the question based on pore size alone.

However, it should be remembered that the diffusing zincate ion has to drag along two hydrated K^+ ions with it, so some differential could be involved. This can be estimated using the value of 80.6 c.c. per mole for hydrated KOH previously calculated. Thus, if one-half the value of 80.6 is assigned to a hydrated K^+ ion, then the total volume per mole for 2 K^+ ions (hydrated) and $\text{ZnO}_2 \cdot 4\text{H}_2\text{O}$ would be 149.1 c.c. per mole. Then,

$$\frac{149.1 \times 10^{24}}{6.023 \times 10^{23}} = 249 \text{ cubic Angstroms}$$

$$d^3 = \frac{6 \times 249}{\pi} = 475$$

$$d = 7.8 \text{ \AA}$$

This value still doesn't appear to be sufficiently larger than those calculated for hydrated KOH to attempt to meet the problem by reduction of pore size in separators.

The question might also be asked: is there any experimental evidence bearing on the situation in terms of relative diffusion rates through membranes? In Table 5 of APL-TDR-64-85 (Final Report on Air Force Contract Nr. AF33(657)-10643, dated 1 August 1964) flux rates for KOH and zincate ion diffusion through regular pore size fibrous sausage casing (RPS) were measured to be 1.1×10^{-3} for KOH under a concentration difference of 12 M and 4.0×10^{-6} for ZnO_2 for a concentration difference of 1.3 M (in $45\% \text{ KOH}$). Using an estimated average value of D for KOH of $1.4 \times 10^{-5} \text{ cm}^2/\text{sec}$, and a value of 1.8×10^{-6} for D of zincate ion in $44\% \text{ KOH}$, the value of flux for KOH might have been expected to be

$$\frac{14}{1.8} \times \frac{12}{1.3} = 72 \text{ times that for zincate ion. Thus, } 4.0 \times 10^{-6} \times 72 = 288 \times 10^{-6} \approx 0.3 \times 10^{-3}, \text{ and for this membrane KOH}$$

diffusion was $1.1/0.3 = 3.7$ times larger than expected in terms of our previous conclusion regarding the possibility of obtaining screening on a pore size basis. This could mean that some screening of zincate ion was being achieved. Comparing the small pore size (SPS) membrane in the same table of reference, the factor was $0.75/0.22 = 3.4$, which represents less screening than was achieved by the regular pore size material. Going on down the table, values of the screening factor lying between 1.3 and 4.6 (the latter for control fibrous sausage casing) are obtained. For the best of the RAI materials, i.e., 2.2XH (Table 6, same reference) a value of 3.2 for the screening index was found. These data, if reliable, would indicate some hope for being able to obtain screening of zincate ion through pore size reduction in spite of the previously estimated values for ionic (molecular) sizes.

It can only be concluded that additional information is necessary, either by way of preparation of smaller pore size membranes or by way of more refined measurements of ionic sizes, or both.

Soluble Silver

While no experimental work has been done on the determination of the size of soluble silver species, some information is available. First of all, negative ions do not vary greatly in terms of ionic dimensions* and, furthermore, if the soluble silver species is AgO^- , it should have a smaller hydration sheath than the doubly charged zincate ion. From the experimental point of view, however, in the just-mentioned Tables of reference, values of soluble silver flux equivalent to those for zincate ion were measured. On this basis, it is concluded that remarks apropos of zincate ion diffusion also apply to diffusion of the soluble silver species.

*See Stern and Amis, "Ionic Sizes," Table 14, p. 30, Chem. Rev. 59, Feb. 1959.

See also Monk, "Electrolytic Dissociation," Table 14.4, p. 271, Academic Press, New York, 1961.

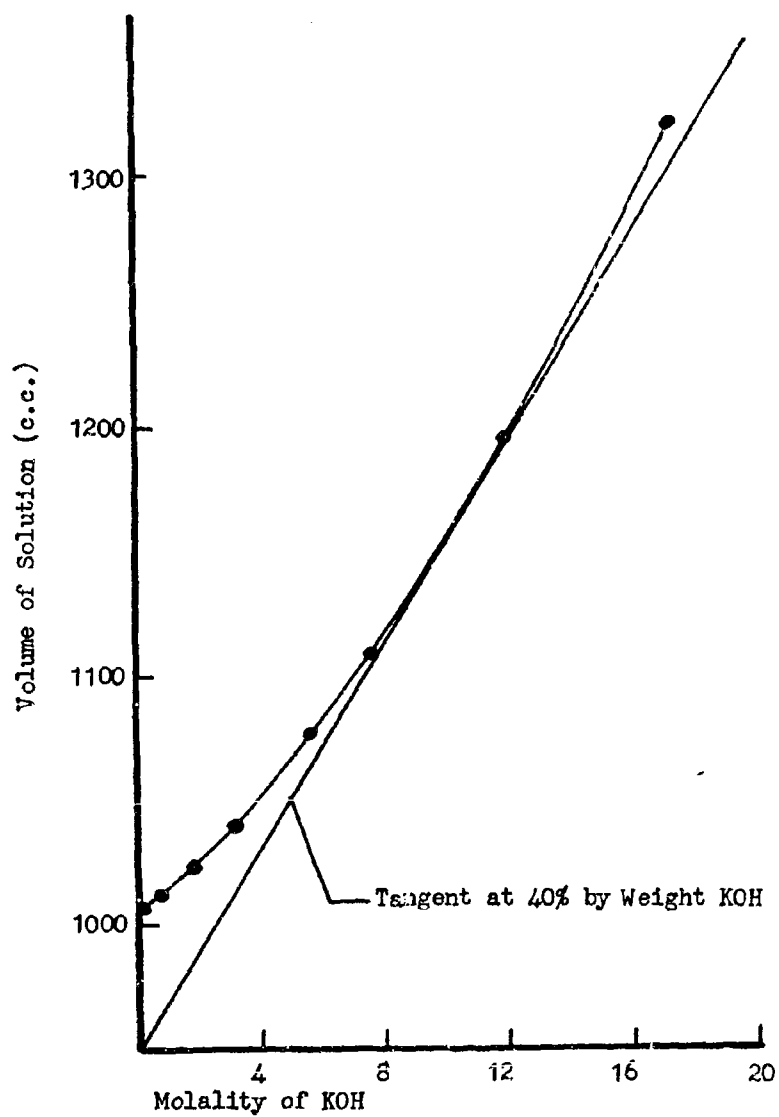


Figure 1. Volume vs. Molality KOH Solutions at 68°F.

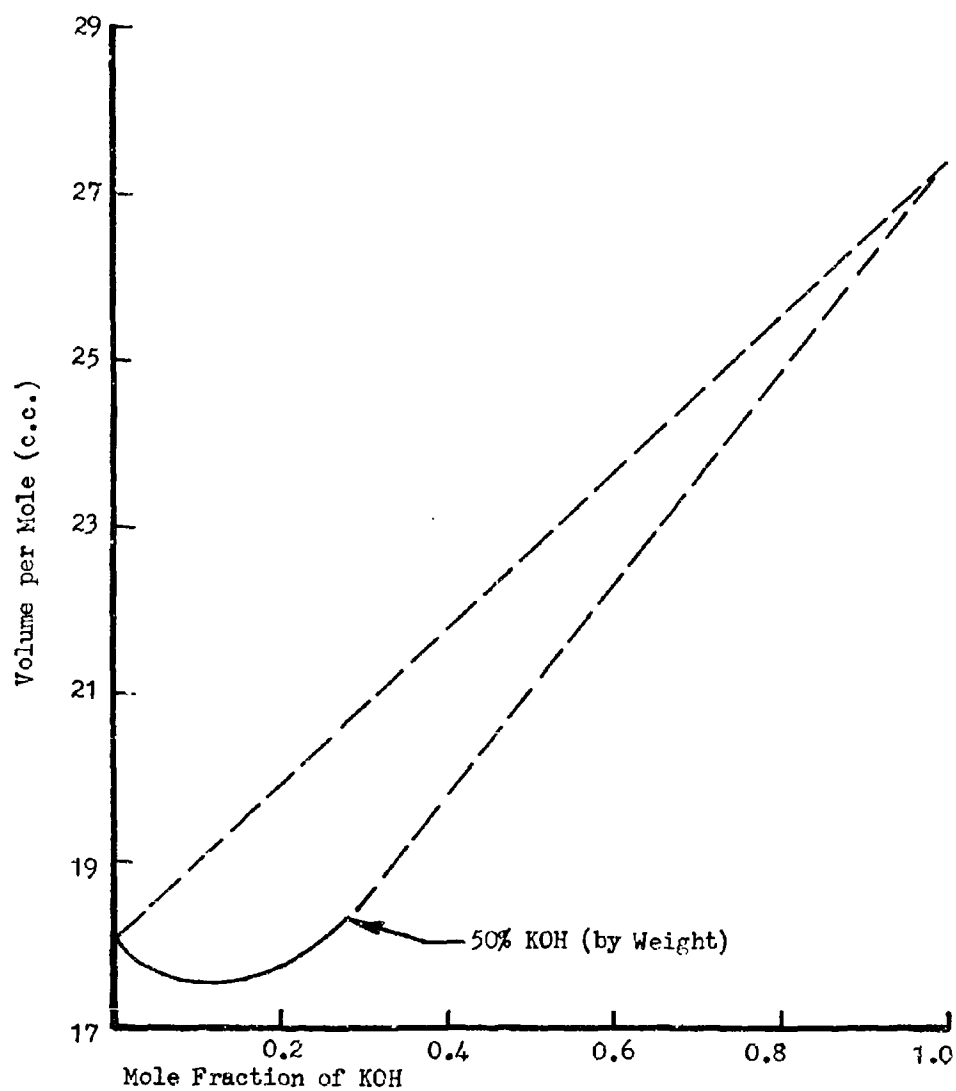


Figure 2. Illustrating Non-Ideality of KOH Solutions

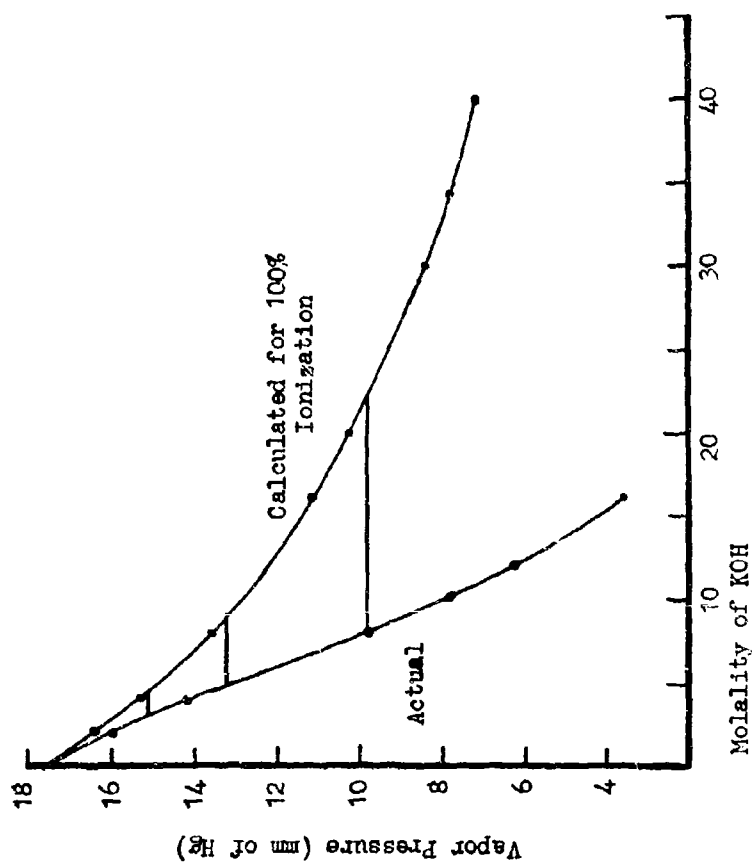


Figure 3 Vapor Pressure of Solutions of KOH. 68°F.

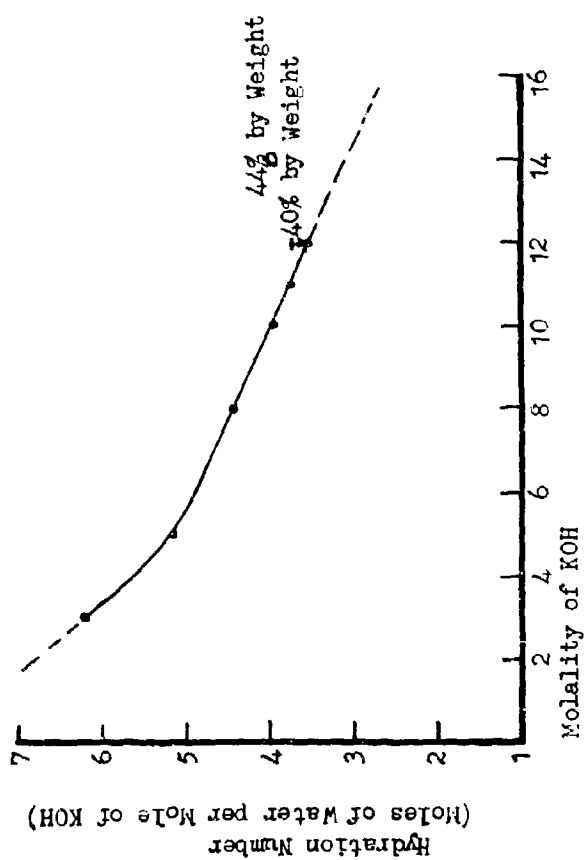


Figure 4. Hydration of KOH. 68°F.

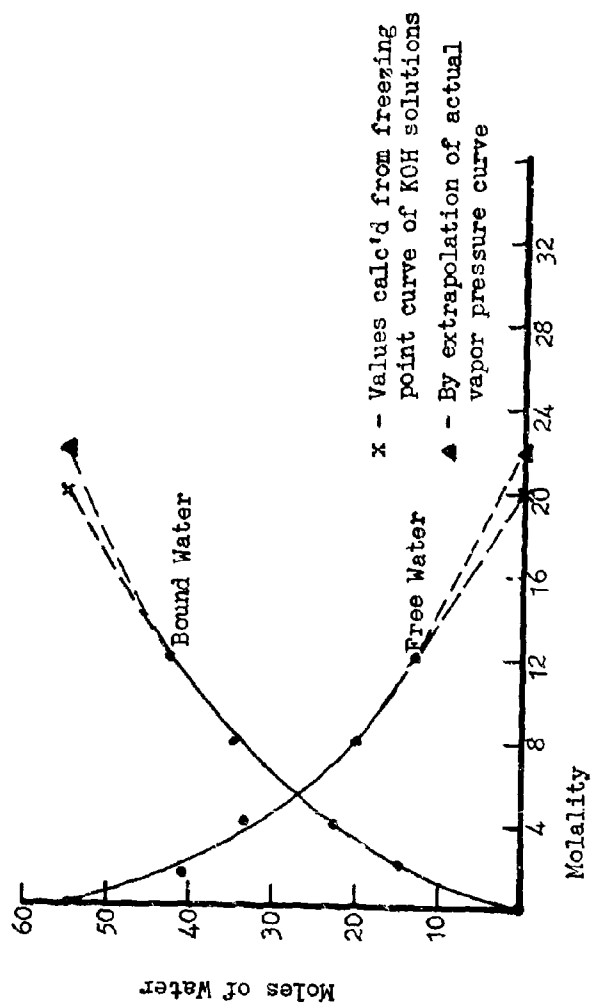


Figure 5. Bound and Free Water in KOH Solutions. 68°F.

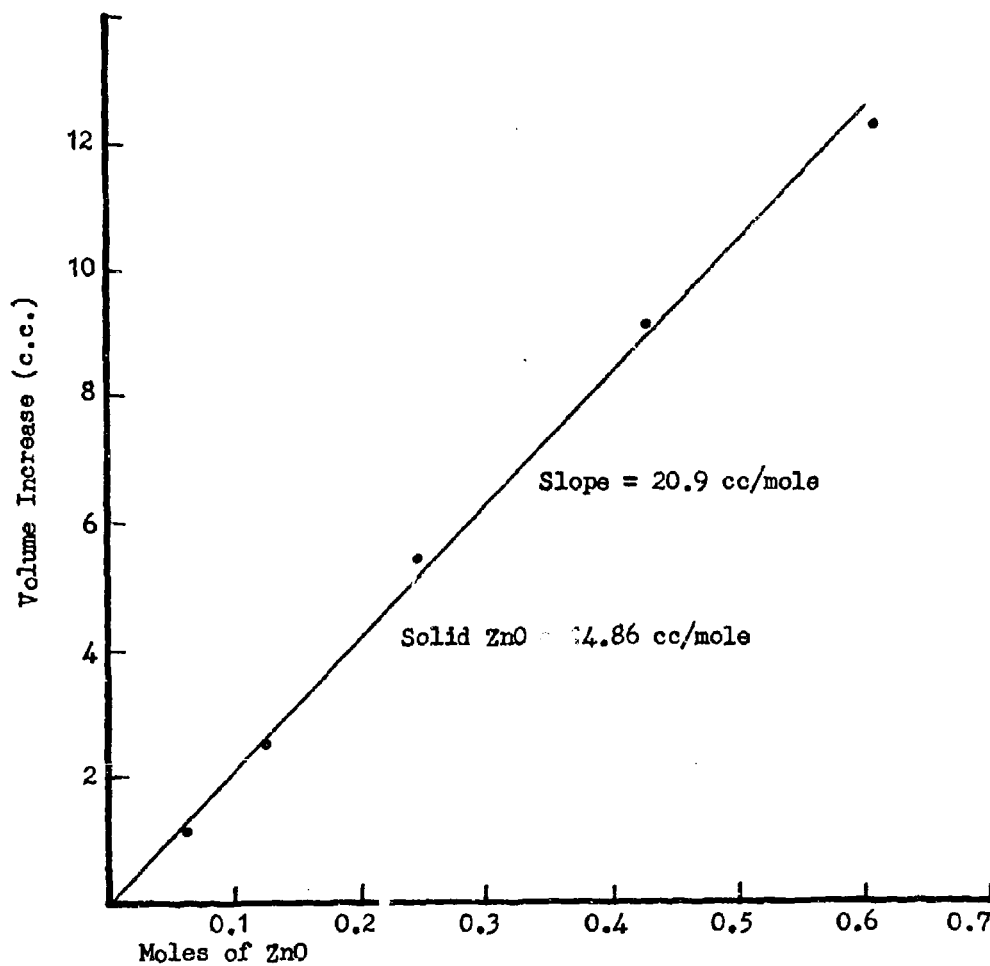


Figure 6. Volume Change of Solutions of ZnO in 45% KOH. 72°F.

APPENDIX VI

DEVELOPMENT OF IMPROVED SEPARATOR MATERIALS FOR
THE ALKALINE SILVER OXIDE-ZINC BATTERY



36-40 37th Street
Long Island City, N. Y. 11101
212 Empire 1-2170

Permion - Specialty Membranes
Radiation Chemistry
Polymer and Electro Chemistry
Water Resources Technology

RAI 407

DEVELOPMENT OF IMPROVED SEPARATOR MATERIALS FOR
THE ALKALINE SILVER OXIDE-ZINC BATTERY

RAI SUB-CONTRACT D-R164719
CONTRACT NO. AF 33(615)-3487

WITH

DELCO-REMY
DIVISION OF GENERAL MOTORS
ANDERSON, INDIANA 46011

Prepared by:

Vincent D'Agostino
Joseph Lee
Gyula Orban
Arthur Canter

FINAL REPORT

PERIOD - APRIL, 1967 - AUGUST, 1968

April 28, 1969

FOREWORD

The work described in this report was performed during the period 1 April 67 to 30 August 1968 under Sub-contract DR 164719 of Air Force Contract AF 33(615)-3487.

The authors wish to acknowledge the valuable guidance of Dr. J. J. Lander and Mr. J. Keralla.

Particular acknowledgement is given to Dr. D. Mertz of Brookhaven National Laboratories for his helpful discussions relating to the studies on beta radiation.

ABSTRACT

Study on development of a separator suitable for silver-zinc secondary batteries has been investigated in detail. Families of separators prepared by radiation grafting of pre-crosslinked polyethylene were characterized. It has been found that the following parameters are of fundamental importance in design of a membrane for secondary batteries: (1) The type of resin used in preparing the film, particularly the molecular weight distribution of the resin, (2) the crosslinking densities of the resin, particularly the dose level of its uniformity and (3) the type of monomers grafted onto the base film. In addition, the percent graft and its uniformity and various preparative procedures such as environment of irradiation and washing procedure in KOH, are also of significant importance.

The separators were characterized by tests such as exchange capacity, electrical resistance, zinc penetration, thermal stability at elevated temperatures in caustic, cycle life in a 3-plate cell, swelling, tensile strength and zinc diffusion. All separators were screened for electrical resistance and cycle life at 40% depth of discharge in a 1.2 amp.-hour 3-plate cell. Larger cells of 25-amp-hour capacity were evaluated by Delco-Remy at various depth of discharge and using a variable number of layers of selected separators. Results indicate that separators prepared from a resin having a narrow molecular weight distribution which is precrosslinked with 90 Mrads of radiation and subsequently grafted with methacrylic acid gives the longest cycle life. This membrane is better than the cellulose sausage casing control. The common failure mode for grafted membranes was by loss of capacity rather than shorting which was the common failure mode for cellulose. This together with the absences of zinc on the grafted separator during cycle life test indicate a different type of transport mechanism for the grafted separator as distinct from the cellulosic separator.

The test-tube quantities of grafted separators have been scaled up for production in small reactors. A 5000 foot sample was delivered to Delco-Remy at the end of this contract.

TABLE OF CONTENTS

		<u>Page</u>
	ABSTRACT	iii
1.0	INTRODUCTION	1
1.1	History of Membrane Development	2
2.0	EXPERIMENTAL	4
2.1	Preparation of Final Sample	4
2.1.1	Procurement of Film	4
2.1.2	Crosslinking of Film	6
2.1.3	Rolling Film Prior to Grafting	8
2.1.4	Grafting	8
2.1.5	Washing	9
2.2	Characterization of the Grafted Separator	10
2.2.1	Exchange Capacity	10
2.2.2	Determination of Uniformity of Graft	11
2.2.3	Electrical Resistance	14
2.2.4	Zinc Penetration	14
2.2.5	Thermal Stability in 40% Potassium Hydroxide	18
2.2.6	Cycle Life Testing in Three Plate Cells	18
2.2.7	Swelling Characteristics	18
2.2.8	Tensile Strength	22
2.2.9	Zinc Diffusion	22
3.0	RESULTS AND DISCUSSIONS	23
3.1	Radiation Crosslinking of Films	24
3.2	Effect of Base Film on Separator Properties	36
3.3	Radiation Grafting of Films	49
3.3.1	Effects of Monomer Concentration on Percent Graft	50
3.4	Effect of Monomer Type	61
3.4.1	Potassium Hydroxide Extraction at 70°C and 145°C	65
3.4.2	Cycle Life at Elevated Temperature	68

TABLE OF CONTENTS (Continued)

		<u>Page</u>
3.5	Testing Results of Grafted Membranes	74
3.5.1	Sample Submitted on Completion of Phase I	74
3.5.2	Samples Submitted Upon Completion of Phase II	83
3.5.3	Final Sample Selection and Specifications	83
4.0	CONCLUSIONS	92
5.0	RECOMMENDATIONS	94
6.0	REFERENCES	96
APPENDIX I	MATERIALS AND SUPPLIERS	98

LIST OF TABLES

<u>Table</u>		<u>Page</u>
1	Dose-Depth Relationship of Crosslinked Films	26
2	Dose-Depth Relationship of Crosslinked Films	26
3	Surface, Exit and Average Dose of Crosslinked Film for 5000 Foot Sample	32
4	Effects of Base Film and Precrosslinked Dose on Cycle Life	37
5	Characteristics of the Base Films	45
6	Intercept and Slope of Charlesby-Pinner Curve	48
7	Effect of Monomer Concentration on Percent Graft. Bakelite 0602 Precrosslinked 90 Mrads; Dose Rate of Grafting 9214 rads/hr; Total Dose 1.55 Mrads	53
8	Relationship Between Percent Graft of Methacrylic Acid and Exchange Capacity of the Membrane	61
9	Screening Test of the Six 100-Ft. Samples in a 3-Plate Cell at 40% DOD	62
10	Thermal Sterilization Data	66
11	Cycle Life of Grafted Membranes at 40% DOD in 3 Plate Cells at 50°C Using 1 Layer of Membrane	70
12	Average Resistance and Dimensional Change of B-DFD-0602 Acrylic Acid Graft as a Function of Electrolyte Concentration and Time	75

LIST OF TABLES (Continued)

<u>Table</u>		<u>Page</u>
13	Preliminary Membrane Evaluation	76
14	Relationship Between Hull Test and Cycle Life Test	80
15	Characterization of Six 100 Foot Samples Submitted on Completion of Phase One	81
16	Characterization of Three 500 Foot Samples Submitted on Completion of Phase Two	84
17	Characterization of Three 500 Foot Samples Submitted on Completion of Phase Two	86
18	Characterization of Three 500 Foot Samples Submitted on Completion of Phase Two	87
19	Characterization of 5000 Foot Sample Submitted on Completion of Phase III	88
20	Characterization of 5000 Foot Sample Submitted on Completion of Phase III	89

LIST OF ILLUSTRATIONS

<u>Figure</u>		<u>Page</u>
1	FLOW DIAGRAM FOR MEMBRANE PREPARATION AND QUALITY CONTROL	5
2	COLORIMETER FOR DETERMINATION OF GRAFT UNIFORMITY	12
3	RESISTANCE CELL	15
4	MEMBRANE RESISTANCE MEASUREMENT APPARATUS	16
5	CYCLE TEST EQUIPMENT	19
6	SCHEMATIC FOR CUT-OFF VOLTAGE REGULATION	20
7	POWER SUPPLY FOR REGULATING SYSTEM	21
8	THEORETICAL AND ACTUAL DOSE-DEPTH CURVES	27
9	DOSE-DEPTH CURVE FOR 1.5 MeV ELECTRONS	28
10	EXPERIMENTAL DOSE-DEPTH RELATIONSHIP FOR 1.4 MeV	30
11	EXPERIMENTAL DOSE-HALF DEPTH RELATIONSHIP FOR 1.4 MeV	31
12	GEL FRACTIONS OF IRRADIATED PHILLIPS 1712 VS. DOSE	33
13	GEL-DEPTH RELATIONSHIP FOR PHILLIPS 1712 POLYETHYLENE FILM IRRADIATED WITH 1 MeV ELECTRONS	34
14	EFFECT OF BASE FILM AND PRECROSSLINKED DOSE ON CYCLE LIFE	38
15	DIFFERENTIAL MOLECULAR WEIGHT DISTRIBUTION CURVE FOR PHILLIPS 1712	39

LIST OF ILLUSTRATIONS (Continued)

<u>Figure</u>		<u>Page</u>
16	DIFFERENTIAL MOLECULAR WEIGHT DISTRIBUTION CURVE FOR USI-280	40
17	DIFFERENTIAL MOLECULAR WEIGHT DISTRIBUTION CURVE FOR B-DFD-0602	41
18	CUMULATIVE MOLECULAR WEIGHT DISTRIBUTION CURVE FOR PHILLIPS 1712	42
19	CUMULATIVE MOLECULAR WEIGHT DISTRIBUTION CURVE FOR USI-280	43
20	CUMULATIVE MOLECULAR WEIGHT DISTRIBUTION CURVE FOR B-DFD-0602	44
21	GEL FRACTIONS OF IRRADIATED POLYETHYLENE FILMS	46
22	INFRA-RED SPECTRA OF GRAFTED MEMBRANE	51
23	EFFECT ON MONOMER CONCENTRATION ON PERCENT GRAFT	54
24	RELATIONSHIP BETWEEN RATE OF GRAFTING AND MONOMER CONCENTRATION	56
25	EFFECT OF PERCENT GRAFT ON THE ELECTRICAL RESISTANCE IN 40% KOH	57
26	COMPARISON OF GRAFT UNIFORMITY BY COLORIMETRIC METHOD	59
27	RESISTANCE AND PERCENT GRAFT VS. EXCHANGE CAPACITY	60
28	CYCLE LIFE TEST OF SAMPLE FILMS AT 60% DEPTH OF DISCHARGE AND 25°C	63
29	EXTRACTION IN 40% KOH	69

LIST OF ILLUSTRATIONS (Continued)

<u>Figure</u>		<u>Page</u>
30	PERMEATION OF ZINCATE THROUGH 2.2 XH SERIES 2	71
31	TEMPERATURE VS. RESISTANCE OF GRAFTED FILM	73
32	ZINC FLUX THROUGH B-DFD-0602	91

1.0 INTRODUCTION

The silver oxide-zinc couple is undoubtedly one of the best for design of a high energy density battery. The problems associated with this system are primarily associated with washing of the zinc electrode and the inadequacy of cellulosic separators to meet the requirements for long term cycle life.

The separator system has been the weakest component in the development of an improved silver-zinc battery. Ideally, a separator must be resistant to the chemical environment encountered in the battery. Generally this requires resistance to varying concentrations of potassium hydroxide up to 45 percent and resistant to the oxidative effects of silver oxide and silver peroxide at temperatures from 40°F to sterilizing conditions of 135-145°C. Generally, however, the operating temperature is 75°F. The necessary function of the separator is to prevent "shorting" by zinc dendrite penetration and/or silver diffusion.

A separator should also have a low resistance and absorb sufficient electrolyte to prevent "drying" of the plates. The swelling characteristics of the membrane must not be excessive. Cellulosics swell considerably in the electrolyte environment. This permits tight packing of the battery. Grafted polyethylenes swell to a lesser degree. The variations can be accounted for by the battery design engineer provided the membrane properties are reproducible. This then, i.e., the reproducibility, is a most important primary requirement of any separator. The reproducibility of separators investigated in this research program was a fundamental consideration and was accomplished by a strict review of all aspects of materials and processes used in preparing the membranes. Results of battery testing on membranes developed during this research effort have been extremely encouraging. As important, the parameters associated with "building" a separator have been identified. As in all research, the results of this program indicate areas for further improvement.

The quality control of all materials used in this program was stressed throughout. The history of events leading to initiation of this program is given in the following section and is done to stress the importance of thoroughly characterizing the materials used in developing membranes.

1.1 History of Membrane Development

In April, 1963, RAI Research Corporation was awarded a separator development program by the Air Force Aero Propulsion Laboratory of Wright Patterson Air Force Base. The objective of this program was to develop a membrane for use as a separator in secondary silver-zinc cells. This work was accomplished under Air Force Contract No. AF33(657)-10643, Task No. 817304 of Project No. 8173. RAI Research Corporation was subcontractor to Delco-Remy Division of General Motors Corporation, the prime contractor.

A number of grafted membranes were fabricated during the course of that program. Various combinations of fluoro-carbon acrylic acid and polyethylene-acrylic acid separators were developed and evaluated at RAI and at Delco-Remy. In general, it was found that a crosslinked highly grafted, low density polyethylene separator was superior to any other variation fabricated. This separator, which was designated 2.2XH, was a crosslinked, low density polyethylene acrylic acid copolymer. Cycle testing of this material in three plate cells gave excellent results at 25% depth of discharge. In 25 amp-hour cells tested at Delco-Remy the 2.2XH separator also proved very encouraging. In these tests the 2.2XH was used in multiple layers. Cells using four layers of 2.2XH as the separator and cycled at 25% depth of discharge at room temperature gave 2,700 cycles without failures.(1) It is significant to note that controls using cellulose under the same test conditions had passed 1500 cycles. This amounted to an 80% improvement in cycle life for batteries using the 2.2XH membranes over the cellulose.

Subsequent to these findings, samples of 2.2XH, manufactured using identical conditions and materials procured from the same suppliers, gave poor results. Because of these later results an intensive in-house program was initiated to determine the reason for the failure to reproduce the original excellent separator. Testing at RAI included evaluation of monomer types, grafting rates, grafting levels, solution concentrations, addition of chain transfer agents, purity of solvents, crosslinking levels of the base film and variations in the base polymers. These tests indicated a strong dependence of the finished separator on three basic variables, the base

polymer, the crosslinking level and the monomer type grafted. Because of the prime dependence of the final separator on the base film an investigation was undertaken to determine if our film supplier had in any manner changed the base film used in the manufacture of the original 2.2XH. After lengthy discussions it was found that the base resin used by our supplier was changed from a Bakelite resin with a 0.922 density to a USI resin with a 0.922 density and that two grades of the USI 0.922 density resin were used. These differed in antioxidant level. Further checking of invoices revealed that samples of 2.2XH made under the Delco-Remy contract were purchased in 1963 at which time the Bakelite resin was used by the extruder. Film purchased in 1965 from the same supplier was made with USI resin 280.

The culmination of all these occurrences was the development of separator materials superior to any films previously made. The theoretical implication of our results indicated that long cycle life battery separator materials could be made by a proper attention to the polymer characteristics of the base film and to radiation crosslinking and grafting procedures. It had been theorized at the beginning of the current program, that the reason for failure of the 2.2XH separator made from the USI 280 resin was due to the low molecular weight averages of this resin. In particular, failure was believed due to the low molecular weight fraction in this resin, which is of advantage to film extruders but which is apparently detrimental to the development of separators. The low molecular weight fractions were believed to lead to failure by short circuiting. These fractions, when grafted, are made quite hydrophilic and could be leached from the separator during use. This action could result in the development of pores which, in turn, would lead to failure by zinc dendrite growth and shorting.

The effect of the three basic parameters, as well as control of the preparation steps, particularly the grafting, constituted the research and development goal of this program. The results which follow substantiate the original premise and note the importance of each of the three basic parameters. Further it has been shown that the importance of the base resin is not depended on the molecular weight averages but rather the molecular weight distribution. The importance of this characteristic was shown to be related to the efficiency of crosslinking.

2.0 EXPERIMENTAL.

The materials and suppliers used are given in Appendix One. The film extruders supplying the film are also given in Appendix One, along with outside facilities used to crosslink the base films and to graft the final separators.

2.1 Preparation of Final Sample

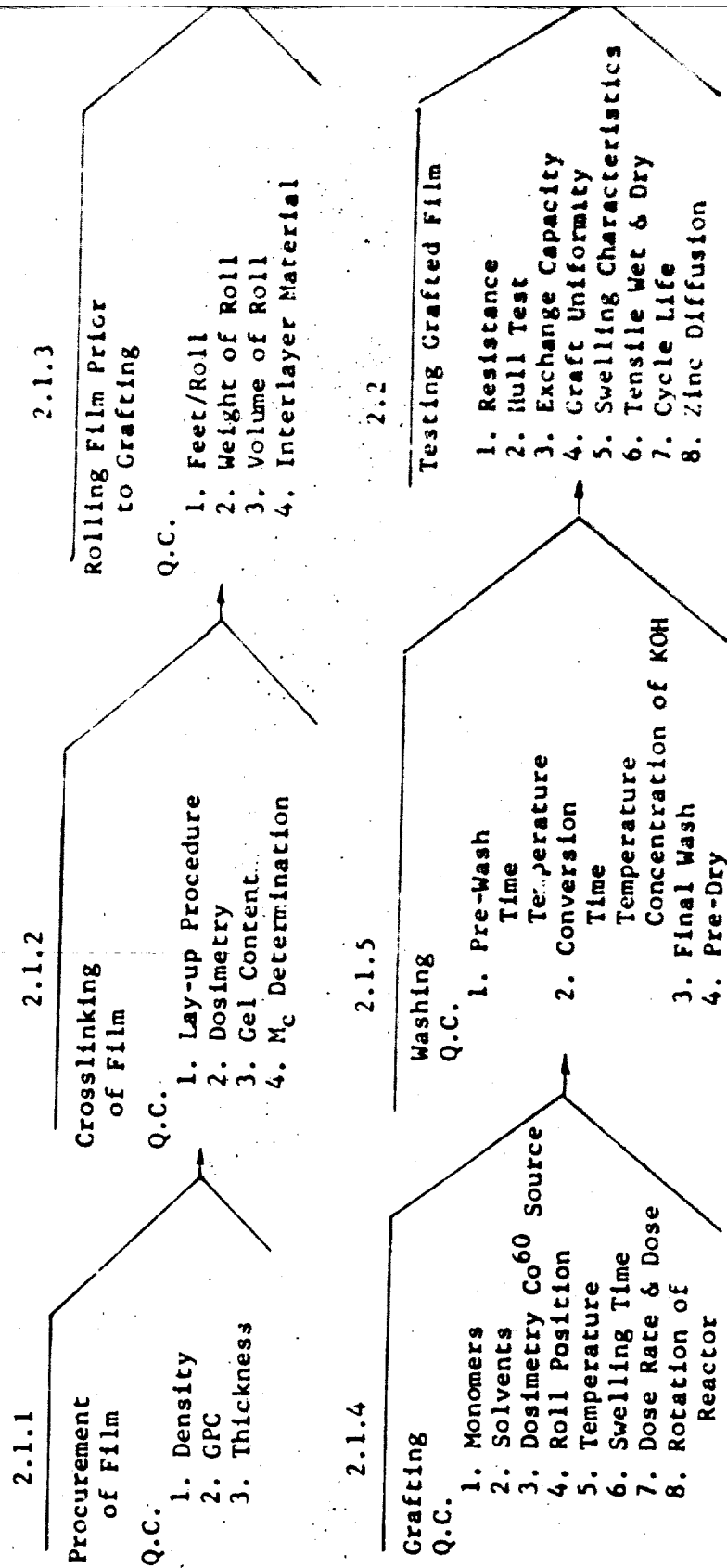
Figure 1 is a flow diagram which indicates procedural and control steps used in preparing the 5,000 foot final sample sent to Delco-Remy near completion of this contract. The procedures given below are based on the preparation of this final sample submitted to Delco-Remy.

2.1.1 Procurement of Film

The resin to be used in preparing the film was purchased from Union Carbide Corporation and is designated Bakelite DFD-0602. The density of this resin was checked along with the weight average (\bar{M}_w) and number average molecular weights (\bar{M}_n). The molecular weight distribution for this resin was determined using gel permeation chromatography (GPC). The results of this analysis are given in Table 5 in a following section. The significance of the distribution is given in a subsequent section.

The resin, as received, was extruded as a one mil film by the Phillip-Johanna Company of Ladd, Illinois. Subsequent to completion of this program a new extruder has been used to supply film. The original extruder could not hold the gauge of one mil to a tolerance better than twenty percent. The current supplier has maintained a tolerance of better than ten percent.

FIGURE 1 FLOW DIAGRAM FOR MEMBRANE PREPARATION
AND QUALITY CONTROL



2.1.2 Crosslinking of Film

The rationale for the crosslinking procedure given here is detailed in a subsequent section. One mil film was folded in twenty-five foot lengths. The film was thirteen inches in width. Seventy-three layers of film were "stacked" uniformly on each other, enclosed in a polyethylene bag and purged by first subjecting the bag to a vacuum and then back filling with pre-purified nitrogen and, subsequently, heat sealing. The film was then irradiated using a 1.5 MeV Dynamitron accelerator. The package was subjected to a nominal dose of 5 megarads per pass for a total of ten passes. The bag was then reversed, back to front, and irradiated under identical conditions for another ten passes. Dosimeters⁽²⁾ were used to determine the actual dose-depth relationship of the film. Strips of blue cellophane dosimeters were placed at every tenth layer of polyethylene film, and after irradiation their transmission was read at 635 mu using a Beckman spectrophotometer. The actual dose the film received is related to the optical density and was read from a standardized calibration curve.

Gel studies were conducted to check the extent of crosslinking as a function of depth and dose⁽³⁾. This is done by placing the irradiated films in individual stainless steel cages and, in turn, each cage is placed into a 4-oz. jar filled with xylene. The xylene contained 0.1% phenylbeta-naphthylamine to prevent oxidative degradation of the films during extraction. The solvent was maintained at 115°-120°C. in an oil bath, and changed daily for two days. After the extractions were completed the films were vacuum-dried at 90°C. for 24 hours, weighed and the percent gel was calculated from the equation

$$\text{Gel} = \frac{W_G}{W_I} \times 100$$

where W_G is the weight of the insoluble fraction (i.e., gel) and W_I is the initial weight of the film before extraction.

When polyethylene is subjected to a crosslinking dose greater than thirty megarads the gel content is no longer of significant value in determining the crosslink density. To note the change in crosslink density at high irradiation dose the M_C value was determined. This parameter indicates the molecular

weight between crosslinks in a treated film and was obtained from a plot of the sol fraction of the gel curves vs. the radiation dose. The detailed calculations necessary to give the M_C value are given in a subsequent section. The equations used are as follows:

$$S + S^{\frac{1}{2}} = \frac{P_0}{q_0} + \frac{1}{q_0 u r} \quad 1$$

where S = Sol fraction = (1-gel content)
 P_0 = the fracture (scission) density per unit dose
 q_0 = the crosslink density per unit dose
 u = the number average degree of polymerization
 r = total dose

S , is obtained from 1-gel content
 r , is the dose and is set experimentally
 u , is calculated from the GPC curve

The M_C value is determined from the slope of a plot of equation one.

$$m \text{ (slope)} = \frac{1}{q_0 u} \quad 2$$

$$q_0 = \frac{1}{mu} \quad 3$$

$$q \text{ (total crosslinking)} = q_0 \times r \quad 4$$

$$M_C = \frac{W}{q} = \frac{W}{q_0 r} = \frac{Wmu}{r}$$

where W is the molecular weight of the repeating unit in the polymer.

2.1.3 Rolling Film Prior to Grafting

The crosslinked film was prepared for grafting by interwinding with a wide mesh cheesecloth to give a roll approximately ten inches in diameter. This roll contains five hundred feet of film. The cheesecloth was 15 inches wide. The film was rolled loosely to permit diffusion of monomer into the roll during grafting. Ideally the film should be rolled under constant tension, since this was not possible the roll size and weight were controlled. The finished rolls were placed in the grafting solution sparged with nitrogen and then allowed to equilibrate for twenty-four hours. The procedure was modified during the course of the contract by pulling a vacuum on the roll to insure removal of air pockets. This modification of procedure, however, did not effect the grafting results and was not made part of the final procedure.

2.1.4 Grafting

The dose rate and dose were determined on small samples and set at 10,500 rads/hr. 1.51 megarads total dose. The dosimetry of the vault was determined by personnel at Industrial Reactor Laboratories using standard techniques. The temperature of the radiation vault was about 75°F.

The grafting solution was made using 26.4 percent glacial methacrylic acid, 70.0 percent benzene and 3.6 percent carbon-tetrachloride. The solution was thoroughly mixed and five gallons was added to a stainless steel reactor. The roll was prepared as described under 2.1.3 on a stainless steel three-inch diameter hollow core and was placed in the reactor. The roll of film and interlayer were positioned on the core so that the roll was kept approximately ten to twelve inches from the bottom of the reactor and the center of the polyethylene was at the center of the vertical height of the can.

The reactors are thirty inches in height. After positioning the roll in the reactor a cover is bolted on the vessel. There is a port in the cover approximately one inch in diameter to allow for pressure relief which might develop during initial phases of the reaction. The film was allowed to swell in the

monomer solution for twenty-four hours and then placed in the radiation vault. The reactors are placed on rotators and revolved at about 25/revolutions per minute during radiation. At the dose rate specified (10,500 rads/hour) the reactors are exposed to the Co^{60} gamma rays for 144 hours. The total dose received being 1.51 megarads.

It is important to predetermine the position of the Cobalt 60 source and the container to insure the alignment of the vertical center of the source with the center of the polyethylene film in the reactor. This is necessary since the equal dose rate lines are "parabolic" in shape about a line perpendicular to the center of the source. Thus in addition to a uniform dosimetry about the source in a horizontal plane the dosimetry in the vertical plane can be maintained. The uniformity of the vertical dosimetry about a line perpendicular to the floor (i.e., paralleled to the reactor) improves as the reactor distance from the source increases. The distance from the source to the reactor is however set by the strength of the source. Under the conditions of irradiation used here the center on center distance from the source to the reactor was thirty-four inches and the variations in dose rate in a vertical plane along the center of the roll being irradiated was less than five percent.

2.1.5 Washing

The reactor from 2.1.4 was removed after receiving the required dose and the roll in turn was removed from the reactor. The grafted polyethylene was unwound from the cheese-cloth and at this stage was covered with a white homopolymer of methacrylic acid. The initial ten to twenty feet of film were generally unevenly grafted and were discarded. The film was initially washed in hot water at 80°C for 10 minutes. Since the homopolymer was not completely removed under these conditions the time was extended to almost three hours. The graft was converted to the salt form by washing at 80°-90°C in five percent potassium hydroxide. Following this the film was washed at 60°C and then at room temperature in water. The wet film was squeezed between nip rolls to remove as much water as possible and then wound on to paper and

dried. Subsequent to shipment of this material to Delco-Remy it has been found advantageous to roll the final product on polyethylene film and to package in a polyethylene bag.

2.2 Characterization of the Grafted Separator

The grafted separator was characterized by

- 2.2.1 Exchange Capacity
- 2.2.2 Determination of Uniformity of Graft
- 2.2.3 Electrical Resistance
- 2.2.4 Zinc Penetration (Hull Test)
- 2.2.5 Thermal Stability at Elevated Temperature in 40% Potassium Hydroxide
- 2.2.6 Cycle Life Testing in Three Plate Cells
- 2.2.7 Swelling Characteristics
- 2.2.8 Tensile Strength
- 2.2.9 Zinc Diffusion

The procedures for these tests follow:

2.2.1 Exchange Capacity

The exchange capacity of the separator was determined by equilibrating a weighed sample of the separator in standardized potassium hydroxide and then back titrating with a known concentration of hydrochloric acid to determine the equivalence of potassium hydroxide consumed. This is assumed to be the exchange

equivalent of acid groups present in the separator.

$$\text{Exchange Capacity} = \frac{(N_o - N_f) \times 1000}{W_s}$$

5

N_o = original normality of potassium hydroxide
 N_f = final normality of potassium hydroxide
 W_s = dry weight of membrane sample in acid form

The exchange capacity is given in milliequivalence per gram of separator. The equilibration period for the separator in the standardized potassium hydroxide was set at twenty-four hours at 25°C.

2.2.2 Determination of Uniformity of Graft

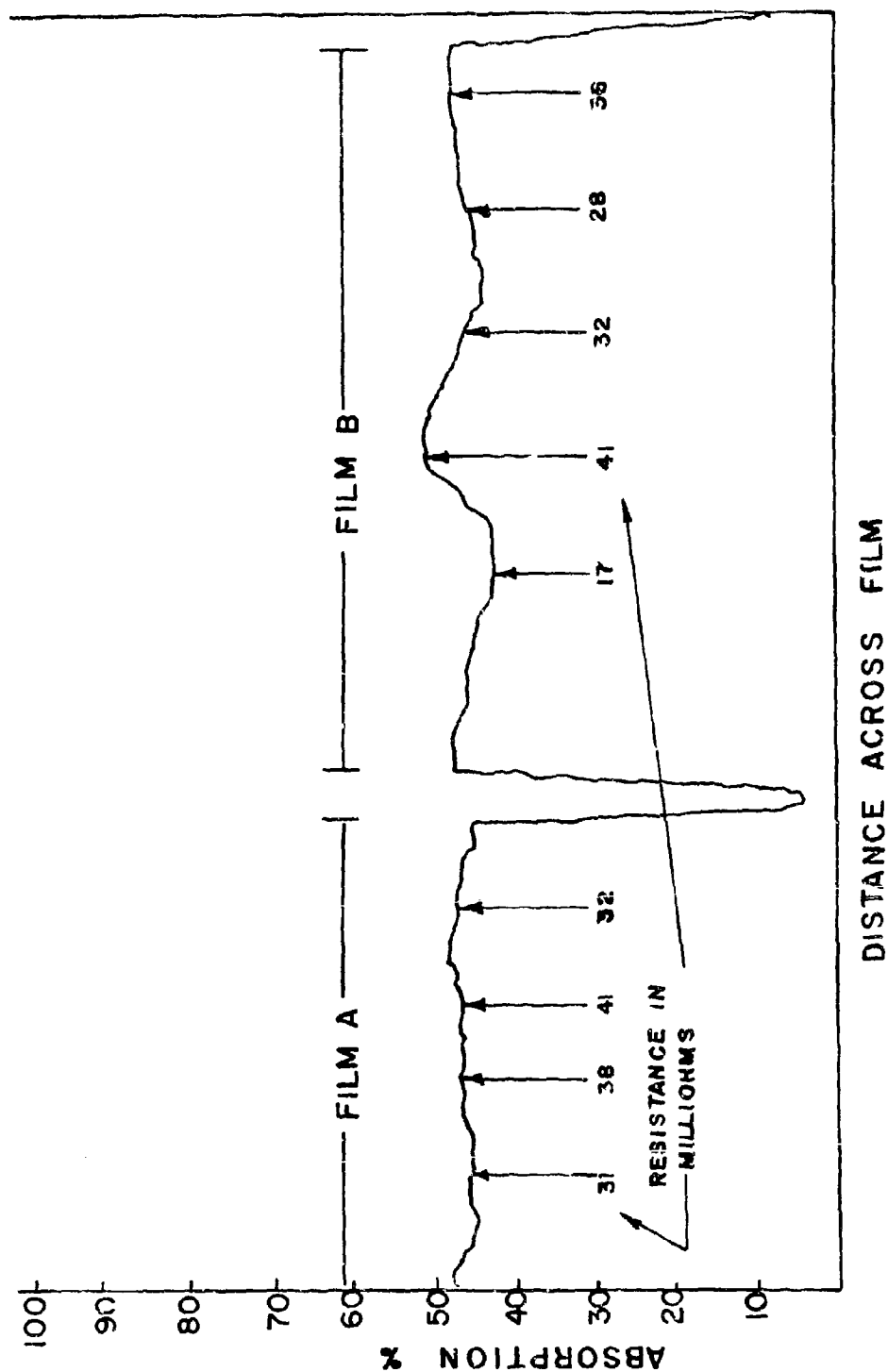
The uniformity of the graft could be determined in a preliminary way by dyeing the grafted sample and then determining the absorption spectrum of the film at a fixed wavelength⁽⁴⁾. This procedure assumes the absorption of dye from solution is proportional to the percent graft and that the optical absorption in turn is proportional to the dye species. Figure 2 is a photograph of the colorimeter built in this laboratory. Figure 26 is a trace of the percent absorption across the width of the separator. The arrows in this trace indicate the resistance of samples removed and checked at various locations. There appears to be a general relationship, as would be expected, but the sensitivity of the instrument used is not adequate. It is not easy to distinguish between sections of the film based on the change in absorption when the difference in resistance is eight milliohms-in².

The basic procedure requires modification wherein the carbonyl function would be measured using ultra-violet radiation rather than dyeing and recording the visible spectrum. Infrared is not satisfactory for quantitative analysis here because the samples contain water.



FIGURE 2
COLORIMETER FOR DETERMINATION
OF GRAFT UNIFORMITY

DETERMINATION OF GRAFT UNIFORMITY BY COLORIMETRY



2.2.3 Electrical Resistance

Electrical resistance of the grafted film was measured in 40% KOH at room temperature using a Plexiglass cell as shown in Figure 3. The circuitry for the resistance measurement apparatus is shown in Figure 4. The resistance of the separator is obtained as the difference between the cell resistance with and without the separator, in milliohms-in.². The resistance was determined as follows:

$$R_{\text{separator}} = R_{\text{(cell + separator)}} - R_{\text{(cell without separator)}}$$
 where

R stands for the electrical resistance of the material. Resistance is measured using an AC bridge at 1000 cycles.

2.2.4 Zinc Penetration

The zinc penetration times were determined using a Hull Test⁽⁵⁾. The procedure as standardized at these laboratories follows:

Size of Cathode Plate: 3-7/8" x 2-1/2"
Anode Plate: 2-1/2" x 2-1/2"

Electrolyte: 45% KOH in a 1 molar ZnO solution

Current: 1 Ampere

Size of Film: 6" x 5"

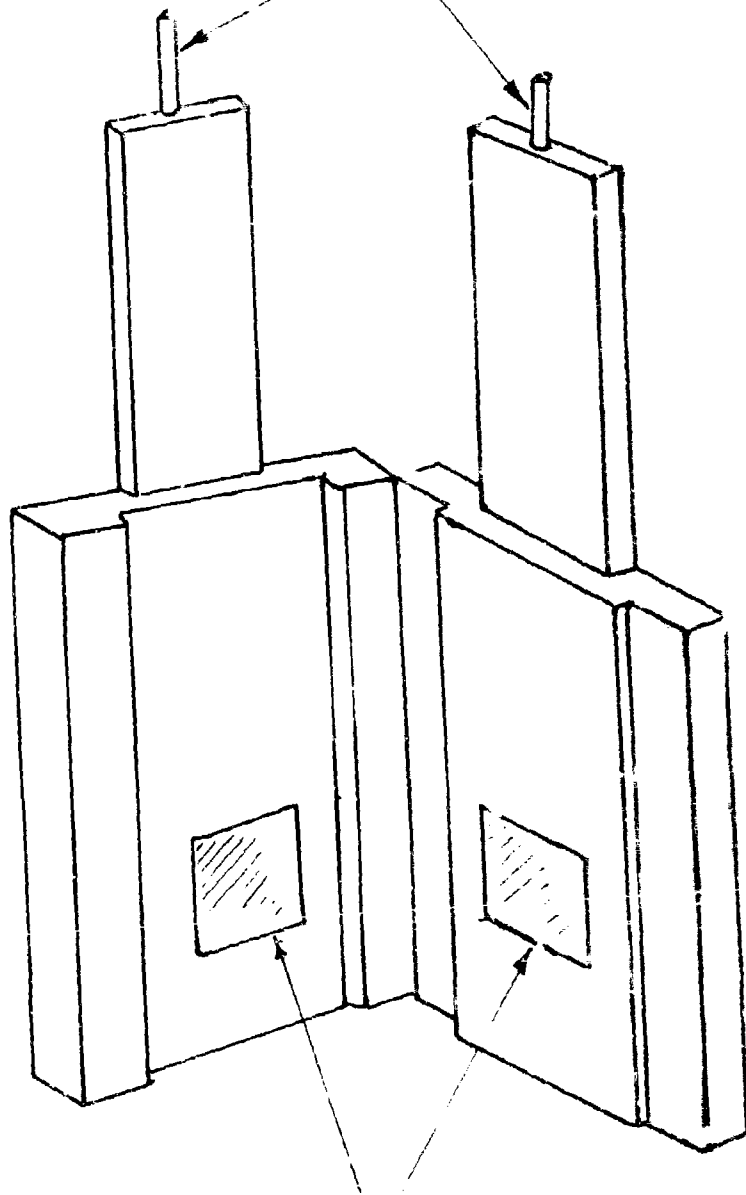
Cleaning Steps for Film:

Hot KOH → H₂O → Methanol (CH₃OH)

I. PREPARATION OF ZINC PLATES

The larger plate must have its edges and corners sanded smooth to prevent any punctures or tears in the film.

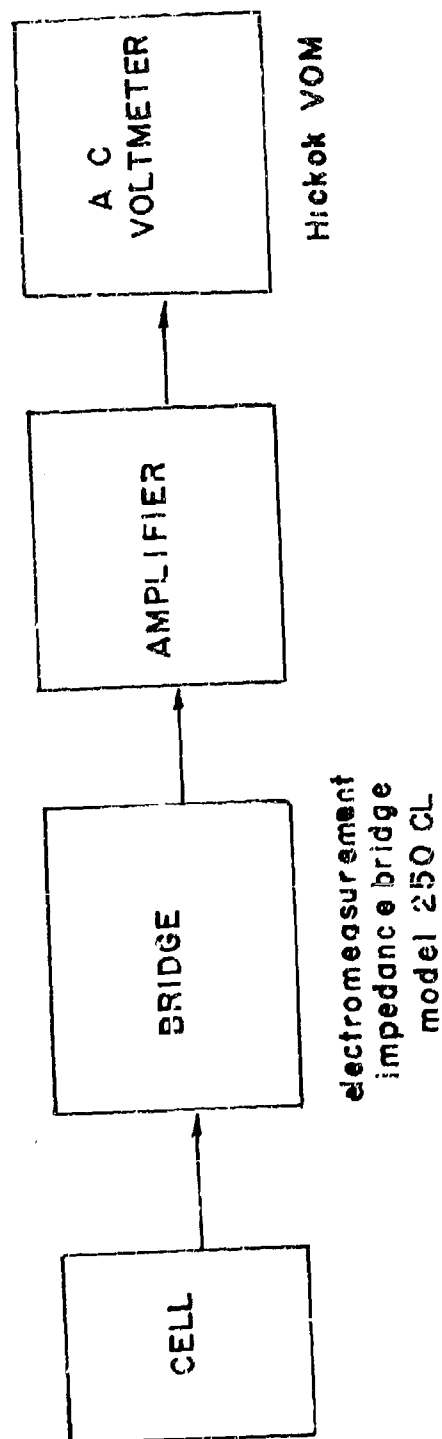
LEADS TO IMPEDANCE BRIDGE



PLATINIZED PLATINUM ELECTRODES

RESISTANCE CELL
FIGURE 3

FIGURE 4 MEMBRANE RESISTANCE MEASUREMENT
APPARATUS



After the sanding, both plates are washed in a solvent, such as acetone, to remove any surface dirt. The smaller plate is connected to the positive terminal.

II. PREPARATION OF FILM FOR TEST USE

A piece of film measuring 6" x 5" should be cut from the desired sample to be tested. Cuttings should be taken from a clean area of the film and should always be handled carefully, by the edges, in order to avoid a puncture or a tear.

Because this film is to be used in a basic environment, we must convert it to its basic form. This is done by washing the film in a hot (80° - 85°C.) 5% KOH bath for approximately 25 - 30 minutes. The film is then rinsed in deionized water to remove the KOH, and then in methanol, removing any water, either on the surface or in the pores. The film is towel blotted until dry.

III. FITTING FILM ON PLATE

The prepared piece of film must now be fitted to the larger (3-7/8" x 2-1/2") plate. The film is first folded in half along its length covering the plate evenly. That film extending beyond the sides of the plate is folded backwards and securely taped. That film remaining above the plate is cut, so that it fits tightly around the plate with no excess. This plate is placed in the Hull Test Unit and connected to the negative terminal. The connection must be in contact with the zinc plate, and is therefore, slipped under the film. The connecting clip should clamp onto the cell wall. After this is done, the 45% KOH-ZnO solution is poured to the filling line on the test cell. The current is then passed at 1 ampere. A timer should be used and set at 15 minute intervals. The test for dendrite formation is a visual one with most of the films showing dendrite formation at the closest distance between the plates. The time when the dendrites just penetrate the film is recorded as the failure time.

2.2.5 Thermal Stability in 40% Potassium Hydroxide

The thermal stability of the separator was determined from tests conducted in 40% potassium hydroxide. The separator was placed in a stainless steel bomb and potassium hydroxide was added. The bomb was then capped and heated at 70° or 145°C. for 7 or 14 days. The weight loss of the film under these conditions was used as a measure of the stability of separator to thermal sterilization.

2.2.6 Cycle Life Testing in Three Plate Cells

Cycle life of various separators was screened and evaluated by testing in three plate cells, two silver and one zinc. The cells had a capacity of 1.2 amp. hours and were cycled over a two-hour regime at forty percent depth of discharge. The discharge cycle was 35 minutes at 800 ma while the charge cycle was for 85 minutes at 350 ma. The cut-off voltage for failure was set at 1.3 volts and charge cut-off was 1.96 volts. The cycle testor is seen in Figure 5. Circuits for control of cut-off voltage are given in Figures 6 and 7. Independently 25 amp-hour cells were used in evaluating this separator. These cells were cycle-tested at 25%, 40% and 60% depth of discharge by Delco-Remy.

2.2.7 Swelling Characteristics

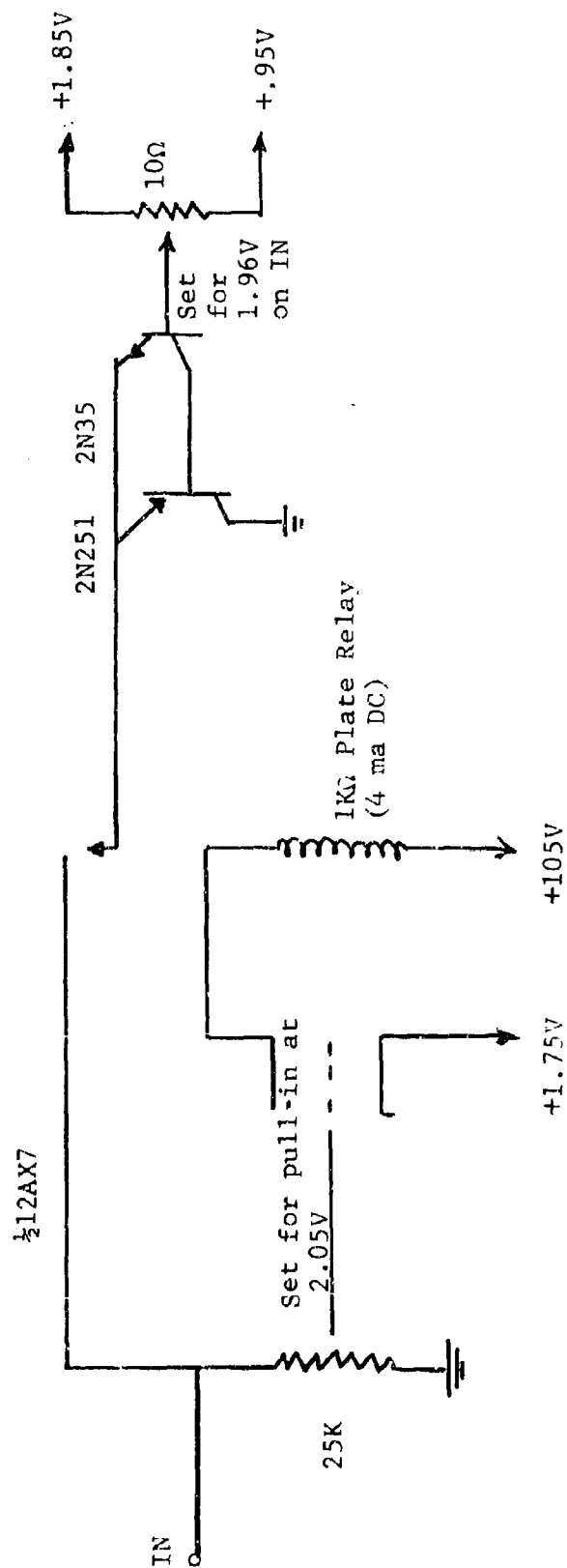
Duplicate pieces measuring 2" x 2" are cut from the grafted film for each concentration of electrolyte to be evaluated. The film pieces are dried to a moisture content of less than 10% by keeping at 40°C for 2 hours. This moisture content can be checked by drying to constant weight at 60°C under vacuum overnight. The film is not normally used in the absolute dried state since it is very brittle and cracks. All samples tested are in the salt form.

The duplicate pieces of film are placed in beakers containing the desired concentration of KOH and equilibrated over two hours at room temperature. The membranes are then removed blotted dry and measured. Data is reported as change in length and width.



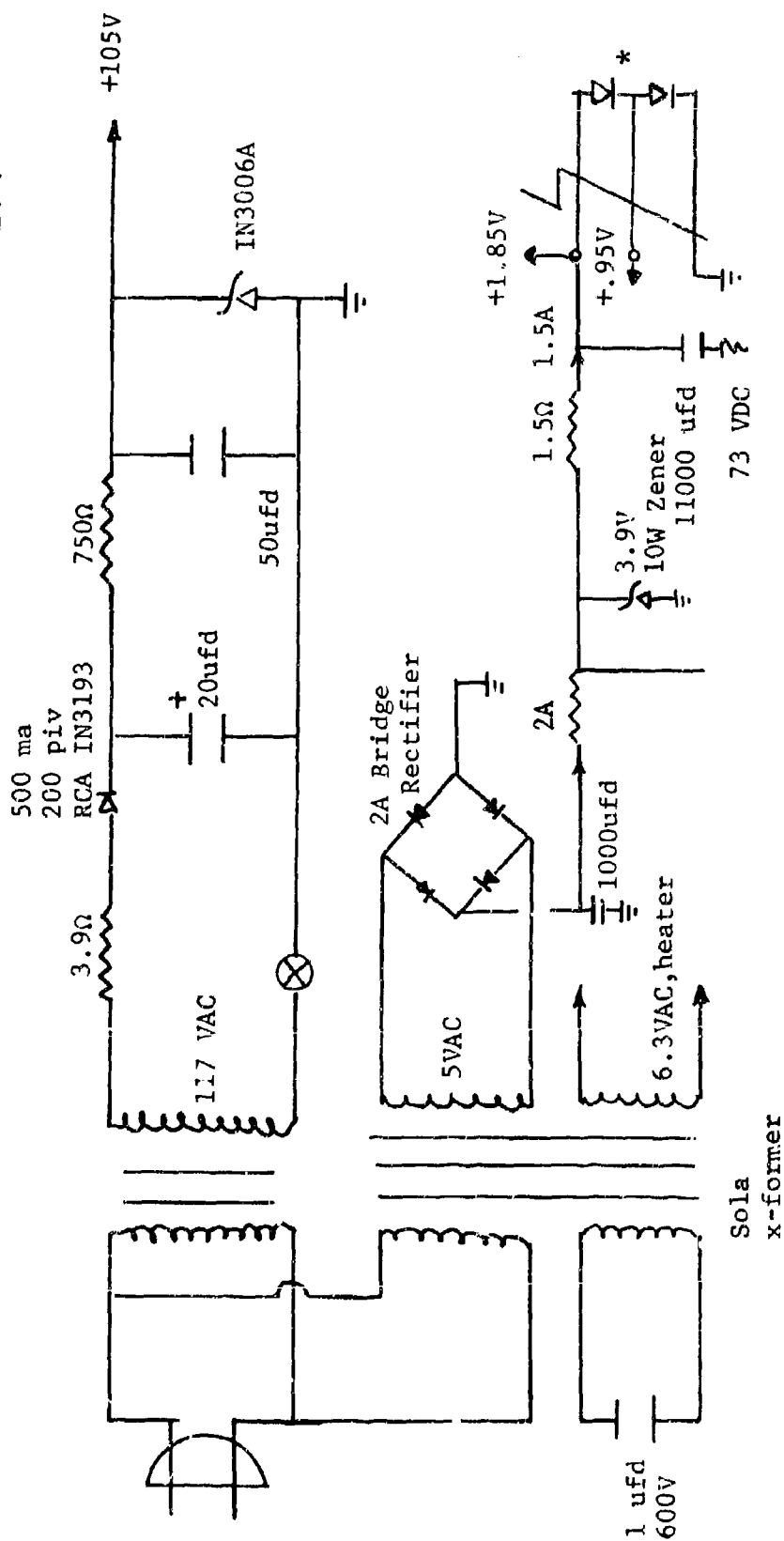
FIGURE 5 CYCLE TEST EQUIPMENT

FIGURE 6 REGULATING SYSTEM FOR CUT-OFF VOLTAGE



Twelve such circuits, consisting of ultrasensitive vacuum tube relays switching ON/OFF complementary-symmetry configuration transistor shunt-regulators.

FIGURE 7 POWER SUPPLY FOR REGULATING SYSTEM



* Temperature Probe in ambient $\pm 10^{\circ}\text{C}$.

Triple regulated reference voltages, available at very low impedance to voltage dividers, are made possible by sola transformer + zener diode + voltage temperature probe (held in oven) employing forward saturated silicone diodes.

2.2.8 Tensile Strength

The tensile strength was determined using a table Instron Tensile Testor. Tensile strength was taken on both wet and dry samples in accordance with ASTM D882-56T⁽⁶⁾. The strain rate was kept constant at 0.2 inches per minute. Stress-strain curves were recorded and the tensile strength is calculated at break.

2.2.9 Zinc Diffusion

The diffusion of zincate ion through the separator was determined according to the procedure given by Cooper and Fleischer⁽⁷⁾.

3.0 RESULTS AND DISCUSSIONS

The results of preliminary investigations indicated the necessity to explore in depth three distinct areas. These were the characteristic of the base polymer, the methods and extent of crosslinking and the grafting procedures and monomer type used in preparing the grafted separator.

It appeared at that time that the choice of resin made in preparing the separator film should be based on the melt index of the polyethylene. More detailed investigation undertaken here however, contradict the primary importance of the melt index and indicate that the molecular weight distribution is a better indicator to follow in selecting a base resin for preparation of a separator to be used in secondary silver-zinc batteries. The importance of having a resin with a narrow molecular weight distribution is related to the efficiency with which beta radiation crosslinks the resin. The crosslinking efficiency has been shown to increase as the molecular weight distribution of the polyethylene decreases. It has been demonstrated that the cycle life of batteries can be increased by using separators which have been more highly crosslinked. The importance of the procedure used in crosslinking the polyethylene film has also been demonstrated to be directly related to the uniformity of the crosslinked film and, though not specifically confirmed, it is believed to strongly influence the uniformity of the grafting process.

Only two monomers have been studied in detail. These monomers were selected based on previous experiences wherein their utility was demonstrated. A number of other monomers were investigated in only a cursory manner because of the limitations of time. In addition to radiation grafting a proprietary chemical grafting procedure was used to prepare a membrane comparable in chemical characteristics to one of the promising radiation grafted membranes. The limited results from this investigation indicate that the chemical grafting procedure is inferior to the radiation grafted separator for the secondary silver-zinc application. The use of chemical grafted membranes for limited secondary, primary and/or limited secondary sterilizable membranes however, is nevertheless possible. This area requires additional research.

In addition to grafting crosslinked base resins the reverse procedure was used to prepare a membrane. The P-1712 was grafted with acrylic acid, and subsequently crosslinked. Preliminary results indicate crosslinking grafted membranes gives separators which are comparable to those prepared by the direct grafting process. In addition the grafting proceeds considerably easier since the grafting step occurs prior to crosslinking. It is believed that the reverse procedure may be satisfactory for crosslinking acrylic acid grafted membranes but is not satisfactory for post crosslinking methacrylic acid grafted membranes. Additional research and testing is necessary to take advantage of this preliminary finding.

The areas briefly discussed above are developed in depth in the following sections.

3.1 Radiation Crosslinking of Films

It is well known that with electron radiation the dose received by a film varies with the thickness of the material into which the electrons are travelling(8). Thus, it is possible when a parallel beam of fast electrons impinges on the surface of matter, that the energy absorbed per gram of matter may be greater at a depth below the surface. The effect is not due to any increase in ion density along the electron track, but merely results from the scattering of the initial parallel beam. After scattering, the electrons are moving, on the average, obliquely to the forward direction of the beam, and leave more energy behind in a thin layer of matter which is normal to the beam direction.

The dose depth relationship for an electron accelerator can be determined by placing cellophane dosimeters at various depth in the material being irradiated and evaluating the change in the absorption of the blue cellophane. Initial testing to determine the dose-depth relationship was performed on a package of stacked polyethylene sheets. One hundred and forty-one sheets were placed in a polyethylene bag with dosimeters and irradiated. The resulting dose-depth data is given in Table 1 for nominal 1 MeV electrons, and is also depicted in Figure 8. Curves A and B are plots of the

two runs made by RAI personnel using identical machines setting on an RDI Dynamitron. The voltage was set at 1 MeV. Curve C is a theoretical plot for 1 MeV electrons. The points D indicate data obtained by RDI for a single polyethylene slab and was not corrected to unity density. The Figure shows that the curves deviate from the theoretical 1 MeV plot and are more indicative of a lower energy electron than the settings indicate. This deviation is due to experimental conditions and machine characteristics. The fact that the experimental curve does not duplicate the theoretical curve is of minor importance for our purpose since the main aim of the experiment was to produce films with known doses. What is more important is that curves A and B duplicate each other since this indicates the precision and reproducibility of each run. However, it is apparent from this data that dosimeters are necessary in future runs as a quality control measure to assure reproducible crosslinking of the films.

Although the exact dose (and for that matter the degree of crosslinking) is known, the amount of usable films within a desired dose range is very limited. This is illustrated by selecting the 90 Mrad dose level. From Table 1 it is seen that only the film between the 19th and 37th layers is usable from the first crosslinking run. The second irradiation yields 90 ± 5 Mrads crosslinked film between the 15th and 20th layers. From the curves it appears that we could use film from the 33rd to 68th layer (based on corrected depth) for the first irradiation. For the second irradiation we would eliminate from this range film from the 43rd to 62nd layer. It can be readily seen from this analysis that a better procedure for crosslinking film was available.

A new simple procedure which has been adapted assures uniform crosslinking of all the film irradiated and reduces the deviation between films to less than 2.3%. This procedure involves irradiating the half penetration thickness of the corrected depth dose curve to one half the required dose and then reversing the packaged film, back to front, and irradiating again for one half the required dose. The total dose received by the stack of film using this technique is illustrated in Figure 9. As shown in the solid curve, the surface dose at the first layer of the stack corresponds to about 60% of the maximum dose at the 73rd layer of the film, which is as would be expected from the theoretical dose-depth relationship. The dotted curve represents the total dose imparted to the whole stack of film, which now is almost a

Table 1

Dose-Depth Relationship of Crosslinked Films

Data From 1st Irradiation

Layer No.	Corrected ^(a) Depth (Mils)	Dose Per Pass Mrads	Total Dose Mrads	Gel %
1	23.81	2.64	73	72
10	33.01	3.00	84	89
19	42.56	3.22	90	90
28	51.96	3.35	94	91
37	62.16	3.30	92	88
46	70.42	3.10	87	84
55	80.16	2.74	77	87
67	97.46	2.20	62	86
79	104.76	1.66	47	81
85	110.27	1.35	38	78
91	116.76	1.08	30	74
97	122.61	0.84	24	66

Table 2

Dose-Depth Relationship of Crosslinked Films

Data From 2nd Irradiation

1	23.81	2.35	65.8
5	27.96	2.50	70.0
15	38.41	3.25	91.0
20	42.30	3.35	93.8
30	53.96	3.65	102.2
40	64.36	2.95	82.6
45	69.76	2.70	75.6
50	74.76	2.80	78.4
60	84.76	2.50	70.0
65	90.16	2.25	63.0
80	106.76	2.00	56.0
98	123.76	1.15	32.2
126	-	0	0
141	-	0	0

(a) The average film thickness was 1.13 mils for a nominal 1.0 mil material

(b) The electron prior to impinging on the film penetrates

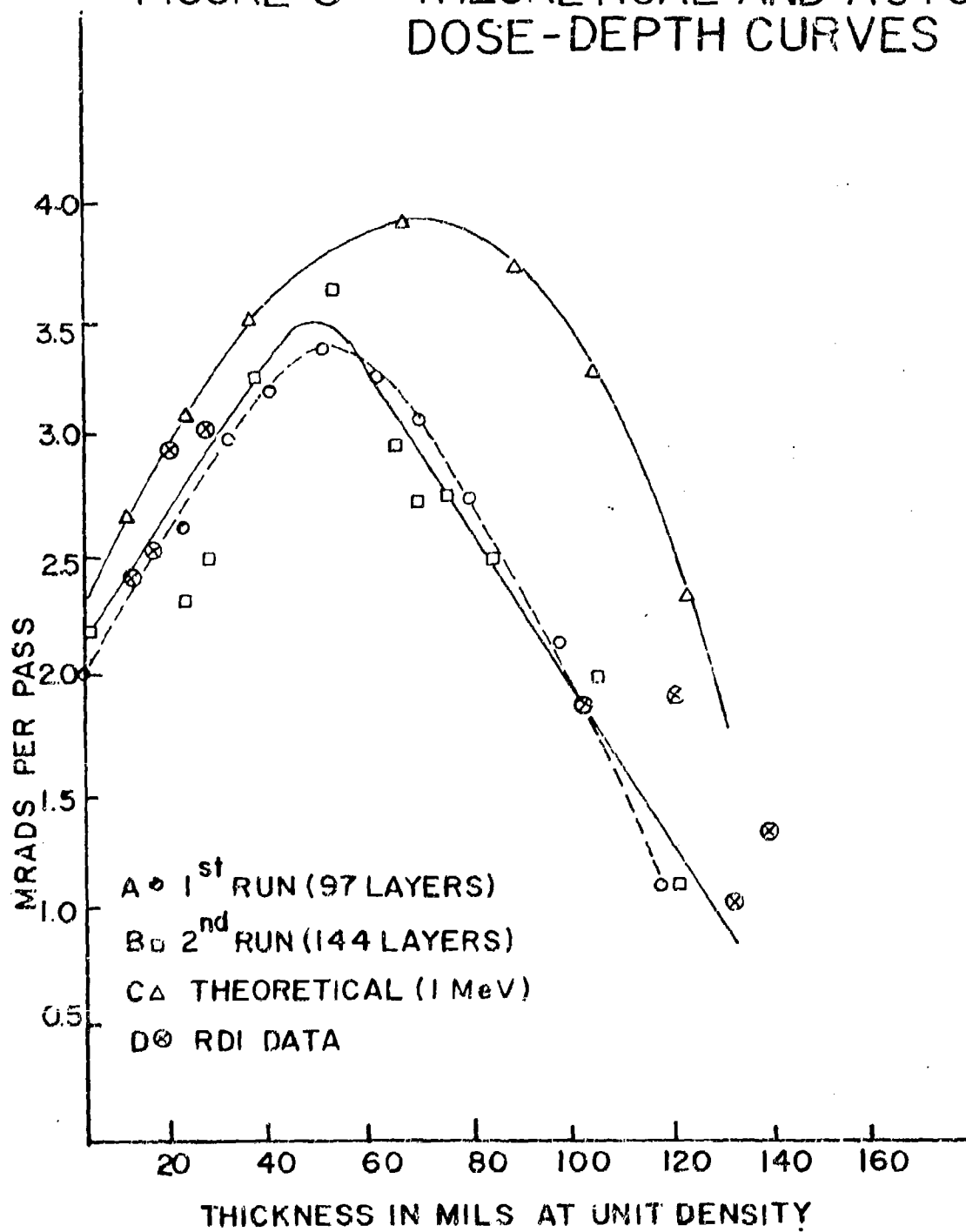
1. 2 mil titanium window

2. 6 inches of air and

3. 6 mils of polyethylene (i.e., the bag)

This is equivalent to 22.76 mils of unit density: the depth of film = layer number x average thickness x .922 + 22.76.

FIGURE 8 THEORETICAL AND ACTUAL DOSE-DEPTH CURVES



DOSE-DEPTH CURVE FOR 1.5 MeV ELECTRONS

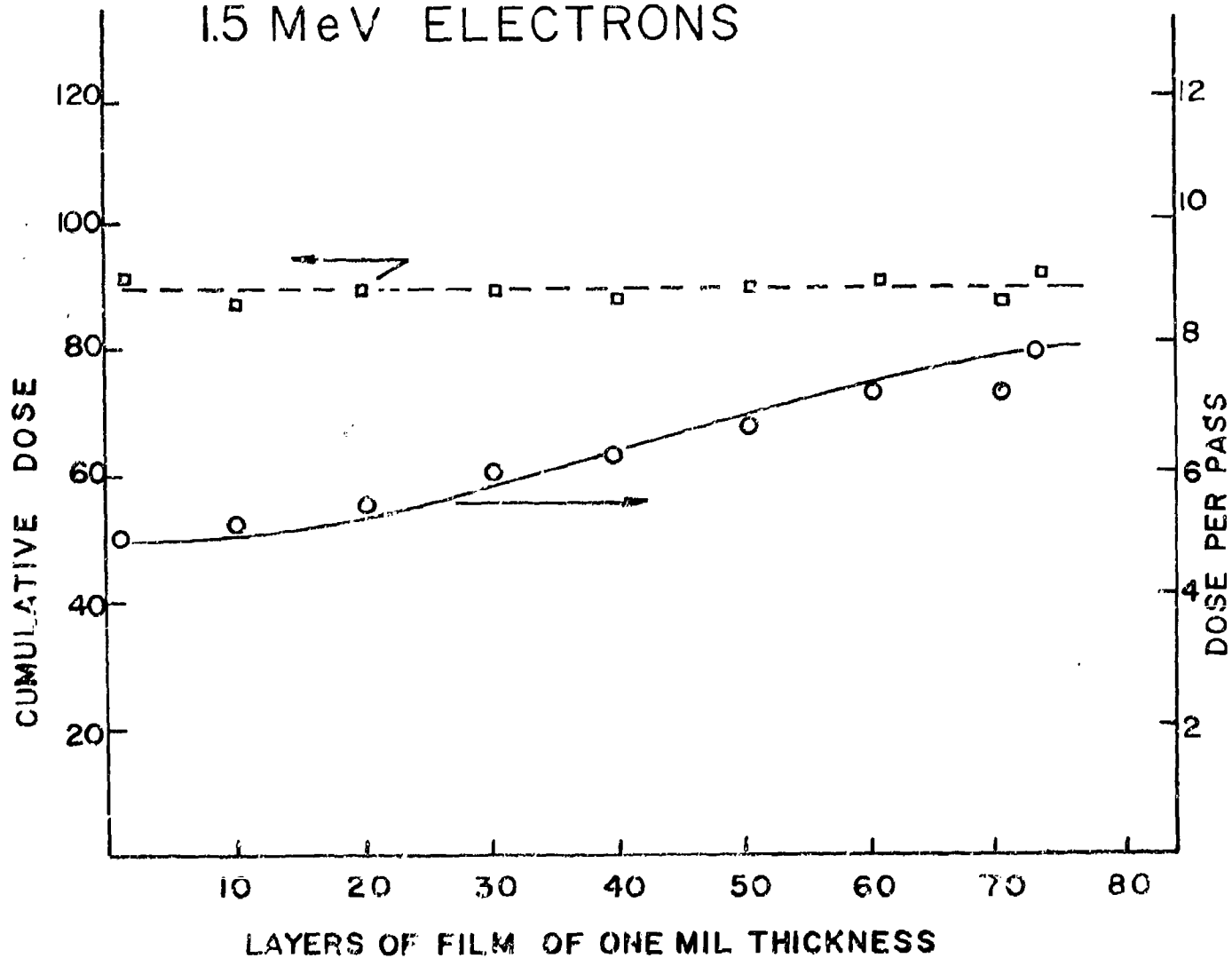


FIGURE 9

straight line. The dose received was calculated to be 89 ± 2 Mrads. The linearity of the curve reflects the uniformity of dose received.

Ideally the film stack should be reversed every second pass. However using the technique indicated above and reversing the film stack only once gives excellent results. The 5000 feet of film irradiated for phase three of this program was done using this procedure. The dose-depth relationship for 1.4 MeV and for the dose-half-depth relation found are given in Figures 10 and 11. The surface and exit dose for every pass was also determined using dosimeters. These figures are shown in Table 3. This procedure gives an average total dose of 94.3 Mrads but is not a true indicator of the dose received by each layer of film since it includes the six mil bag.

The importance of the development of this method which assured uniformity of crosslinking cannot be stressed too strongly. The extent of crosslinking has also been shown to be of significant importance. The effects of ionizing radiation on polyethylene have been extensively reviewed by Charlesby⁽⁹⁾. Polyethylene, on reaction with ionizing radiation degrades and crosslinks simultaneously. The ratio of degradation to crosslinking (P_0/q_0) is given as 0.2 which indicates a predominance of crosslinking.

The effect of the radiation dose on the film irradiated here was determined from the gel content and the M_c value. As crosslinking progresses the linear polyethylene is converted to a three dimensional structure which is insoluble in common solvents for the uncrosslinked polyethylene. The procedure for determining the gel content is given in the experimental sections. The effect of irradiation on gel formation is given in Figure 12. The gel formation as a function of depth is given in Figure 13. These figures were derived from data obtained from the initial irradiation using 1 MeV electrons. The gel content rises rapidly up to a dose of 30 Mrads and falls off rapidly with thickness above 120 mils.

These figures reflect the importance of using a minimum of thirty megarads to effect a significant degree of crosslinking, maintaining a maximum thickness of 120 mils when

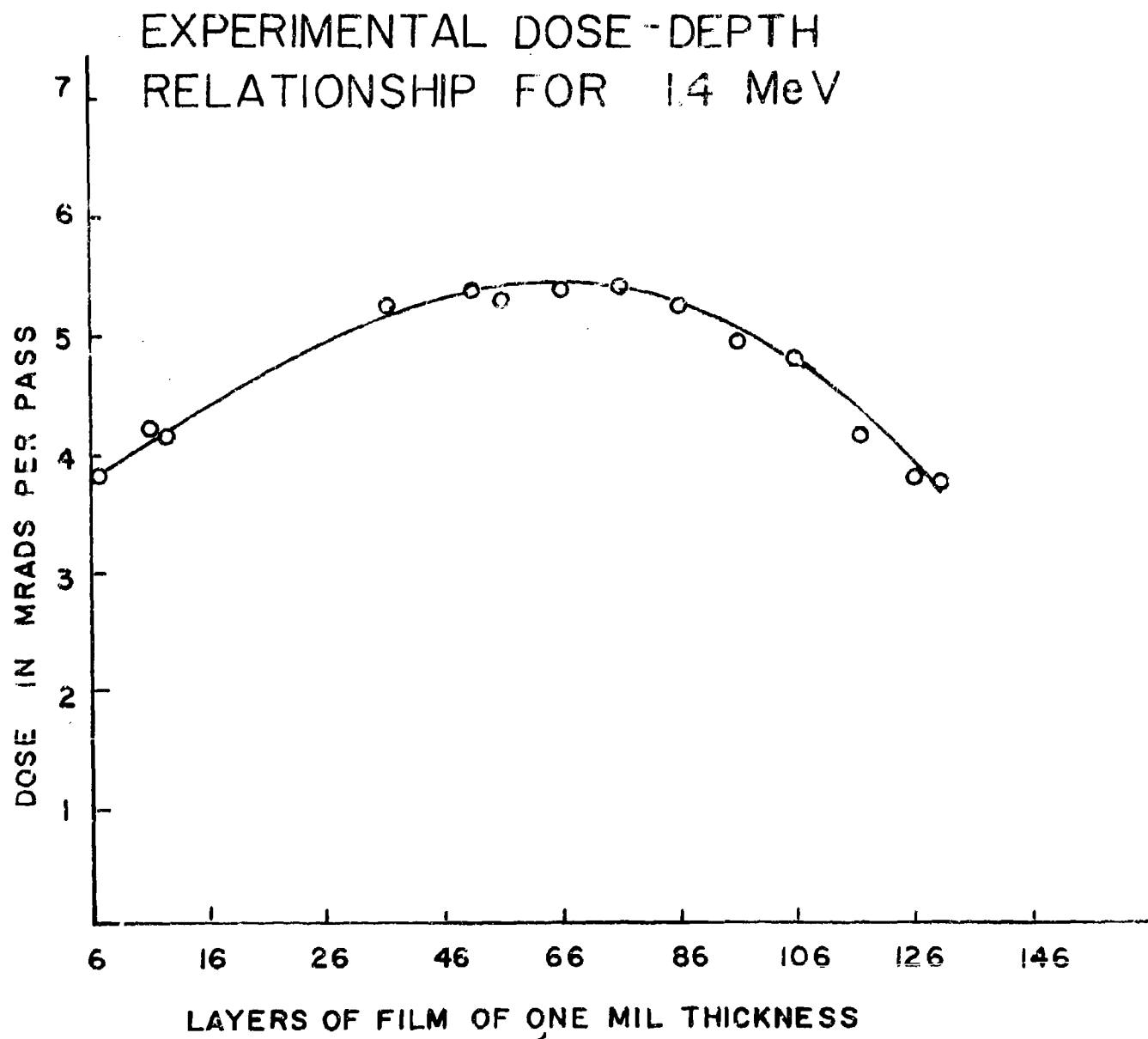


FIGURE 10

EXPERIMENTAL DOSE-HALF DEPTH
RELATIONSHIP FOR 1.4 MeV

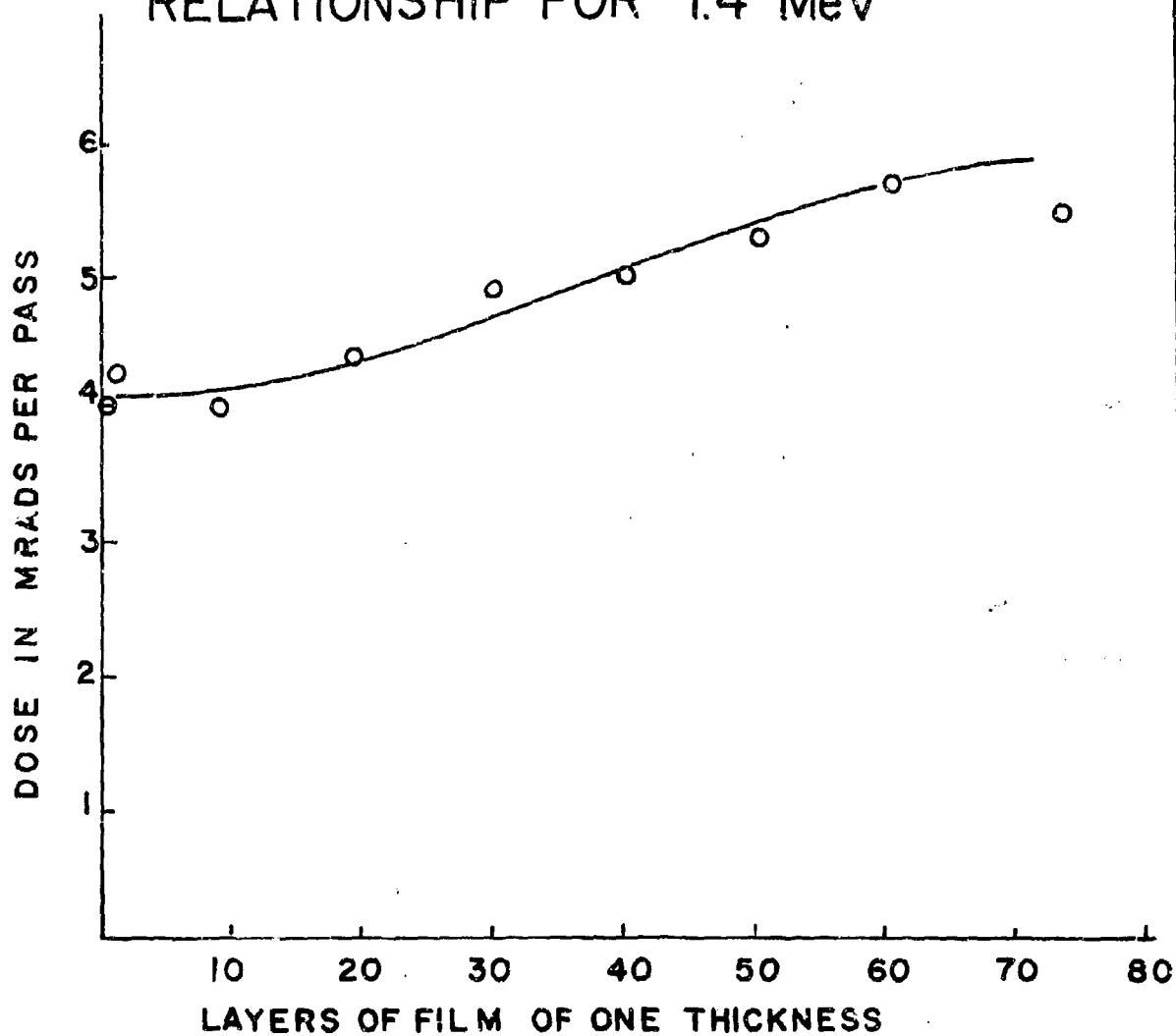


FIGURE II

Table 3

Surface, Exit and Average Dose of Crosslinked Film
for 5000 Foot Sample

Pass	Dose Mrad		Average
	Surface	Exit	
1	3.8	5.5	4.65
2	3.8	5.5	4.65
3	3.8	5.5	4.65
4	3.8	5.5	4.65
5	5.0	7.24	6.12
6	4.75	6.88	5.81
7	3.75	4.70	4.23
8	3.75	4.70	4.23
9	4.00	5.00	4.50
10	3.75	5.00	4.38
11	4.00	5.20	4.60
12	4.00	5.20	4.60
13	4.10	5.25	4.65
14	4.10	5.50	4.80
15	4.20	5.15	4.68
16	4.20	5.25	4.72
17	4.00	5.00	4.50
18	3.75	5.50	4.63
19	4.00	5.25	4.63
20	4.20	5.00	4.60
Total			94.31

FIGURE 12 GEL FRACTIONS OF
IRRADIATED PHILLIPS 1712 VS DOSE

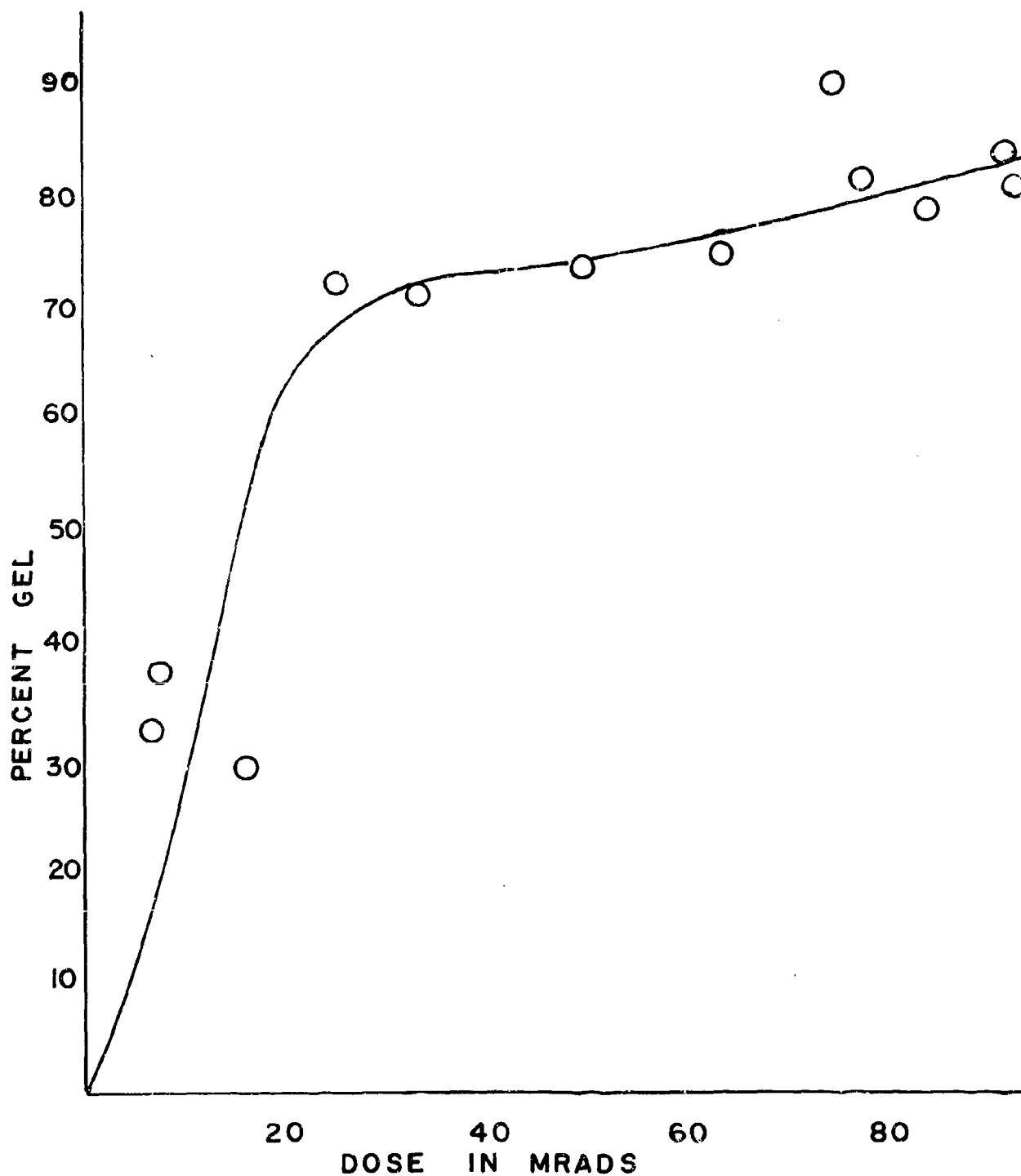
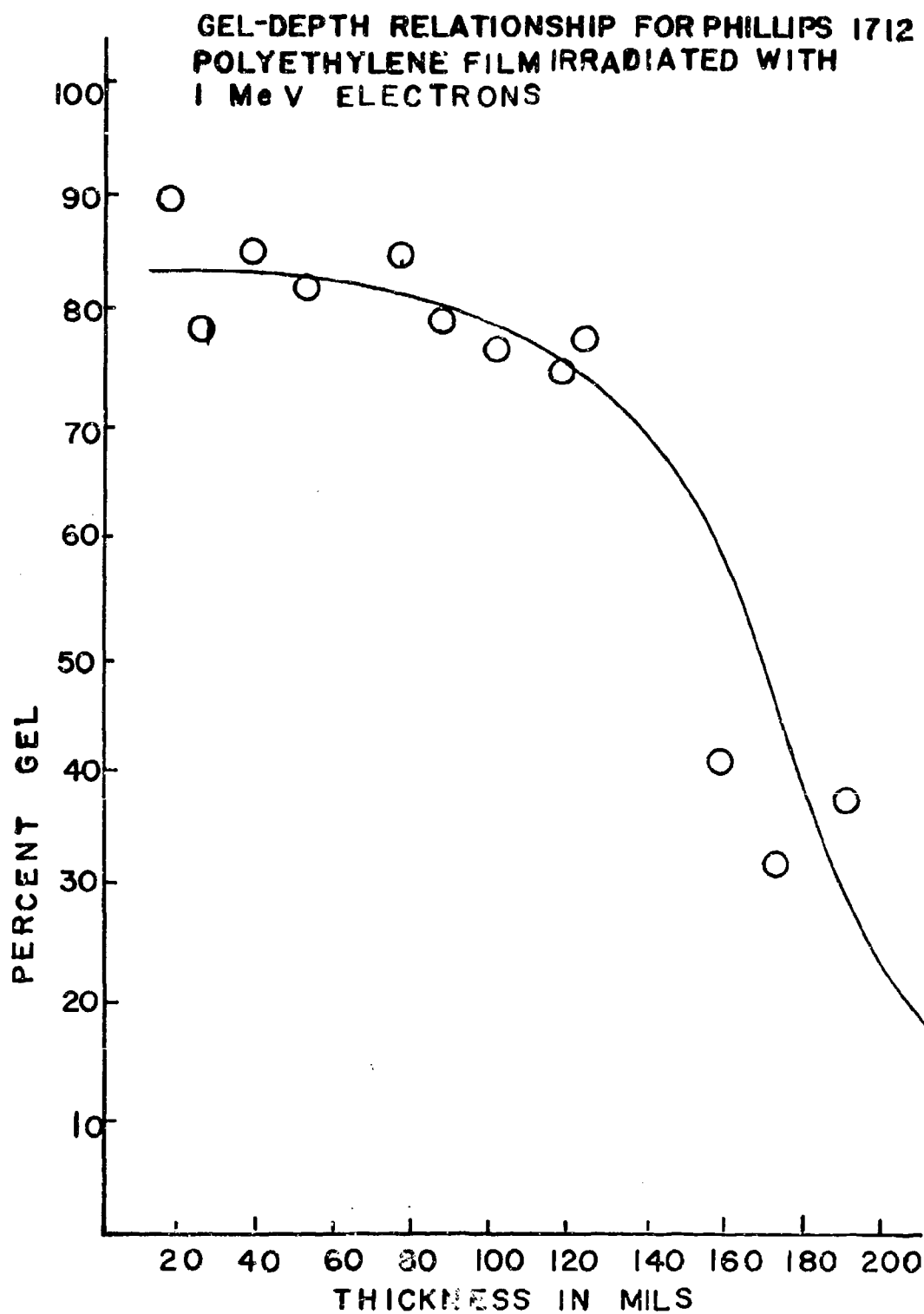


FIGURE 13



irradiating with 1 MeV electrons and using a more sensitive parameter for measuring crosslink density above 30 Mrads of irradiation.

As noted, above 30 Mrads. the gel content is a poor indicator of the dose and crosslinking density since the gel content at 40 Mrads of radiation is not much different from that produced at 100 Mrads. Above 30 Mrads it is, therefore, necessary to determine the M_c values of the crosslinked film. This value is related to the molecular weight between crosslinks. As the radiation dose increases, the M_c value decreases significantly. This is indicative of a continuation of crosslinking beyond the gel stage and a tightening of the film network. This additional crosslinking could be responsible for the decreased diffusion of zincate into the film and the subsequent plating of the zinc in the film. The determination of the M_c value is given in more detail in another section of this report.

3.2 Effect of Base Film on Separator Properties

The molecular properties of the base polymer used in preparing film for use in secondary silver-zinc batteries is of singular importance. The crystallinity, molecular weight distribution and absence of low molecular weight fractions are controlling parameters relating to the efficiency of crosslinking and the extent of extraction in a caustic environment when the graft is a cationic exchanger.

The three base films selected for evaluation after preliminary screening were precrosslinked to 30, 50 and 90 megarads, grafted with acrylic acid and cycle-tested under identical conditions. Films with zero and 70 Mrads were also tested. The results of these tests are given in Table 4 and Figure 14.

Two factors are evident from Figure 14 (1) as the pre-crosslinking dose is increased, the cycle life of the grafted film increases and (2) the cycle life is some function of the base films at high dose. Since the three films all received the same dose, the difference in cycle life can only be explained by differences in the properties of the resins alone.

Properties of the resin obtained from the manufacturer were density and melt index. More important data for our purpose was obtained from gel permeation chromatography (GPC)⁽¹⁰⁾. The interpretation and methods of GPC analysis are too involved to discuss here. The reader is referred to the literature particularly that cited in reference 10. Essentially, the GPC chromatogram gives a size distribution of the polymer species, and by calibrating against certain standards, the number average and weight average of the polymeric material can be determined. The relationship between molecular weight and elution volume (the calibration curve) has been obtained mostly for linear polymers. Branched low density polyethylene has only been recently studied by Wild and Guliana⁽¹¹⁾. Their calibration curve for low-density polyethylene has been used to obtain the molecular properties of the three films evaluated. Figures 15, 16 and 17 are the differential molecular weight distribution curves for Phillips 1712, USI-280 and Bakelite DFD 0602. Figures 18, 19 and 20 are the cumulative molecular weight distribution curves for these films. Data relating to these resins are given in Table 5.

Table 4

Effects of Base Film and Precrosslinked
Dose on Cycle Life

Expt No.	Type of Film	Pre- crosslinked Dose (Mrads)	Monomer Type	Cycle Life in 3 Plate Cell at 40% Depth of Discharge
211-32-2	P 1712	90	AA	182 Shorted
211-36-2	P 1712	50	AA	46 Shorted
211-38-2	P 1712	30	AA	42 Shorted
211- 6-6	P 1712	0	AA	30 Shorted
211-48-1	P 1712	70	AA	112 Shorted
211-32-1	USI-280	90	AA	190 Shorted
211-36-1	USI-280	50	AA	46 Shorted
211-38-1	USI-280	30	AA	7 Shorted
211-122-P	USI-280	0	AA	19
211-47-1	USI-280	70	AA	108 Shorted
211-32-3	B DFD 0602	90	AA	316 Shorted
211-36-3	B DFD 0602	50	AA	47 Shorted
211-38-3	B DFD 0602	30	AA	34 Shorted
211-56-2	B DFD 0602	0	AA	35 Shorted
211-52-7	B DFD 0602	70	AA	130 Shorted

EFFECT OF BASE FILM AND PRECROSSLINKED DOSE ON CYCLE LIFE

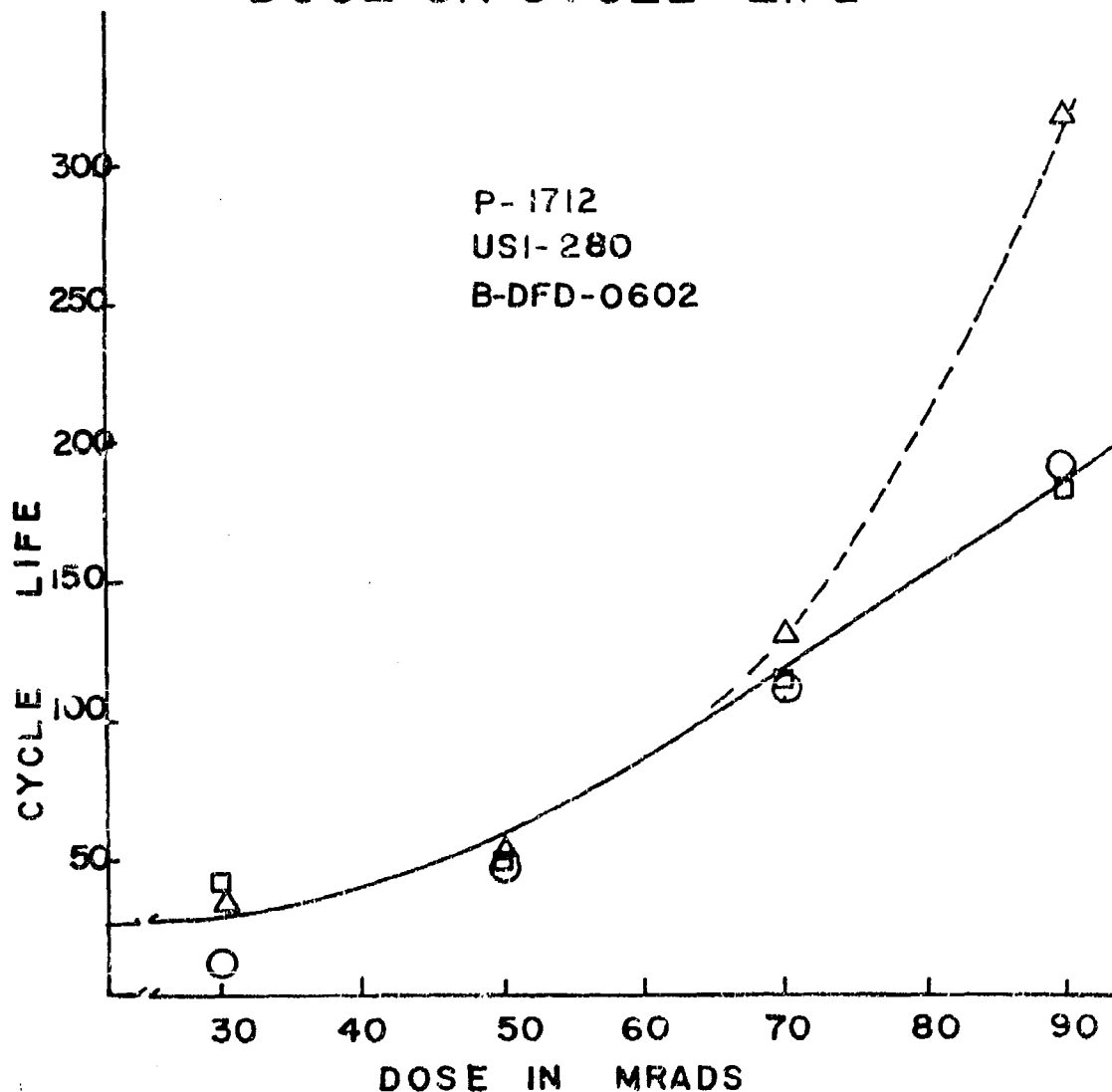
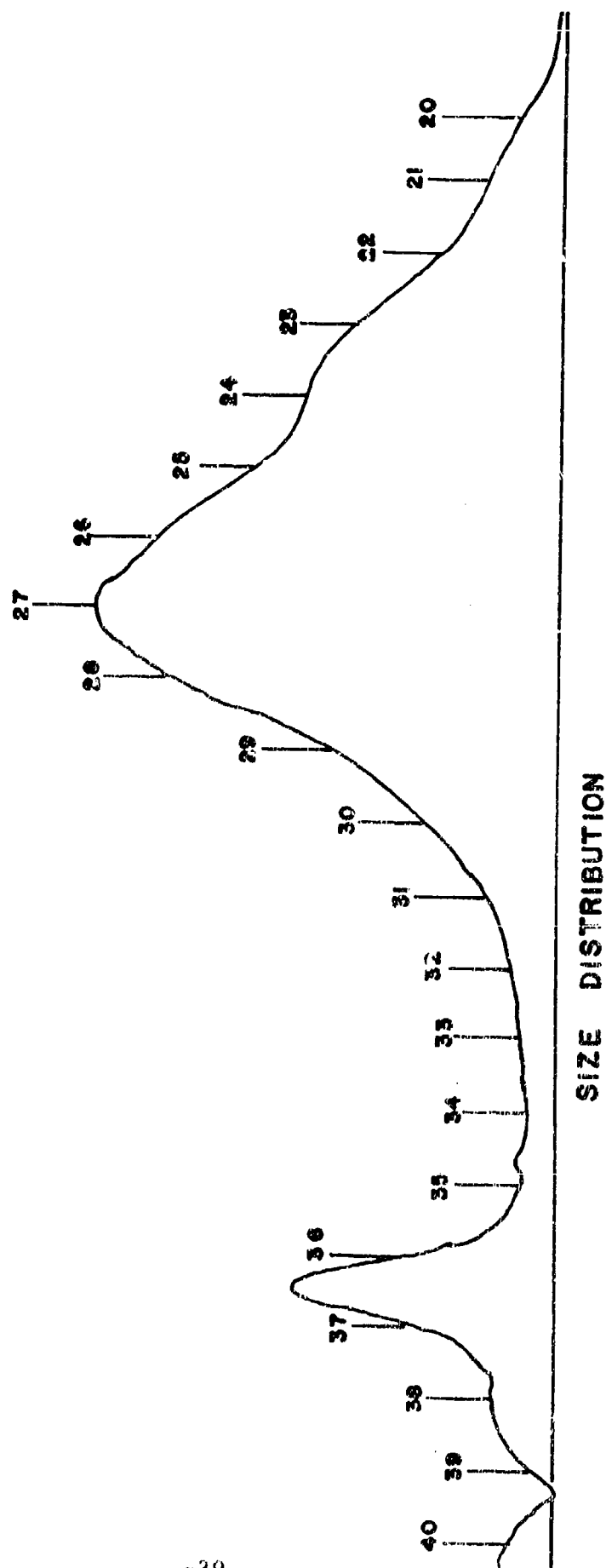


FIGURE 14

FIGURE 15 DIFFERENTIAL MOLECULAR WEIGHT
DISTRIBUTION CURVE FOR PHILLIPS 1712



DIFFERENTIAL MOLECULAR WEIGHT
DISTRIBUTION CURVE FOR USI-280

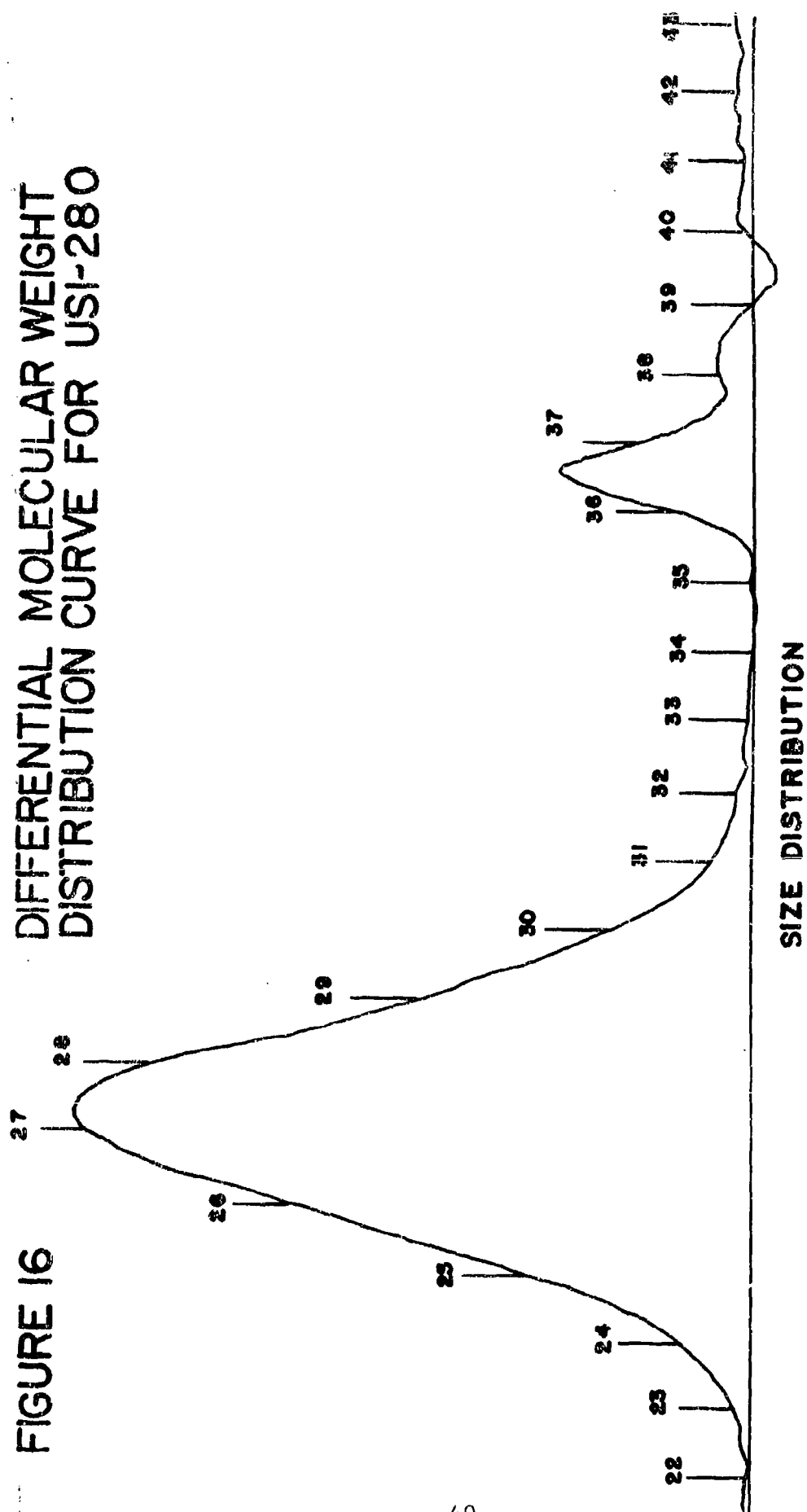


FIGURE 17 DIFFERENTIAL MOLECULAR WEIGHT DISTRIBUTION CURVE FOR B-DFD-0602

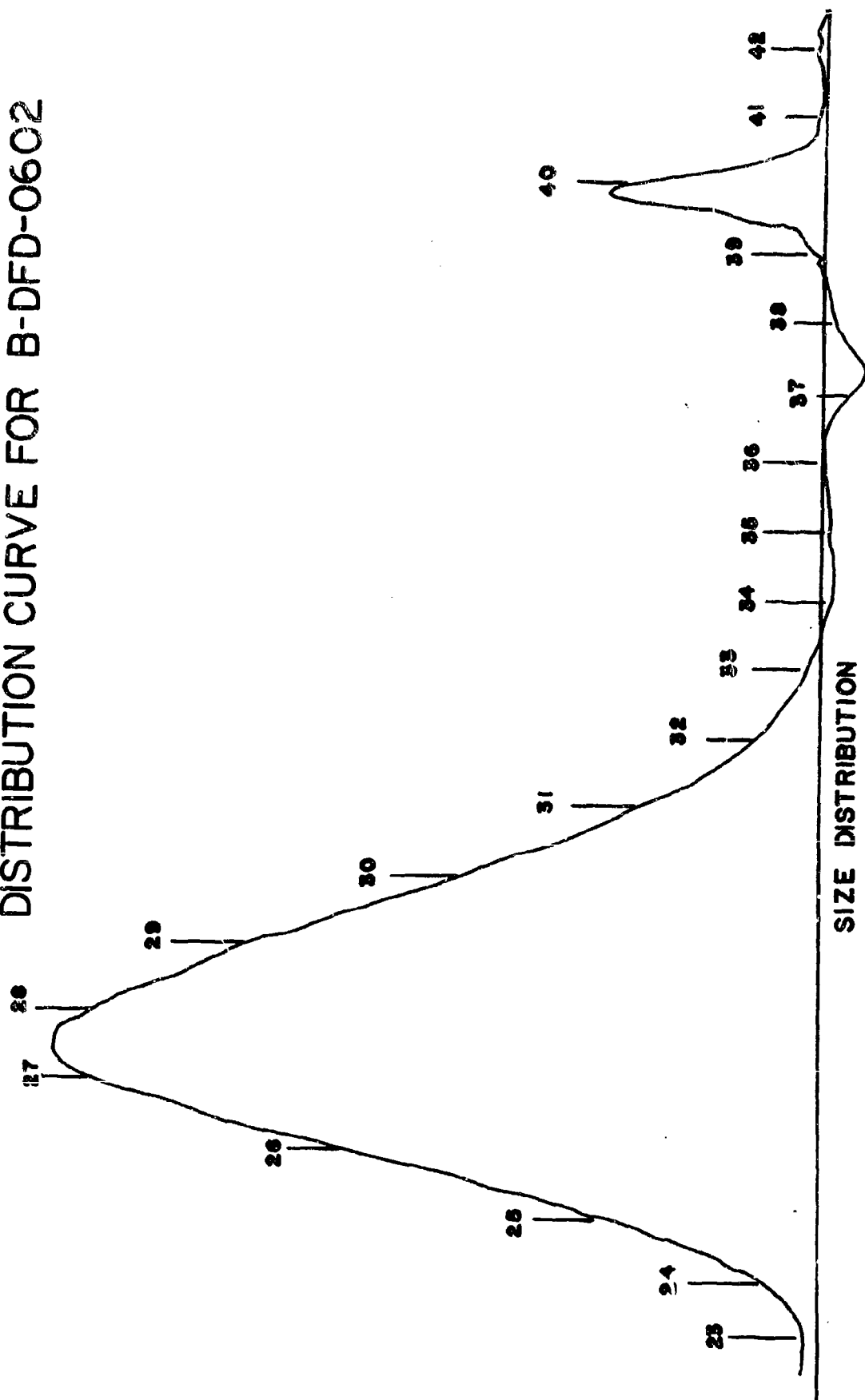


FIGURE 18 CUMULATIVE MOLECULAR WEIGHT
DISTRIBUTION CURVE FOR
PHILLIPS 1712

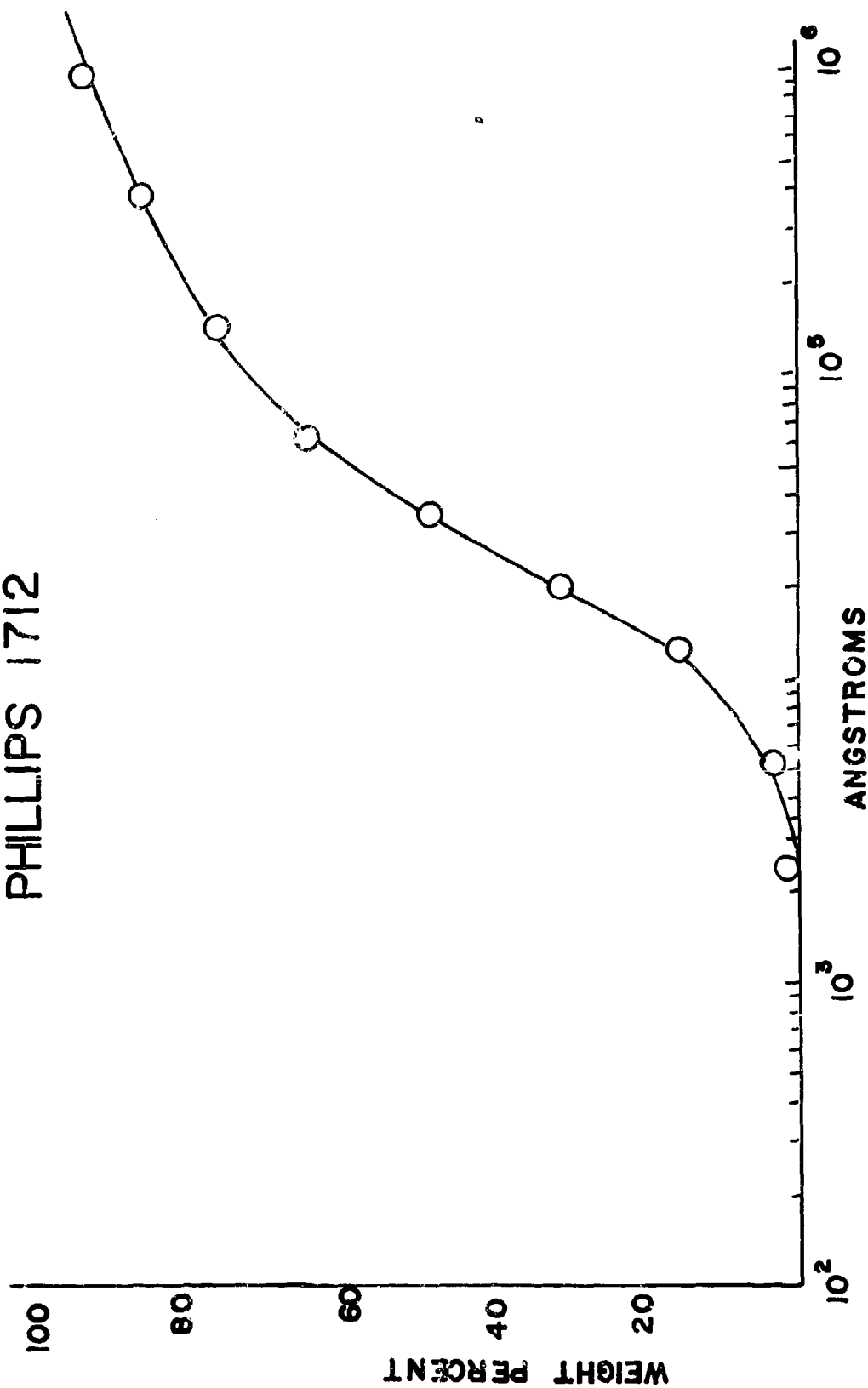


FIGURE 19 CUMULATIVE MOLECULAR WEIGHT
DISTRIBUTION CURVE FOR
USI-280

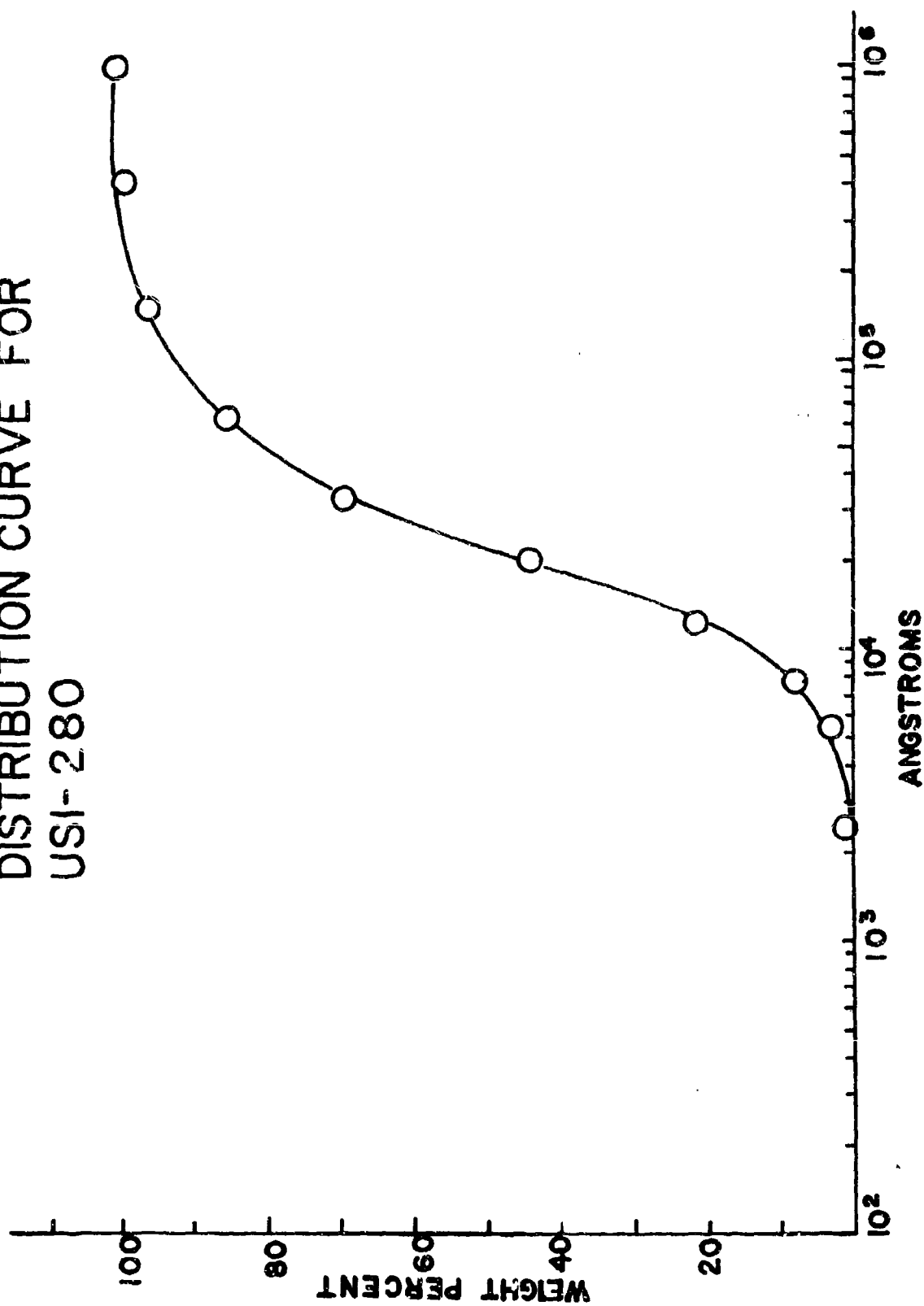


FIGURE 20

CUMULATIVE MOLECULAR WEIGHT
DISTRIBUTION CURVE FOR
B-DFD-0602

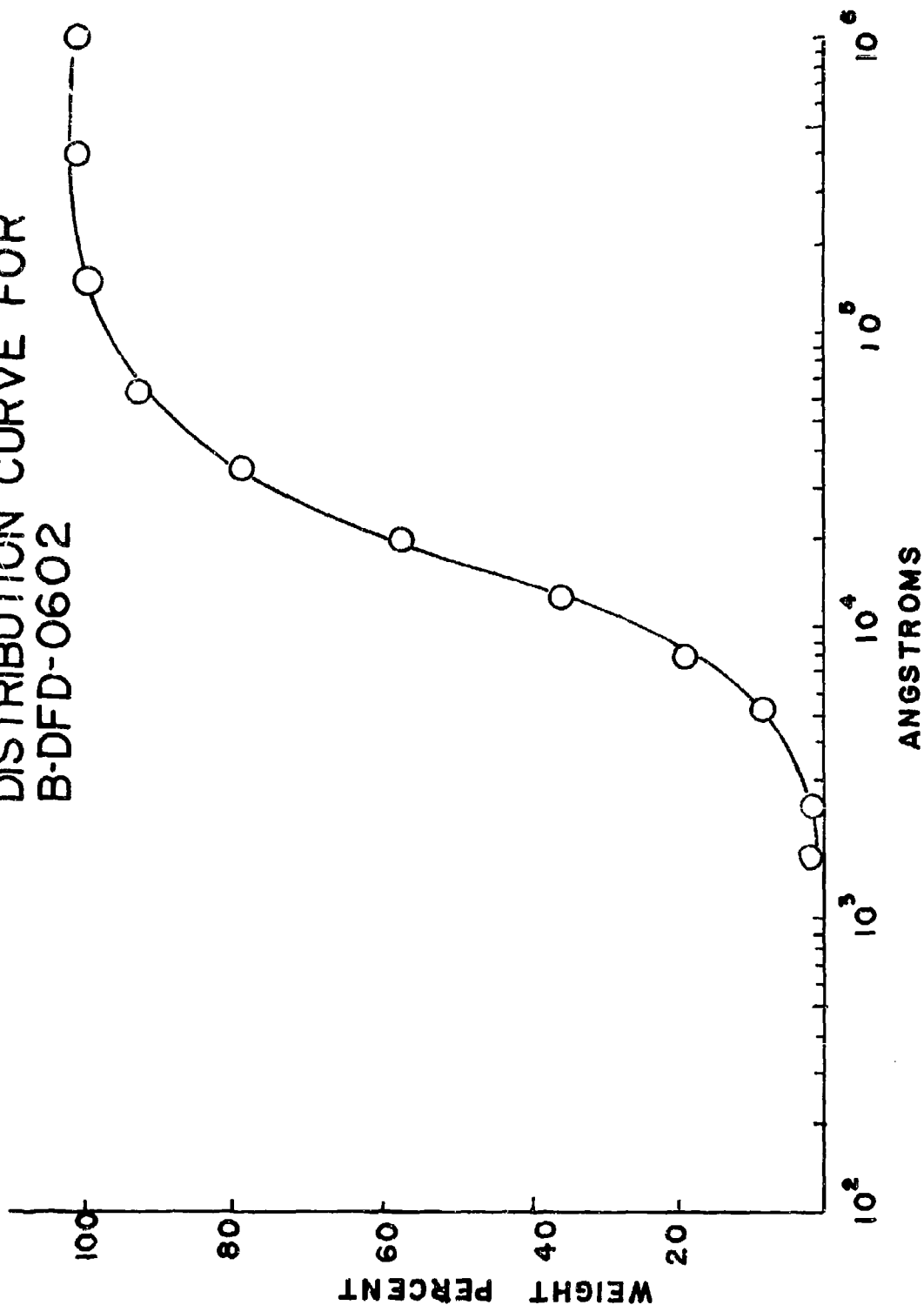


Table 5

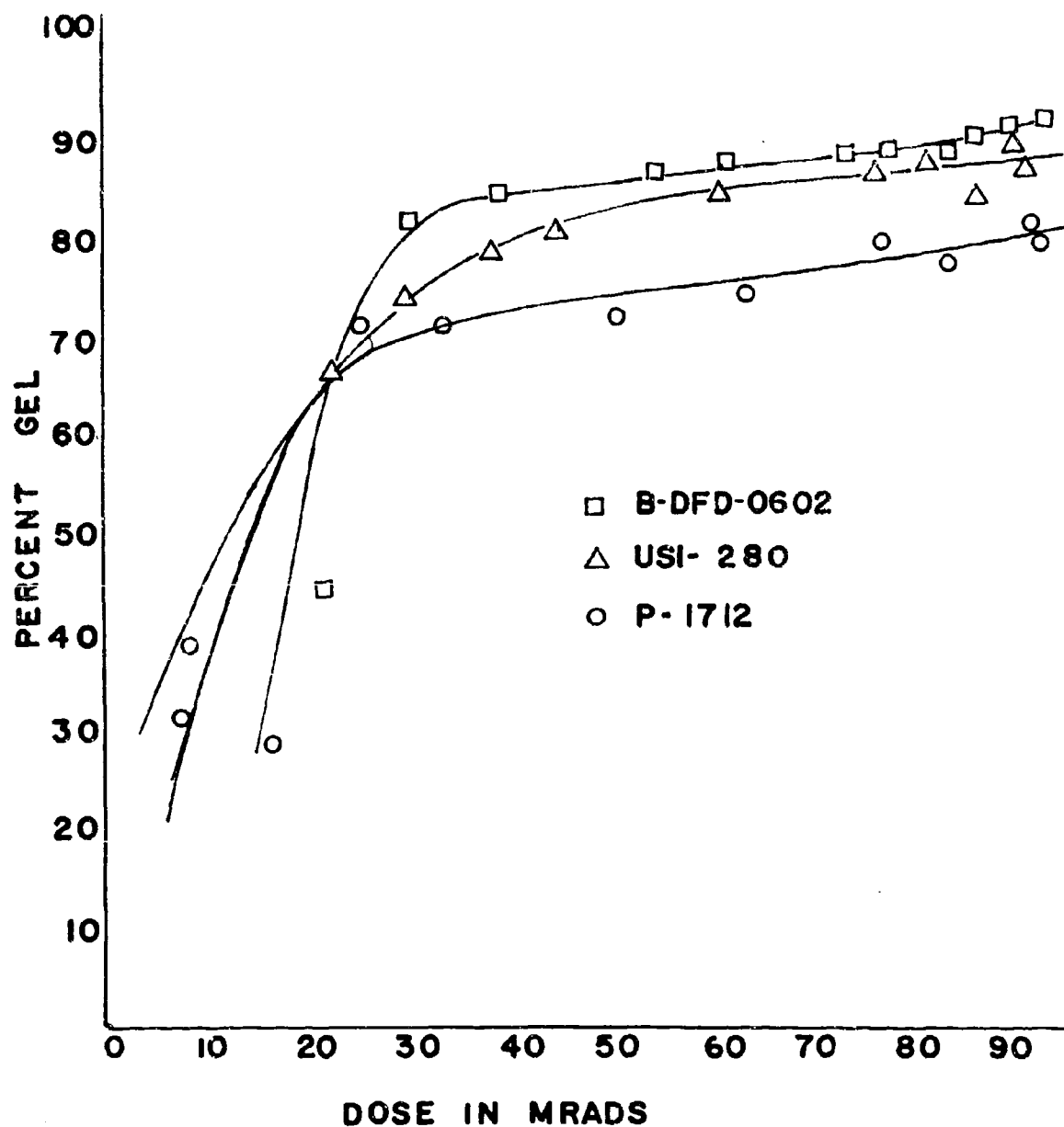
Characteristics of the Base Films

Film	From Manufacturer		From GPC		
	Density	Melt Index	\bar{M}_n	\bar{M}_w	\bar{M}_w/\bar{M}_n
P 1712	0.917	1.20	29,261	223,078	7.6
USI-280	0.922	1.40	22,362	58,303	2.6
B DFD 0602	0.922	0.75	17,135	34,468	2.0

The GPC curves are very instructive in that they show that the highest molecular weight resin does not correlate with lowest melt index. The data from Table 5 shows that the Phillips 1712 resin has the highest molecular weight averages but also has the widest molecular weight distribution. The Bakelite DFD 0602 resin has a relatively low molecular weight but has a very narrow distribution. Both the USI-280 resin and the Bakelite DFD 0602 appear to have a normal log distribution while the Phillips 1712 is bipopulate in character.

Charlesby⁽⁹⁾ has shown that the efficiency of radiation crosslinking is directly related to the molecular weight distribution. He has noted that above a particular molecular weight the narrower the molecular weight distribution, the more efficient the crosslinking per unit dose. Indeed, such behavior has been beautifully demonstrated by the gel-dose curve in this study. Figure 21 is a plot of the percent gel vs. dose. From this figure it can be seen that above 30 Mrads the percent gel is greater at equal doses for that resin having the lower molecular weight distribution and the gel content for the resin increases in the order Bakelite DFD 0602 > USI-280 > Phillips 1712. This order would be expected from the \bar{M}_w/\bar{M}_n i.e., the molecular weight distribution. Table 5 correlates with the gel curve as an inverse function.

FIGURE 21 GEL FRACTIONS OF
IRRADIATED POLYETHYLENE FILMS



At high radiation doses, above 30 Mrads, the change in gel content per unit change in dose is small. The relationship between crosslink density of each film at high radiation doses is more readily followed by the crosslink density q or the molecular weight between crosslinks M_c . In general, when the crosslinking efficiently is determined the sol fraction S , which is 1-gel fraction, is correlated with dose. Charlesby has shown that a plot of $S + S^{\frac{1}{2}}$ vs. $\frac{1}{r}$ is linear for a random molecular weight distribution and $\frac{1}{r}$ is approximately linear for many other forms of molecular weight distribution⁽⁹⁾. The equation relating sol fraction and total dose is given by

$$S + S^{\frac{1}{2}} = \frac{P_0}{q_0} + \frac{1}{q_0 u r} \quad 6$$

Where S = sol fraction, P_0 = fracture density per unit dose, q_0 = crosslinking density per unit dose, u = number average degree of polymerization and r = the total dose.

Assuming that the films all have random molecular distribution which is true for the Bakelite DFD 0602 and USI-280, but slightly off for Phillips 1712 both the slope and the intercept of the Charlesby-Pinner curve can be used to calculate the crosslinking density and M_c . The slope of the $S + S^{\frac{1}{2}}$ vs. $\frac{1}{r}$ curve is

$$m \text{ (slope)} = \frac{1}{q_0 u} \text{ and } q_0 = \frac{1}{mu} \quad 7$$

it then follows that

$$q = q_0 r \text{ or } q_0 = \frac{q}{r}$$

and $\frac{1}{mu} = \frac{q}{r} \text{ or } q = \frac{r}{mu}.$

From $M_c = \frac{w}{q}$ and (7) we get 8

$$M_c = \frac{wmu}{r} \quad 9$$

where w is the molecular weight of the repeating unit in the polymer. The intercept of the $S + S^2$ vs. $\frac{1}{r}$ curve is

$$C = \frac{P_0}{q_0} \quad 10$$

which is scission to crosslinking ratio and is obtained by extrapolating $1/r$ to zero, as r goes to infinity.

Data on the Charlesby-Pinner curve of the three films is given in Table 6.

Table 6

Intercept and Slope of Charlesby-Pinner Curve

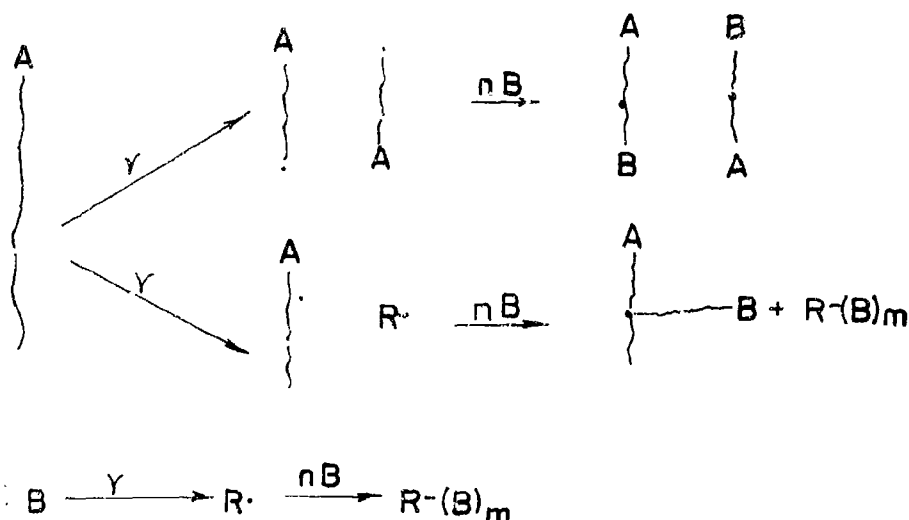
Base Resin	$\frac{P_0}{q_0}$	u	$\frac{1}{q_0 r}$	q_0	M_c
P 1712	0.38	1,045	18.99	0.51×10^{-4}	6.22×10^3
USI-280	0.29	798	13.39	0.94×10^{-4}	3.31×10^3
B DFD 0602	0.32	612	9.32	1.75×10^{-4}	1.77×10^3

This table shows that the Bakelite DFD 0602 has a much greater crosslinking density than the USI-280 which in turn has a greater crosslinking density than the Phillips 1712. Data given in this table is for film irradiated to 90 Mrads. The crosslink density, q_0 , of a model paraffin, octadecene in which u equals 18 has been given in the literature as 1.4×10^{-4} (12). If the last column in the table, the M_c value, is normalized by dividing each value by 1.77 it is readily seen that the crosslink density of the Bakelite DFD 0602 is double the USI-280 and over 3.5 time that

of the Phillips 1712 resin. This data reflects the tightness of the network structure of the three films and is indicative of a reduced "pore size".

3.3 Radiation Grafting of Films

Although there are numerous methods of grafting given in the literature, (13) (14), the method used here is that of direct grafting. It involves irradiation of a polymeric film in a solution of an organic acid monomer. Schematically,



where $A \sim A$ is the polymer, $A\cdot$, $A \sim \cdot$ are polymeric free radicals, $R\cdot$ is a low molecular weight radical or hydrogen atom, and B is the monomer. If the polymer is of the degradation type, then under radiation, the resultant reaction gives a block copolymer only, i.e., $A \sim B$. If, however, the polymer is of the crosslinking type, then the reaction yields a graft copolymer, i.e., $A \sim A$, and homopolymer $R-(B)_m$.

Since polyethylene crosslinks on exposure to radiation⁽⁹⁾ the formation of both graft copolymer and homopolymer is to be expected. Another source of homopolymer is due to radiolysis of the monomer acid itself. The grafting scheme given above is very simple. It must be realized, however, that there are many parameters unknown that affect grafting such as G_R values of

the polymer, monomer, solvent and interlayer (G_R is the free radical yield per 100 eV absorbed in the irradiated medium) the energy transfer process, the dose, the dose rate, the atmosphere, the additive, the diffusion of monomer to the polymer film, the temperature of the system, and the interdependence of all these parameters as the grafting reaction proceeds. The interplay of these parameters makes the study of grafting very complex. Detailed studies on grafting are found in references (3), (9) and (13). Of importance in this report is the fact that the grafted membranes should have the required electrical properties. Under the conditions given in the Experimental Section, our resultant grafted membranes have about 70 - 80% graft by weight, and an electrical resistance in 40% KOH of about 20 - 60 milliohm-in.² at room temperature.

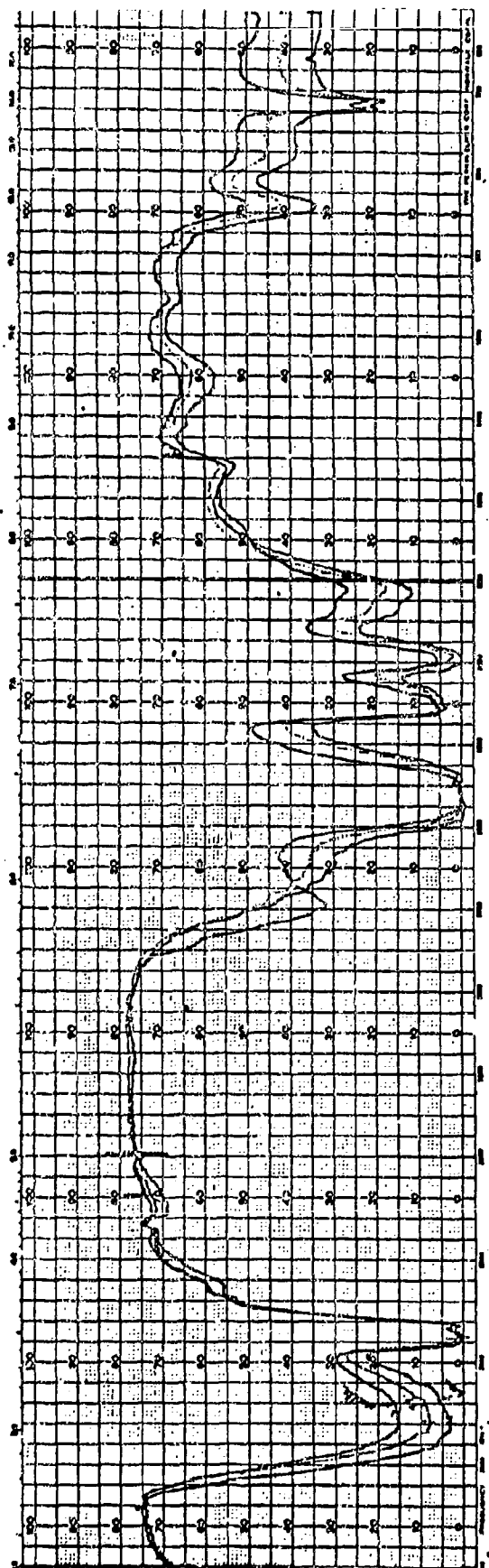
The substantiation that we have a grafted film having a primary bond between the polyacrylic or methacrylic acid formed and the polyethylene backbone is evidenced by the stability of the graft in 40% KOH, retention of the exchange capacity after extraction at elevated temperature, cycle life in a battery and its infrared spectrum. Figure 22 is an infrared spectrum of the grafted membrane. The characteristic carbonyl peak persists regardless of the extraction conditions used to remove the ionic polymer.

3.3.1 Effects of Monomer Concentration on Percent Graft

Accurate kinetic data is important in designing a procedure to give a uniform graft polymerization. In principle, conventional free radical polymerization reactions and kinetics should be applicable to radiation grafting systems. In practice, however, the situation is not quite straight forward because the interplay of various parameters and reaction conditions. The gel effect, chain transfer, phase separation, and diffusion effects are but a few of the many factors which can seriously affect the reaction kinetics.

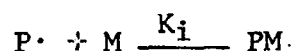
The simplified grafting kinetics for radiation grafting has been described by Chapiro(3). This consists of initiation, propagation, termination and chain transfer. The following rates are

FIGURE 22 INFRARED SPECTRA OF GRAFTED MEMBRANE

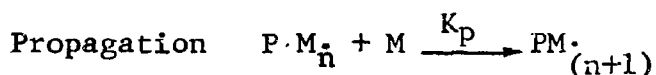




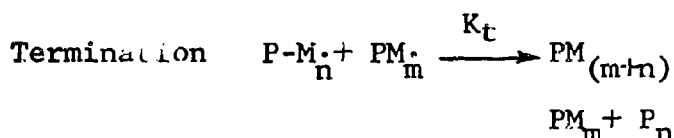
Rate = $k_d I$



Rate = $k_i (P\cdot) (M\cdot)$



Rate = $k_p (PM_n\cdot) (M)$



Rate = $2k_t (PM\cdot)^2$



Where I = Intensity of radiation

P = Polymer backbone

$PM\cdot$ = Polymeric radical

$P_m, P_n, P_{(m+n)}$ = Graft copolymer

M = Grafting monomer

SX = Chain transfer agent.

If one assumes that the length of the grafted chain is long, that the free radicals are in its steady state, and the chain transfer can be neglected, the rate of grafting is then given by

$$R_p = k_p (PM_n\cdot) (M)$$

$$= k_p \left(\frac{R_i}{2k_t} \right)^{\frac{1}{2}} (M) = k_p \frac{k_d (I)^{\frac{1}{2}} (M)}{2 k_t^{\frac{1}{2}}} \quad 11$$

This equation predicts that the rate of polymerization is proportional to the square root of radiation intensity, and to first power of monomer concentration. Table 7 gives data on the grafting of Bakelite DFD 0602 film precrosslinked to 90 Mrads with methacrylic acid, under constant dose rate and total dose conditions.

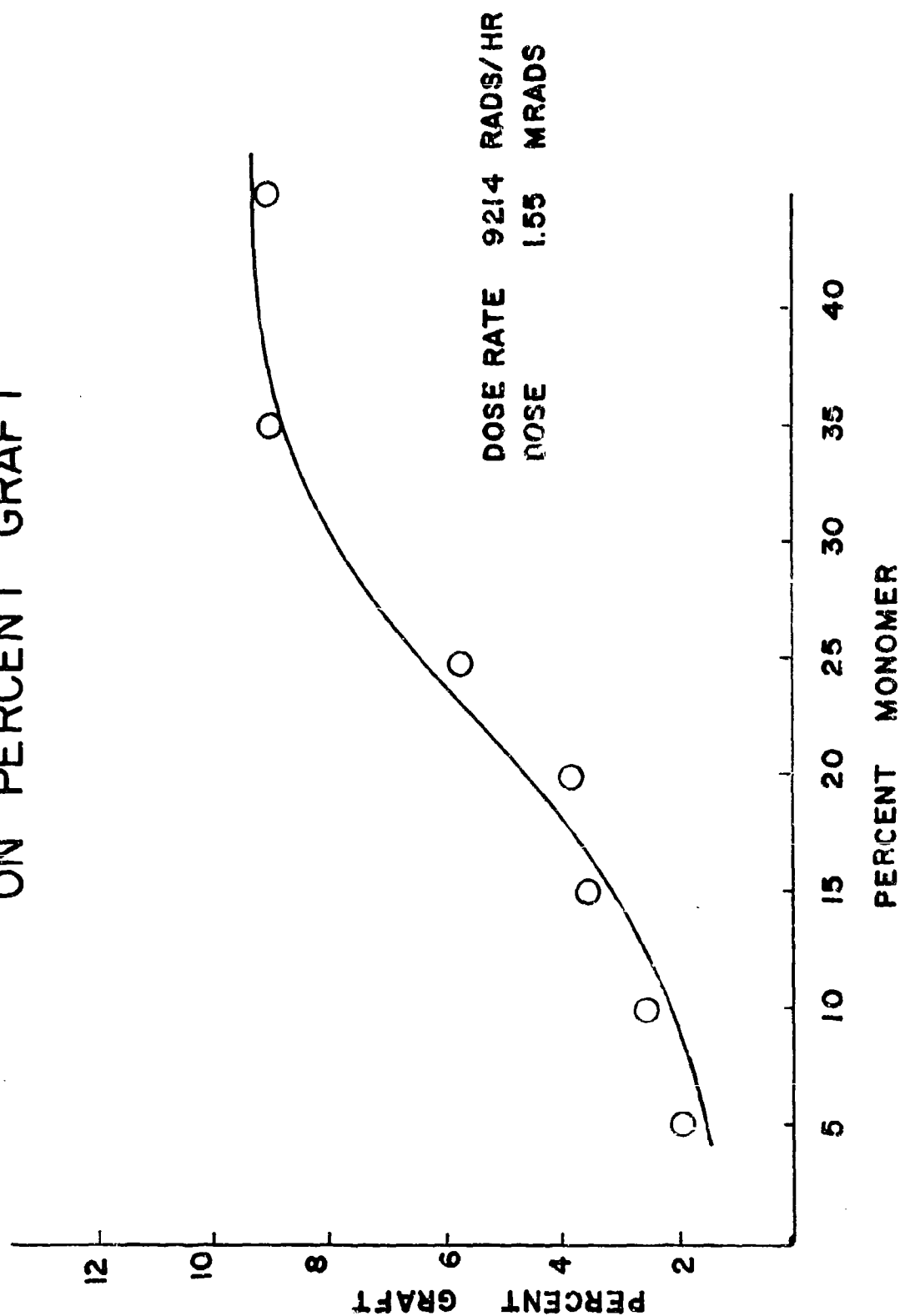
Table 7

Effect of Monomer Concentration on Percent Graft.
Bakelite 0602 Precrosslinked 90 Mrads; Dose Rate
of Grafting 9214 rads/hr; Total Dose 1.55 Mrads

Sample No.	Monomer Concentration	% Graft	R_p % hr ⁻¹	Resistance
213-30-5	25% MA	56.50%	0.336	76.2 Milliohm-in ²
213-30-6	20% MA	36.67%	0.218	103.5
213-30-7	15% MA	33.85%	0.201	126.0
213-30-8	10% MA	24.33%	0.145	179.5
213-30-9	5% MA	19.23%	0.114	480
213-30-10	35% MA	89.32%	0.532	41.8
213-30-11	45% MA	91.93%	0.547	33.0

It is obvious that the percent graft increases with increasing monomer concentration, and levels off at about 35 to 45% monomer concentration, as seen in Figure 23. If we divide the percent graft by the time of grafting, an average

FIGURE 23 EFFECT OF MONOMER CONCENTRATION
ON PERCENT GRAFT



rate of grafting polymerization R_p is obtained in percent graft per hour. An approximate linear relationship between the rate of polymerization and the monomer concentration exists as required by the equation.

$$R_p = k_p \left[\frac{R_i}{2k_t} \right]^{\frac{1}{2}} (M) = \frac{k_p k_d (I)^{\frac{1}{2}} (M)}{2k_t^{\frac{1}{2}}}$$

The slope of this equation $k_p \left[\frac{R_i}{2k_t} \right]^{\frac{1}{2}}$ is obtained from a plot of R_p vs. M .

Figure 24 shows such a relationship, disregarding the highest monomer concentration where other factors such as the rate of diffusion of monomer effect the kinetics. If we can show also that the rate of grafting is proportional to the square root of I the intensity of radiation, it is quite possible that the grafting reaction proceeds according to the above mechanism scheme.

The effect of percent graft on the electrical resistance of the separator is also tabulated in Table 7 and is shown in Figure 25. From this figure it is seen that the electrical resistance rises abruptly below 30% graft. This brings in an intriguing question of uniformity of graft. Actually, the percent graft in Table 7 is a grand average of the increase in weight over a film area of 1 x 25 ft². A non-uniform graft could exhibit both high and low electrical resistance spots, which are very undesirable in a battery. In general, visual inspection is a gross indicator of the uniformity of graft, but certainly is not totally reliable. A quality control method was developed to check the uniformity of graft. The method makes use of light absorption of the functional group in the grafted chain. The carboxyl group of acrylic or methacrylic acid has been shown to absorb both ultra-violet (250 mμ) and infrared light (5.8μ)(15). In addition, basic dyes that are accepted by the carboxyl groups absorb visible light. The infrared spectrum of an acrylic acid-grafted separator has been shown in Figure 22, for the top, middle and bottom part of the separator as it came from the reactor drum. In all the bands, the bottom part of the

FIGURE 24 RELATIONSHIP BETWEEN RATE OF GRAFTING AND MONOMER CONCENTRATION

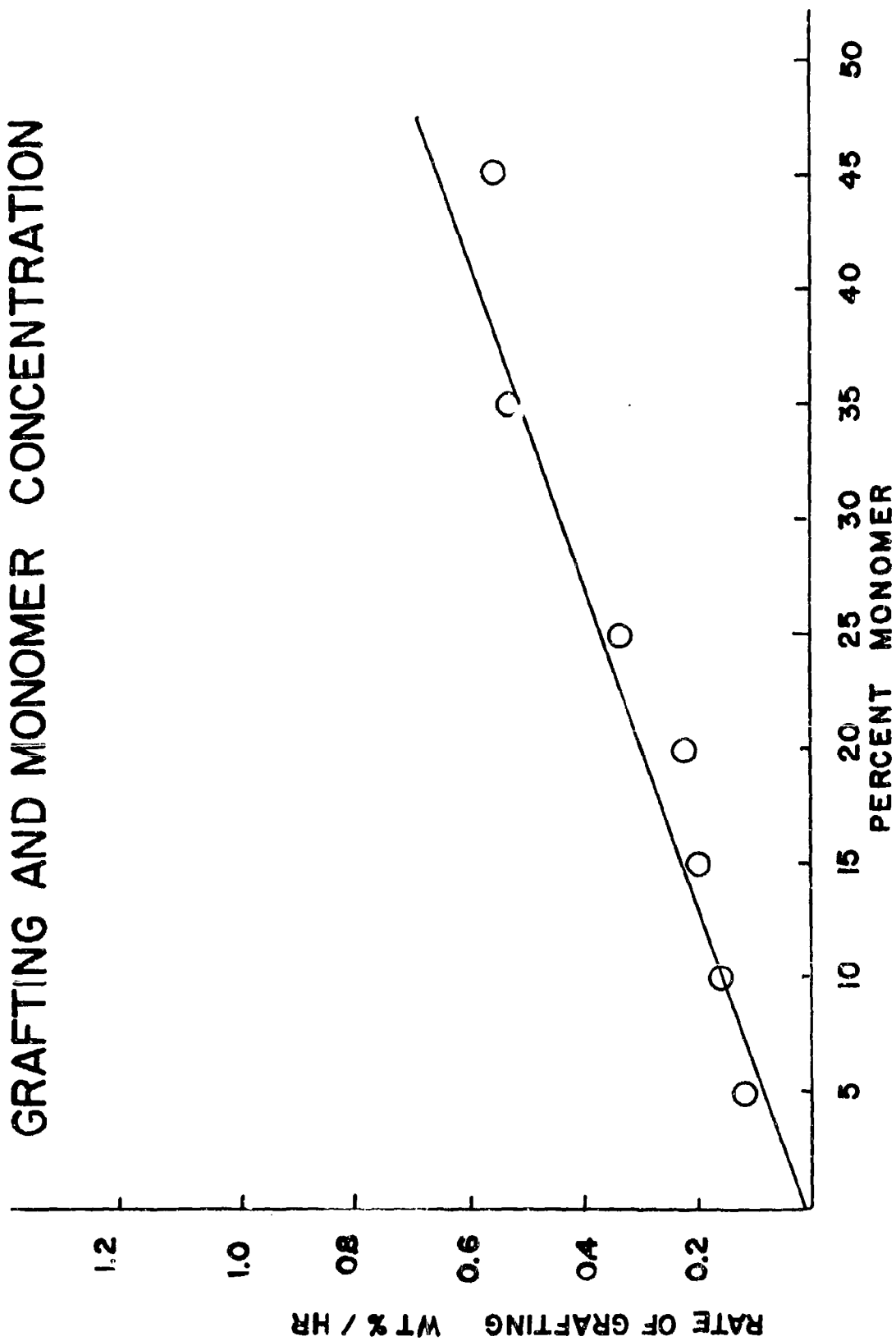
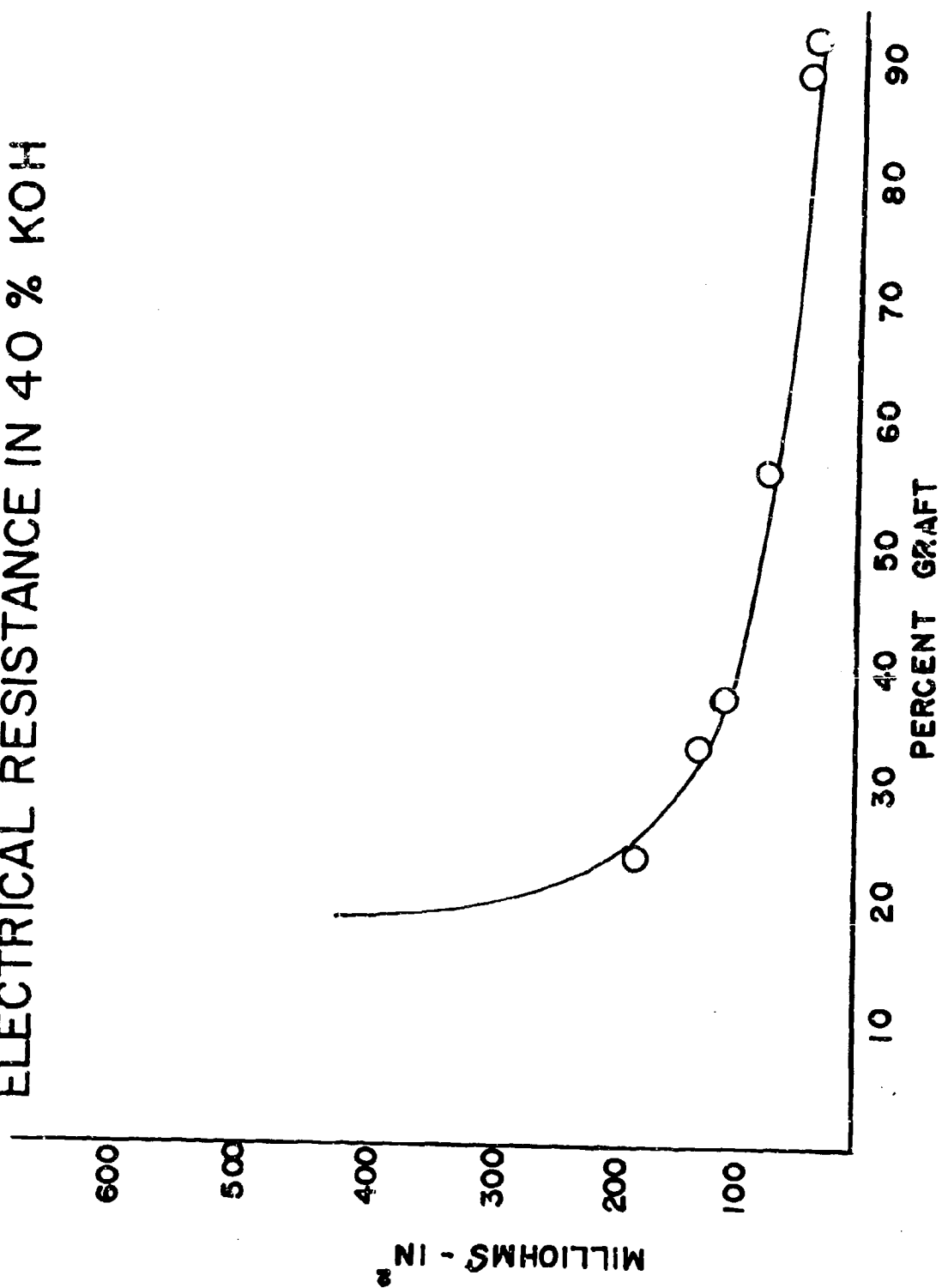


FIGURE 25 EFFECT OF PERCENT GRAFT ON THE ELECTRICAL RESISTANCE IN 40 % KOH



separator absorbs more than the top which in turn absorbs more than the middle part of the film. Assuming that the absorption is proportional to the concentration of the absorbing species, this means that the graft is more concentrated in the bottom, less in the top and least in the middle. If now we fix the wavelength where the band absorbs most, say 7.1, and scan the film over a distance, the recorded spectrum should indicate the uniformity of the graft. Figure 26 shows a spectrum of two films, dyed and scanned in the visible region of light. As a reference, the electrical resistance of the two films is also measured. It can be seen that the resistance fluctuation is less in film A than in film B, which indicates that film A is more uniform than film B in graft though their total percent graft may be the same. This basic procedure appears to be applicable for determining the uniformity of the grafted film. The specific instrument built during this program is not however, sufficiently sensitive. Further, the application of ultra-violet absorption would permit a direct reading of the percent graft. The homopolymer could also be removed using organic solvents so that the grafted monomer would be in the acid form and the film would be essentially anhydrous. This phase of the program requires additional development but the procedure initiated here appears promising as a control for graft uniformity.

Figure 27 is a plot of the percent graft against exchange capacity and the resistance against exchange capacity. As noted above in Figure 25 at low percent graft the resistance drops rapidly and then at above 30% graft the rate of decrease in resistance with a change in percent graft is very much decreased. It is believed that the reason for this change in rate is due to the inability to convert the acid completely to the salt form at the higher graft levels.

When plotting percent graft vs. exchange capacity the plot is asymptotic to an exchange capacity value. If, however, we plot resistance vs. exchange capacity, we note that at higher exchange capacities the resistance falls and continues to fall at a definite rate (this is only true if we plot one set of grafted samples). This data seems to indicate that the resistance decreases not as a function of percent graft but as a function of the fraction of the graft in the salt form. Also the percent graft is linear with exchange capacity in the low percent graft range. As the percent graft increases the exchange capacity levels off. This data is also given in Table 8.

FIGURE 26 DETERMINATION OF GRAFT
UNIFORMITY BY COLORIMETRY

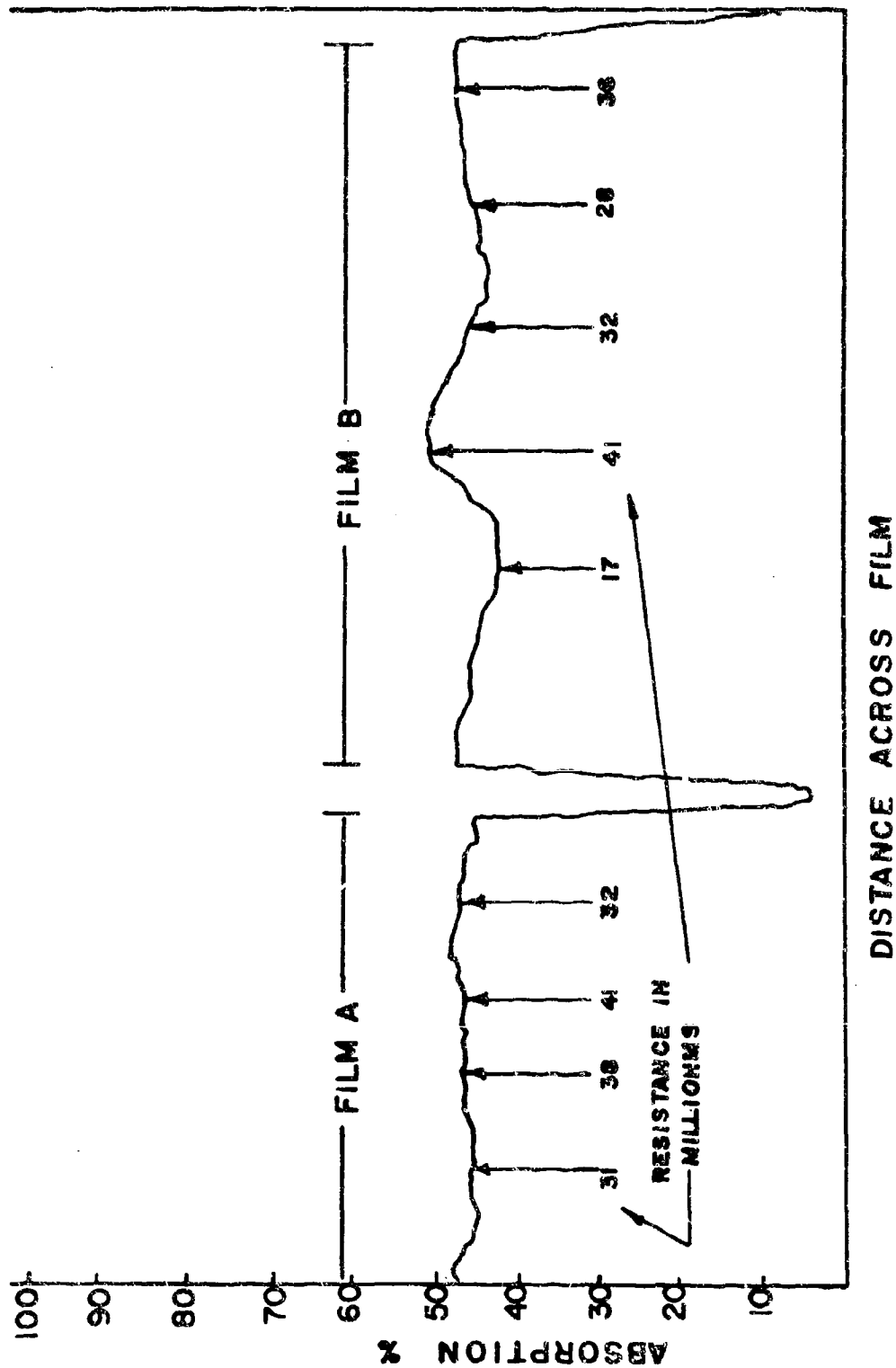
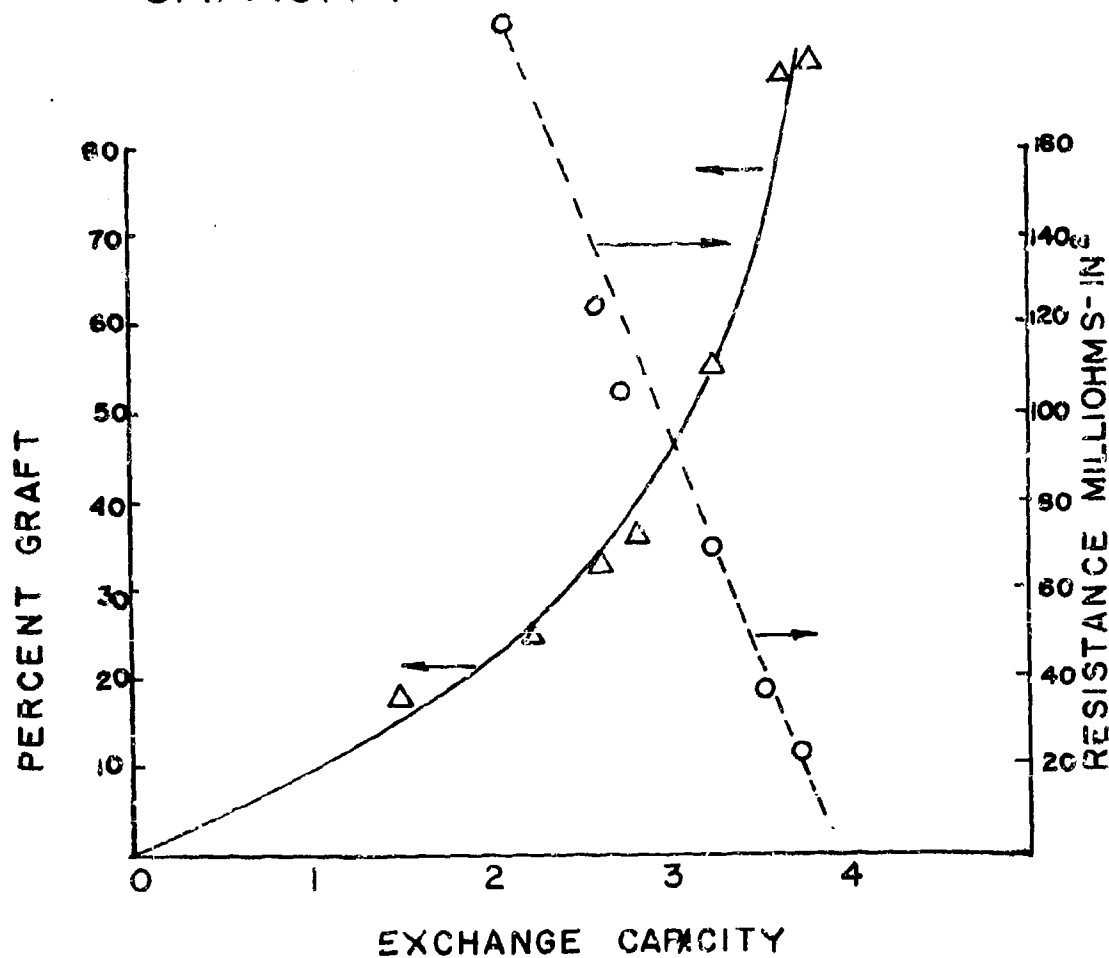


FIGURE 27 PERCENT GRAFT
AND RESISTANCE VS EXCHANGE
CAPACITY



This data was taken from 90 Mrads crosslinked Bakelite DFD 0602 film grafted with various percents methacrylic acid.

Table 8

Relationship Between Percent Graft of Methacrylic Acid and Exchange Capacity of the Membrane

Sample No	Pre-crosslinked Dose	Percent Graft	Exchange Capacity M.eq./Gram
213-30-5	90 Mrad	56.50%	3.34
213-30-6	90 Mrad	36.67%	2.80
213-30-7	90 Mrad	33.85%	2.72
213-30-8	90 Mrad	24.33%	2.24
213-30-9	90 Mrad	19.23%	1.44
213-30-10	90 Mrad	89.32%	3.55
213-30-11	90 Mrad	91.93%	3.63

3.4 Effect of Monomer Type

The effect of monomer type grafted on the cycle life can be seen from Table 9 and Figure 28. Three 100-ft. samples prepared using the three base films precrosslinked to about 90 Mrads, were grafted with acrylic acid and methacrylic acid. According to the cycle life test from 25 AH cells, which was conducted in the Delco-Remy laboratories, the methacrylic acid graft performs much better than the acrylic acid grafts.

Table 2

Screening Test of the Six 100-Ft. Samples in a 3-Plate Cell at 40% DOD

Sample No.	Material	Dose Range (Mrads)	Acid Graft	Resist- ance (m-ohm-in. ²)	Hull Test (Min.)	Exch. Capacity	Cycle Life	Control
47-1-1-1-1	USI-280	96.4-94.8	AA*	58	667	3.2	154S ⁺	150S
47-1-1-1-2	USI-280	96.4-94.8	AA	58	-	5.3	66S	
48-1-2-2-1	P-1712	81 - 94.8	AA	58	233	2.0	128S [#]	150S
48-1-2-2-2	P-1712	81 - 94.8	AA	85	-	2.0	112GL	
48-1-2-2-3	P-1712	81 - 94.8	AA	62	-	-	138GL	
49-1-3-3-1	B-DFD-0602	82 - 91.8	AA	32	210	-	245S	42S
49-1-3-3-2	B-DFD-0602	82 - 91.8	AA	31	2220	3.2	321S	
49-1-3-3-3	B-DFD-0602	82 - 91.8	AA	30	1260	4.1	182S	
49-1-3-4-1	B-DFD-0602	82 - 91.8	AA	30	-	-	267S	
50-1-4-1-1	USI-280	94.8-95.5	MA**	34	85	-	120S	174S
50-1-4-1-2	USI-280	94.8-95.5	MA	42	-	3.0	306S	
50-2-4-2-3	P-1712	81.5-93.8	MA	28	95	-	192S	174S
50-2-4-2-2	P-1712	81.5-93.8	MA	28	-	-	70S	
50-3-4-3-2	B-DFD-0602	91.0-95.5	MA	32	-	-	206S	114S
50-3-4-3-5	B-DFD-0602	91.0-95.5	MA	34	-	-	306S	

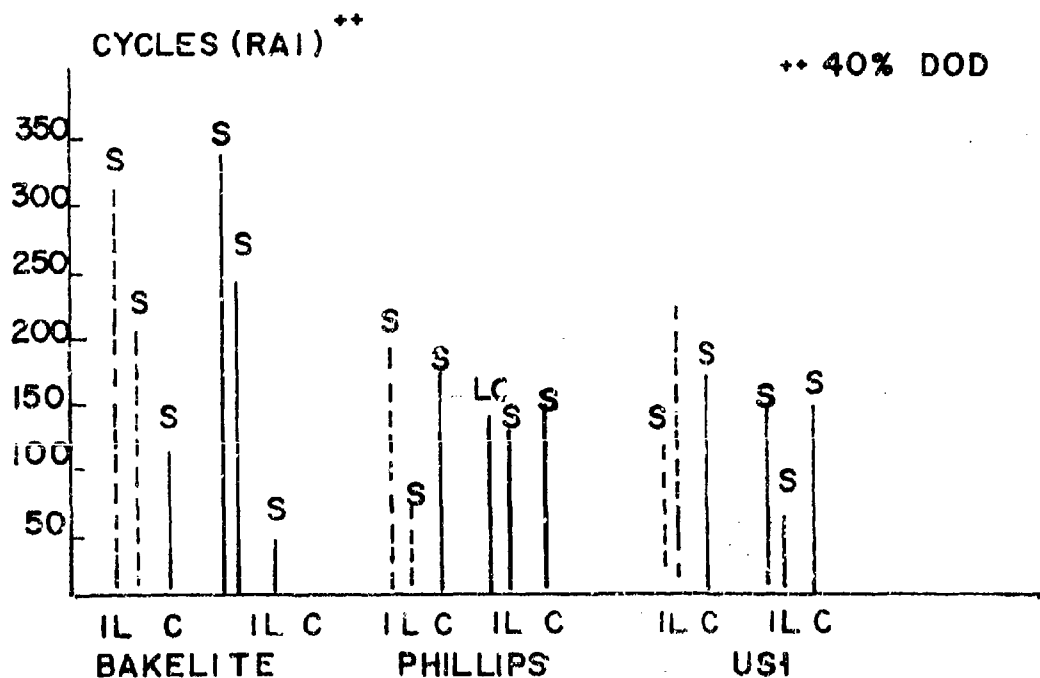
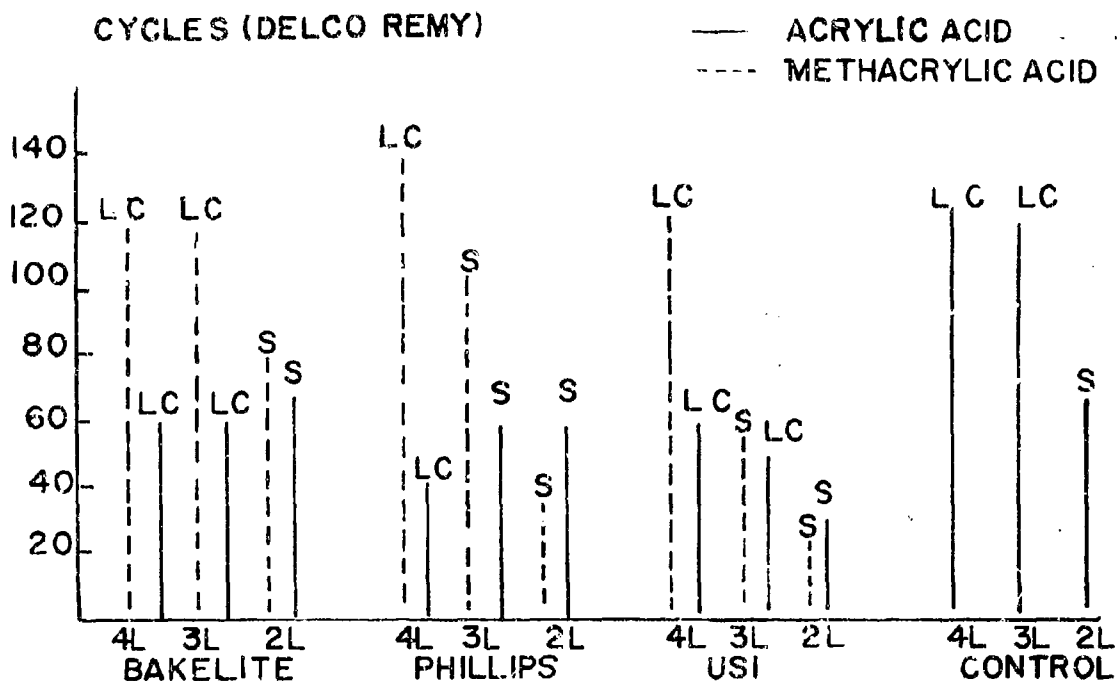
* Acrylic Acid

** Methacrylic Acid

+ Short

Capacity Loss

FIGURE 28 CYCLE LIFE TEST OF SAMPLE FILMS AT 60 % DEPTH OF DISCHARGE



These results may be explained by steric effects since the methacrylic acid has a bulky methyl group as compared to the hydrogen atom of acrylic acid so that the zincate and silver ions experience more steric resistance during their transport. On the other hand, there is evidence that the methacrylic acid grafted side chain ionizes more easily than the acrylic acid grafted side chain. Morawetz, et al., (16) have shown that the pK_a for polymethacrylic acid changes very little, but the pK_a for polyacrylic acid increases as the extent of ionization increases. The pK_a increase makes it more difficult to ionize the polyacrylic acid as the neutralization proceeds. This is supported by the fact that methacrylic acid graft has a lower electrical resistance than the acrylic acid graft, and its wet-out time is faster than the acrylic acid graft. In fact, we believed that the degree of neutralization in the grafted cation-exchange membrane is an extremely important factor which should be more thoroughly investigated since it represents the electrostatic charge built onto the membrane. This charge may be most important in decreasing zincate ion transport. This mechanism of repulsion is not possible with a neutral membrane like cellophane in which transport of ions is based on size and diffusion factors with the cellophane separator acting more or less like a molecular sieve. What is more significant in the ion-exchange membrane is that superimposed of the molecular sieve factor which is built in by precrosslinking the base film to have a tight network, there is the charge factor which is built in by grafting so that the film acts as a charge barrier. It is well known that in a neutral rubber membrane, the diffusion of methane, a large molecule, is more rapid than the diffusion of nitrogen, a small molecule. Evidently, something other than the pore size factor alone of the membrane must be accounted for. In addition, Lander (17) has reported that the size of a hydrated zincate ion is about the same as a hydrated KOH molecule in the electrolyte. Based on pore size of the separator, it is difficult to envision a membrane that will allow hydrated potassium and hydroxide ions to permeate through without letting the zincate ion through. The same result has also been reported by McBreen (18) who by measuring the relationship between membrane conductivity and zincate diffusivity, concluded that "the likelihood of finding a membrane which will not allow zincate ions to diffuse and at the same time would conduct hydroxyl ions at a reasonable rate is rather remote". It is very likely that the above conclusions are true for neutral membranes like cellophane since the relationship between membrane conductivity and zincate

diffusion is linear. The larger the membrane conductivity, the faster the zincate diffusion.

However, the possibility of "separating" the zincate and hydroxide ions using an ion-exchange type membrane should exist. This was recently reviewed by Professor Gregor⁽¹⁹⁾ who thought "that the problem of maintaining a proper molecular pore structure in a silver-zinc battery system can probably be met only by the introduction of ionic groupings into a properly prepared matrix, and not in the realm of neutral membranes". In our case, the properly prepared matrix is the crosslinked polyethylene structure, and the ionic groupings are the grafted carboxylic acids.

3.4.1 Potassium Hydroxide Extraction at 70°C and 145°C

Extraction in 40% potassium hydroxide at 70 and 145°C is designed to check the thermal stability of the grafted film in hot alkali medium. In a sense, the test can be used as a criteria for thermal sterilization. The effect of pre-crosslinked dose on the thermal stability of the grafted film is given in Table 10. Of significance is the electrical properties of the film after going through the thermal cycle. This will be discussed in a later section. When some material is extracted, the weight change is negative. When some material is added on the film, the weight change is positive. Theoretically, when nothing is extracted from the film, the weight change should be zero. The data is shown in Table 10.

Although the extracted fractions have not been identified, it may be speculated that they are the sol fraction of grafted and ungrafted polyethylene since the temperature of extraction (145°C) exceeds the melting point of polyethylene which is about 110°C. The amount of extractables for 0, and 30 Mrads material, however, corresponds to much less than what might be expected from the sol-gel curves. For membranes with 90 Mrads crosslinking there should be about 90% gel and 10% sol. The extracted fraction is what might be expected. At present, this weight loss is not entirely understood since a 10 to 20% weight loss would produce macroscopic voids in the film.

Table 10

Thermal Sterilization Data

Sample No.	Dose of X-Link (Mrads)	Type of Film	Dose of Graft (Mrads)	% Wt. Change 7 Days at 70°C. in 40% KOH	% Wt. Change 14 Days at 70°C. in 40% KOH	% Wt. Change 7 Days at 145°C. in 40% KOH	% Wt. Change 14 Days at 145°C. in 40% KOH	Grafting Solution
211-6-1	0	P-1712	1.02	-17.5	-9.8	-12.3	-34.8	A
211-6-3	0	P-1712	1.69	-14.8	-15.4	-31.1	-32.4	B
211-6-4	0	P-1712	1.02	-10.5	-12.5	-18.0	-18.0	C
211-6-5	0	P-1712	1.35	-8.3	-12.2	-28.3	-13.6	C
211-6-6	0	P-1712	1.02	-21.3	-12.8	-17.2	-13.0	B
211-6-7	0	P-1712	2.37	-24.3	-9.9	-9.2	-11.8	B
				Av. -16.1	Av. -12.1	Av. -19.4	Av. -20.6	
211-38-1	30	USI-280	1.24	-16.9	-18.6	-13.3	-14.1	F
211-38-3	30	B-DFD-0602	1.24	-5.9	-16.3	-20.2	-13.4	F
211-38-4	30	USI-280	1.24	-14.0	-16.5	-21.8	-12.0	G
211-38-5	30	P-1712	1.24	-32.0	-25.1	-17.5	-16.8	G
211-38-6	30	B-DFD-0602	1.24	-15.7	-24.4	-13.9	-16.5	G
				Av. -14.0	Av. -16.8	Av. -14.4	Av. -12.1	
211-36-1	50	USI-280	1.24	-7.0	-7.4	-9.2	-11.3	F
211-36-2	50	P-1712	1.24	-7.3	-11.6	-8.4	-10.5	F
211-36-3	50	B-DFD-0602	1.24	-4.9	-3.9	-8.9	-7.5	F
211-36-4	50	USI-280	1.24	-6.3	-5.9	-11.7	-11.0	G
211-36-5	50	P-1712	1.24	-5.6	-4.6	-8.2	-7.4	G
211-36-6	50	B-DFD-0602	1.24	-5.4	-5.6	-7.9	-9.7	G
				Av. -6.1	Av. -6.5	Av. -9.0	Av. -9.6	

(Continued)

Table 10 (Cont'd.)

Sample No.	Dose of X-Link (Mrads)	Type of Film	Dose of Graft (Mrads)	% Wt. Change 7 Days at 70°C. in 40% KOH	% Wt. Change 14 Days at 70°C. in 40% KOH	% Wt. Change 7 Days at 145°C. in 40% KOH	% Wt. Change 14 Days at 145°C. in 40% KOH	Grafting Solvent
211-32-1	90	USI-280	1.00	- 5.66	- 5.33	- 4.17	- 4.26	B
211-32-2	90	P-1712	1.00	- 4.97	-10.61	- 2.38	-10.06	B
211-32-3	90	B-DFD-0602	1.00	- 7.64	- 5.97	- 3.49	- 5.35	B
211-40-4	90	P-1712	1.24	-12.47	-14.32	- 5.28	- 6.10	G
211-40-5	90	B-DFD-0602	1.24	- 5.05	- 8.78	- 4.71	- 6.11	G
211-40-6	90	USI-280	1.24	- 8.42	-13.05	- 2.86	- 4.32	G
				Av. - 7.3	Av. - 7.2	Av. - 4.5	Av. - 6.0	

Solution Components	A	B	C	D	E	F	G
Benzene	33.5	67.0	35.0	(5-35)	66.4	70.0	70.0
Methylene Chloride	33.5	-	35.0	35.0	-	-	-
Acrylic Acid	30.0	30.0	30.0	30.0	30.0	29.0	29.0
Carbon Tetrachloride	3.0	3.0	-	(30.0)	3.6	1.0	1.0

However, if the extracted fraction is due to decarboxylation of the grafted chain, no voids would form but the membrane would increase in electrical resistance. This has not been to be the case since the extracted film always have improved conductivity. Cycle life at elevated temperature using grafted membranes also shows significant improvement over cellophane controls. In order to understand the effect of thermal sterilization, careful identification of the extracted fraction is necessary, and work should continue in this area for thermally sterilizable membranes.

The extraction data at 145°C is graphically given in Figure 29. In general, the lower the temperature or the time for extraction the smaller the percent extracted. In addition as the precrosslinked dose increased the extractable fraction decreased. This data confirms the importance of crosslinking in preventing leaching of membrane fractions and is indicative of what might occur during room temperature cycling.

3.4.2 Cycle Life at Elevated Temperature

The cycle life of batteries using grafted membranes at 50°C is much better than the cycle life of batteries using cellophane separators. The data from limited tests is given in Table 11. These results are in line with the previous discussion which indicated that for cellophane the diffusivity of the zincate ion increases with rise in temperature so that shorting by zinc dendrite formation is more likely at 50°C than at room temperature. The poor stability of cellophane at elevated temperature due to chemical degradation is also another factor. The diffusivity of the zincate ion, however, decreases with a rise in temperature for grafted membranes⁽¹⁸⁾, as seen in Figure 30, which was taken from reference 18. Also of significance in Figure 30 is the dependence of zincate diffusivity on the concentration of the electrolyte, which is not expected for the cellophane type membrane, but is typical of the ion-exchange type grafted membrane.

FIGURE 29
EXTRACTION IN 40% KOH

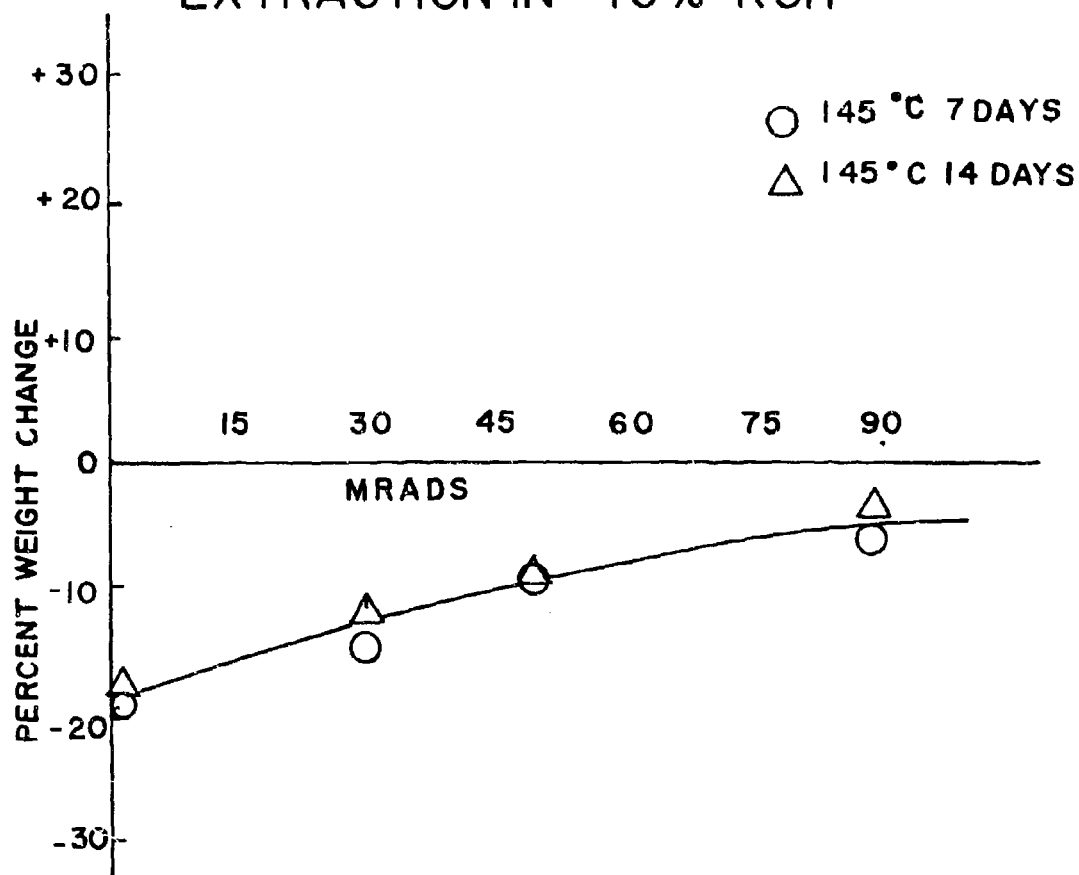


Table 11

Cycle Life of Grafted Membranes at 40% DOD in 3
Plate Cells at 50°C Using 1 Layer of Membrane

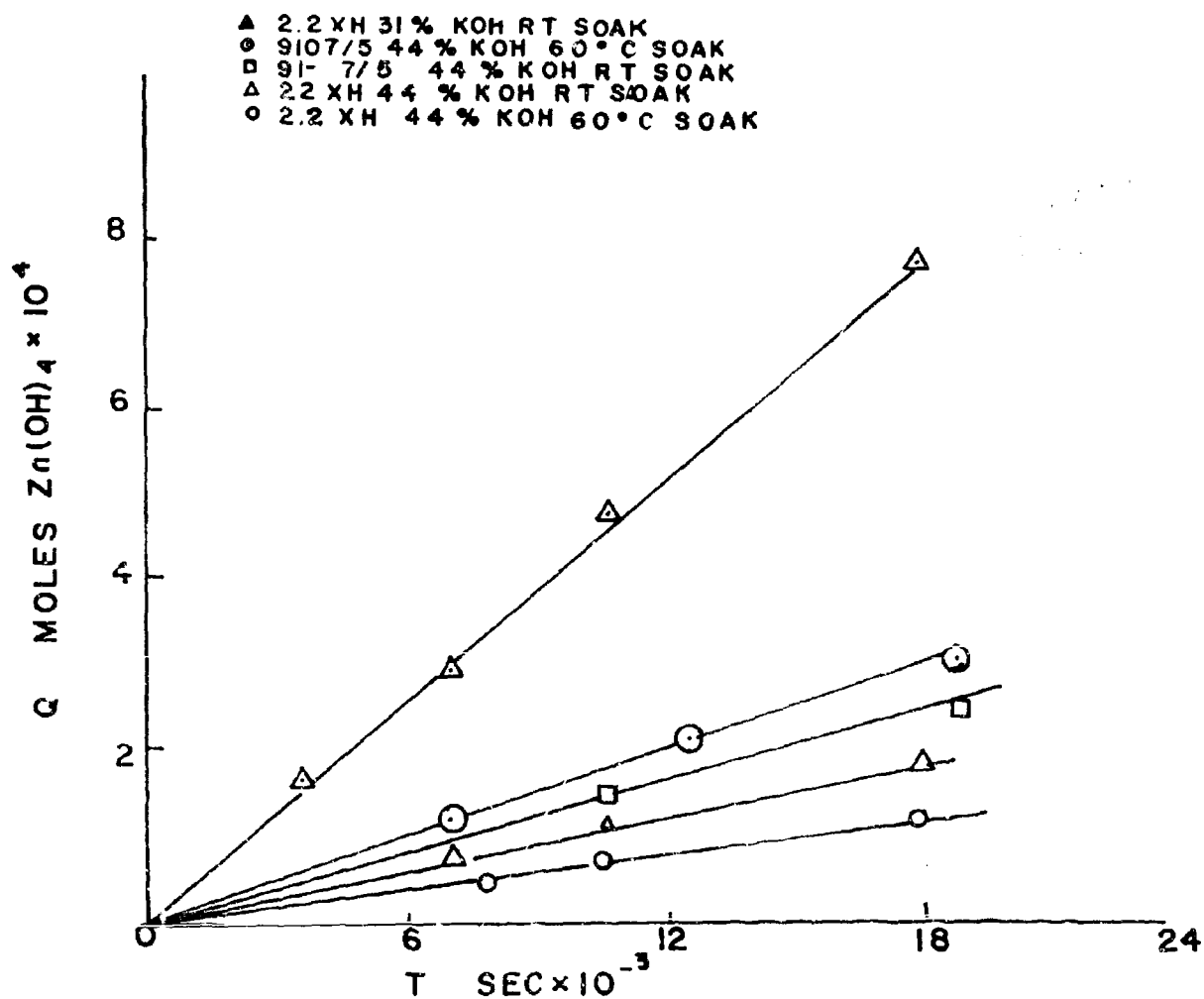
Sample No.	Material	Dose (Mrads)	Graft	Cycle Life	Remarks
211-49-1	B-DFD-0602	90	AA*	170	C.L. ⁺
211-49-1	B-DFD-0602	90	AA	50	C.L.
211-49-1	B-DFD-0602	90	AA	124	C.L.
211-50-3	B-DFD-0602	90	MA**	310	Shorting
211-50-3	B-DFD-0602	90	MA	474	C.L.
211-50-3	B-DFD-0602	90	MA	280	Short
Control 1	-	-	-	50	Short
Control 2	-	-	-	104	Short

* Acrylic Acid

** Methacrylic Acid

+ Capacity Loss

FIGURE 30 PERMEATION OF
ZINCATE THROUGH 2.2 XH SERIES 2⁽¹⁸⁾



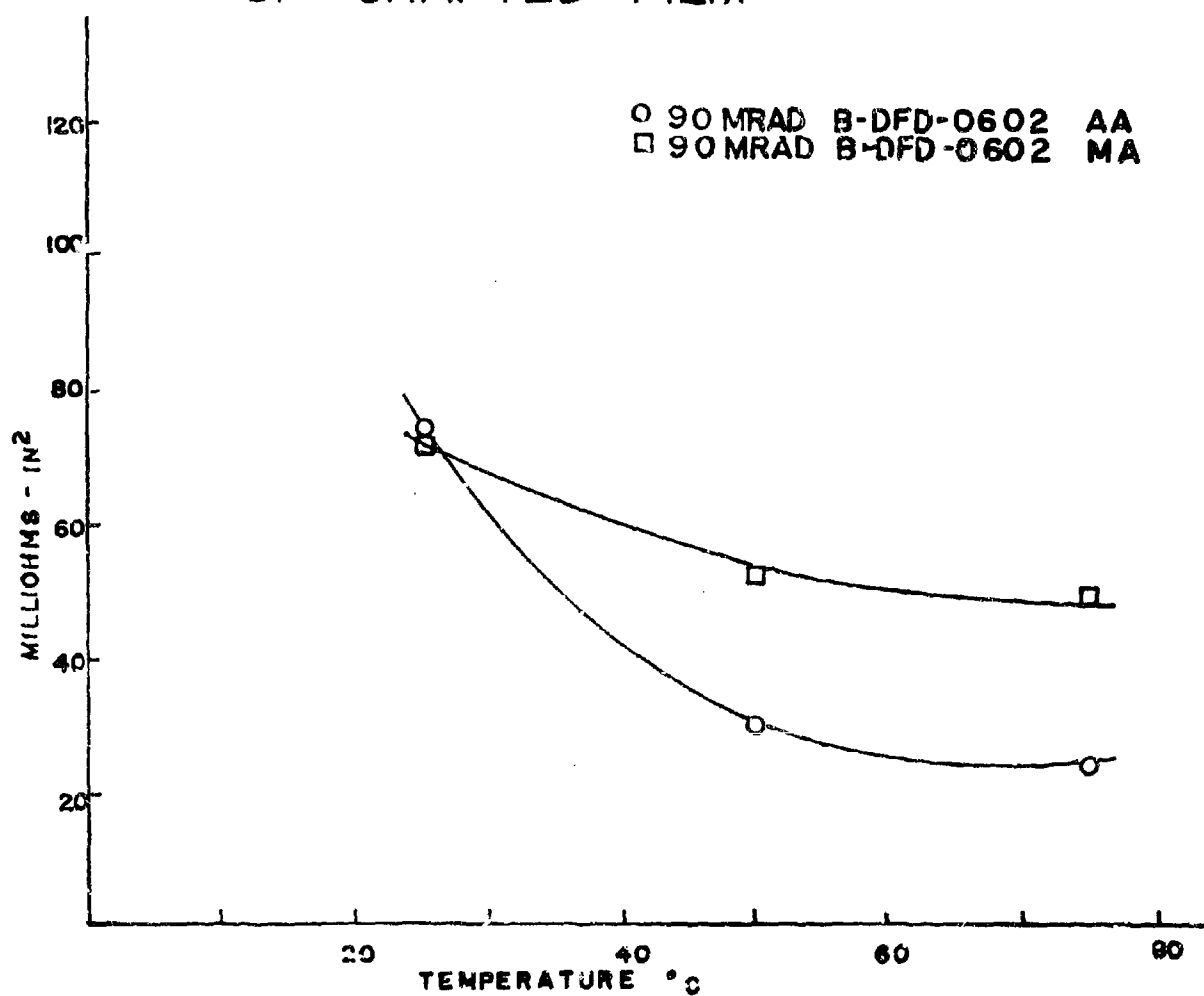
The results given above can be explained qualitatively by application of the theory of polyelectrolytes. What appears to be occurring with an increase in temperature is a concomitant increase in the titration of the acid to the salt form in the grafted membrane. This increase in salt formation could account for the lowering of the electrical resistance at elevated temperature as shown in Figure 31. It also substantiates the premise that decarboxylation does not occur at 70°C since the resistance of the film is decreased.

As more and more of the grafted acid is converted to the salt form, the charge density along the grafted chain increases. Since the zincate ion bears a double negative charge and the carboxylate is also negatively charged the zincate ion effectively sees a tortuous electrostatic path, and is excluded from the membrane. The highly crosslinked film does not swell in the environment and thereby maintains a high charge density in addition to maintaining the "pore size". It is believed that these factors could account for McBreen's results of decreased zincate diffusivity with rise in temperature. It is also important to note that the zincate ion being double charged would have a high charge density.

The dependence of the zincate diffusivity on electrolyte concentration can be explained by the salt effect on polyelectrolytes. At 31 percent potassium hydroxide concentration the charges on the grafted chain are probably less shielded than at the higher concentration so that the polymer is more highly expanded at the lower concentration. This effect results in a decrease in diffusivity in the higher potassium hydroxide concentration.

Both the electrical resistance and dimensional change of the grafted membrane (B-DFD-0602, 90 MR, acrylic acid) have been measured as a function of potassium hydroxide concentration and time and it was found that the resistance of the acrylic acid grafted separator varied unpredictably as a function of time but increases with increasing KOH concentration. The results from evaluation of film are given in Table 12. This effect which is believed due to an increase in pK_a of the acrylic acid as the concentration increases should not be as severe for polymethacrylic acid since its pK_a changes only slightly with increase in concentration. Finally, the size of the hydrated zincate ion, and for that matter, all the other ions in the electrolyte may change with temperature, but the extent of change for hydrated zincate ion, hydrated hydroxide ion and

FIGURE 31 TEMPERATURE VS RESISTANCE
OF GRAFTED FILM



hydrated potassium ion may not be the same with temperature. It may be expected that the degree of hydration will decrease with increasing temperature so that although at room temperature the size of hydrated zincate ion and hydrate hydroxide ion are about the same, they may not be the same at elevated temperature and a membrane might separate them purely on size alone.

3.5 Testing Results of Grafted Membranes

Prior to submission of sample membranes under phases I, II and III of this contract numerous materials were evaluated on different base resins with various grafting solution and at various crosslinking levels. Data on these materials are given in Table 13. Testing of these samples included resistance, hull tests and cycle life. In addition the crosslinked samples were evaluated for gel content, M_c value and in some instances tensile strength of wet and dry samples. Hull test results for some of these samples are given in Table 14.

3.5.1 Sample Submitted on Completion of Phase I

The samples submitted after completion of phase one are given in Table 15. Six samples were submitted. These were coded as indicated in Table 15. The films used in preparing these samples were crosslinked using the original crosslinking procedure. The crosslinking range for these samples was significant. Testing in three plate cells confirmed data presented earlier in this report.

The selection of separators for testing samples was made to investigate two variables, the film type and the monomer type. The importance of crosslinking dose was established and therefore only highly crosslinked films were evaluated. One hundred foot samples of each of the separators was submitted to Delco-Remy for evaluation in 25 Amp./hour cells.

Table 12

Average Resistance and Dimensional Change of B-DFD-0602 Acrylic Acid
Graft as a Function of Electrolyte Concentration and Time

Code Number	Time (Mins.)	5% KOH		10% KOH		20% KOH		30% KOH		40% KOH	
		R	D	R	D	R	D	R	D	R	D
3-3-1	1	26	13.3	48	11.1	10	19.9	79	5.0	54	3.0
3-3-1	10	29	10.1	49	10.1	10	14.8	64	4.0	42	3.0
3-3-1	30	27	10.1	45	8.0	9	10.7	50	5.0	32	4.0
3-3-1	60	21	14.3	38	11.1	5	10.7	50	6.1	37	7.0
3-3-1	180	25	15.4	64	11.1	9	16.8	57	10.3	35	9.0
3-3-1	1200	63	15.4	106	12.2	20	9.7	144	8.2	53	7.0
3-3-1	2640	77	13.3	135	14.3	20	15.8	161	7.1	80	6.0
3-3-1	4080	65	16.4	105	12.2	20	16.8	165	9.2	89	6.0
3-3-2	1	20	12.7	91	11.0	110	8.8	94	7.0	82	4.9
3-3-2	10	19	19.8	72	14.1	86	9.8	72	9.0	68	7.9
3-3-2	30	15	15.7	74	13.1	83	8.8	78	9.0	68	8.9
3-3-2	60	15	14.7	69	15.2	78	8.8	77	10.0	65	8.9
3-3-2	180	17	18.8	72	14.1	71	7.8	75	11.1	60	8.9
3-3-2	1200	16	18.8	73	14.1	71	7.8	75	10.0	56	4.9
3-3-2	2540	13	17.7	66	13.1	58	8.8	72	8.0	59	6.9

R = Resistance in m-ohm/in² in 45% KOH

D = Increase in dimension in percent relative to initial dimension

Table 13
Preliminary Membrane Evaluation

Film Type	Grafting Solution	Cross-linking Dose Mrads	% Graft	Resistance - In ² Milliohms	Cycles To Failure
211-6-1	P-1712	A	78	13	13
2	P-1712	A	109	Not Tested	Poor
3	P-1712	B	97	12	10
4	P-1712	C	102	18	23
5	P-1712	C	83	14	40
6	P-1712	B	63	13	30
7	P-1712	B	103	11	35
211-8-1	P-1712	C	23	15	57
2	P-1712	C	74	14	16
3	P-1712	C	81	16	13
4	P-1712	C	110	14	15
211-18-1	P-1712	D	108	15	-
2	P-1712	D	90	13	-
3	P-1712	D	95	43	-
4	P-1712	D	149	18	-
5	P-1712	D	80	21	-
6	P-1712	D	75	23	-
211-32-1	USI-280	E	71	182	190
2	P-1712	E	75	86	182
3	B-DFD-0602	E	57	96	316
-Visking Control					
-7 (1-20)					113

(Continued)

Table 13 (Cont'd.)

Film Type	Grafting Solution	Cross-linking Dose Mrads	% Graft	Resistance -in ² Millionths	Cycles To Failure
211-36-1	U-280	50	77	14	46
2	P-1712	50	71	21	46
3	B-DFD-0602	50	67	25	47
4	USI-280	50	50	27	14
5	P-1712	50	47	30	76
6	B-DGD-0602	50	40	31	191
211-38-1	USI-280	30	92	19	7
2	P-1712	30	89	20	42
3	B-DGD-0602	30	75	18	34
4	USI-280	30	82	24	81
5	P-1712	30	67	112	26
6	B-DFD-0602	30	71	180	59
211-40-1	P-1712	90	Over Grafted	-	-
2	B-DFD-0602	90	Over Grafted	-	-
3	USI-280	90	Over Grafted	-	-
4	P-1712	90	55	147	-
5	B-DFD-0602	90	60	271	-
6	USI-280	90	58	275	-

(Continued)

Table 13 (Cont'd.)

Film Type	Grafting Solution	Cross-linking Dose Mrads	% Graft	Resistance - In Ω	Cycles To Failure
211-42-1	P-1712	90	57	374	-
2	B-DFD-0602	90	76	228	-
3	USI-280	90	69	300	-
4	P-1712	90	78	189	-
5	B-DFD-0602	90	81	122	-
6	USI-280	90	86	159	-
211-54-1	B-DFD-0602	84	0	-	-
2	B-DFD-0602		0		
5	B-DFD-0602	30		70	136
211-52-1	B-DFD-0602	107		Too High	-
2	NA-301	82		158	45
3	NA-107	88		198	70
4	B-DFD-0602	62		59	Delco-Remy
5	B-DFD-0602	61		50	Delco-Remy
6	B-DFD-0602	57		74	166
7	B-DFD-0602	65		42	130
8A	R-DFD-0602	29		57	138
8B	S-565	27		26	62
9	B-DFD-0602	38		59	130
10	B-DFD-0602	32		98	110
11	B-DFD-0602	90*		95*	

(Continued)

Table 13 (Cont'd.)

Film Type	Grafting Solution	Cross-linking Dose Mrads	% Graft	Resistance Milliohms -In ²	Cycles To Failure
211-56-1	P-1712	90**	103	45	142
2	P-1712	15x	103	45	124
3	P-1712	90y	63	45	84

* Post crosslinked with Divinylbenzene (Resistance went from 45 to 95).
 ** Post crosslinked 1 without divinylbenzene to 90 Mrad, and 3 with DVB to 90 Mrads.
 x Post crosslinked with DVB (15 Mrads).
 y Post crosslinked with DVD (90 Mrads)

Solution Components	GRAFTING SOLUTION PERCENT										
	A	B	C	D	E	F	G	H	I	J	K L
Benzene	33.5	67.0	35.0	(5-35)	66.4	70.0	70.0	76.4	76.4	70	70 67
Methylene Chloride	33.5	-	35.0	35.0	-	-	-	-	-	-	-
Acrylic Acid	30.0	30.0	30.0	30.0	30.0	29.0	-	-	-	26.4	30
Carbon tetrachloride	3.0	3.0	-	(30-0)	3.6	1.0	1.0	3.6	3.6	3.6	3.6 3.0
Methacrylic Acid						29.0					
3.3 Dimethylacrylic								20.0			
Cis - 2,5 Dimethylacrylic								2.0			
Vinylacetate										3.0	

Table 14

Relationship Between Hull Test and Cycle Life Test

Sample No.	Time to Dendrite Growth	Cycle Life 40% DOD
211-32-1	1 hr. 30 minutes	190
211-32-1	2 hr. 35 minutes	
211-32-2	4 hrs.	182
211-32-2	4 hrs.	
211-32-3	1 hr. 10 minutes	316
211-32-3	7 hr. 45 minutes	
Control	2 hours 20 minutes	
Uncrosslinked AA Graft	20 minutes	
211-36-1	40 minutes	46
211-36-2	30 minutes	46
211-36-3	3 hours	47
211-36-4	1 hour 55 minutes	14
211-36-5	2 hours 15 minutes	76
211-36-6	3 hours 45 minutes	191

Table 15

Characterization of Six 100 Foot Samples
Submitted on Completion of Phase One

Code (a) No.	Film (b)	Monomer (c) (d) Type	Cross-linking (g) Dose (Mrads)	Resistance mohms -In 2	Hull Test	Ex- change Ca- pacity	Cycle (f) Life
47-1-111	USI-280	AA	96.4-94.8	40-75	667	3.2	154
47-1-112	USI-280	AA	96.4-94.8	40-75		5.3	66
48-1-211	P-1712	AA	81 - 94.8	40-75	233	2.0	
48-1-212	P-1712	AA	81 - 94.8	85		2.0	
48-1-213	P-1712	AA	81 - 94.8	49-85			60
48-1-214	P-1712	AA	81 - 94.8	35-45			
48-1-215	P-1712	AA	81 - 94.8	35			
48-1-216	P-1712	AA	81 - 94.8	20-40			
49-1-331	B-DFD-0602	AA	82 - 91.8	18-46	240		245
49-1-332	B-DFD-0602	AA	82 - 91.8	15-46	2220	3.2	321
49-1-333	B-DFD-0602	AA	82 - 91.8	13-42	1260	4.1	
49-1-334	B-DFD-0602	AA	82 - 91.8	13-42			
49-1-341	B-DFD-0602	AA	82 - 91.8	15-38			267
50-1-411	USI-280	MA	94.8-95.5	34	85		120
50-1-412	USI-280	MA	94.8-95.5	42		3.0	300
50-1-413	USI-280	MA	94.8-95.5	30			
50-1-414	USI-280	MA	94.8-95.5	35		3.0	
50-1-415	USI-280	MA	94.8-95.5	60			

(Continued)

Table 15 (Cont'd.)

Code (a) No.	Film (t)	Monomer (c) (d) Type	Cross- linking Dose (Mrads)	Resist- ance mohms -In ²	Hull Test	Ex- change Ca- pacity	Cycle (f) Life
50-2-421	P-1712	MA	81.5-93.8	30			
59-2-422	P-1712	MA	81.5-93.8	28			70
50-2-423	P-1712	MA	81.5-93.8	28	95		
50-2-424	P-1712	MA	81.5-93.8	22		3.2	
50-2-425	P-1712	MA	81.5-93.8	30		3.3	
50-3-431	B-DFD-0602	MA	91.0-95.5	24-38	210	3.2	137
50-3-432	B-DFD-0602	MA	91.0-95.5	28-38			206
50-3-433	B-DFD-0602	MA	91.0-95.5	34-44	150		42
50-3-434	B-DFD-0602	MA	91.0-95.5	24-34		3.1	118
50-3-435	B-DFD-0602	MA	91.0-95.5	26-42			

(a) All code numbers omit prefix 211, for 211-47-1-111 - the first three number 211-47-1 indicate book/page, experiment number - the last 3 digits, 111, are used only when a larger (500 ft) reactor is used. These digits indicate reactor number (1) roll and part of roll tested (1).

(b) U = USI Resin 280-50; P = Phillips, Marlex 1712; B = Bakelite DFD-0602

(c) AA = Acrylic Acid, grafting solution = 26.4% AA, 3.6% CC 1₄, 70% Benzene

(d) MA = Methacrylic Acid, grafting solution = 26.4% MA, 3.6% CCl₄, 70% Benzene

(e) Dose rate was 10,500 rads/hour, for all samples.

(f) Cycle life - was determined on 3 plate cells (2 Gg, 12n) at 40% DOD. All failures are by shorting.

(g) During this part of the program a procedure for absolute control of the crosslinking was not established therefore^a crosslinking range for the irradiation is given.

3.5.2 Samples Submitted Upon Completion of Phase II

The cycle test data from in battery testing of separators submitted under phase one confirmed the importance of the base resin. The results of tests on three plate 1.2 amp. hour cells tested at RAI and twenty five amp-hour cells cycled tested at Delco-Remy are in accord. These tests indicate that the separators prepared using Bakelite DFD-0602 with acrylic acid and methacrylic acid were better than other separators prepared with different base resins.

Based on these findings separators 211-50-3 and 211-49-1 were selected for further testing in batteries and therefore 500 feet of each membrane was prepared and submitted for testing on completion of phase two.

The third sample submitted for evaluation on completion of phase two was a chemically grafted separator. This separator is coded 213-141-1 and 213-141-2 since the same separator was made under identical conditions but at two different times. The results of resistance testing cycle life and resistance as a function of time in 40% potassium hydroxide is given in Tables 16, 17 and 18.

The Hull test for the 211-50-3 and 211-49-1 separator were in excess of three hours.

3.5.3 Final Sample Selection and Specifications

Cycle testing of samples from phase two substantiated preliminary findings. The 211-50-3 separator which was a methacrylic acid graft on a highly crosslinked narrow molecular weight film was found to be best. The specification for the 5000 foot sample are given in Table 19. Resistance values are given in Table 20. The zinc flux determination was by the procedure given by Lander(20).

Table 16

Characterization of Three 500 Foot Samples Submitted
on Completion of Phase Two

Code No.	Resist- ance mohms -in ²	Code No.	Resist- ance mohms -in ²	Code No.	Resist- ance mohms -in ²	Code No.	Resist- ance mohms -in ²
<u>211-50-3</u>							
411	52	<u>451</u>	36	127	68	<u>213-143-1</u>	<u>213-143-2</u>
412	52	542	51	128	68	1	1
413	52	453*	38	129	65	2	2
414	51	453*	46	1210	70	3	3
415	46	454	60	1211	70	4	4
416	50	455	44	1212	82	5	5
417	38	456	46	1213	72	6	6
418	51	457	43	1214	72	7	
419	54	458	60	1215	72	8	
<u>211-49-1</u>							
421	60	<u>111</u>	62	1216	72		
422	49	112	57	1217	80		
423	48	113	69	1218	65		
424	50	114	60	1219	87		
425	52	115	65	1220	84		
426	45	116	50	1221	80		
427	47	117	51	1222*	72		
428	48	118	46	1222*	80		
431	49	119	69	311	57		
432	46	1110	70	312	59		
433	45	1111	46	313	48		
434	45	1112	57	314	43		
				315	61		
				316	67		

Table 16 (Cont'd.)

Code No.	Resist- ance		Code No.	Resist- ance		Code No.	Resist- ance		Code No.	Resist- ance	
	mohms	-in ²		mohms	-in ²		mohms	-in ²		mohms	-in ²
435	49		1113	55		317	77				
436	68		1114	58		318	75				
437	52		1115	70		319	80				
438	44		1116	70		3110	77				
439	37		1117	70		3111	73				
			1118	58		3112	52				
441	54		1119	59		3113	71				
442	42					3114	62				
443	47		121	56		321	45				
444	43		122	67		322	77				
445	43		123	31		323	65				
446	45		124*	67		324	60				
447	34		124*	72		325	70				
448	58		125	68		326	60				
449	48		126	63		327	62				
						328	61				
						329	57				
						3210	64				

Samples No.: 711-49-7
211-50-4

Table 17

Characterization of Three 500 Foot Samples
Submitted on Completion of Phase Two

Code No.	Cycle Life at 40% DOD		Test Terminated
	No. Cycles to Capacity Loss	Cycles to Short	
211-49-1*	284,	-	Film cut
211-49-1	216,264,310	-	310
211-49-1	106,362,384	-	384
			261
211-49-1	72,261,	-	
211-49-1	414	-	414
211-50-3	220,372	-	372
211-50-3	284,386,538	-	588
211-50-3	244,335	-	335
211-50-3	424,447	-	447
213-141-1	-	120	-
Control Visking 7		60	-
Control Visking 7		202	-
Control Visking 7		104	-
Control Visking 7		154	-

All testing was on 3 plate 1.2 amp hour cells cycled at 350 MA charge for 85 minutes and 350 MA discharge for 35 minutes (2 hour cycle). Cells had 2 silver and on zinc plate and use one layer of separator - cut off voltage set at 1.96 volts on charge.

Table 18

Characterization of Three 500 Foot Samples
Submitted on Completion of Phase Two

Electrical Resistance in 40% KOH at Room Temperature
as a Function of Time

Code No.	Resistance Milliohm-Sq. In.			
	2-4 min.	35 min.	300 min.	1440 min.
<u>211-49-1</u>				
1	80	41	41	64
2	61	49	42	39
3	56	58	48	67
4	42	53	40	33
5	93	86	77	66
6	86	81	81	64
<u>211-50-3</u>				
1	63	60	60	68
2	61	62	50	41
3	75	61	60	44
4	69	62	60	63

Table 19

Characterization of 5000 Foot Sample
Submitted on Completion of Phase III

Resin	Bakelite DFD-0602
Film	Blown (1.0 mil \pm 20%)
Density	0.922
GPC Curve	Figure 17
\bar{M}_w/\bar{M}_n	2.0
M_c	\approx 1770
Crosslinking Dose	89 \pm 2 Mrads
Graft Type	Methacrylic Acid
Grafting Solution	Methacrylic Acid - 26.4% Carbontetrachloride 3.6% Benzene 70%
% Graft	\approx 75-90%
Resistance (Avg.)	49 milliohm -in ²
Grafting-Dose Rate	10,500 rads/hour
Dose	1.51 Mrads
Hull Test	> 3 hours
Cycle Life 40% DOD, 2 Hour Cycle, 3 Plate (1 Layer Film)	> 300
Tensile Wet	1200
Dry	1500
Zinc Flux (mole/in ² minute)	1.14 x 10 ⁻⁶ (Figure 32)

Table 20

Characterization of 5000 Foot Sample
Submitted on Completion of Phase III

Electrical Resistance in 40% KOH at Room Temperature

Code No.	Resistance mohm-in ²	Code No.	Resistance mohm-in ²	Code No.	Resistance mohm-in ²	Code No.	Resistance mohm-in ²
<u>211-50-3</u>							
1-1-1-	56.3	2-1-1	62.0	3-1-1	53.3	4-1-1	35.0
1-1-2	56.3	2-1-2	62.3	3-1-2	51.0	4-1-2	47.0
1-1-3	55.3	2-1-3	64.7	3-1-3	49.0	4-1-3	49.3
1-1-4	53.7	2-2-1	62.0	3-2-1	38.7	4-1-4	37.3
1-2-1	51.0	2-2-2	62.7	3-2-2	43.7	4-1-5	41.7
1-2-2	44.3	2-2-3	61.3	3-2-3	44.7	4-2-1	31.3
1-2-3	48.7	2-3-1	52.7	3-3-1	52.3	4-2-2	27.0
1-2-4	52.0	2-3-2	55.3	3-3-2	60.7	4-2-3	45.0
1-3-1	48.7	2-3-3	56.3	3-3-3	44.0	4-2-4	41.7
1-3-2	56.0	2-4-1	57.0	3-4-1	55.0	4-3-1	32.7
1-3-3	49.7	2-4-2	47.3	3-4-2	57.0	4-3-2	43.7
1-3-4	51.3	2-4-3	43.7	3-4-3	41.7	4-3-3	51.3
1-4-1	61.0	2-4-4	56.3	3-4-4	55.0	4-3-4	48.0
1-4-2	61.3	2-4-5	48.0	3-5-1	35.7	4-3-5	50.3
1-4-3	59.3	2-4-6	49.3	3-5-2	53.3	4-4-1	54.0
1-5-1	49.7	2-4-7	66.0	3-5-3	58.7	4-4-2	59.0
1-5-2	50.7			3-5-4	68.0	4-4-3	58.3
1-5-3	27.7					4-4-4	37.7
1-5-4	42.0					4-4-5	36.0

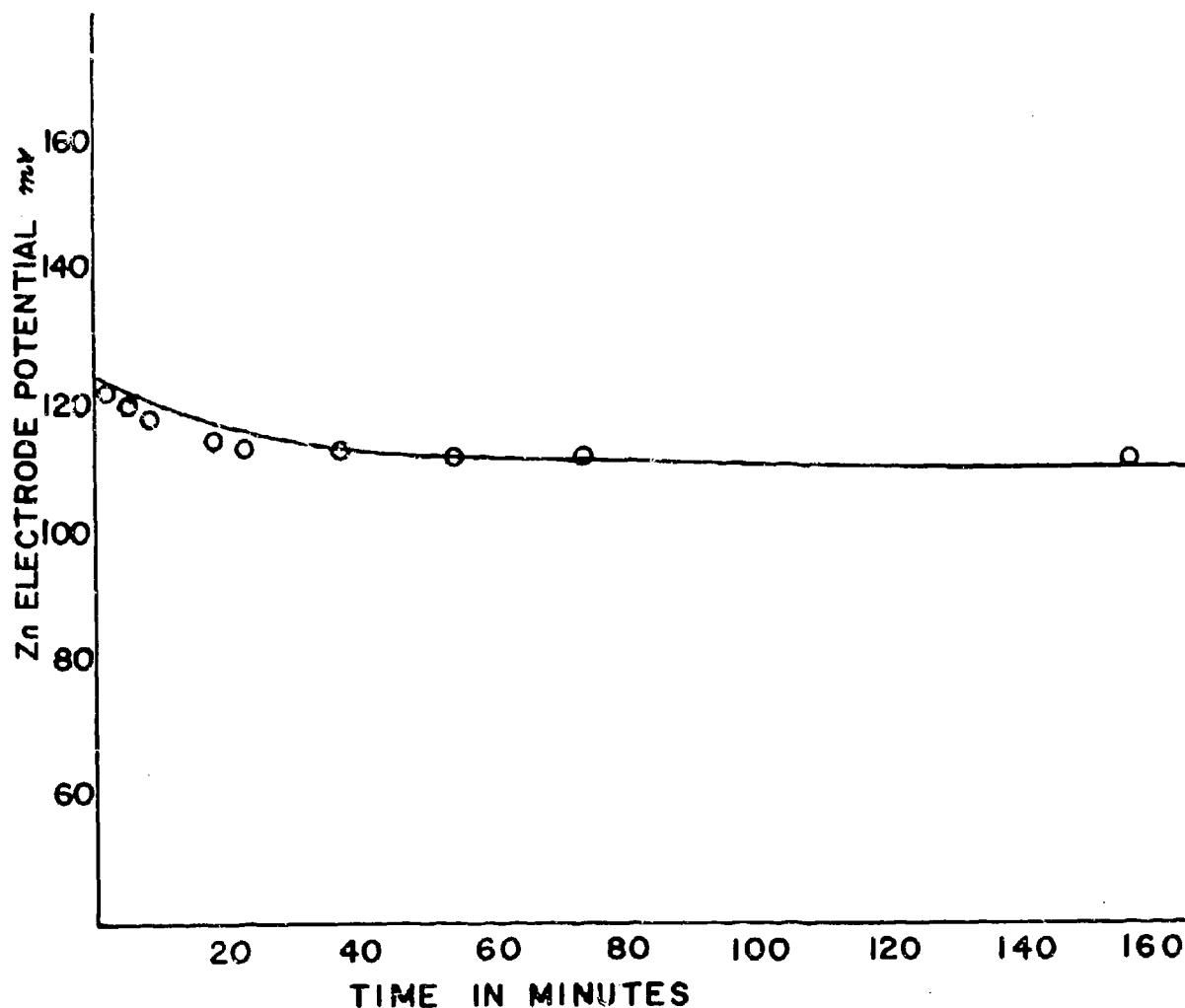
Reactor #1			Reactor #2			Reactor #3			Reactor #4		
Average	51		Average	57		Average	51		Average	42	
Minimum	28		Minimum	44		Minimum	36		Minimum	28	
Maximum	61		Maximum	66		Maximum	68		Maximum	59	

Table 20 (Cont'd.)

Code No.	Resistance mohm-in ²	Code No.	Resistance mohm-in ²	Code No.	Resistance mohm-in ²	Code No.	Resistance mohm-in ²
<u>211-50-3</u>		<u>211-50-3</u>		<u>211-50-3</u>		<u>211-50-3</u>	
5-1-1	48.7	6-6-1	55.5	7-1-1	67.7	4-5-1	43.7
5-1-2	33.7	6-1-2	62.3	7-1-2	66.3	4-5-2	37.0
5-2-1	60.0	6-2-1	62.7	7-2-1	68.7	4-5-3	41.7
5-2-2	56.7	6-2-2	63.0	7-2-2	68.0	4-5-4	34.7
5-3-1	33.7	6-3-1	71.3	7-2-3	69.3	4-5-5	26.7
5-3-2	28.7	6-3-2	59.3	7-3-1	65.0		
5-4-1	20.3	6-4-1	55.7	7-3-2	66.3	8-1-1	56.3
5-4-2	55.3	6-4-2	58.7	7-3-3	64.7	8-1-2	48.7
5-4-3	54.7	6-5-1	67.7	7-4-1	72.3	8-1-3	64.7
5-5-1	57.0	6-5-2	65.0	7-4-2	67.7	8-2-1	54.7
5-52	53.7	6-5-3	61.7	7-4-3	69.3	8-2-2	69.3
		6-5-4	65.0	7-5-1	74.7	8-3-1	64.7
9-1-1	67.3	6-5-5	65.0	7-5-2	69.3	8-3-2	68.7
9-1-2	66.3	6-5-6	63.0	7-5-3	66.7	8-4-1	62.3
9-2-1	67.7					8-4-2	52.7
9-2-2	65.3					8-5-1	60.3
9-3-1	61.7					8-5-2	61.7
9-3-2	64.3						

Reactor #5	Reactor #6	Reactor #7	Reactor #8
Average	Average	Average	Average
46	62.6	68.3	60.4
Minimum	Minimum	Minimum	Minimum
20	55.3	65.0	61.7
Maximum	Maximum	Maximum	Maximum
60	71.3	74.7	69.3

FIGURE 32 ZINC FLUX THROUGH
GRAFTED BAKELITE DFD 0602



A family of polyethylene separators has been prepared. Results of testing on these materials lead to the following conclusion.

- (1) There are at least three important parameters which must be set in order to prepare polyethylene separators useful in secondary silver-zinc batteries. These parameters are:
 - (a) base resin: the base resin must have a narrow molecular weight distribution. This distribution is important to assuring optimum crosslink density
 - (b) Crosslinking: the cycle life of batteries is a direct function of the extent of crosslinking of a particular polyethylene resin. The greater the crosslinking dose given a resin the greater will be the cycle life
 - (c) Monomer type: the cycle life is effected by the type monomer grafted onto the base resin. Methacrylic acid grafted separators are preferred over acrylic acid separators if the intended application is for long term cycle life.
- (2) Grafting crosslinked films is more difficult than grafting noncrosslinked films. Methacrylic acid grafts more readily than acrylic acid.
- (3) The preliminary results obtained to date indicate that the diffusion of zincate ion into grafted (ionic) membranes decreases with increase in temperature. This conclusion requires additional data for substantiation.

- (4) The resistance of an ionic separator is more a function of the exchange equivalent than the percent graft. It appears that the washing conditions of grafted films is of fundamental importance in converting the graft to the salt form. Low wash temperatures give only partial conversion of the graft to the salt.
- (5) Although more testing is necessary to be definite it appears that crosslinking after grafting is acceptable for acrylic acid grafted separators but not methacrylic acid grafted membranes. This may be directly related to the crosslinking scission ratio of acrylic and methacrylic polymers.
- (6) Uniform crosslinking densities can be obtained on samples by application of the technique described in this report. This technique is described as the "half depth - half dose" irradiation.
- (7) The percent extraction from grafted membranes at elevated temperatures is some inverse function of the extent of crosslinking.
- (8) Separator 211-50-3 which combined all the desired resin, crosslinking and monomer properties gave the best separator evaluated to date for secondary silver-zinc batteries.
- (9) The cycle-life of batteries operated at an elevated temperature increased when crosslinked ionic separators were used but decreased when cellulosics separators were used.

1. The preliminary promising results obtained in cycle testing batteries using ionic separators at elevated temperatures indicates that the optimum condition for cycle testing is above room temperature. Cellulosics degrade at higher temperatures while ionic separators developed here appeared to improve in their capacity to prevent zinc diffusion. It is recommended that additional cycle testing be undertaken as a function of temperature to determine the optimum operational temperature for batteries using ionic separators.

2. The test results from cycle testing 25 amp hour batteries confirm the improvement registered in three plate cells. It is recommended that procedures for scale up and development of this separator be undertaken to establish quality control specification on the processes and product developed. It is also necessary to improve the process to decrease the average resistance of the separator. It is believed that this can be done by optimizing on washing conditions and relating washing conditions to exchange capacity.

3. The method of evaluating graft uniformity started here should be modified to improve the sensitivity of the procedure. It has been shown that the procedure practiced is applicable but can be improved by evaluating the ultra-violet spectra of grafted films rather than dyeing and plotting the visible spectra. This method could be developed as a non destructive in line test.

4. The increase in resistance with decrease in temperature is quite significant for separators having acrylic and methacrylic acid grafts. This may be related to the stiffness of the grafted chain. It is suggested that new membranes for use at cold temperatures could be prepared by grafting flexible chains to the same crosslinked base resin. This could be accomplished by co-grafting a vinyl ether with another monomer such as vinyl acetate or perhaps methacrylic acid.

5. An additional area of investigation which is recommended would be the evaluation of non-ionic grafted membranes having varying percents cationic exchange capacity on the zinc washing characteristics of the plates. It is believed that by using non-ionics with varying predictable ionic character the electro-osmotic effect and its relation to capacity loss could be studied.

REFERENCES

1. J. J. Lander, and J.A. Keralla, "Applied Research investigation of Sealed Silver-Zinc Batteries" Supplementary Report to APL-TDR 64-85, April 1965.
2. E.J. Henley, and R. Richman, *Analyt. Chem.*, 28 1580 (1956).
3. A. Chapiro, "Radiation Chemistry of Polymeric Systems" John Wiley & Sons, Inc. New York (1962).
4. RAI Quarterly Report 388, January, 1968.
5. Private Communications, Dr. J.J. Lander and RAI.
6. ASTM D882-56T, ASTM Standard on Plastics, 12th Edition, March, 1961.
7. J.E. Cooper & A. Fleischer, editors "Characteristics of Separators for Alkaline Silver Oxide-Zinc Secondary Batteries", Aero Propulsion Laboratory, 1965.
8. Trump, et. al. *J. Appl. Phys.*, 21 346 (1950).
9. A. Charlesby, "Atomic Radiation and Polymers" Pergamon Press, 1960.
10. J. Johnson and R. Porter, editor "Polymer Symposia on Analytical Gel Permeation Chromatography" *J. Polymer Sci., Part C*, Interscience Publisher, 1968.
11. L. Wild and R. Guliana, *J. Polymer sci.*, A-2 in press.
12. A. Charlesby, *Rad Res.* 2 96 (1955).
13. H. A. J. Battaerd, and G.W. Tregan "Craft Copolymers", Intersciences Publisher, New York, 1967
14. W. Gabara, S. Porejko, *J. Polymer Sci., Part A1*, 5, 1347 (1967).

15. A. Weissberger, editor "Technique of Organic Chemistry"
Vol. IX, Interscience Publisher Inc., New York 1961.
16. H. Morawetz, "Solution Properties of Macromolecules"
Interscience Publisher, 1967.
17. J. J. Lander and J. A. Keralla, "Technical Report
AFAPL 67-107", August 31, 1967.
18. J. McBreen, "Final Report for Study of Zinc Electrode
for Spacecraft Electrochemical Cells" October 1967.
19. H. P. Gregor, "The Electrochemical Society, Inc. Fall
Meeting - Montreal, Canada, October 6-11, 1968".
20. J. J. Lander, Zinc Diffusion (Chapter 11); "Characteristics
of Separators for Alkaline Silver Oxide Zinc Secondary
Batteries" Ed J.E. Cooper and A. Fleischer.

APPENDIX ONE

MATERIALS AND SUPPLIERS

Glacial Acrylic Acid	Rohm and Haas
Glacial Methacrylic Acid	Rohm and Haas
Vinylacetate (Practical)	Eastman Organic Chemicals
3.3 Dimethylacrylic Acid	Pfaltz & Bauer, Inc.
3 Methymethacrylic Acid	Pfaltz & Bauer, Inc.
Phenybeta-Naphylamine	Eastman Organic Chemicals
Methylene Chloride (Reagent)	Fischer Scientific Company
Zinc Oxide (USP)	Matheson Coleman and Bell
Divinylbenzene (Commercial)	Dow Chemical Company
Benzene	Peerless Petrochemicals Inc.
Methanol	Peerless Petrochemicals Inc.
Xylene	Peerless Petrochemicals Inc.
Potassium Hydroxide Solution (Certified)	Fischer Scientific Company
Potassium Hydroxide (Solid 90-92%)	Allied Chemical Corp.
Bakelite DFD-0602 Resin	Union Carbide Corporation
USI-280	U.S. Industries Chemical Co.
NA-107	U.S. Industries Chemical Co.

Appendix One (Cont'd.)

NA-301

U.S. Industries Chemical Co.

P-1712

Phillips Petroleum Co.

S-565

Sea-Space Systems, Inc.

SERVICES

Gel Permeation Chromatography
(GPC)

Waters Associates Inc.

Extrusion of Film

(1) Phillips-Joanna

(2) Sea-Space Systems, Inc.

Crosslinking (Beta Radiation)

Radiation Dynamics Inc.

Gamma Radiation

Industrial Reactor Laboratories,
Inc.

UNCLASSIFIED

Security Classification

DOCUMENT CONTROL DATA - R&D		
(Security classification of title, body of abstract and indexing annotation must be entered when the overall report is classified)		
1. ORIGINATING ACTIVITY (Corporate author)		2a. REPORT SECURITY CLASSIFICATION
Delco-Remy Division General Motors Corporation Anderson, Indiana 46011		Unclassified
		2b. GROUP
3. REPORT TITLE		
"Silver-Zinc Electrodes and Separator Research"		
4. DESCRIPTIVE NOTES (Type of report and inclusive dates)		
Technical Report 30 June 1967 to 30 June 1969		
5. AUTHOR(S) (Last name, first name, initial)		
Keralla, J. A.		
6. REPORT DATE	7a. TOTAL NO. OF PAGES	7b. NO. OF REFS
30 June 1969	430	0
8a. CONTRACT OR GRANT NO.	8b. ORIGINATOR'S REPORT NUMBER(S)	
AF33(615)-3487		
A. PROJECT NO.		
3145		
c. Task No. 314522	8c. OTHER REPORT NO(S) (Any other numbers that may be assigned this report)	
d.	AFAPL-TR-69-57	
10. AVAILABILITY/LIMITATION NOTICES		
Foreign announcement and dissemination of this report by DDC is not authorized.		
11. SUPPLEMENTARY NOTES	12. SPONSORING MILITARY ACTIVITY	
	Air Force Aero Propulsion Laboratory	
	Wright-Patterson Air Force Base, Ohio	
13. ABSTRACT		
<p>Emulphogene BC-610 used in quantities of .5% to 1% by weight in the negative active material tends to increase cycle life.</p> <p>The use of 1% Pb in the negative active material tends to increase cycle life at 60% depth-of-discharge. The presence of Fe in zinc oxide in concentrations over .010% is detrimental to cycle life at any depth-of-discharge.</p> <p>The use of inert polyethylene crosslinked at 90 Mrads, radiation grafted with methacrylic acid can be used as a satisfactory separator material for long cycling silver zinc cells.</p> <p>Key Words: Storage Battery Secondary Cells Sealed Separators Keralla, J. A.</p>		

DD FORM 1473

UNCLASSIFIED

Security Classification